DYNAMICS OF COUPLED CONTAMINANT AND MICROBIAL TRANSPORT IN HETEROGENEOUS POROUS MEDIA: PURDUE COMPONENT

FINAL REPORT
12/23/1996 – 12/31/1999

J. H. Cushman

June 2000

Prepared for the
U.S. Department of Energy
Assistant Secretary for
Environmental Management
Washington, DC

Prepared by
Purdue University
West Lafayette, IN

DISCLAIMER

Portions of this document may be illegible in electronic image products. Images are produced from the best available original document.

Final Report (6/21/00) for

Grant DE-FG07-97ER62354

for

DOE/EM Project

Dynamics of Coupled Contaminant and Microbial Transport in Heterogeneous Porous Media:
Purdue Component

by

John H. Cushman, Co-PI
Prof. Applied Math
Prof. Environmental Physics
Center for Applied Math
1395 Math Sciences Building
Purdue University
West Lafayette, IN 47907
Phone: 765-494-8041
Email: jcushman@math.purdue.edu

Summary

Dynamic microbial attachment/detachment occurs in subsurface systems in reponse to changing environmental conditions caused by contaminant movement and degradation. Understanding the environmental conditions and mechanisms by which anaerobic bacteria partition between aqueous and solid phases is a critical requirement for designing and evaluating in situ bioremediation efforts. This interdiscipliary research project, of which we report only the Purdue contribution, provides fundamental information on the attachment/detachment dynamics of bacteria in heterogeneous porous media. The multidisciplinary team contributing to the overall project has evolved from previous collaborations between DOE and various universities. Co-investigators include Drs. Ginn, Murphy and Fletcher as well as numerous students and post docs.

Fundamental results resulting from the Purdue collaboration are:

(i) Development of a matched-index method for obtaining 3-D Lagrangian trajectories of microbial sized particles transporting within porous media or microflow cells.

(ii) The application of advanced numerical methods to optimally design a microflow cell for studying anaerobic bacterial attachment/detachment phenomena.

(iii) Development of two types of models for simulating bacterial movement and attachment/detachment in microflow cells and natural porous media.

(iv) The application of stochastic analysis to upscale pore scale microbial attachment/detachment models to natural heterogeneous porous media.

(v) Evaluation of the role nonlocality plays in microbial dynamics in heterogeneous porous media.

Table of Contents

I. Introduction

1. Purpose

In "Estimating the Cold War Mortgage: The 1995 Baseline Environmental Management Report" (BEMR), uncertainty in estimating cleanup cost is associated with the lack of remedial approaches for contamination problems, as well as the lack of knowledge on the effectiveness of the remedies that are available (DOE, 1995a). These difficulties highlight the need for the development of technologies for subsurface contaminant plume containment and remediation (DOE, 1995b). The central challenge of in situ remediation strategies is the control of the transient spatial distribution of contaminants and remediation reagents (e.g., nutrients or microorganisms) in the presence of natural physical and chemical heterogeneities. Currently available predictive tools rely almost exclusively on the representation of passive attachment/detachment processes (e.g., filtration, sedimentation) with the bacterium treated as an inert biocolloid. One of the most intractable aspects of bioreactive transport, however, is active microbial partitioning (e.g., attachment/detachment) under growth and transport in physically and chemically heterogeneous systems (Sturman et al., 1995). Active attachment/detachment is associated with microbial physiologic response to changes in local aqueous concentrations of nutrients and electron-acceptors: this process is treated rarely in field-scale bacterial transport theories, and not at all in available predictive tools.

Understanding coupled contaminant and bacterial transport in real media is critical to the success of potential future bioremediation/biobarrier strategies at DOE sites. Disposal of chlorinated hydrocarbons has generated extensive contaminant plumes in sand/gravel aquifers at DOE's Savannah River Site (SRS) in South Carolina and Paducah Gaseous Diffusion Plant (PGDP) in Kentucky, and such organic solutes interact with natural environments in coupled

complex ways that have serious ramifications for remediation. For example, during the SRS in situ bioremediation demonstration, 90% of the increase in methanotroph biomass arising from degradation of trichloroethylene (TCE) partitioned into the aqueous phase (DOE, 1993). Initially, this methanotroph population was primarily attached to solid surfaces. If this partitioning behavior during bioremediation were understood and could be predicted, the knowledge could be exploited to effectively distribute the biomass across a contaminated area and to plan an injection network so as to minimize costly well construction and dampen or eliminate microbially-induced reductions in hydraulic conductivity. This basic knowledge on the transport response of microorganisms is required for any subsurface remediation involving microbes, including staged approaches that sequentially degrade and immobilize multiple contaminants. Staged approaches (temporal or spatial) can exploit the different transport properties of distinct microbial populations and are especially well suited to DOE mixed contaminant problems.

Factors affecting microbial partitioning behavior are complex and not well-defined. In oligotrophic environments, some microorganisms partition onto the solid phase as nutrients become limiting (Fletcher and Marshall, 1982; Kjelleberg et al., 1985), while the opposite response can occur in a nutrient-rich environment or contaminant plume (Bengtsson, 1989; Murphy et al., submitted). Complicating this scenario is the involvement of active microbiological survival mechanisms that are not well understood at a basic science level. Some microorganisms have displayed active attachment/detachment processes that are transient under changing growth and starvation conditions (Dawson et al., 1981; Kjelleberg and Hermansson, 1984; van Loosdrecht et al., 1987, 1990). It is not yet clear how wide-spread "active attachment/detachment processes" are among microorganisms, but they may be highly

significant in natural environments, where there appears to be appreciable exchange between attached and mobile populations. While some microorganisms use transport as a survival mechanism (to move to a better environment), other microorganisms appear to use attachment as a survival mechanism, as they appear to be less susceptible to potentially lethal environmental effects (Chen et al., 1993) and predation (Leff et al., 1994). Further, nutrients associated with the solid phase and with heterogeneous chemical reactions may be more accessible to attached microorganisms. Although anaerobic bacteria play a significant role in microbial destruction of chlorinated solvents and transformation of metals, very few studies have been reported on the transport of bacteria in porous media under anaerobic conditions (Clement et al., in press). Further, little information is available on the dynamic attachment/detachment of active microorganisms in natural media—information that is critical for designing cost-effective in situ bioremediation strategies for mixed contaminants. Without a fundamental understanding of these processes, field efforts can be severely compromised or even wasted by unexpected consequences, such as biological plugging of the aquifer near injection zones (Cunningham et al., 1991; Semprini et al., 1991). The study of bacterial transport must also account for coupling between microbial partitioning and transport in heterogeneous media. Our ability to control any subsurface manipulation involving transport is severely challenged by the occurrence of natural physical and chemical heterogeneities in, for instance, reactive surface area and hydraulic conductivity. Specifically, the coupled distributions of microbes and aqueous-phase nutrients, and how these distributions change in time under particular pumping and nutrient addition strategies, will depend on the spatial variability (heterogeneity) in the controlling chemical and physical properties.

The purpose of the proposed research is to address the limitations in understanding reactive contaminant transport and dynamic bacterial attachment/detachment under growth and growth-limiting conditions in natural porous media. This research will assess the coupled degradation and transport processes involving biological agents, with focus on the active and passive attachment/detachment and transport processes of anaerobic microorganisms involved in TCE degradation, including their persistence under transient variations in substrate and electron-acceptor availability. The goals of the research are to develop basic knowledge of the fundamental relationship between contaminant transport and active bacterial transport and attachment/detachment under transient local chemical conditions. This knowledge will afford a quantitative understanding of the transient spatial distribution of contaminants and microbial populations during contaminant degradation and microbial growth in physically and chemically heterogeneous media. To accomplish this end, the research includes an integrated effort toward the development of predictive models of contaminant transport and degradation in heterogeneous media, through a combined multi-scale experimental and theoretical approach.

2. Background

Movement of bacteria through porous media, including sediments and fractured rock, is largely determined by the opposing processes of convective transport and the attachment of bacteria to solid surfaces. The different processes involved are understood to disparate levels of sophistication and have been examined in various scientific disciplines varying from soil science to colloid transport to microbial physiology. The purpose of this section is to chart the current state of the sciences involved, in order to identify the foundations for the proposed multidisciplinary research. The section begins with conceptualizations of biomass structure in porous media and proceeds through subsections on active and passive microbial

attachment/detachment (e.g., phase partitioning) processes, to a review of modeling such processes combined with convective-dispersive transport in heterogeneous porous media. The broad scope represents the nature of field contamination problems faced by OEM and reflects the scope of research covered. The following literature review is necessarily comprehensive in order to provide the complete background required by the multidisciplinary nature of the hypotheses put forth.

2.1. Biomass Structures in Porous Media

The proper model representation of the biological phase in porous media is a matter without consensus as noted in the exchanges of Widdowson (1991), Baveye et al. (1992) and Jaffee and Taylor (1992). However in natural contaminated media associated with OEM sites, the rates of contaminant degradation as well as the rates of biomass attachment/detachment are closely linked to the structural form of biomass in natural media, and so any quantitative study of the relevant processes must examine and account for the structures involved. Biomass in the subsurface is represented alternately as 1) a continuous biofilm on the solid surfaces (Taylor and Jaffee, 1990a; Taylor et al., 1990; Dykaar and Kitanidis, 1996); 2) a discontinuous patchy film (e.g., Vandevivere and Baveye, 1992a,b; Rittmann, 1993) or microcolony with specified geometric structure (e.g., Molz et al., 1986; Widdowson et al., 1988); and 3) no assumptions on biomass structure (unstructured models; e.g., MacQuarrie et al., 1990; Sudicky et al., 1990; Zysset et al., 1994; Wood et al., 1994; Murphy et al., submitted). Structured biofilm models are often associated with a focus on pore clogging and permeability changes, which limit transport and hence degradation (Cunningham et al., 1991; Rittman, 1993). Mathematically, the continuous biofilm and microcolony models are often associated with a diffusion limitation on the transport of solutes from aqueous phase to biomass phase where they can be degraded (Wood

9

et al., 1994). The diffusive transport of substrate into the biomass is typically represented by an "effectiveness factor" (e.g., Williamson and McCarty, 1976; Dykaar and Kitanidis, 1996) which is a parameter that reflects the rate limitations on the transport and degradation of solutes within the biomass structure. The "effectiveness factor" encompasses microscopic features of the subsurface biomass system such as biofilm or colony thickness, biofilm density, and colony radius. These quantities are defined at scales well below the scales of quantities used to express mass fluxes in groundwater (e.g., porosity, conductivity), and rigorous linking of representative parameter values across these scales is generally lacking. One exception is the scaling in Dykaar and Kitanidis (1996) of a single pore biofilm model (via the assumption of a periodic media) to derive equations that describe degradation and biofilm growth at the continuum (e.g., centimeter) scale in bulk porous media. However, in addition to requiring a continuous and uniform biofilm of known density, this approach is subject to assumptions that specify an idealized pore geometry, limiting its extension to heterogeneous media. Moreover, biofilm density, a critical parameter in biofilm-based models, is difficult to quantify, particularly in porous media. Literature values of biofilm density range from 10 to 130 kg dry mass/m^3 (Peyton and Characklis, 1993) and depend on several factors such as vicinity to the aqueous phase, type of bacteria, history of substrate supply, and shear force.

Wood et al. (1994) showed that when the mass transfer coefficient across a biofilm is large, as in the case of a relatively thin biofilm or rapid diffusion through the biofilm, the structured model reduces mathematically to an unstructured model. Use of an unstructured approach involves no assumption on biomass structure, which is treated as a volumeless aqueous species that may or may not undergo a partitioning with the solid phase (MacQuarrie et al., 1990; Sudicky et al., 1990; Zysset et al., 1994; Wood et al., 1994). Therefore, the unstructured

approach is more commonly adopted in investigations that focus on kinetic transport in oligotrophic groundwater environments and will be used in this study.

2.2. Microbial Attachment/Detachment Processes in Porous Media

Both conceptual and quantitative representations of biomass partitioning (attachment/detachment processes) in porous media depend strongly on the underlying assumptions made about the structure of the microbial community, as noted above. For instance, in model formulation for both numerical studies and simulation of column experiments, MacQuarrie et al. (1990) and Sudicky et al. (1990) represent attachment/detachment through equilibrium partitioning. Zysset et al. (1994) use a similar approach but represent the attachment/detachment as a kinetically-controlled process. In fact, attachment/detachment is nonexistent in several recently developed models, including those that treat active microbes as an exclusively aqueous-phase component (e.g., MacQuarrie et al., 1990) and those that treat biomass as an exclusively solid-phase (attached) component (e.g., Bower and Cobb, 1986; Molz et al., 1986; Widdowson et al., 1988; Kindred and Celia, 1989; Wood et al., 1994; Dykaar and Kitanidis, 1996). The multiple and conflicting ways in which biomss partitioning has been represented in porous media arise partly from the *absence of basic scientific information regarding the structure of microbial distribution and dynamics of active attachment/detachment processes in porous media*. Active processes have received less attention, while a representation of passive bacterial partitioning, through analogy to colloid transport, has been the focus of many studies. The physical processes involved in passive microbial partitioning are well-documented and are summarized here.

Passive Attachment/Detachment. Several researchers have experimentally investigated *passive* attachment processes that influence the transport of non-growing bacterial cells in one-

11

dimensional porous media columns. A large segment of the literature is dedicated to the development and application of filtration theory-based representations of attachment processes examined in such laboratory experiments, and we focus briefly on these studies. Straining and physical filtration represent the removal of microbes from solution by physical (geometric and electrostatic) forces, as opposed to active biological binding. Straining is the trapping of microbes in pore throats that are too small to allow passage and is exclusively a result of pore geometry (Corapcioglu and Haridas, 1984). Prediction of mass removal by straining, based on purely geometric relations between the effective diameter of biocolloids and the diameter and packing (coordination number) of grains forming the porous media, is detailed by Herzig et al. (1970) and experimentally by Sakthivadivel (1966, 1969). An important result of these analyses for microbial transport is the finding that straining is not significant in idealized packed beds (porous media made up of identical spherical grains) where the colloid diameter is less than 5% of the porous media grain diameter (Herzig et al., 1970; Corapicoglu and Haridas, 1984; McDowell-Boyer et al., 1986; Harvey and Garabedian, 1991).

Physical Filtration. Physical filtration is the removal of particle mass from solution via collision with and deposition on the porous media. Physical forces involved are gravity, partice-particle and particle-solvent collisions (Brownian forces), electrostatic interaction potentials between the particle and the porous media, van der Waals attractive potentials, biocolloid (microbe) inertia, and pore-water hydrodynamic forces (Yao et al., 1971; McDowell-Boyer et al., 1986). Filtration due to gravity is termed sedimentation (McDowell-Boyer et al., 1986; Corapcioglu and Haridas, 1984) and depends on particle buoyancy. Many bacteria and viruses are neutrally buoyant, in which case sedimentation is negligible.

Filtration due to the remaining physical forces (Brownian, electrostatic, van der Waals, and pore-water hydrodynamic) is the dominant mechanism for removal of biocolloids and has received enormous attention, partly as a result of its quantitative tractability (cf. Review by McDowell-Boyer et al., 1986). Physical filtration terminology is often used inconsistently between disciplines; while the term "physical filtration" is used in the engineering literature, "adsorption" is used in chemistry, and "attachment" in the microbiological literature.

Previous research has demonstrated that physical filtration is influence by solute ionic strength due to its effect on electrostatic interactions (Sharma et al., 1985; van Loosdrecht et al., 1989; Scholl et al., 1990; McDowell-Boyer, 1992; Tan et al., 1994), pH (McEldowney and Fletcher, 1988), and mineralogy (Fletcher and Loeb, 1979; Scholl et al., 1990). Shonnard et al. (1994) found significant increases in adsorption of a TCE-degrading bacterium as a result of increased ionic strength of solution in coarse sands. Scholl et al. (1990) and Mills et al. (1994) found that iron hydroxide-coated sands filtered more bacteria than clean sand, which was expected given the effect of iron hydroxide coatings on the interaction potential. Quartzitic materials are predominantly negatively charged, as are most bacteria; thus, the hydrodynamic and attractive (van der Waals) forces must overcome the repulsive electrostatic force for bacterial immobilization to occur. Iron hydroxide-coated sand grains have positive surface charges, thus reversing the electrostatic force from repulsive to attractive and increasing the likelihood of microbial attachment. Hydrophobic interactions can also result in sorption of microorganisms (Fletcher and Loeb, 1979; van Loosdrecht et al., 1987; Fletcher, 1991) and has been investigated by measuring the hydrophobicity of microorganisms and determining their sorption on porous media coated with organic matter (McCaulou et al., 1994). Even small amounts of organic matter on porous media may result in complete retention of microorganisms

on the particle surfaces (Ryan and Gschwend, 1990) which may also be related to active microbial adhesion.

The effect of these physical forces on microbial attachment is quantified in models through averaging the interaction potentials and hydrodynamic forces in the pore-scale behavior of an idealized microbe moving through an idealized porous media. Namely, rates of attachment are derived for a chemically inert spherical particle being transported through a uniformly packed homogeneous bed of spherical grains (Herzig et al., 1970; Shaw, 1976; Tien et al., 1979). The microbial mass removal from the aqueous phase is cast in terms of pore-water velocity, viscosity, and density; media grain size; and media porosity. The resulting relations are well-known (cf. DeMarsily, 1986) and have been widely applied to microbial transport (cf. Harvey et al., 1989; Harvey and Garabedian, 1991). The reversibility of physical filtration (via reduction in solute ionic strength; Scholl et al., 1990; McDowell-Boyer, 1992; Bales et al., 1995), as well as the reversibility incurred by changing the pore-water velocity direction (Sakthivadivel, 1966), is not inherent in filtration theory-based models because the filtration models represent irreversible deposition only under conditions of uniform flow direction and fixed solution chemistry. Thus treatment of detachment is entirely absent in several filtration theory analyses of microbial transport (e.g., Jewett et al., 1995). The evidential significance of detachment processes in experimental studies, however, has led to increased reliance on a (more or less empirical) detachment term in addition to the attachment terms. The resulting "two-site" reactive transport model utilizes irreversible kinetic reactions for attachment at one type of reaction site (in accordance with filtration theory), and either equilibrium or kinetic-reversible terms for attachment and detachment at a second type of reaction site. Examples are given by Harvey and Garabedian (1991), Fontes et al. (1991), Bales et al. (1991), Lindqvist and Bengtsson (1991),

Mills et al. (1991), Kinoshita et al. (1993), Hornberger et al. (1992), and McCaulou et al. (1994). This recent reliance on kinetic detachment is not actually new; dual attachment/detachment mechanisms were modeled similarly in an early study on particulate "clogging/declogging" (Sakthivadivel and Irmay, 1966; Herzig et al., 1970), as noted by Corapcioglu and Haridas (1984). Tan et al. (1994), and Lindqvist et al. (1994) augment the first-order kinetic attachment model with a nonlinear governing factor intended to represent the attachment-limiting effect of site-saturation, while maintaining a linear detachment kinetic. An identical model is recently proposed for colloid transport in Saiers et al. (1994).

Prediction of effective first-order kinetic attachment coefficients via filtration theory has met with mixed success, partly because of the non-ideal and distributed characteristics of natural granular media, and partly due to inherent limitations of the theory (e.g., original filtration theory-based attachment is unlimited and irreversible). The capabilities and shortcomings of the theory in field application are well documented by Harvey and Garabedian (1991).

Size Exclusion. In addition to filtration, size exclusion results in differential bacterial and ion tracer breakthrough times in column (Hornberger et al., 1992; Mayotte et al., 1996) and field (Wood and Ehrlich, 1978; Pyle and Thorpe, 1981; Harvey et al., 1989) experiments. Size exclusion is the phenomenon of transported particles moving faster than the pore water, or at least faster than the average pore-water velocity (as indicated by the breakthrough of a salt tracer). The process is similar to hydrodynamic chromatography (e.g., DeMarsily, 1986). Pore-water velocity within a capillary or pore throat is generally parabolically distributed, with the maximum velocity occurring at the centerline and that at the pore walls equal to zero (DeMarsily, 1986). Conventional transport theory assumes that molecular-scale solutes thoroughly sample the full distribution of velocities in convecting pores of all significant sizes.

Microbes and large colloids, by virtue of their size, preferentially experience the higher velocities near pore centerlines, yielding an average velocity that is higher than that of a molecular (salt) tracer. Thus microbes can precede the tracers down gradient. Results from hydrodynamic chromatography (Dodds, 1982; DeMarsily, 1986) indicate that in idealized porous media, the ratio between bacterial and water average velocities is quite small, usually between 1.0 and 1.1, and that the occurrence of exclusion requires the bacterial diameter be <1% of the media grain diameter, which is common for transport in sandy aquifers. The velocity ratio can be amplified in the presence of ionic forces (this is anion-exclusion, as opposed to size-exclusion). When the electrostatic forces between the media and colloid are repulsive, as is the case with negatively charged microbes in negatively charged quartzitic media, the force field tends to channel the microbes closer to the pore throat centerlines and away from the walls (and the slower velocities; DeMarsily, 1986). Thus the effect may be drastically more pronounced at larger observation scales in natural media, as has been reported in some experiments (Pyle, 1979; Engfield and Bengtsson, 1988; Harvey et al., 1989; Harvey, 1993; Shonnard et al., 1994).

Active Attachment/Detachment. Active attachment/detachment processes are much less well described and understood than passive processes, and efforts to capture the effects of active processes on transport in bulk porous media have just begun (e.g., active detachment, Peyton et al., 1995). Active attachment is often referred to as adhesion and for clarity is treated separately in our discussion from passive electrostatic adsorption which may occur during physical filtration. Several studies have reported that microorganisms exhibit active attachment/detachment processes, which may be a response to local nutrient availability (Dawson et al., 1981; Kjelleberg and Hermansson, 1984; van Loosdrecht et al., 1990), survival mechanisms (Dawson et al., 1981; Wrangstadh et al., 1990; Gilbert and Brown, 1995), and/or

growth (Jenneman et al., 1985, 1986; Reynolds et al., 1989; Sharma et al., 1993). The distinction between a microorganism's response to nutrient availability, survival stress, and growth are not necessarily separable nor independent processes. Furthermore, in contrast to the passive attachment/detachment processes discussed above, numerical representations of these active processes are totally lacking in predictive reactive transport models.

There is considerable variability in the strength and duration of bacterial attachment to surfaces. Many attached bacteria are firmly bound to surfaces and resist strong shear forces. Others are only loosely associated, and are easily removed by shear stresses (Marshall et al., 1971) or may move over surfaces by gliding motility or "rolling" motions (Lawrence and Caldwell, 1987). Moreover, with time the adhesive association may alter and cells may detach. Release of attached bacteria can occur due to enzymatic degradation of adhesive polymers (Boyd and Chakrabarty, 1994), chemical alterations (Marshall et al., 1989), or alterations in the bacterial surface due to changing nutritional conditions (Rosenberg et al., 1983; Vandevivere and Kirchman, 1993; Wrangstadh et al., 1990). Thus, the transport of microorganisms through porous media is strongly dependent not only on their inherent active adhesive properties, but also on their environment and their metabolic activities.

Response to Nutrient Availability. The ability of bacteria to associate with surfaces enables them to utilize surface-adsorbed nutrients that may not be accessible to cells in the aqueous phase. The bacteria may be strongly attached or they may associate only temporarily with the surface to graze nutrients. Both leptospires (*Leptospira biflexa* patoc 1) (Kefford et al., 1982) and vibrios (Vibrio MH3) (Hermansson and Marshall, 1985) were found to attach reversibly to surfaces and utilize ^{14}C-labeled stearic acid that was adsorbed to the surface. In contrast, some substrates partition onto surfaces and are accessible only to organisms that can

attach or graze. For example, *Serratia marcescens* EF190 irreversibly attached to surfaces and rapidly scavenged ^{14}C-labeled stearic acid on the surface. Little label was found in free-living cells (Keffort et al., 1982). Similarly, ^{14}C-labeled bovine serum albumin, which adsorbed rapidly onto particles, was utilized by attached *Pseudomonas* sp. NCIMB 2021, but was essentially inaccessible to bacteria in the liquid phase (Griffith and Fletcher, 1991). Furthermore, the ability to alternate between aqueous and solid phases allows the organism to access nutrients in both phases.

Utilization of surface adsorbed nutrients is influenced by the physico-chemical properties of the surface, which in turn influence strength of binding and adsorption of adsorbed molecules. In some cases, bacterial utilization is enhanced; for example, the degradation of nitrilotriacetate by bacteria attached to sand had a shorter lag time and higher specific activity than with bacteria in the aqueous phase (McFeters et al., 1990). In the case of degradation of tritium-labeled ribulose-1,5-bisphosphate carboxylase (RuBPCase) by the marine *Pseudomonas sp.* S9, the percent degraded decreased with increasing hydrophobicity of the surface (Samuelsson and Kirchman, 1990). Growth rates were higher on a hydrophilic glass surface than on a hydrophobic polyethylene surface initially, but after six hours, rates increased on the hydrophobic surface because of increased adsorption of the RuBPCase. The effects of surface adsorption on substrate accessibility are particularly significant with macromolecules, which tend to bind with high affinity through multiple adsorption sites.

In some cases, adsorption of macromolecules inhibit their utilization by bacteria, presumably because of conformational changes that alter or obscure enzyme binding sites. There are numerous examples of reduced degradation of substrates in the presence of particles (Gordon and Millero, 1985; Ogram et al., 1985). Reduced degradation of naphthalene has been observed

in some soils (Guerin and Boyd, 1992), and there was almost total inhibition of degradation of bromobenzene in simulated groundwater when sand was present (Mills and Eaton, 1984).

There is also evidence that bacterial behavior and/or physiology can be influenced by association with surfaces, and that may indirectly influence their utilization of substrate. Genes may be induced or derepressed (Dagostino et al., 1991; Davies et al., 1993), leading to alterations such as the production of exopolymers (Vandevivere and Kirchman, 1993). There are many parameters that may be altered in the surface microenvironment, compared to the liquid phase, that could influence gene expression; these include not only substrate concentration and type, but also pH, osmolarity, and cell density.

Responses Associated with Survival. There have been numerous observations of enhanced survival of microorganisms on surfaces. This advantage appears to be most pronounced when bacteria are in biofilms, that is they are embedded in a highly hydrated polymeric matrix. There are three possible explanations for this enhanced survival: 1) the intercellular polymer protects against toxic substances by providing a reactive barrier to diffusion, 2) the bacteria in the biofilm have a reduced growth rate because of reduced diffusion of key nutrients, making them less susceptible to toxic substances, and 3) the surface environment results in the derepression or induction of genes associated with survival (Gilbert and Brown, 1995). It is possible that bacteria have evolved mechanisms to induce attachment in situations where association with a surface provides a strong selection pressure. With the marine Vibrio DW1, starved cells became more adhesive than unstarved bacteria (Dawson et al., 1981). This observation has led to the speculation that adhesion may be a response to starvation, enabling the organisms to associate with a surface where nutrients may be more accessible. In contrast, starvation of a marine Pseudomonas species resulted in synthesis of polymers that

19

resulted in cell detachment (Wrangstadh et al., 1990). Thus, it is impossible to generalize about the effects of starvation on adhesion, except to say that nutrient deficiency may alter the adhesiveness of the cell in either a positive or negative direction. Moreover, the alterations in surface adhesiveness vary and are characteristics of the particular type of nutrient limitation, e.g. carbon, nitrogen, phosphorus (Brown and Melling, 1969; Ellwood and Tempest, 1972; Holme, 1972; Lambert, 1988).

Once attached to a surface, the "fitness" or survival of the organism may be influenced by alterations in gene expression. As mentioned above, there are many parameters, which may be altered at the surface microenvironment, that can influence gene expression. These include oxygen tension (Smith and Neidhardt, 1983; Clark, 1984), pH, cell density and metabolite concentration, osmolarity, and inorganic ions (Goodman and Marshall, 1995). Attachment to a surface allows for the establishment of stable communities that rely on transfer of metabolites, an activity that is much more important for anaerobes than for aerobes. Also the surface microenvironment may facilitate the establishment and maintenance of anoxic sites, and precipitated metal sulfides may provide additional protection.

Response to Growth. The process of growth has been recognized as a mechanism by which bacteria penetrate porous media under static or flowing conditions (Jenneman et al., 1985, 1986; Reynolds et al., 1989; Sharma et al., 1993). Reynolds et al. (1989) suggested that as nonmotile cells grow, they fill the locally available pore space and new cells are physically displaced into the next portion of the porous media. For cells that are attached to porous media, the physical displacement may occur simply from cell division, ejecting the cell into the pore space. Under flowing conditions, as encountered in groundwater systems, the progeny may be transported until straining or attachment to the porous media occurs. The process of cell

division-mediated transport can be represented numerically by assuming an initial distribution of cells with all growth partitioning to the aqueous phase.

Peyton and Characklis (1993) reported that active detachment rates were strongly growth rate dependent and were not significantly affected by shear stress. Peyton et al. (1995) used an advection-dispersion model to analyze data from Lundman (1992) and observed the effective detachment coefficient to increase with increasing substrate concentration (and hence the growth rate). Clement et al. (1996) used first-order detachment and attachment models to analyze Jenning's (1994) experimental data. The detachment coefficient values estimated for the actively-growing, denitrifying population was observed to be higher than the non-growing bacterial detachment rates reported in the literature. Thus, growth not only results in increased numbers of cells, but may also result in dispersal by facilitating cell detachment.

2.3. Modeling Biological Reactions in Porous Media

Assessment of subsurface biological activity and contaminant biodegradation requires knowledge of rates of utilization of both nutrient and electron acceptors by the microorganisms, the corresponding rates of growth of the microorganisms, and their levels of activity. During subsurface bioremediation, new cells are produced by the actively growing ambient microbial cells that metabolize supplied nutrients and contaminants. Growth of microorganisms in natural subsurface environments will depend on changes in environmental variables such as pH, temperature, presence of inhibitory toxic materials, presence of competing populations, and availability of nutrients and substrates required for cell growth.

These processes are usually quantified through the use of descriptive mathematical models that either incorporate the structure of the metabolism process, or represent the degradation through unstructured process models. Advanced structured models may be used to

describe the effects of variables such as pH, temperature, etc., on cell-level metabolic processes (Williams, 1967). However, in environmental applications, the difficulty or impossibility of measuring each of the many parameters associated with structured models has often led to the use of simpler semi-empirical, unstructured models (cf. Wood et al., 1994). If the metabolic reaction is jointly limited by the availability of a required substrate and the electron-acceptor, the reaction rate can be modeled by a dual-Monod form of kinetic model. Molz et al. (1986), Widdowson et al. (1988), Kindred and Celia (1989), Taylor and Jaffe (1990b), Kinzelbach et al. (1991), Zysset et al. (1994), Wood et al. (1994), Ginn et al. (1995), Clement et al. (1996) all describe several forms of Monod-based kinetic equations used for modeling different types of microbial metabolisms. These studies account for biomass growth through a simple linear conversion of mass of nutrient degraded to biomass increase. On the contrary, some field studies have assumed subsurface microbial metabolic reactions as instantaneous reactions that are independent of microbial concentrations (Rifai et al., 1987; Chiang et al., 1989; Wiedemeier et al., 1995). These studies assumed oxygen (an electron acceptor) to react instantaneously with hydrocarbon plumes, leading to complete mineralization of a stoichiometric equivalent of hydrocarbon (electron donor). Subsurface aerobic bacteria were assumed to mediate the instantaneous reaction; however, their presence was not explicitly considered. Rifai and Bedient (1990) compared an instantaneous reaction model to a double-Monod kinetic model and concluded that the instantaneous model was adequate when reaction rates are large. Even though the study assumed the existence of constant amount and uniform distribution of bacterial cells throughout the subsurface, the kinetic model ignored cell growth, decay, and transport.

Several modeling studies have ignored the explicit presence of bacteria in both aqueous and attached phases and their dual role in contaminant removal (Molz et al., 1986; MacQuarrie et

al., 1990; Chen et al., 1992). A few studies have considered the presence of cells at various phases, but they have also assumed microbial reaction kinetics to be independent of the phase in which cells reside (Taylor et al., 1990c; Zysset et al., 1994; Clement et al., 1996; Murphy et al., submitted). This may not be an adequate assumption because, as noted above, cells attached to the solid phase may behave differently from the cells suspended in the aqueous phase. Van Loosdrecht et al. (1990) reviewed the influence of solid surfaces on microbial activity and concluded that the presence of solid surfaces may or may not affect microbial substrate utilization rates and growth yields. The effect would depend on the nature of the organism, type and concentration of substrate, and nature of solid surface. In addition to microbial growth, solute sorption effects could also influence microbial reaction at various phases (Brusseau and Rao, 1989). Degradation rates in natural media may also reflect different levels of microbial metabolic activity, which depend on the history of nutrient availability to the microorganism and the history of the growth of the microorganism (e.g., Wood et al., 1994). A method for accounting for the resulting lag in microbial degradation capability under a change from nutrient-limiting to nutrient-rich conditions is described in Wood et al. (1994, 1995). In Wood et al. (1995) a model incorporating metabolic lag, in addition to Monod-type degradation kinetics, is applied to the data of Chen et al. (1992). Further modeling studies supported by experimental evidence are needed before general conclusions can be made about phase-dependent microbial reactions in porous media.

2.4. Heterogeneity, Transport, and Scaling Issues

Because the processes governing the transport of contaminants and bacteria in the saturated subsurface often are subject to significant natural heterogeneity, any attempt at characterizing the processes at the field scale must, at some level, account for the effects of the

heterogeneities on the processes of contaminant and microbial convection/dispersion, contaminant degradation, microbial growth, and microbial attachment/detachment. The most direct deterministic approach of full characterization of physical and chemical aquifer properties that vary with space is impossible because of the inaccessibility of the subsurface. The result is that simulation model components representing coupled reactive contaminant and microbial transport that are developed and validated under laboratory conditions (with controlled single-scale heterogeneities at most) may not reflect field processes accurately. In fact, such models may not even serve for prioritizing governing processes in the field.

Spatial variability (heterogeneity) in aquifer physical or chemical properties naturally occurs on multiple scales as a result of geologic processes involved (cf. Cushman, 1990). Heterogeneities in physical/chemical properties occur on scales at and below the *observation scale* (e.g., the field scale for OEM needs). Generally speaking, the heterogeneities that occur on the observation scale (such as imperfectly layered hydrofacies structures that may extend 10-100 meters horizontally) must be characterized in the field, e.g., via borehole sampling or hydraulic or geophysical tests. Effects of heterogeneities at lower scales, which are unresolvable because of their inaccessibility or small scale or both, must be imcorporated in model components through upscaling approaches. Such approaches usually involve mathematical/statistical averaging of mass balance equations that represent heterogeneity through parameters that are space random functions with known correlation properties. Models averaged in this way allow use of laboratory-validated processes in determination of field-scale measures, such as plume dimensions. However, they do not typically allow prediction of small scale measures (such as contaminant and/or bacterial arrival at an observation well), nor can such approaches handle nonlinear and/or strongly coupled reactions, which severely complicate the averaging. One

24

alternative that can handle these complications is the streamtube-ensemble approach (e.g., Ginn et al., 1995), which represents the transport as through an ensemble of one-dimensional streamtubes, thus separating the effects of physical heterogeneity on flow from the potentially coupled and nonlinear reactions. For certain processes the upscaled model may simply be the same as the small-scale model with averaged or effective parameter values. Alternatively, an upscaled process such as dispersion, which is conventionally represented through the convection-dispersion equation (CDE) with constant parameters, in general requires a new form altogether (e.g., nonlocal dispersion; Cushman and Ginn, 1993; Cushman, 1996). When the transported solute is degraded by an attached or aqueous phase biomass, the present of physical heterogeneities can render the CDE approach inaccurate (Ginn et al., 1995).

Similar difficulties afflict the accuracy of microbial transport models in the presence of heterogeneities. Although the "two-site" models that are almost universally used to describe microbial attachment/detachment appear to be relatively useful for transport in column experiments with homogeneous media, laboratory-determined reaction rate parameters may not be indicative of field conditions (Harvey et al., 1987, 1989, 1993). Whereas column studies often involve injection of prepared bacteria into pristine media; conditions in the contaminated field typically involve active consortia of microbes in the aqueous and/or attached phases, possibly as an actively growing biofilm. Moreover, mechanisms of bacterial transport at the field scale differ from those characterized in batch or column studies as a result of heterogeneity and the dependence of hydraulic and chemical properties on scale. Examples include heterogeneity and the dependence of hydraulic and chemical properties on scale. Examples include heterogeneity in grain size (affects passive attachment and size exclusion), heterogeneity in grain surface chemistry (affects active and passive attachment); and heterogeneity in hydraulic

conductivity (affects convection and macrodispersion). Complexities from any one of these factors can significantly complicate transport: for instance, Harvey et al. (1993) report on an *in situ* multitracer experiment in which the relative order of breakthroughs of bacteria, microspheres, and salt differed for three sample locations within one vertical meter of a single sampling well. In that study, significantly different retardation factors were required to explain the effects of depth within the well. The ramifications of chemical and physical heterogeneities on active microbial attachment/detachment and convective transport under growth conditions are generally unknown. Under this condition, and in recognizance of the nonlinear coupling among the attachment, transport, and growth processes, careful upscaling is necessarily an integral and active part of the proposed research.

Upscaling Approaches. Upscaling is the accounting of the influence of heterogeneities on intermediate scales from the laboratory to the field, and thus links measurements on small scales to observations on large scales. Some progress has been made on upscaling the processes of inactive bacterial transport (i.e., convection-macrodispersion and passive attachment). The effect of groundwater convective velocity fluctuations that arise from heterogeneous hydraulic conductivity is known as macrodispersion and is upscaled through modification of coefficients of the convective-dispersive transport models to incorporate dependencies on time or space (e.g., Dagan, 1989), or most generally on increments of time and space (Cushman and Ginn, 1993; Hu et al., 1995; Cushman, 1996).

Treatment of the effect of heterogeneities on coupled bioreactive contaminant and bacterial transport requires scaling of the interactions between the bacteria and solute nutrients and electron-acceptors, and between the bacteria and the solid phase. Linear interactions that are kinetically-controlled and nonlinear equilibrium interactions recently have been incorporated

into stochastic macrodispersive models. Studies typically involve perturbation approaches to scaling of uncoupled reaction and transport processes in porous media exhibiting simple patterns of physical and/or chemical heterogenities. In the perturbation approach, the parameters appearing in the equations that govern the fate and transport of the solute and microbial component are expressed in terms of the sum of a deterministic or average part and a stochastic or random part, and various statistical assumptions are applied to the random part to develop useful models from the "perturbed" equations. Some recent applications include i) the extension of the low-order perturbation method (Dagan, 1989; Kitanidis, 1988) in Chrysikopoulos et al. (1992), Bellin et al. (1993), Quinodoz and Valocchi (1993), Selroos and Cvetkovic (1994), and Cvetkovic and Dagan (1994); ii) the averaging of from one to many simulations of the reactive transport system (Sudicky et al., 1990; Bosma et al., 1993), and iii) the averaging of higher-order perturbation forms of the equations of reactive transport (Hu et al., 1995). Under these approaches, the chemical and physical heterogeneities are represented as random fields (specifically, the constitutive model parameters have been represented as random fields with specific spatial correlation structures), and the effect of physical heterogeneities is represented through an effective mixing parameter termed the "macrodispersivity" tensor, for use in equivalent field-scale convection-dispersion-reaction (CDR) models. Many of these studies have indicated that the macrodispersivity tensor depends on the presumed statistics of the reaction properties (e.g., Quinodoz and Valocchi, 1993; Cvetkovic and Dagan, 1994; Hu et al., 1995). In a numerical study of aerobic degradation in physically heterogeneous media, Sudicky et al. (1990) demonstrate that while the effective dispersion parameter ("macrodispersivity", derived from low-order perturbation approaches) may be useful for describing the behavior of a

conservative solute, it inherently predicts excessive mixing between nutrient and oxygen rich pore waters and thus overestimates aerobic degradation.

In all of these studies, with the exception of the non-local model of Hu et al. (1995), the heterogeneities are idealized in that they occur on a single scale that is small relative to the model scale, and they are most often represented as second-order stationary spatial random fields (e.g., Cressie, 1991) with known probability distribution and finite spatial correlation structure. Thus, these results may be limited in field application if these assumptions are violated, such as when multiple scales of heterogeneity occur, or when heterogeneity patterns are better represented by more complex probability distribution functions (pdfs) and/or correlation structures (e.g., Scheibe and Cole, 1994). The low-order perturbation approach requires that nonlinearities in the reactions be of minimal importance, and that the transformation of different components be uncoupled. However, nutrient-limited degradation is strongly nonlinear as reflected in the relatively simple dual-Monod kinetics model, and contaminant concentrations are fully coupled to both aqueous and attached phase microorganism concentrations through microbial growth. Couplings associated with transience in the reactive capacity of the solid or microbial phases (e.g., due to sorption site limits or to microbial growth, respectively) have been untreated with the exception of the streamtube-ensemble approach of Ginn et al. (1995), which allows the fully nonlinear and coupled problem to be specific in terms of streamtube (one-dimensional) reactive transport. This can, in turn, be averaged to predict contaminant arrivals at a well or control plane.

II. Goals (Purdue Component)

1. Develop matched-index methods for obtaining 3-D Lagrangian trajectories of microbes in porous media and microflow cells.

2. Use advanced numerical methods to optimally design a microflow cell and model microbial transport in such a system. Apply sticky Brownian motion with motility and chemotaxis to study microbes in the flow cell.

3. Develop methods, based on stochastic perturbation approaches, for upscaling to natural geologic formations and examine the role played by uncertainty in B.C.s.

4. Evaluate the role of nonlocality in the transport of chemicals and microbes.

III. Accomplishments

1. A Method for Reconstructing Microbial Trajectories in Microflow Cells

1.1. Introduction

Microflow cells have played a large role in phase I of this project. Specifically movies of the evolution of microbes in flow cells have been obtained which show the diffusive-convective transport of the microflora as well as the microbes sticking to the pore walls. To analyze this data for modeling purposes it is expedient to obtain the particle trajectories in 3-D. This is not a trivial problem, especially if the microflow cell contains a porous medium.

We have pioneered the development and use of three-dimensional particle tracking velocimetry for this purpose (Moroni and Cushman, 2000a,b,c) and we have used these experimental tools to obtain relevant data on several test problems. Specifically, these test problems involve matched-index porous formations and both classical stochastic models and more modern statistical mechanical approaches. We describe these in the remainder of this section.

1.2. 3-DPTV Method

A porous medium homogeneous at the bench scale (Fig. 1) has been constructed by filling a parallelepiped tank ($30\times30\times50$ cm^3) with 1.9 cm Pyrex spheres. The spheres are packed randomly but distribute homogeneously on the bench scale. The porosity is 42 %. Glycerol is used as fluid phase because at the appropriate temperature it has the same refractive index as the spheres. Thus the Pyrex solid matrix and glycerol combined are transparent to the appropriate wavelength light. A pump is used to fill the test section and later to extract the fluid phase.

The choice of tracers depends on the information one wants to gather. Because we are studying dispersion of a passive tracer carried by the mean flow, the dimension of the tracer has

to be small compared to the grain size. The ratio between its specific weight and that of the liquid has to be such that buoyancy effects are minimal. Furthermore, since the flow field is reconstructed using an image analysis technique, the tracer has to be highly reflective. Appropriately sized air bubbles satisfy our requirements. A bubble diffuser fed with a compressor has been used to inject the tracer particles.

The air does not wet the solid, the bubbles are small (0. 1 mm) compared to the grain size (1.9 cm), and because of the high viscosity of glycerol, the small bubbles remain trapped inside the fluid phase and flow passively. The noise caused by minimal deposition of the bubbles on the sphere surfaces has been avoided by filtering the acquired images.

The test section is lighted using a high power lamp (1000W). In order to assure a uniform lighting of the medium and to avoid the direct interaction among the light and the cameras, a mirror has been used to create a light beam from the top of the test section.

The acquisition and storage system consists of two CCD high-resolution cameras (1024×1024-pixels), two-camera unit controls and a workstation to manage the acquisition process, image digitalization and storage. Each CCD camera has been positioned on an optical bench. The benches are arranged on a rigid cube so the optical axes are orthogonal. A He-Ne laser has been used to guarantee the benches are parallel to the two faces of the test section. The distance between the cameras and the test section (2 meters) has been chosen so as to maintain parallel optical rays. Further, this distance minimises distortion errors. The diaphragm opening has been chosen, for this light intensity to obtain a field depth of about 22-cm. Each field (planes x_1x_3 and x_2x_3) has dimension 22×22 cm^2.
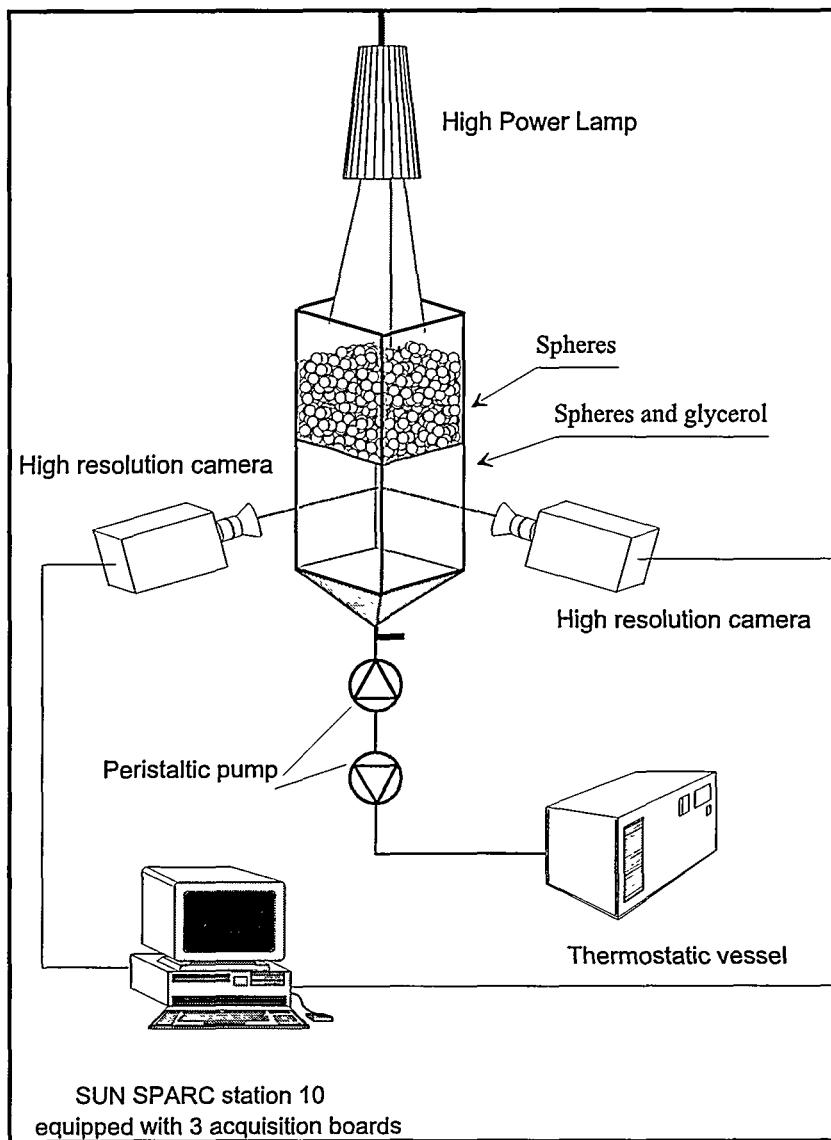
Figure 1. Experimental set-up

At start up, 3D-PTV experiments must be calibrated. By placing a 2D grid on the faces of the parallelepiped test section, acquiring two coupled images (one for the nearest faces and one for the farther ones) and comparing them, it is possible to determine the precision of the device. This procedure allows us to determine the tolerances that can be used during the 3D-trajectory reconstruction.

The grids, acquired respectively from the nearest and farthest faces, can be overlapped with an error = 0.5 %. Comparison between images acquired from the same direction in the

32

nearest and farthest faces gives us an error of at most 10% in the deviation of the optical rays from parallel. Four cm-wide dark screen is placed around the tank cross-section and this coupled with the diaphragm opening and light intensity gives a field of view only in the midsection of the chamber. This reduces our error to below 10%. Furthermore, an algorithm for correcting the errors caused by an incorrect positioning of the tracer particles has been developed. For more details see Moroni and Cushman (1999a).

Figure 2 displays the steps used to obtain reliable images.

Thresholding of the image during the acquisition phase is used to separate the foreground from the background. A binary image is obtained. In this way each pixel has a value equal to 0 if it belongs to the background or non zero if belongs to a tracer particle. An average of 70 images is acquired for each run of the experiment. The superposition of the images can be carried out without loss of information. Each image is digitised in a 1024×1024-element, 256 gray level matrix. One megabyte of memory and 1.5 sec are necessary for storage. To improve the acquisition rate and reduce the amount of memory required for each experiment, the superposition of the single images acquired has been carried out. An increasing threshold has been applied to the images acquired in order to maintain information about the acquisition time.
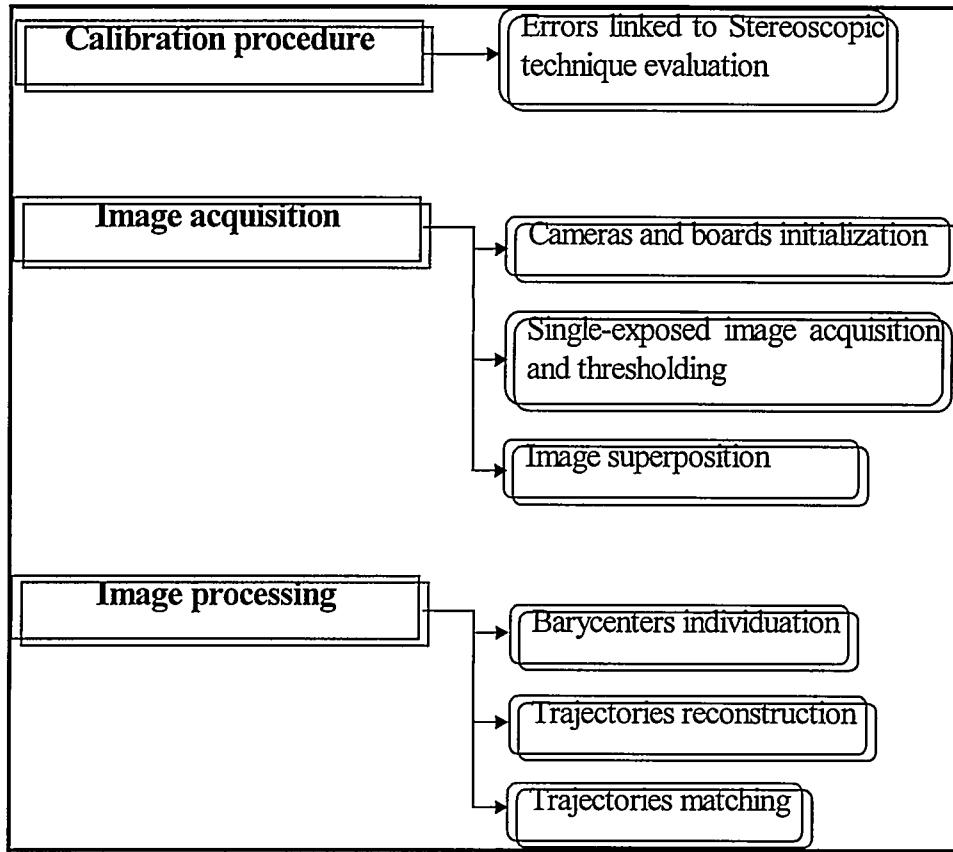
Figure 2. 3D-PTV steps

The stored images are then analyzed to determine particle barycenters and their area. A complicated algorithm to determine the barycenter of connected same-grey level pixels (spots) has been developed for barycenters reconstruction (see Moroni and Cushman, 1999a for details).

The trajectory reconstruction algorithm arranges the barycenters with increasing acquisition times and forms the trajectories. Roughly, the reconstruction algorithm works as follows. Successive spots are studied inside a circle of radius "toll" (which takes into account the local acceleration) with center positioned on the end of the extension of the distance between the last two points belonging to the examined trajectory (Fig. 3).
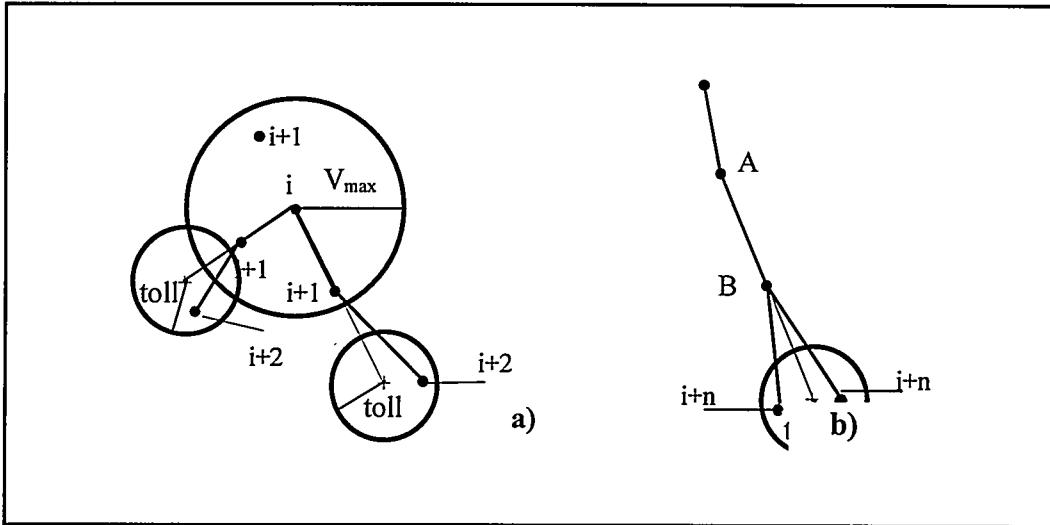
Figure 3. Trajectories reconstruction

Barycenters belonging to a possible trajectory are considered for further exploration, and the algorithm disregards trajectories with more than one displacement in common and with more than 50 % of spots in common. Among the retained trajectories starting from the same spot, the longest one is chosen.

By matching the 2D trajectory projections the 3D displacements can be obtained (Guezennec *et al.*, 1994) (Fig. 4). Each trajectory is labelled at the beginning of the reconstruction procedure. The algorithm compares each trajectory found on the x_3x_2 plane with all those reconstructed on the x_1x_3 plane.
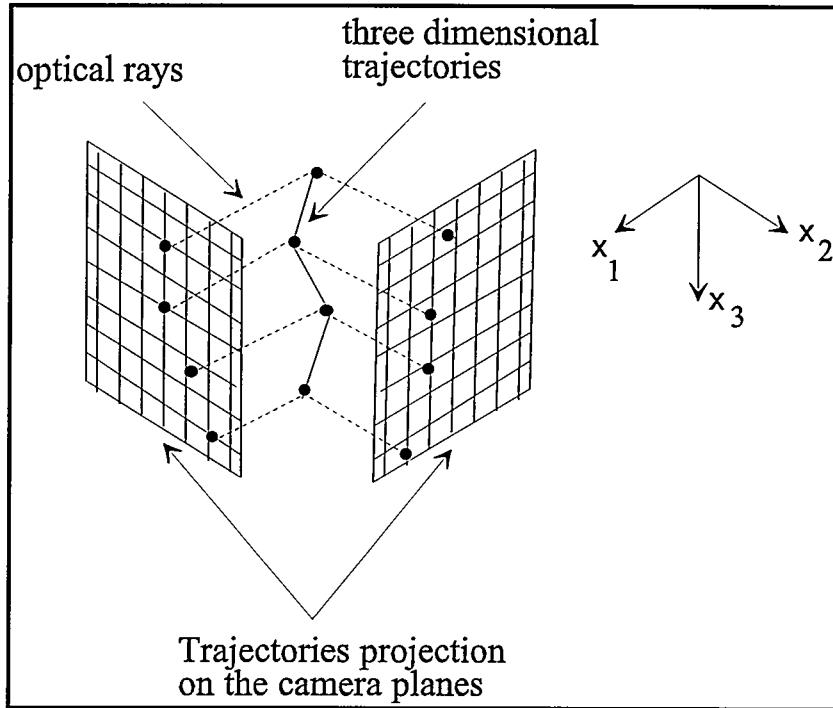
Figure 4. 2-D trajectories matching

The matching procedure is carried out by introducing a tolerance, ε, (determined as a result of the calibration procedure) for the difference between the x_3 coordinates of two spots recorded at the same acquisition time and belonging to the pair of examined trajectories. Matching conditions in the x_3 direction have to be satisfied with at least three points belonging to the examined trajectories. When more than one trajectory satisfies this criterion, the mean longitudinal velocities are computed and the trajectory with the velocity closest to the track is chosen.

1.3. Preliminary Results

Four different mean flow rates were studied (Table 1) and characterized by their respective Reynolds numbers. An average of 40 images were acquired for each flow rate, and averages were obtained using all the images acquired under the same experimental conditions.

A typical representation of the reconstructed trajectories is presented in Fig. 5. Henceforth we only study one mean-velocity. More extensive results can be found in Moroni and Cushman (1999a, b). The trajectories were truncated when statistics were not adequate for the computation of averages associated with the mean-square displacements, normalized velocity covariances, the self part of the intermediate scattering function, the classical dispersion tensor, the generalized dispersion tensor and velocity distributions.

Table 1. Mean velocities and Reynolds numbers

	Vel1	Vel2	Vel3	Vel4
Re	0.049	0.085	0.105	0.129
Mean Velocity (cm/sec)	0.211	0.366	0.450	0.551
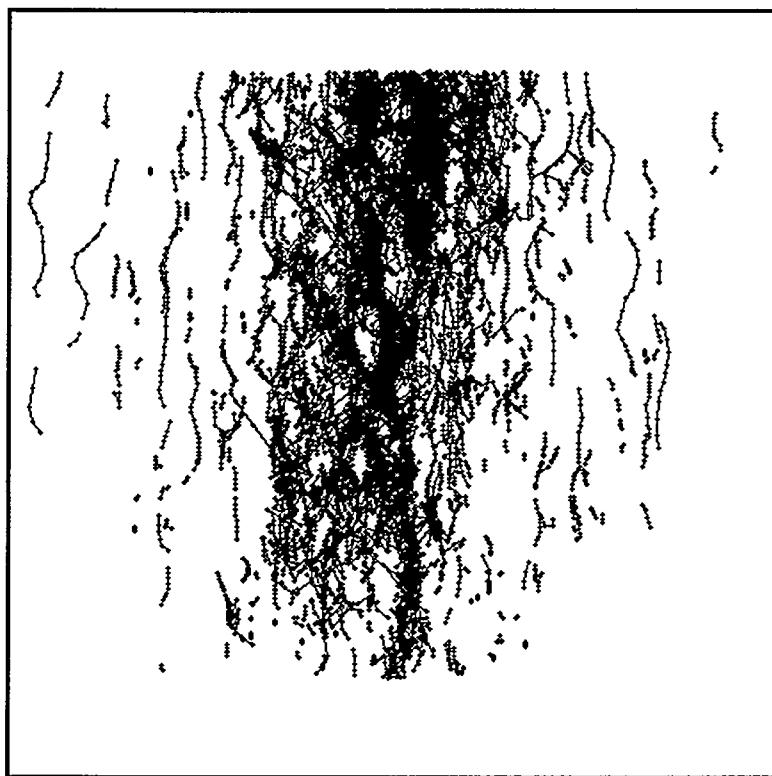
Figure 5. Reconstructed trajectories (Image 7, <v>=(0, 0, 0.211))

The probability density functions (pdf) for the transverse and longitudinal components of the fluctuation velocity have been evaluated and are shown in Fig. 6. The velocity data have been normalized by the square root of the fluctuating-velocity variance for comparison to a normalized gaussian distribution.

There is a good agreement between the pdf for the transverse components (u, v) and the gaussian distribution. This result is quite different from Cenedese and Viotti (1996) and Cenedese et al. (1997) who using analogous analysis found a symmetrical shape that is not gaussian. More details can be found in Moroni and Cushman (1999a).
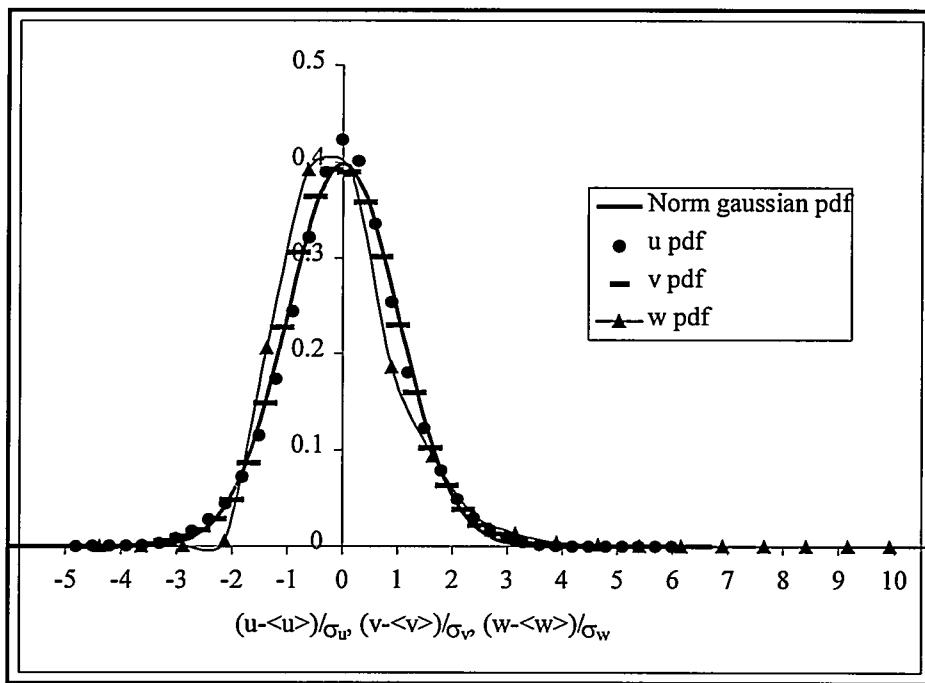
Figure 6. Normalized velocity probability densities

The pdf of the longitudinal component of the velocity fluctuation (w) does not appear gaussian. The velocity distribution is asymmetrical much like that of Kutsovsky *et al.* (1996). The percent of negative velocity in this experiment is very low, as there is little recirculation in this system.

Figure 7 displays the normalized lagrangian velocity covariances:

$$\rho_{ij}(\tau) = \frac{C_{v_{ij}}(\tau)}{\sigma_{v_j} \sigma_{v_j}}$$

(1)

The averages are taken over all trajectories.
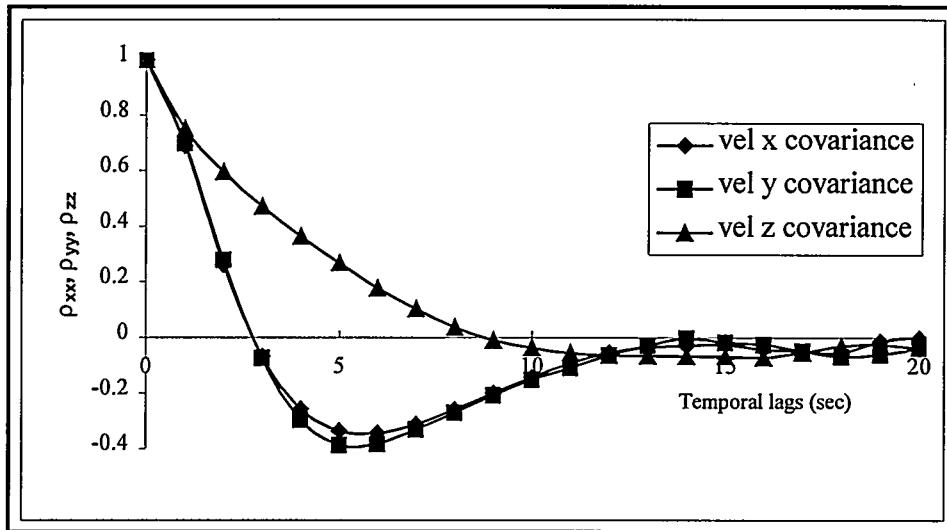
Figure 7. Normalized longitudinal and transversal velocity covariances

The lagrangian integral scales, in the various directions, as given by the integral of ρ_{ii}, are

T_{xx}= 1.41 sec, T_{yy}= 1.44 sec, T_{zz}= 3.25 sec.

The mean-square displacements are presented as log-log plots in Fig. 8. It is known from classical analysis that such plots are linear when the classical Fickian limit is obtained. The longitudinal component appears to reach a Fickian limit, but it is not clear from the data whether the transverse components do so.
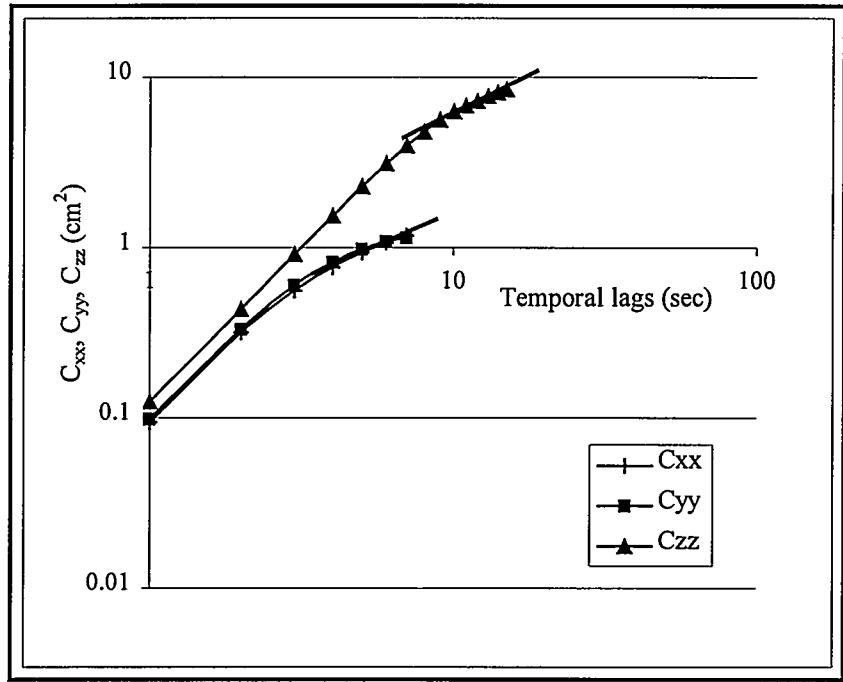
Figure 8. Mean-square displacements

1.4. Summary

Three dimensional particle tracking velocimetry (3-DPTV) methodologies were developed and tested on a match-index porous system. The test medium consisted of Pirex and glycerol with air bubbles used to simulate microbes ($\sim$ 0.1 mm). 3D trajectories were reconstructed and analyzed to obtain lagrangian velocity distributions, mean-square displacements, velocity covariances, time integral scales and the classical dispersion tensor. In subsequent phases of this work the trajectory reconstruction technique can be used with actual microflow cell experiments involving sticky anerobial microbes.

2.   Hydrodynamic Aspects of Pore Scale Microbial Dynamics

2.1   Introduction

Bacterial motility is of importance to a wide spectrum of applied scientific disciplines, including human health, food science, and bioremediation. Understanding the mechanisms of bacterial motility involves knowledge from several scientific disciplines: anatomy, genetics, chemistry, and physics (Berg, 2000). Emphasis to explain bacterial movement has been given to flagellated organisms, like *E. coli*. The behavior of motile cells near a solid surface has been extensively studied in the absence of bulk flow, but relatively little is known about motile cell behavior in advective flow fields (Carmesano and Logan, 1998). The present work addresses the movement of single-cell, non-flagellated organisms subject to an advective flow. It also includes attachment and detachment from walls. The movement of single-cells can be described in terms of run lengths, run times (runs), turn angles (tumbles), and index of directional persistence of a cell. The trajectory of a single-cell resembles that of a Brownian particle, continuously alternating runs and tumbles. The macroscopic behavior can be characterized by a motility coefficient, analogous to a diffusion or dispersion coefficient. The relationship between single-cell description and bulk behavior is of interest.

Biondi et al. (1998) studied swimming bacteria (*E. Coli*) in restricted geometries, measuring cell velocity, tumbling probability and turn angle of single cells in micro channels. They concluded that only when capillaries are smaller than three times the diameter of the bacteria, there exists a visible change in the bacteria's motility with respect to their motility in unrestricted media. The macroscopic motility in unrestricted geometry according to their result is increased by a factor proportional to the size of the system. Sticking to the glass surfaces did not occur in their experiments.

Hydrodynamic drag is believed to reduce the diffusion coefficient of a particle moving in a restricted geometry (enhanced drag in restricted channels). Berg and Turner (1990) have previously hypothesized that as the size of the cell becomes comparable to the size of the pore, there exist an increase in motility coefficient due to the restriction of the movement in the axial direction. They observed random motility coefficients of wild-type *E. coli* increased by a factor in excess of 2 when the micro capillary in which they move was reduced from 50 μm to 10 μm . The later investigators results were conducted observing cell-population dynamics, in contrast to Biondi et al. (1998) who observed individual cells.

Carmesano and Logan (1998) studied the effect of fluid velocity on the transport of motile and nonmotile bacteria. They observed that the collision efficiency, α (defined as the ratio of particles that attach to soil grains to particles that collide with the soil) decreases as the mean velocity decreases. Testing against nonmotile bacteria, they hypothesized that swimming cells were able to avoid sticking to soil grains at low fluid velocities, while at high fluid velocities bacteria could not reduce attachment. They also suggested that previous deposited cells provide a more favorable surface for adhesion than a native soil. Since their results were obtained using sand columns, they merit a further investigation at the pore scale to confirm or correct some of their claims. Main discrepancies with filtration theory were checked for consistency using nonmotile cells, but in the procedure, the attaching mechanisms may be altered. Nonetheless differences were observed and other researchers results (Camper et al., 1993) are consistent in the hypothesis that is, beyond a velocity threshold, single cell motility will not affect cell retention in the media.

Phillips et al. (1994) measured in separate experiments the motility of *E. coli*. They determined the distribution of cell velocities was slightly skewed from normal, and the run

length time distributions were exponential. They were unable to measure turn angles between consecutive runs because cells would not remain in the focal plane long enough. The values of the variables that could not be measured were taken for their analysis from Berg and Brown, (1972). They also found the macroscopic behavior of population motility can be predicted from microscopic observations. In particular the expressions proposed by Othmer et al., 1988, and Rivero et al., 1989 were suitable for the conditions tested.

The need for cost effective ways of dealing with subsurface contaminant plumes either by cleanup or by containment is a well documented (DOE, 1995a) problem with no ready solutions. One promising technique for the remediation of polluted sites is the use of microorganisms which degrade organic toxins if sufficient nutrients, usually in the form of electron acceptors, are provided. An important factor in the engineering of biobarriers/bioremediation is the microbial partitioning that takes place between the aqueous and solid phases. Factors that affect such partitioning are numerous, but include such things as growth and starvation conditions (Dawson et al.1981, van Loosdrecht et al. 1987,1990), limiting of nutrients (Fletcher and Marshall, 1982), potential toxicity in the aqueous phase (Chen et al. 1994) as well as local surface properties of the porous medium. The importance of the biomass in a porous medium cannot be underestimated, since it plays a crucial role in the degradation rates of contaminants (as nutrients necessary for the process may not be available in the solid phase).

Here we present a model for the dynamics of a microorganism undergoing random forces in addition to a convective transport. Since the proper representation of the biological phase is a matter without consensus (as noted in the exchanges of Widdowson, 1991 and Jaffe and Taylor 1992), and since we do not want to restrict ourselves to clogging and permeability changes which are the focus of continuous biofilm models, we present a model which will serve as a basis for an

unstructured biological population. We focus on the individual dynamics of a single microbe, or a system of such particles in a relatively low concentration so that they have little effect on the surrounding environment and each other. One may think of this as the initial stage before a type of colonization of the surface occurs. The random forces can be thought of as a sum of Brownian forces together with random swimming forces generated by a bacteria in a homogeneous liquid. We assume the random forces are normally distributed and independent. The normality assumption is an averaging over different particle trajectories. We comment that the model can be extended to include chemotactic forces if one assumes they are of the same order as either the molecular Brownian forces, in which case one replaces the normality of the random walk assumption with a non-symmetric random walk; or on the same order as the convective forces, in which case one can superimpose the vector fields arising from the chemotaxis and convection to obtain a net vector field for the average movement. In particular the run and tumble behavior of certain types of bacteria (Berg and Brown, 1972) can be taken into account.

In addition to the random forces in the liquid phase our model introduces a stickiness parameter which relates the attachment/detachment process or physico-chemical interactions between microbes and the solid matrix. It is crucial to incorporate time lags due to interaction with the soil matrix, if one hopes to understand the effects a microbial population would have on a contaminant convecting through the matrix.

This model describes bacterial motility using three components. The first solves for the laminar flow field in a specified geometry. The second incorporates single-cell movement by this convective flow subject to drag, inertial, and Brownian forces caused by the fluid flow (drag and inertial) and the bacteria motility (Brownian: modeled as random). And thirdly a probabilistic model for attachment and detachment is proposed.

2.2. Model

Laminar flow in a microflow cell. To isolate and observe bacterial motility under convective fluid transport, a flow cell was designed that can be placed under the microscope and images of individual bacteria taken. Similar methodologies have been developed earlier (e.g., Berg and Turner, 1990; Phillips et al., 1994; Barton and Ford, 1997; Biondi et al., 1998) to observe single-cell movement. Three designs were tested (see Fig. 9) which included fully three dimensional flow features (Fig. 9a,b,c), and two-dimensional features (Fig. 9d). Pore size distribution in natural systems is variable. Fine pores in fine sands range from 2 to 20 µm. The smallest dimension (thickness) considered in the flow cells is 20 µm. It is constant for flow cells a and d, and variable for flow cell b,c. The flow rates used correspond to those typical of groundwater flow velocities; 10^{-4} to 10^{-6} m/s.

Analytical solutions for creeping (laminar) flows are available with certain geometries (e.g., parallel plates, cylindrical tubes, etc.) but in general, once geometrical features differ from these regular geometries one must resort to numerical solutions. The commercially distributed CFD code FLUENT was used to solve for the laminar flow field.

The first geometry analyzed corresponds to a rectilinear box (as depicted in Fig. 9a) connected to inlet and outlet conduits. The inlet and outlet tubes have smaller cross sectional area than the flow cell's body. Figure 10 shows a cross sectional view of the velocity field (10a), total pressure (10b) at z = d/2, with d = 0.2 mm the flow cell thickness, and wall shear stress (10c). The abrupt expansion between the inlet conduit and the flow cell body causes stagnation zones and curvature in the flow streamlines (Fig. 10d).

To avoid large stagnation zones which can trap bacteria and affect breakthrough (or introduce an unknown retardation), the design shown in Fig. 9bc was devised. The thickness of

B. Chamber shown without connecting silicone gel and a clear top-small coverslip.

Silicone Dam

Outlet Tubing

Glass Slide

Glass Slide

Inlet Tubing

6 Small Cover Slips

Large Top Cover Slip

Silicone Dam

Large Bottom Cover Slip
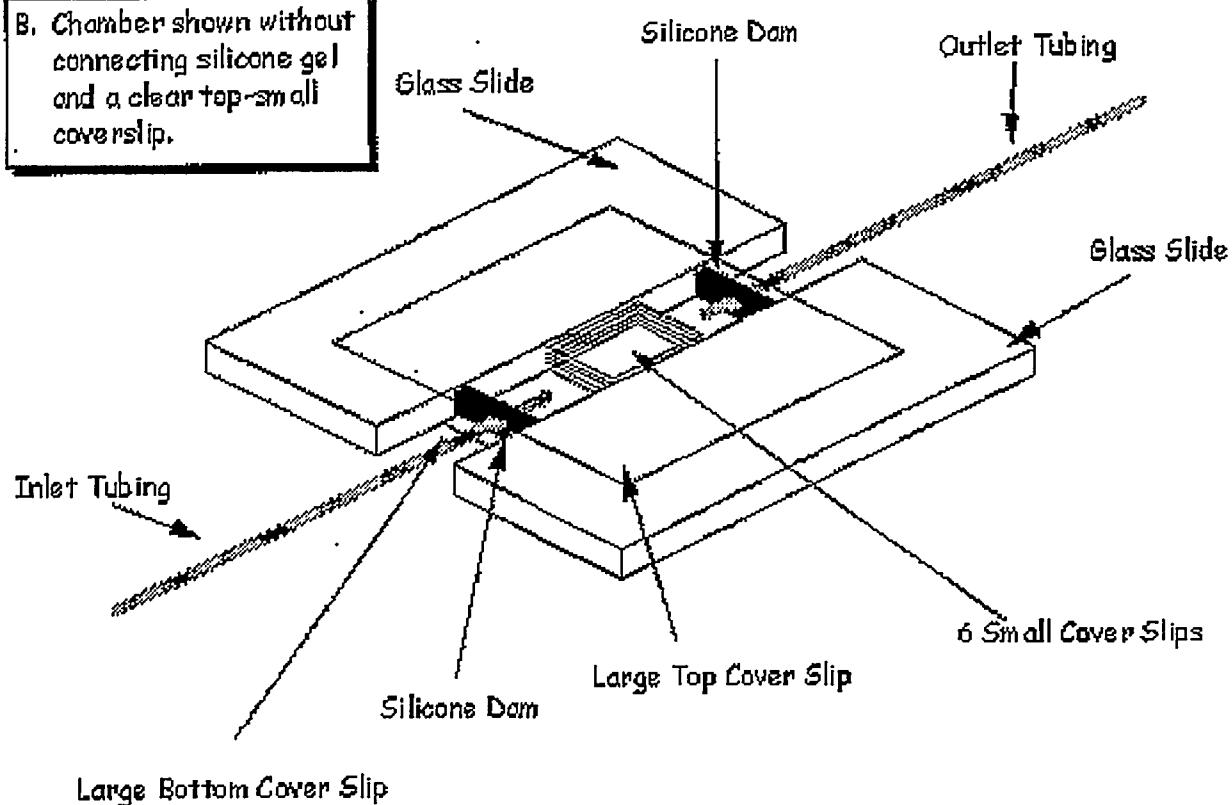
C. Chamber shown with connecting silicone gel and a colored top-small coverslip.

Connecting Silicone
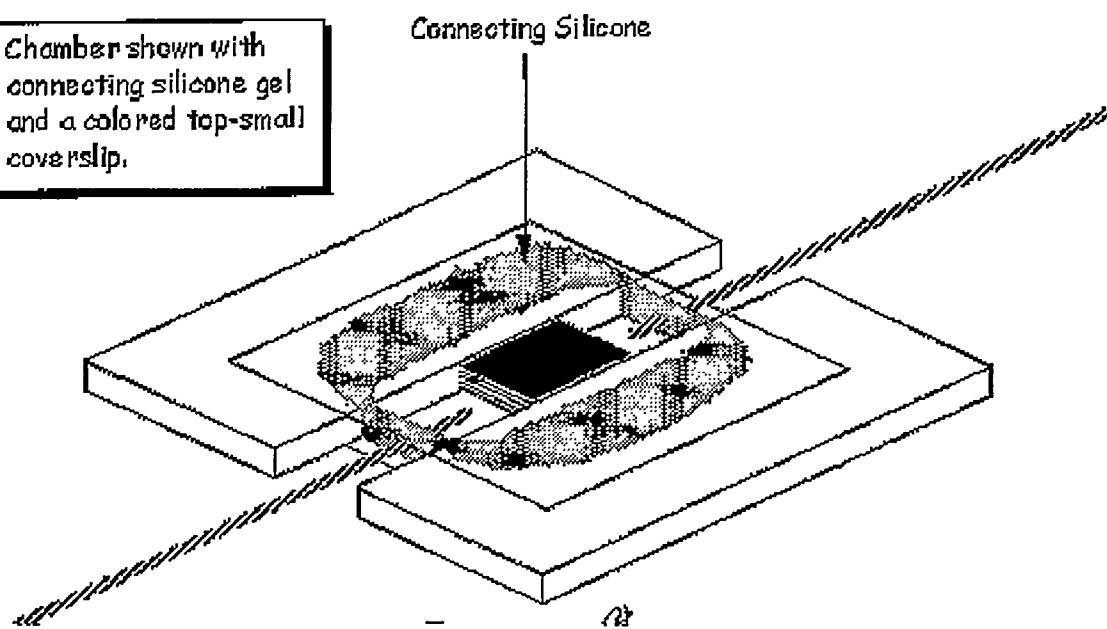
Figure 9a. Parallelepiped box with constant thickness.

46
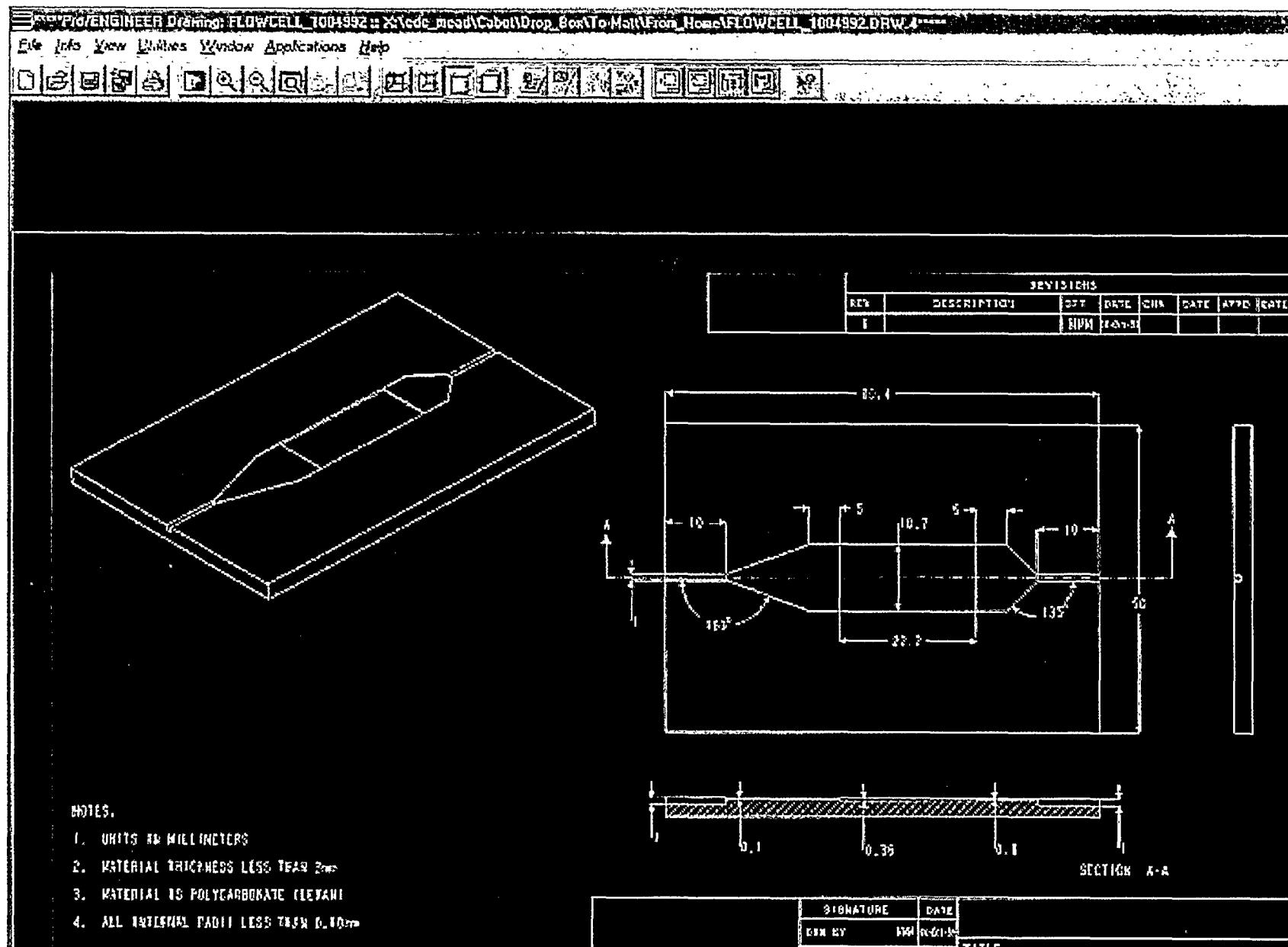
Figure 9b. Funnel-shaped transition between inlet/outlet ducts and flow cell body with variable thickness.

47
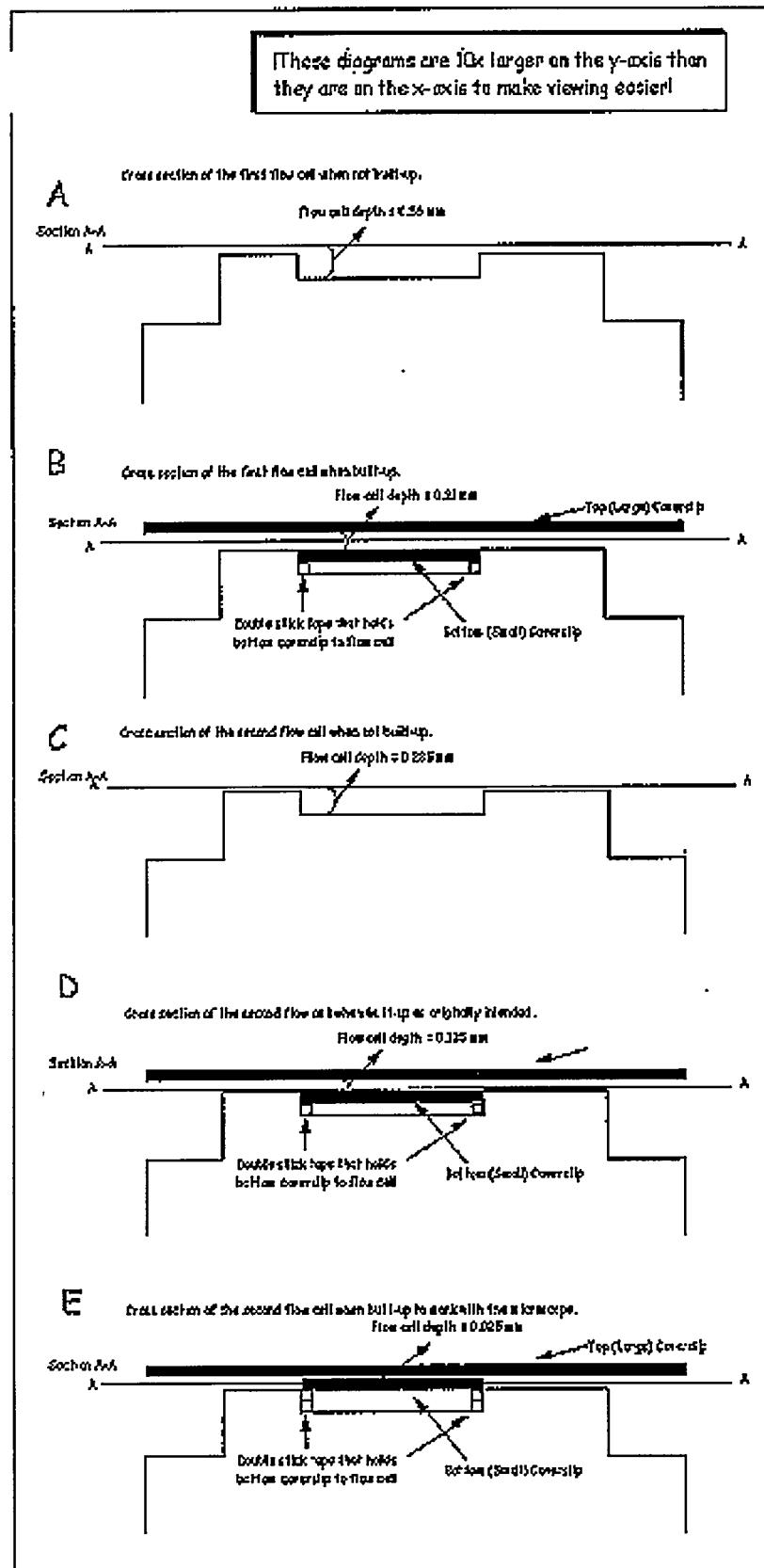
Figure 9c. Parallelepiped box with constant thickness.

Figure 9d.

Contours of Velocity Magnitude (m/s)

Apr 21, 2000
FLUENT 5.2 (3d, segregated, lam)
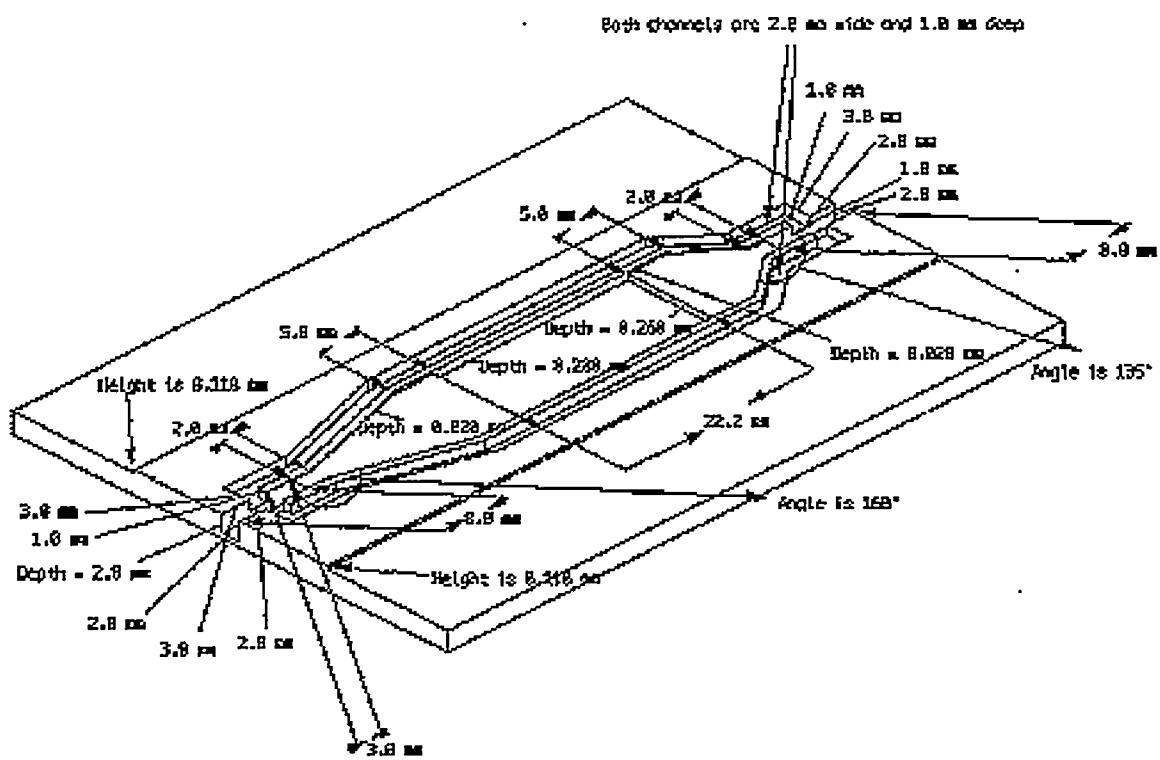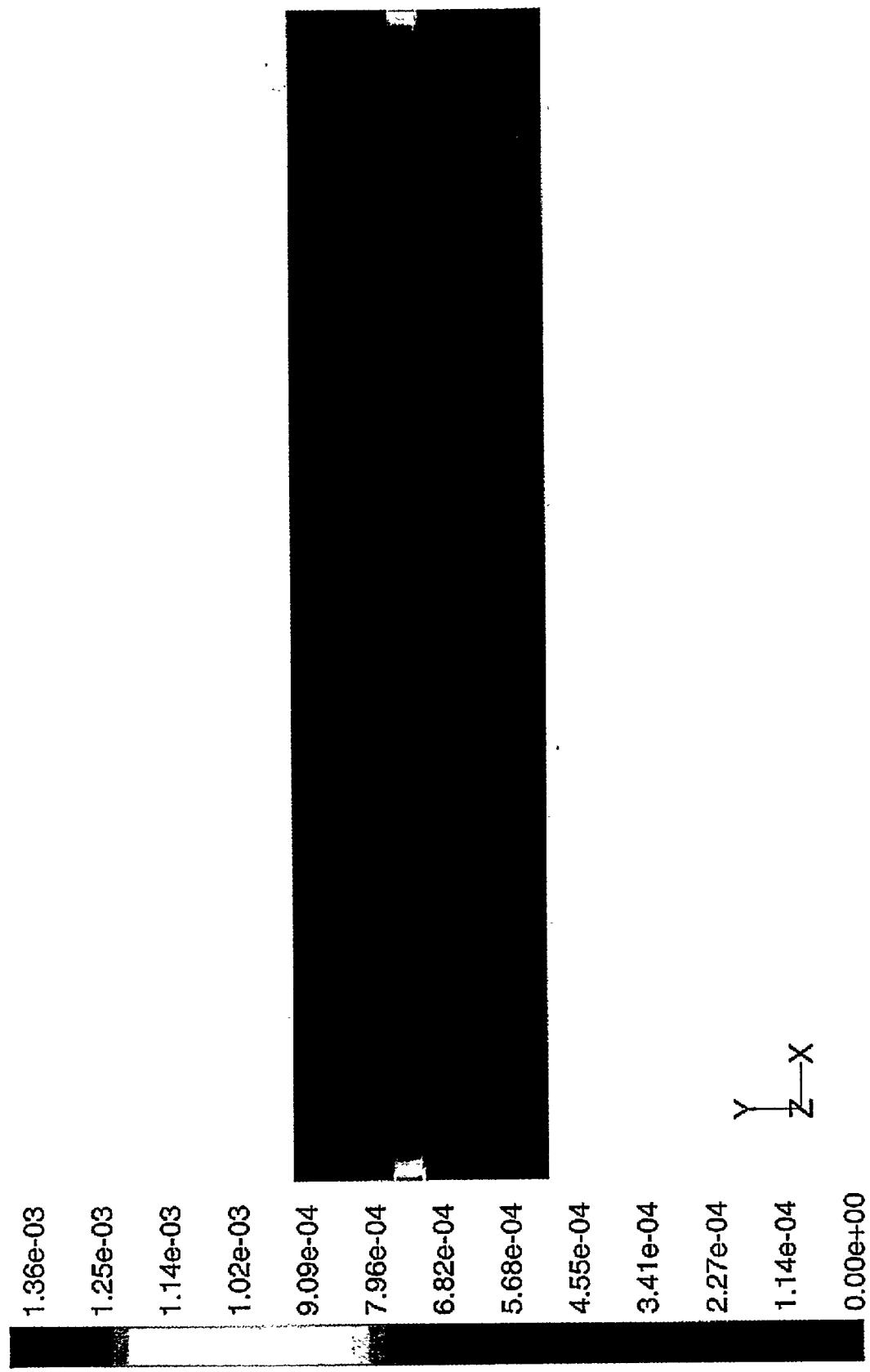
Figure 10a. Total velocity.

7.62e+02
6.85e+02
6.09e+02
5.33e+02
4.57e+02
3.81e+02
3.05e+02
2.28e+02
1.52e+02
7.62e+01
-2.31e-03

Contours of Total Pressure (pascal)

Apr 21, 2000
FLUENT 5.2 (3d, segregated, lam)
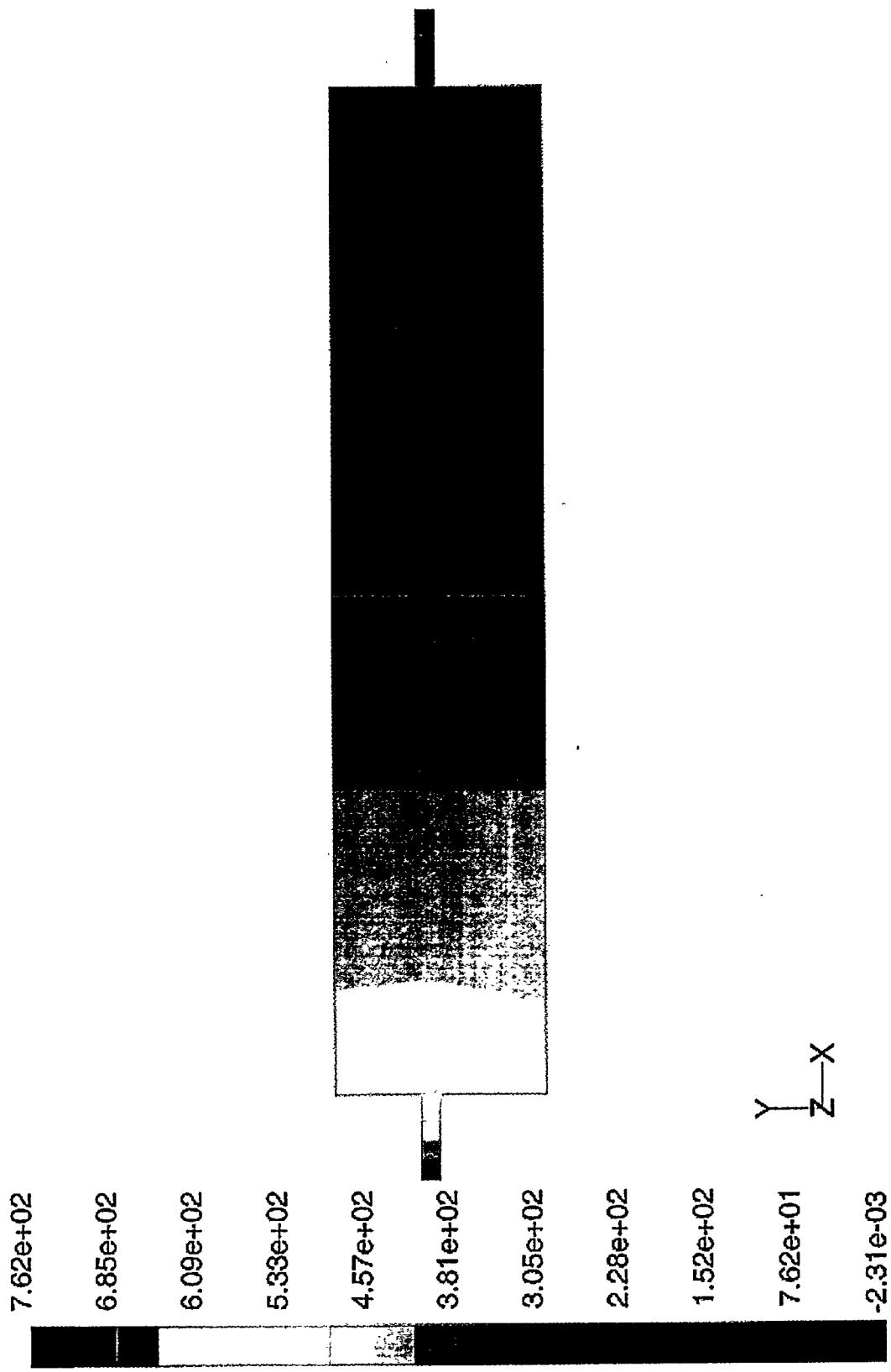
Figure 10b. Total pressure.

51
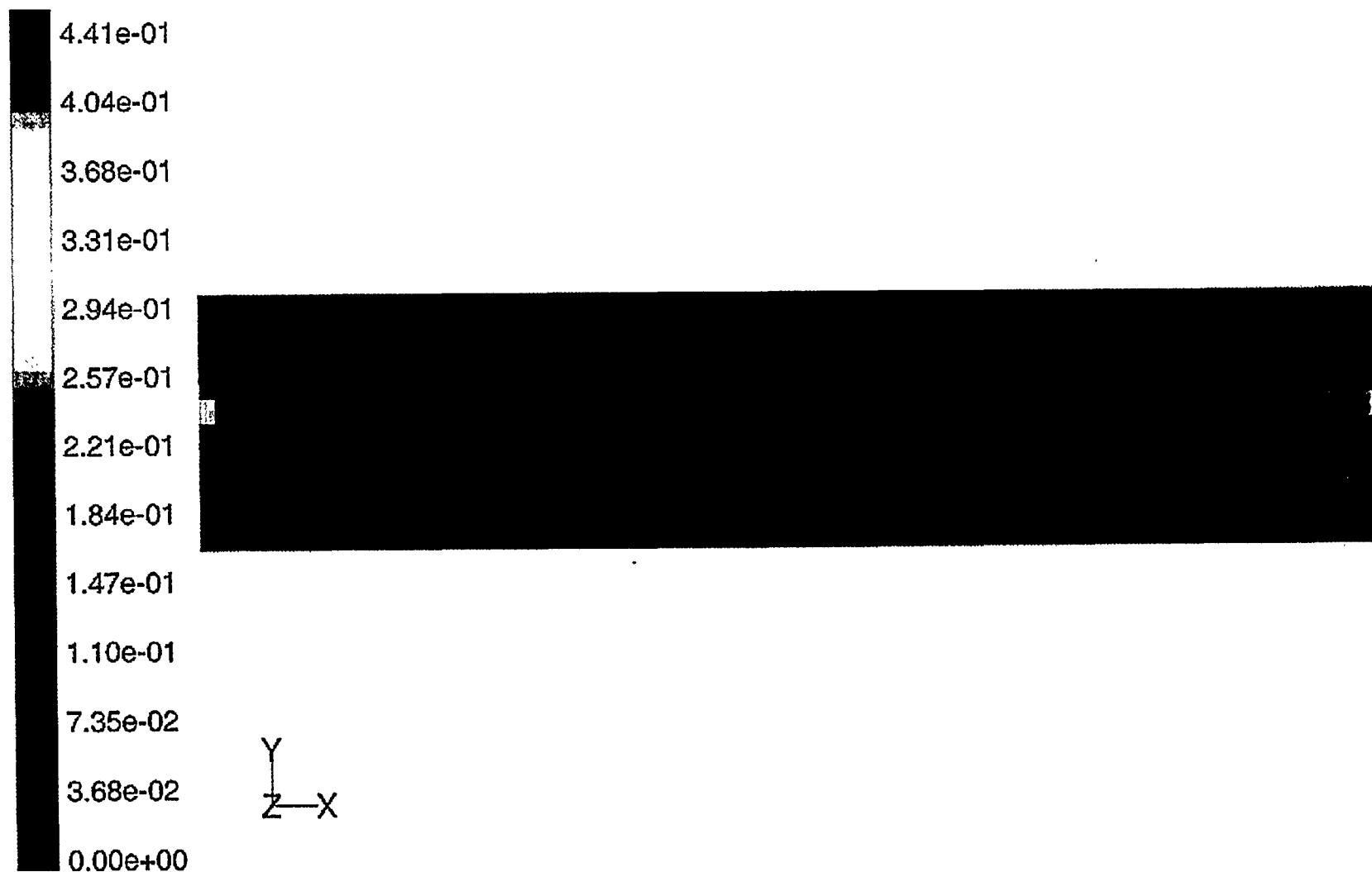
Contours of Wall Shear Stress (pascal)

Apr 21, 2000
FLUENT 5.2 (3d, segregated, lam)

Figure 10c. Wall shear stress.

3.85e+02	
3.53e+02	
3.21e+02	
2.89e+02	
2.57e+02	
2.25e+02	
1.93e+02	
1.61e+02	
1.29e+02	
9.64e+01	
6.43e+01	
3.22e+01	
1.47e-01	

Y
Z—X

Contours of Vorticity Magnitude
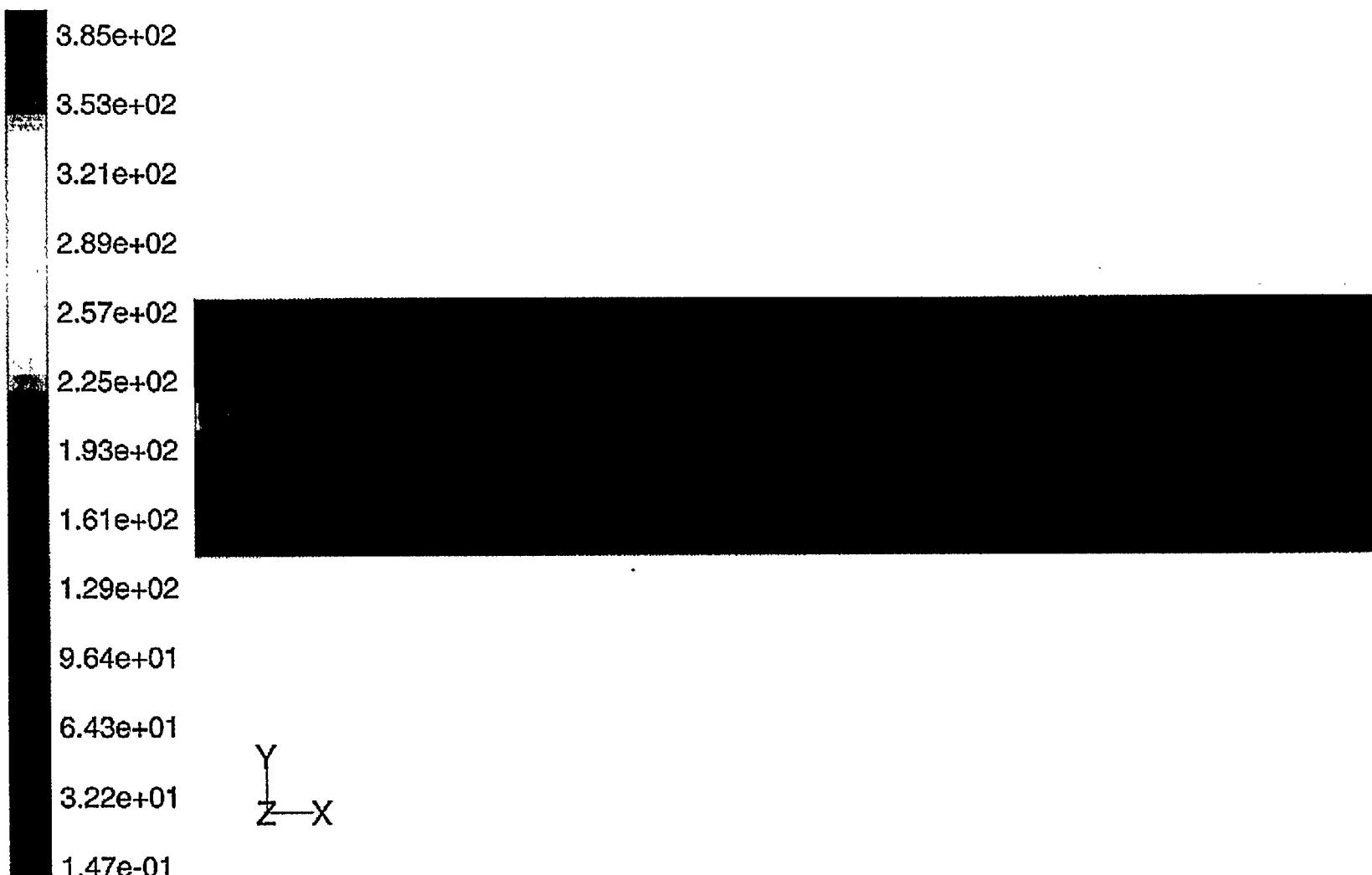
Apr 21, 2000
FLUENT 5.2 (3d, segregated, lam)

Figure 10d. Path lines.

| 1.50e-04 |
| 1.37e-04 |
| 1.25e-04 |
| 1.13e-04 |
| 1.00e-04 |
| 8.75e-05 |
| 7.50e-05 |
| 6.25e-05 |
| 5.00e-05 |
| 3.75e-05 |
| 2.50e-05 |
| 1.25e-05 |
| 0.00e+00 |

Contours of Velocity Magnitude (m/s)
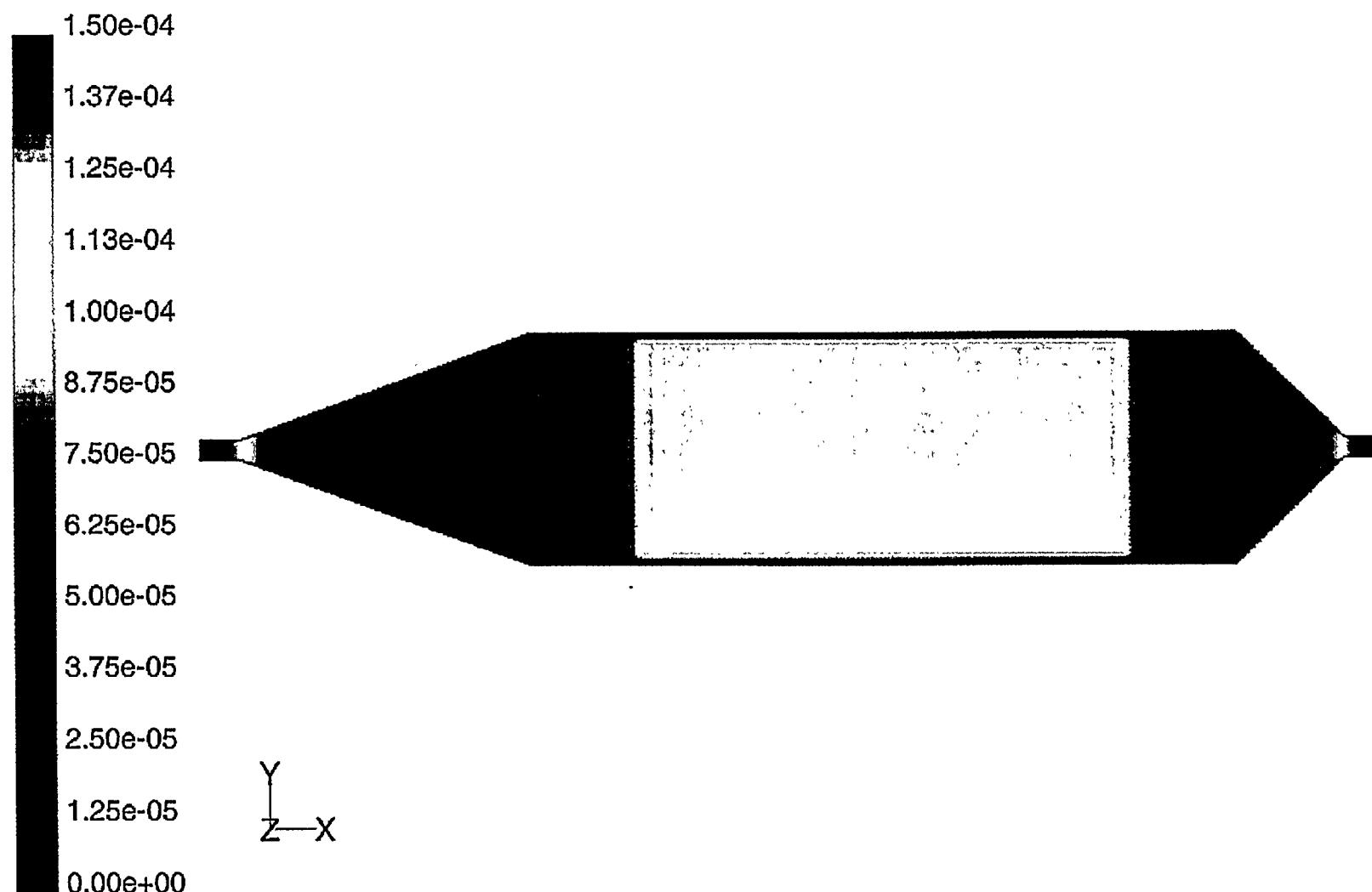
Mar 28, 2000
FLUENT 5.0 (3d, segregated, lam)

Figure 11a. Total velocity.

2.66e+01

2.44e+01

2.21e+01

1.99e+01

1.77e+01

1.55e+01

1.33e+01

1.11e+01

8.86e+00

6.64e+00

4.43e+00

2.21e+00

-1.43e-04

Y
|
Z—X
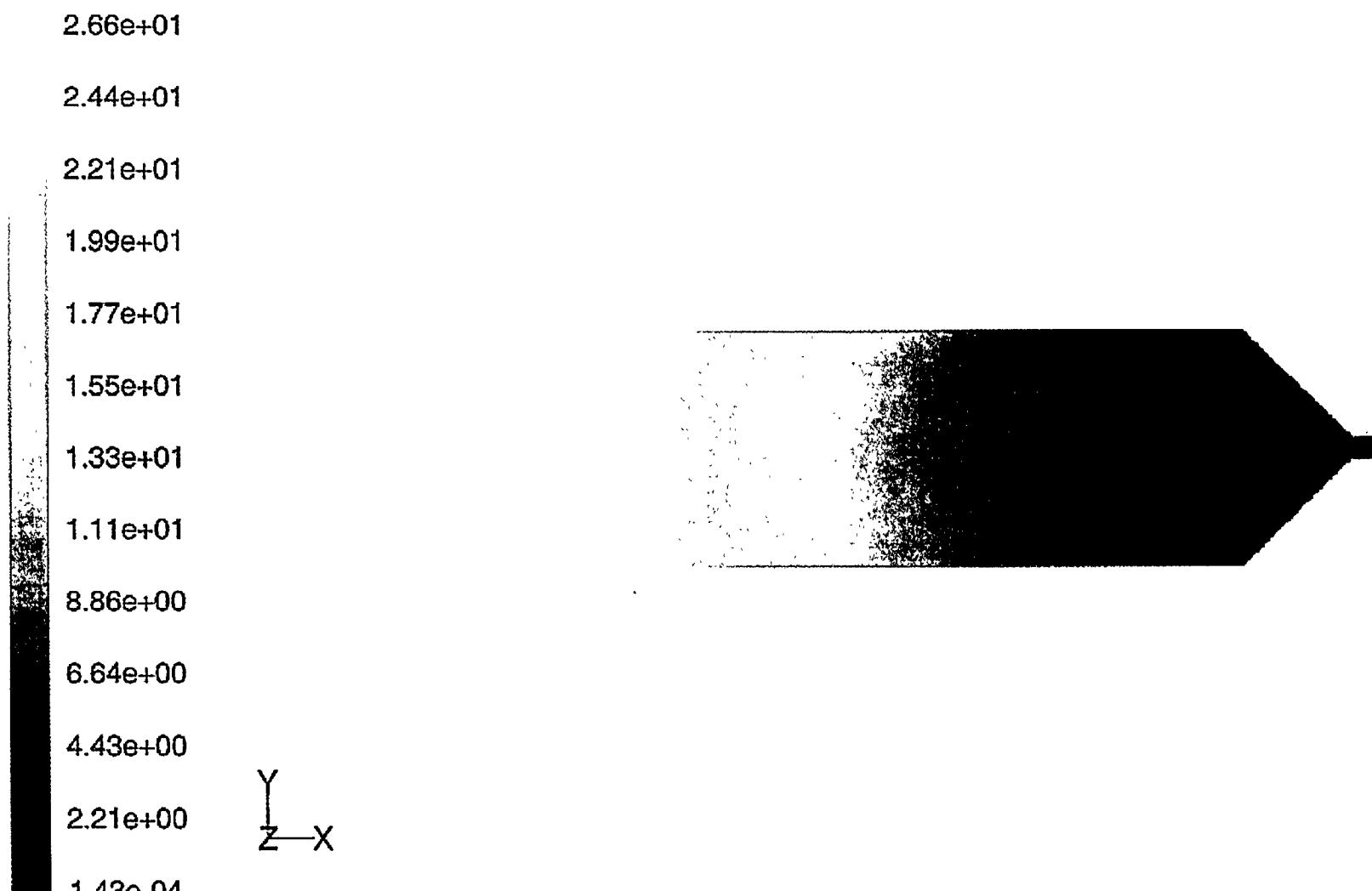
Contours of Total Pressure (pascal)

Mar 28, 2000
FLUENT 5.0 (3d, segregated, lam)

Figure 11b. Total pressure.

Contours of Wall Shear Stress (pascal)

Mar 28, 2000
FLUENT 5.0 (3d, segregated, lam)
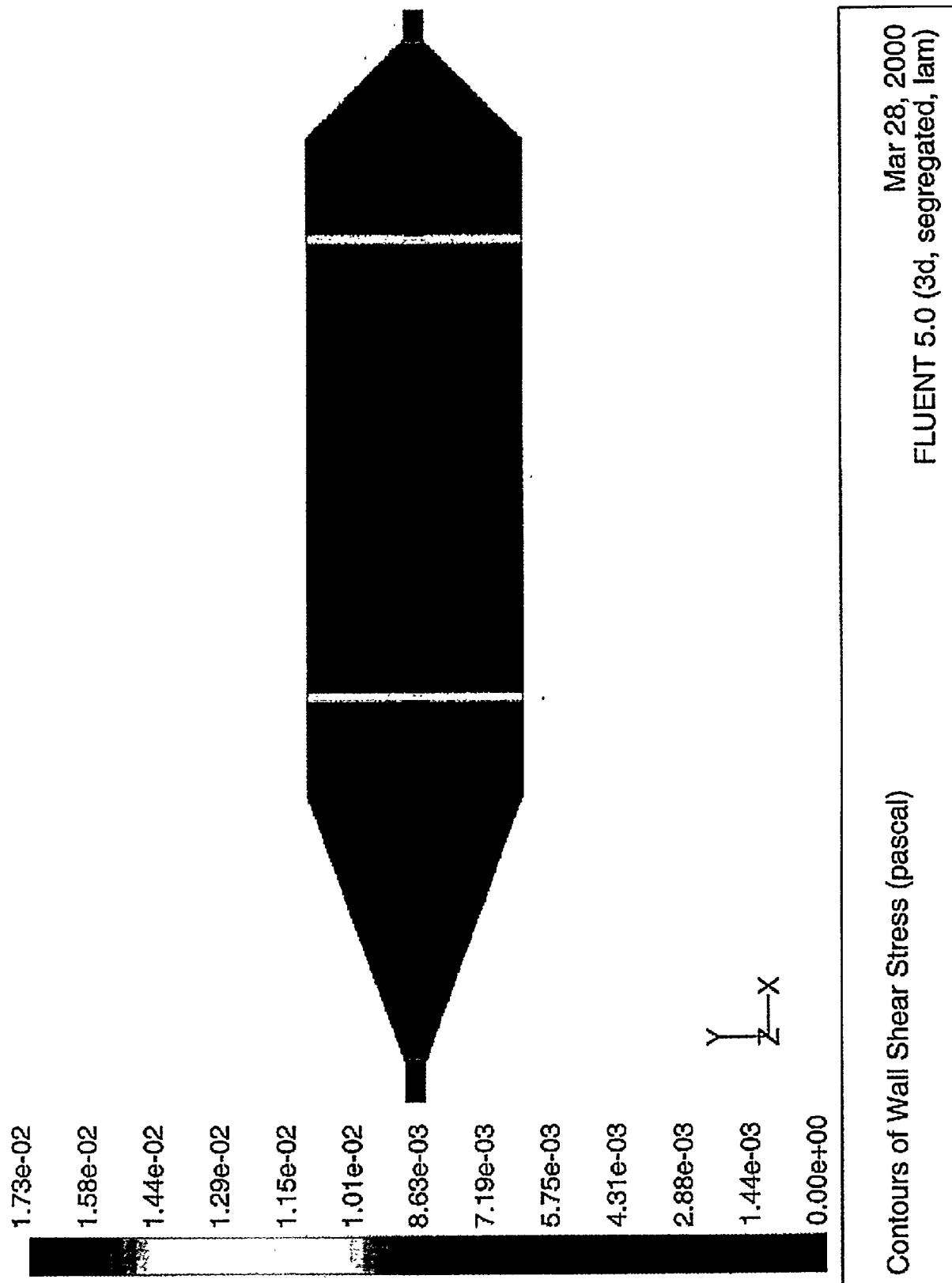
Figure 11c. Wall shear stress.

56
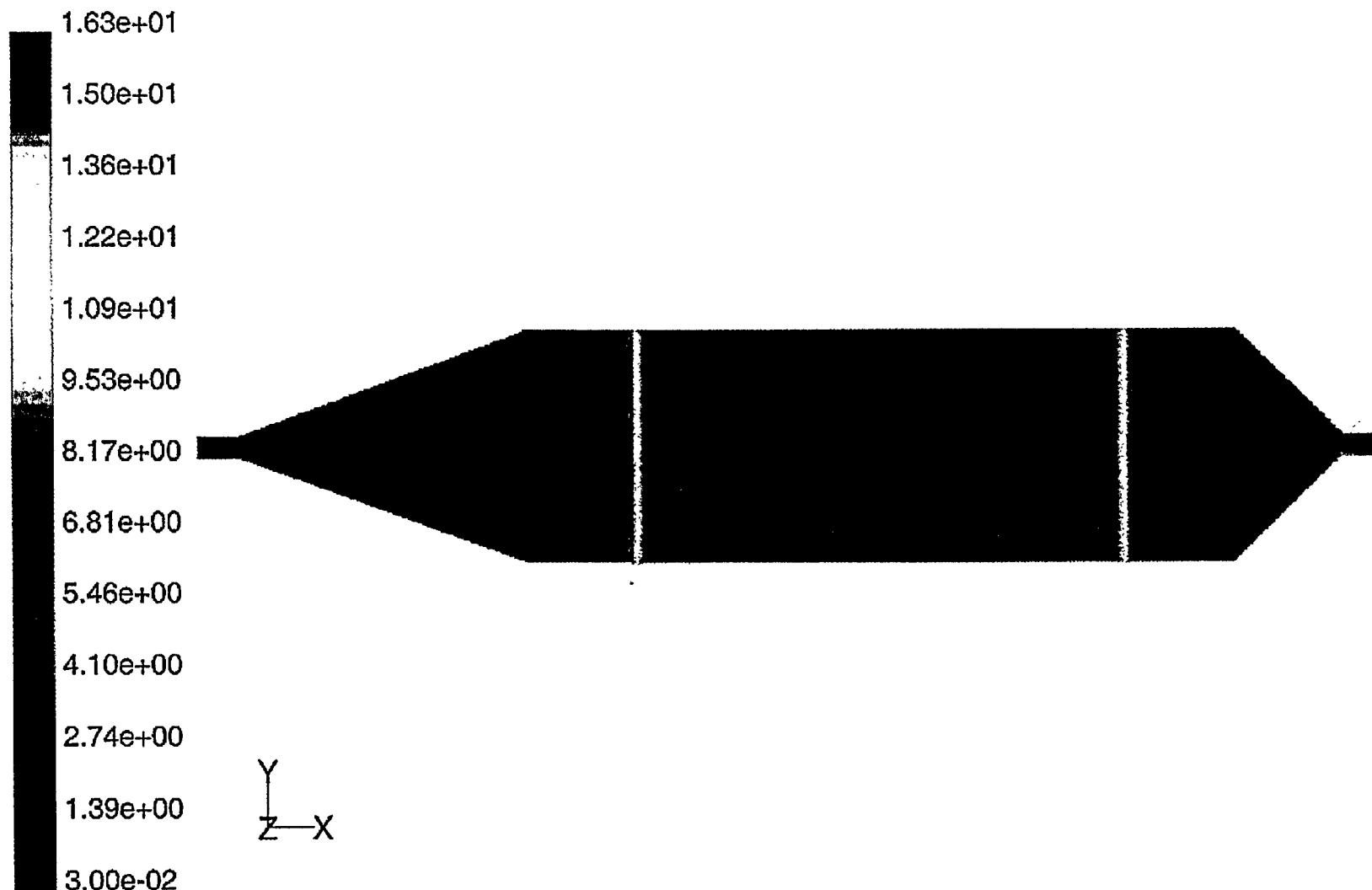
Contours of Vorticity Magnitude

Mar 28, 2000
FLUENT 5.0 (3d, segregated, lam)

Figure 11d.

this cell is variable. In the inlet and outlet funnel-shaped regions the thickness is 130 μm, and in the center region of the flow cell body the thickness of 30 μm. This introduces, in a simplified way, a geometric feature that is present in real pores, i.e., change in the flow cross sectional area. Figure 11 shows the velocity, pressure, and wall shear stress along defined cross sections. The three dimensional character of the flow creates zones where particle collisions with walls are more likely, therefore one prefers to analyze bacterial motility and attachment characteristics in flow cells where these three dimensional features are not present.

Finally, Fig. 12 corresponds to Fig. 9c, where thickness is constant. Wall shear stress is maximum at the flow cell inlet pipe and decrease as the cross sectional area (normal to flow direction) increases. This offers an opportunity to study the effect of wall shear forces on attachment characteristics and bacterial motility.

Bacteria as a discrete phase. Once the flow field is obtained, microbes are released and tracked. A sufficient number of particles are released to obtain representative statistics of the cell transit time through the pore. Particles are released from different points at the entrance, and followed across the domain, allowing them to stick to the flow cell wall when they collide with it. The probabilistic model describing the attachment/detachment will be discussed in the next section. Many bacteria of interest for groundwater bioremediation have sizes between 1 and 10 μm. At this size, Brownian forces may be negligible compared to drag forces for the characteristic groundwater velocities. However, given that the single cell motility occurs randomly, the forces generated by the cells in their swimming are modeled with a fictitious Brownian force.

1.15e-03	
1.06e-03	
9.60e-04	
8.64e-04	
7.68e-04	
6.72e-04	
5.76e-04	
4.80e-04	
3.84e-04	
2.88e-04	
1.92e-04	
9.60e-05	
0.00e+00	

Y
Z—X
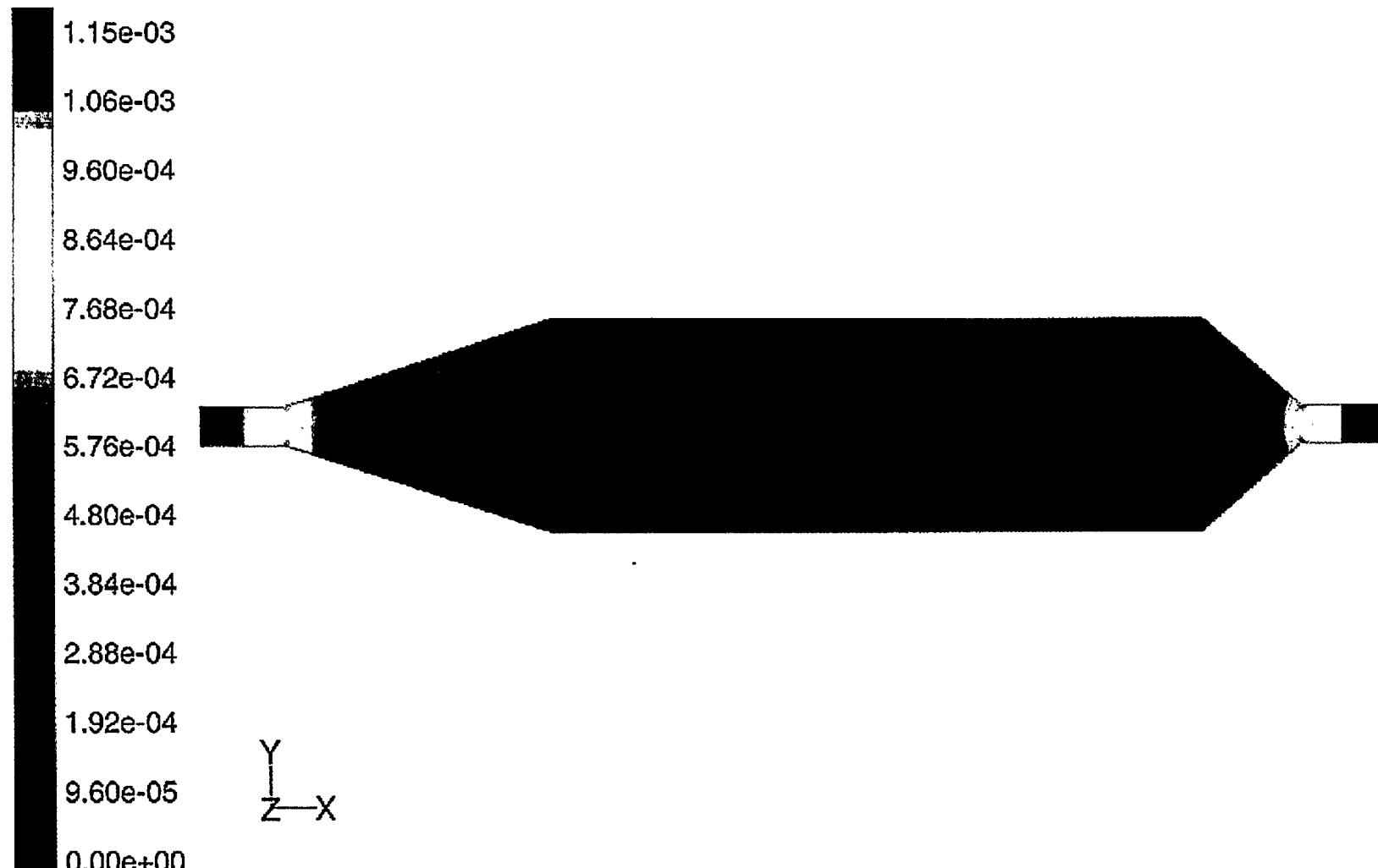
Contours of Velocity Magnitude (m/s)	Mar 29, 2000
	FLUENT 5.0 (3d, segregated, lam)

Figure 12a. Total velocity.

3.36e+02
3.08e+02
2.80e+02
2.52e+02
2.24e+02
1.96e+02
1.68e+02
1.40e+02
1.12e+02
8.40e+01
5.60e+01
2.80e+01
-1.11e-03

Contours of Total Pressure (pascal)

Mar 29, 2000
FLUENT 5.0 (3d, segregated, lam)
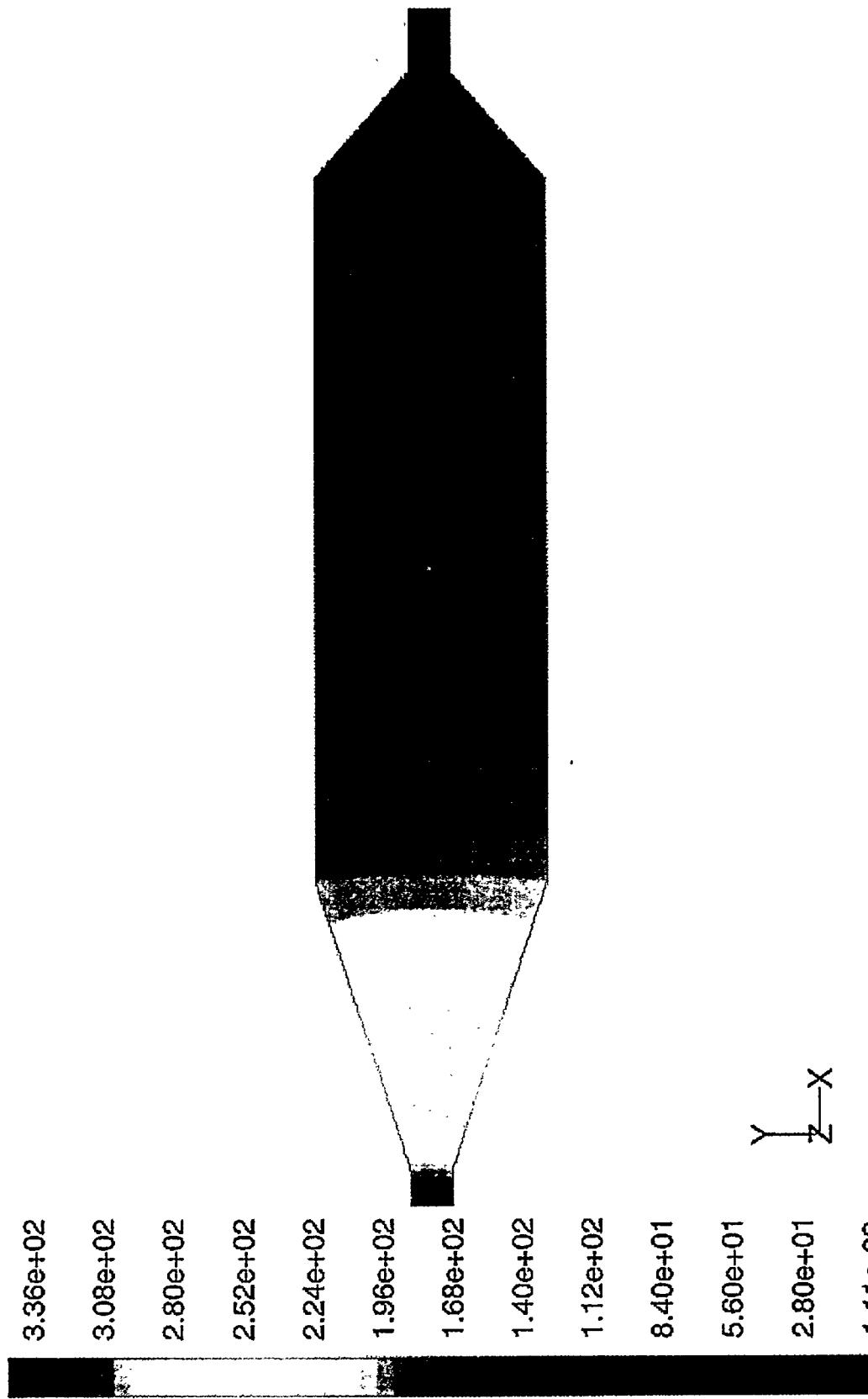
Figure 12b. Total pressure.

Contours of Wall Shear Stress (pascal)

Mar 29, 2000
FLUENT 5.0 (3d, segregated, lam)

Figure 12c. Wall shear stress.

2.16e+02
1.98e+02
1.80e+02
1.62e+02
1.44e+02
1.26e+02
1.08e+02
9.00e+01
7.20e+01
5.40e+01
3.60e+01
1.80e+01
0.00e+00

Contours of Vorticity Magnitude
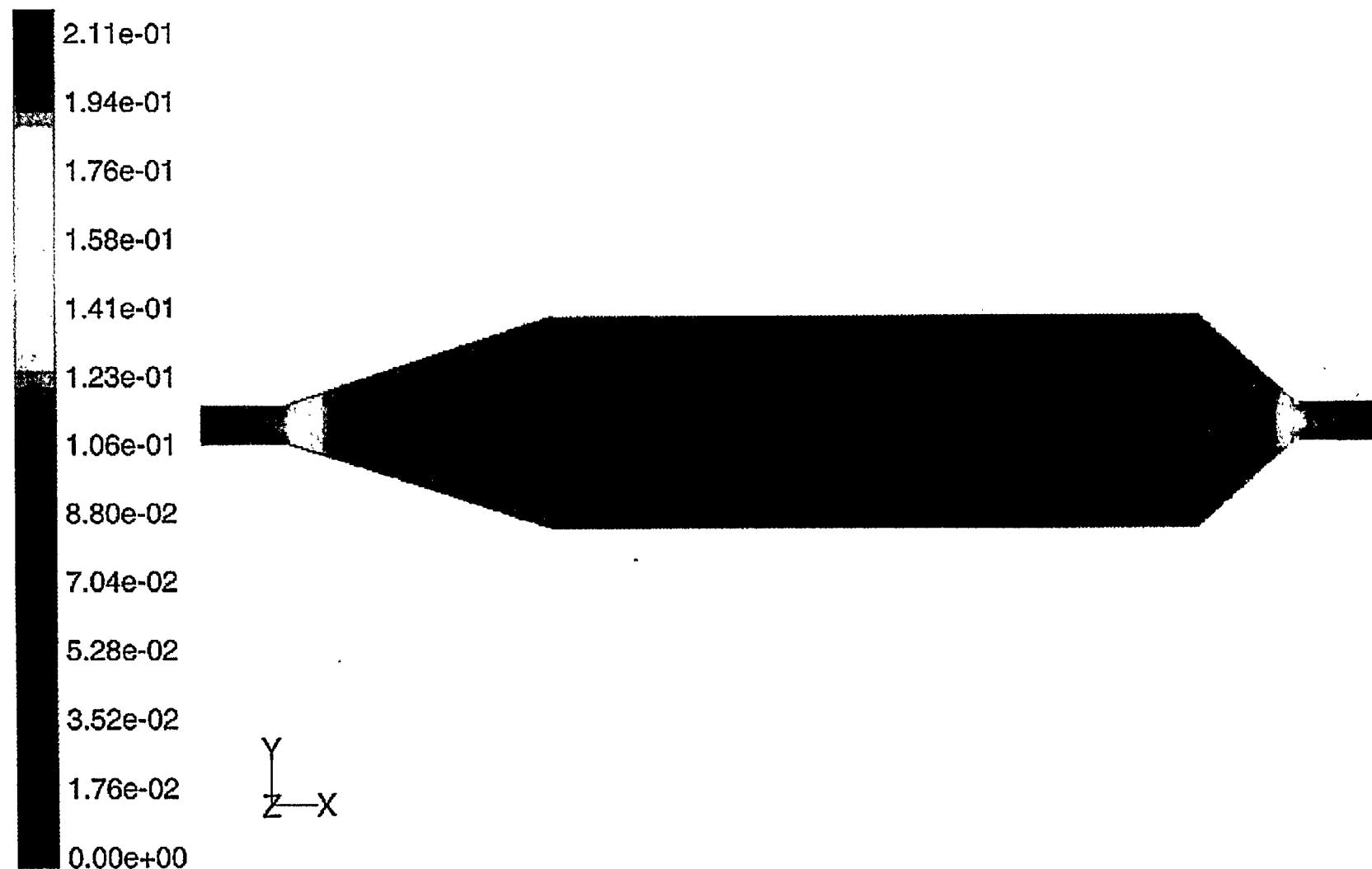
Mar 29, 2000
FLUENT 5.0 (3d, segregated, lam)
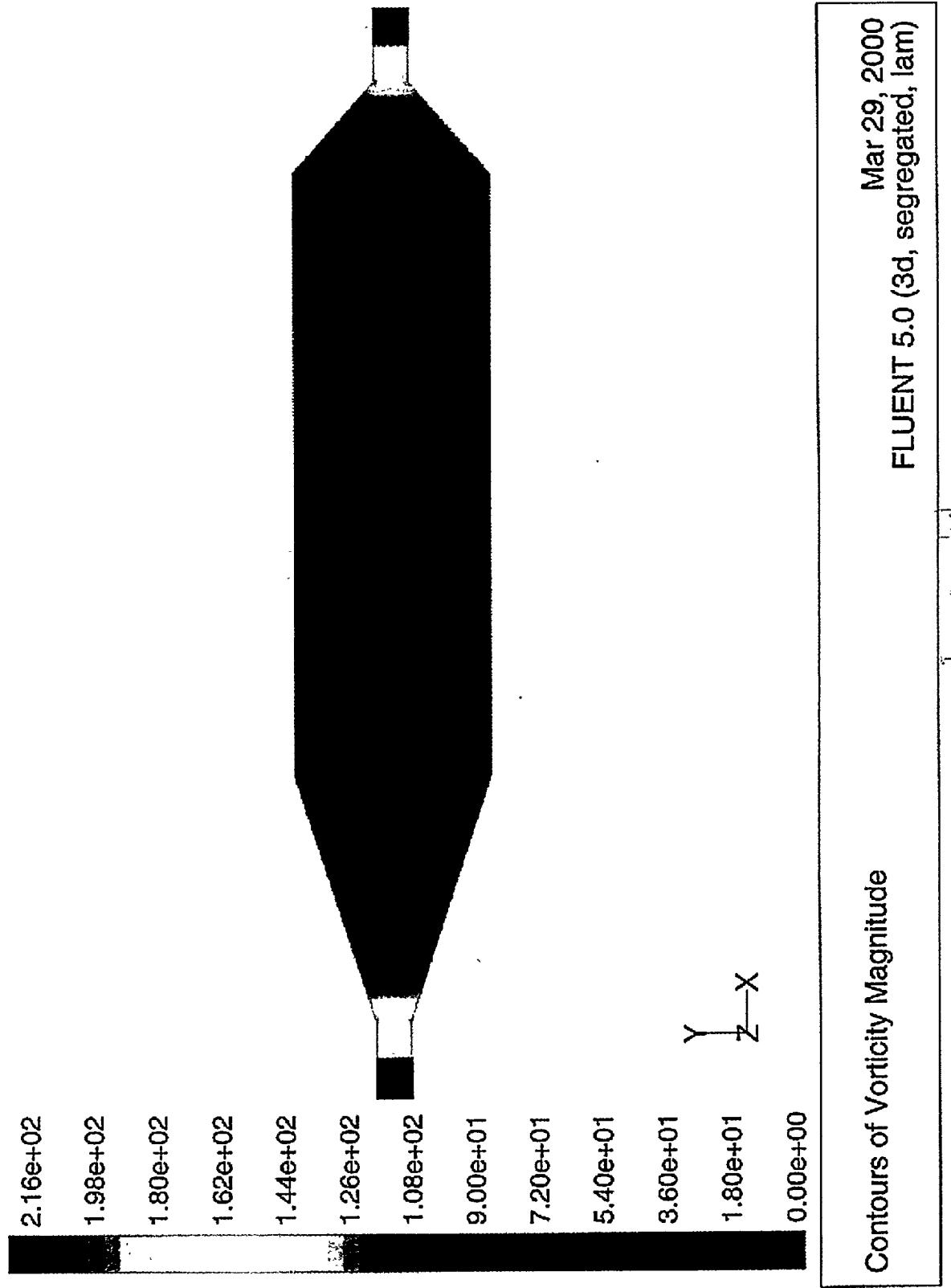
Figure 12d.

FLUENT allows one to trace a particle using a Lagrangian reference frame. The particle

velocity, $u = \left(u_{px}, u_{py}, u_{pz} \right)$, with (x,y,z) denoting a three dimensional coordinate system, is

related to the drag and Brownian forces through the equation

$$\frac{du_{pi}}{dt} = F_D \left(u_i - u_{pi} \right) + F_{Bi} + g_i \frac{\left(\rho_p - \rho \right)}{\rho_p} \tag{2}$$

where u_i represents the fluid velocity in direction i, F_D represents the drag coefficient, and F_{Bi} is

the Brownian force. The term involving gravity, **g**, accounts for buoyancy forces due to density

differences between the fluid ρ and the discrete phase ρ_p. The drag force, $F_D \left(u_i - u_{pi} \right)$, is

given by

$$F_D = \frac{18\mu}{\rho_p D_p^2} \frac{C_D \, \mathrm{Re}}{24} \tag{3}$$

with μ the fluid's molecular viscosity, D_p the particle's diameter, and Re the relative Reynolds

number defined as

$$\mathrm{Re} = \frac{\rho D_p \left\| u_p - u \right\|}{\mu} \tag{4}$$

The bacteria modeled in this study, Desulfomonile tiedjei, is far from spherical and therefore it is

better to use a drag force model for non-spherical particles, as provided by Haider and

Levenspiel (1989). In this case

$$C_D = \frac{24}{\mathrm{Re}} \left(1 + b \, \mathrm{Re}^{b_2} \right) + \frac{b_3 \, \mathrm{Re}}{b_4 + \mathrm{Re}} \tag{5}$$

where the coefficients b_1, b_2, and b_3 (Equations given in Appendix A) are functions of the shape

factor $\phi = s/S$ which is the ratio of the surface areas of a sphere having the same volume as the

particle, s, to the actual surface area of the particle, S. If we consider Desulfomonile tiedjei to be of cylindrical shape, of height five times the diameter of the circular face, then $\phi = 0.7$.

The Brownian force, F_B, is intended to represent the single cell motility, characterized as a random process with measurable parameters. In a strict sense, Brownian forces are caused by bombardment of the fluid (or solvent) around the particles (cells), and their relative magnitude with respect to inertial or drag forces decreases as the particles increase in size. For a thermal non turbulent environment the Brownian force may be characterized by a white noise process with spectral distribution (Li and Ahmadi, 1992)

$$S_{ij}^{n} = S_o \delta_{ij} \tag{6}$$

where δ_{ij} is the Kronecker delta function, and

$$S_o = \frac{216 v k_B T}{\pi^2 \rho D_p^5 \left(\frac{\rho_p}{\rho}\right)^2 C_c} \tag{7}$$

where k_B is the Boltzman constant, v is the kinematic viscosity, and T is the absolute temperature of the fluid. Brownian forces are more important for sub-micron particles, and in a convective flow environment like the one studied here, as a particle decreases in size, the drag and inertial forces decrease relative to the Brownian force.

In the context of this work, we must scale Brownian forces so that they represent the tumble and run random mechanism of bacterial motility. Since equation (7) is the model for Brownian forces included in FLUENT, we must scale either temperature T, or particle diameter D_p until the overall random bacterial motility matches the modeled particles tracked. As seen in relationship (7), a change in scale of one order of magnitude in the particle diameter causes a change of five orders of magnitude in the Brownian force, while F_B is linearly dependent on the temperature T.

We modify the particle diameter for the Brownian forces, but not for the drag and inertial forces, since motility does not affect these. FLUENT provides a way to maintain dynamical similarity by modifying the particle density as to keep the ratio of inertial to drag forces constant, while changing the ratio of Brownian to drag forces.

Most knowledge of single cell motility has been gathered using flagellated organisms like *E. Coli.* Little is known about motility of non flagellated bacteria. From the particle/hydro-dynamic point of view, a number conjectured mechanisms for bacteria motility have been suggested. These conjectures have yet to be proven with direct observation.

Changing direction of resultant drag force. By changing orientation and shape (S-shape) the bacteria have some control over the direction they move within a convective field. This is observed under the microscope as the cells flex and curl. This swimming mechanism will change the direction in which the resultant drag force is being applied from the fluid to the individual bacteria, generating self-displacement. This component of bacteria motility is modeled using Brownian dynamics as described above. If the bacteria are looking for attachment sites, this activity will increase the probability of collision against a wall and reduce the mean free path compared to an inert particle of the same size. It is important to note that adhesion and swimming mechanisms will effect each other and the overall bacteria motility.

Particle rotation and vorticity. It is known that particles traveling in convective flows through capillaries are subject to rotation. This effect increases with particle diameter (proportional to cubed diameter) and has an observable effect on the particle dynamics (with vorticities typical of a pore laminar flow). In a classic experiment by Segre and Silberberg (1961), particle migration across streamlines was observed. In a capillary tube, rotating particles are subject to Magnus forces, and the balance between such a force and the drag force occurs in

65

an annular region around which particles travel. If there exist a motility mechanism to limit cell rotation, then they will follow the fluid streamlines.

Electromagnetic effects. As found by Schie and Fletcher (1999), negatively charged cell surfaces effect bacteria adhesion to surfaces. As a consequence transport in the aqueous phase will be influenced. Fast (as in anion exclusion) and slow transport (as in diffusion close to a wall) may also occur. Only the appropriate experiments and measurements can provide the necessary characteristics to include in the biotransport model.

Modeling bacterial pore wall attachment/detachment. One of the objectives of the experimental work by collaborators is to measure single-cell attachment and detachment to develop a probabilistic model that better describes the process in aggregated scales (Darcy scale and larger). Preliminarily, we present two hypothetical models that remain to be tested and calibrated against measurements. In the first, once a single cell collides with a pore wall, it sticks for a time, t_w. This sticking time is assumed to have an exponential distribution (in addition, a log-normal time distribution has been modeled). The second model accounts for a phenomenon qualitatively observed for bacteria attachment. If the microbe finds suitable conditions for life at the attachment site, it may remain there for a long time. In fact, the attachment may be irreversible. It is reasonable therefore to consider that the attachment time, t_w, is bimodal. That is, attachment always occur, but there will be a fast time scale detachment if conditions are not suitable, or a slow time scale or irreversible attachment. If we define P_f as the probability of finding one fast time attachment, the simplest model we could imagine is that probability being constant. In reality, the value of P_f is associated with factors like distribution of nutrients and competing bacterial species, and if a coupled model for those is available, a more sophisticated

66

P_f with a space dependent probability can be modeled. If the attachment/detachment of bacteria occurs kinetically, then P_f will be time dependent. For the sake of this report we will explore the simplest case in which P_f is constant. The probability of a slow attachment time occurring will be $P_s = 1 - P_f$.

2.3. Results

In this section emphasis is given to the flow cell design shown in Fig. 9d because the current experiments are being performed on it. Extensive results however exist for the three geometries and are available upon request. During the following discussion, references to the coordinate system (x,y,z) are frequent, and so the system is defined as follows: (i) x is the main direction of flow, aligned with the inlet and outlet pipes longitudinal axis, $0 < x < 60.4$ mm; (ii) y is direction of the flow cell's width, $-5.35 < y < 5.35$ mm; and (iii) z is direction of the flow cell thickness.

Cell design 1. In absence of random motility (absence of random Brownian force), the particles will follow stream lines and only a few collisions will occur at the wall between the flow cell body and the outlet pipe. These collisions are mainly due to the deceleration of the flow in the main flow direction (x direction) nearing the mentioned wall. Inertial forces cause the particles to decelerate at a slower rate (balance between drag forces and inertial forces) in the x direction, therefore they may collide against the wall.

Cell design 2. Figure 11 displays variables for the flow cell geometry shown in Fig. 9b,c. The thickness or z dimension of the flow cell is variable. The flow cell was operated with a flow rate of q=100 μm=2.777 10^{-11} m^3/s. The pressure drop (27 Pa in 70.4 mm, or 384 Pa/m) is equivalent to a 0.384 m head loss in 1 km of mean flow length. The funnel shaped inlet

expansion and outlet contraction generate a y component of the velocity, and the variable thickness generates a z component of the velocity.

A number of particles (N=1600) of diameter 1 μm are released from the cross section at x=0.005 m and tracked through the flow cell. In absence of Brownian motion, Fig. 13a shows the exit time distribution at the cross section x=0.0554 m. A number of particles (around 400 out of the 1600) exhibit delayed times (long tail) due to physical retardation occurring at locations where sudden contraction in the cross sectional area occurs. Allowing diffusion to occur reinforces this point. Figure 13b shows this condition. The exit time distribution does not have the long tail as before, although the mean arrival time in the two situations is the approximately the same $\overline{t_e} = 2700s$. If a Gaussian curve is fitted to the early breakthrough (no tail) of Fig. 13a, the corresponding standard deviation is $\sigma_{te} = 360$ s. For Fig. 13b, the standard deviation is $\sigma_{te} = 1030$ s. It can be concluded that the pore scale geometry and biochemistry have a strong synergism. Its consequences must be analyzed in detail when a macroscale averaged model is used in porous media.

Cell design 3. The following analysis corresponds to the flow cell geometry shown in Fig. 9d.

Flow field. The flow cell was operated with a flow rate of q=2.777 10^{-11} m^3/s. The pressure contours are shown in Fig. 12b. The pressure drop of 350 Pa in 70.4 mm, 4972 Pa/m, is greater (around five fold) than a selected typical value for geologic medium (1000 Pa/m, that is equivalent to a 1 m head loss in 1 km of flow length). Figure 12a shows the total velocity at a xy plane, z=10^{-5} m=10 μm.
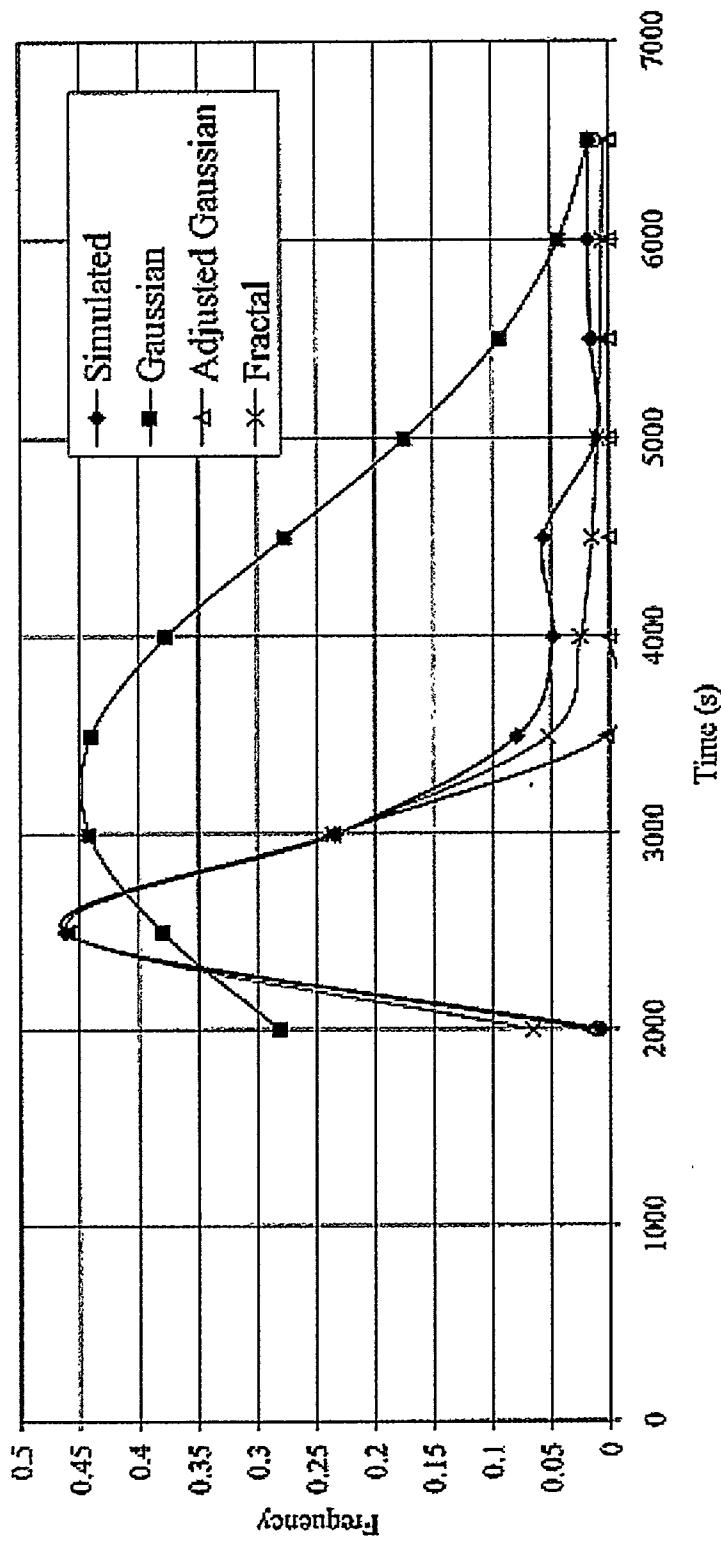
Figure 13a. Exit times of particles for flow cell design 2. No Brownian motion allowed. Elastically bouncing particles, no attachment to wall.
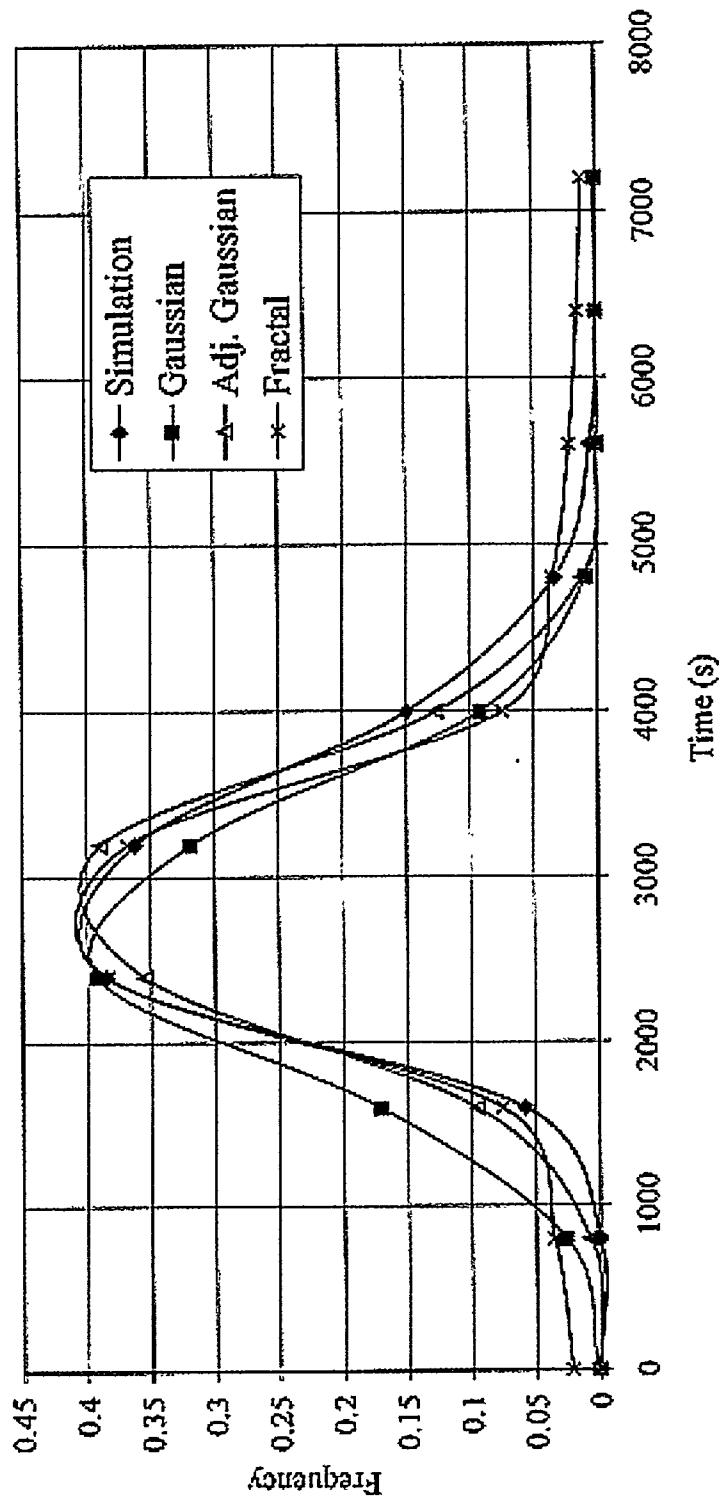
Figure 13b. Exit times of particles for flow cell design 2. Brownian motion allowed. Elastically bouncing particles, no attachment to wall.

70

After passing the entrance, the flow decelerates. There exits an important y component to the velocity field, as shown in Fig. 14a,b,c. The angled, funnel-like shape of the expansion renders a smooth transition and eliminates stagnation zones. Figures 14a,b,c shows details of the velocity at $z=10^{-5}$ m. There are zones of low and high velocity near the sharp angled corners of the flow cell. Figure 14b,c displays the magnitude of the velocity at the section $z=2x10^{-6}$. Through most of the domain the velocity profile in the z direction is nearly parabolic, like pressure driven flow between two infinite plates.

Rotation of the bacterial cells coupled with wall shear stress may play a role in the motility mechanisms developed by the bacteria. For instance, if the bacteria can stop the rotation the flow field is transferring to it, it will travel along streamlines, otherwise free rotation causes the particle to move between streamlines. It is not known if bacteria posses such sophisticated motility. Figure 14d shows the vorticity nearing the flow cell's wall, $z=0$ or $z=2x10^{-5}$ m. Higher vorticity is associated with larger velocity changes, and the flow cell walls may be thought of as sources of vorticity. Nearing the center of the flow cell, $z=10^{-5}$m, the vorticity decreases considerably (14e), when approaching the wall, a particle will spin faster. Figure 14g shows the wall shear stress. The bacteria may experience adverse conditions in zones of greater shear stress like the narrow inlet and outlet pipes.

Figure 15a,b displays particle (1 μm) paths, for the flow cell shown in Fig. 9d. In absence of random motility (absence of random Brownian force), the particles will follow streamlines and collisions will not occur within the domain. Magnus forces (resulting from particle rotation) have not been considered here, although the significant velocity gradients in the z direction (aligned with the microscope optical axis) and the relative size of the particle (1 μm) with respect to the smallest flow domain dimension (20 to 35 μm) indicate they may have an observable

effect. At the pore scale we may see an aggregated effect of Magnus forces, but in a porous medium in which the particles will jump from pore to pore in a complex geometry, this effect may be averaged out and possibly can be modeled in mechanical dispersion. A sample of 360 particles was injected at the zy cross section $x=5 \times 10^{-3}$ m, uniformly (Fig. 16a shows the arrival time in a zy cross section $x=55.4 \times 10^{-3}$) through the cross section. The particles do not interact with each other or with the flow field. Particles traveling in streamlines close to the walls $z=0$ and $z=2 \times 10^{-5}$ have greater breakthrough times (by a factor of around 3) than those traveling along the center plane's $z=10^{-5}$ streamlines. This Taylor dispersion of the particles within the cell can be characterized by the mean and variance of arrival times to the zy section $x=55.4 \times 10^{-3}$, which is the end of the funnel shaped contraction. The mean arrival time is $\overline{t_e} = 409$ s and the standard deviation is $\sigma_{t_e} = 206$ s. The arrival times are not Gaussian (as can be seen in Fig. 16a) but have an asymmetric distribution tailing towards longer times than the mean arrival time. This distribution depends on the flow cell geometry.

Next consider 1 μm particles with Brownian motion. Figure 16b shows this case. First assume there is no attachment at the wall, but a particle bounces elastically when it collides against a wall. The Taylor dispersion indicated above for the non-Brownian particle changes, with new mean arrival time $\overline{t_e} = 371$ s and standard deviation $\sigma_{t_e} = 55$ s. The slight reduction in average time and the important reduction in the standard deviation are due to the particles jumping between streamlines, consequently each particle samples more velocity zones in the z direction than in the previous case and the arrival times are less disperse. More important, the distribution is Gaussian as shown in Fig. 16b. This shows how aggregating the effects of Brownian motion on a convective flow changes the character of the larger scale observations.

We turn our attention now to the nature and location of the collisions of the particles against the flow cell walls, as it forms part of the attachment/detachment process. An average of 1.04 collisions/particle/mm traveled in the x direction occur, mainly with the faces parallel to the xy plane, z=0, and z=20 μm (85.8% collisions occur at those planes). Another significant number of the collisions occur at the narrowing stretch of the main cell (12.9%) at the inclined planes that form the funnel shaped contraction. These collisions result from the particle inertia and hence the particles decelerate at lower rates than the flow, crossing streamlines in the process. In contrast, only 1.25% of the total collisions occur at the entrance expansion, which is both smoother and located opposite to the particles main flow direction. The Brownian force increases the probability of the particles colliding against the wall.

After a collision with the wall, a particle attaches to the wall for some time (models discussed in section 2.3), then detaches and returns to the flow. The particle can return into the flow with no momentum, or bounce elastically (i.e. to recover the momentum it had before attachment). The latter scenario is plausible when the bacteria have electrostatic forces to detach from the wall and gain velocity into the liquid phase (as reported by Busscher et al., 1998).

Consider a three dimensional random walk, and look at the exit time distributions the main direction of flow, x in this case. Figure 17 shows one single particle's x coordinate in time for the three situations, (a) elastic bouncing at the wall, (b) attaching and detaching from the wall at each collision with a log-normal(0,1) attachment time, and (c) attaching and detaching from wall with a bimodal time with P_s=0.1, fast time attaching distribution log-normal(0,1), and slow time attaching distribution normal(100,50).

To obtain a statistically significant sample, consider 360 particles released at the flow cell inlet. Figure 18b shows the x coordinates of such particles as a function of time, for the bimodal

attachment/detachment with P_s=0.1. (Figure 18a shows the corresponding plot for elastically rebounding particles.) Figure 18c depicts a histogram (equivalent to a breakthough curve or exit times pdf) of the arrival times at an exit cross section located at x=0.0554 m. The histogram has been normalized as a pdf, and three analytical models, Gaussian, hyperbolic cosine, and exponential-fractal have been adjusted to fit the curve (least squares method). The exponential-fractal model best fits this pdf.

Increasing bacterial motility. Consider the case when Brownian forces dominate inertial forces. This case is studied by changing D_p. We take D_p =0.1 µm. Changing the size of the particles does not have any impact on their trajectories when no Brownian motion is present (Magnus forces not considered). The smaller particles follow the streamlines with identical times. In this case the time arrival of the 360 particles at x=55.4x10^{-3} m has mean $\overline{t_e} = 384.5$ s and standard deviation $\sigma_{t_e} = 14.5$ s (Brownian force acting). Compared with D_p=1 µm particles, the mean arrival time is slightly greater, accounting for a longer pathline, and the standard deviation is significantly smaller (by a factor of 3), indicating that particles sample the velocity field more thoroughly and Taylor dispersion will therefore be smaller.

This results from the random force allowing the particles to wander in both the z and y directions and sample more of the velocity field (xy projection of pathlines for the later differ considerably from xy projection of streamlines). The distribution of exit times is Gaussian.

The number of collisions with the wall that a particle experiences (on average) per unit length traveled in the main direction of flow is 3.2 collisions/particle/mm (in the x direction). Using the same bimodal attachment model as before, with P_s=0.05, attachment and detachment are modeled with log-normally distributed short and normally distributed long attachment times. Figure 19 shows breakthrough curves for three cases. Case (a) has P_s=0.05, short attachment

times re log-normal (1.5,2), and long times are normal(100,50). The dark blue curve in Fig. 19 is the result of simulation for this case (a), resulting in a two-peaked breakthrough. A Gaussian curve ($\overline{t_e} = 6263$ s, $\sigma_{te} = 2261$ s), has been fit to the earlier peak, which embodies most of the mass. This fit by no means implies the process is Gaussian but gives an idea about symmetry and basic statistics of the breakthrough curve. Case (b) is the earliest breakthrough, with P_s=0.05, short times are log-normal (0,1), and long times are normal (100,50) (time units: seconds). A Gaussian model reasonably fits the breakthrough curve, with mean $\overline{t_e} = 1680$ s, and standard deviation $\sigma_{te} = 549$ s. Case (c) uses P_s=0.1, that is, the probability of attaching for a longer time after a collision is 10% instead of 5%.
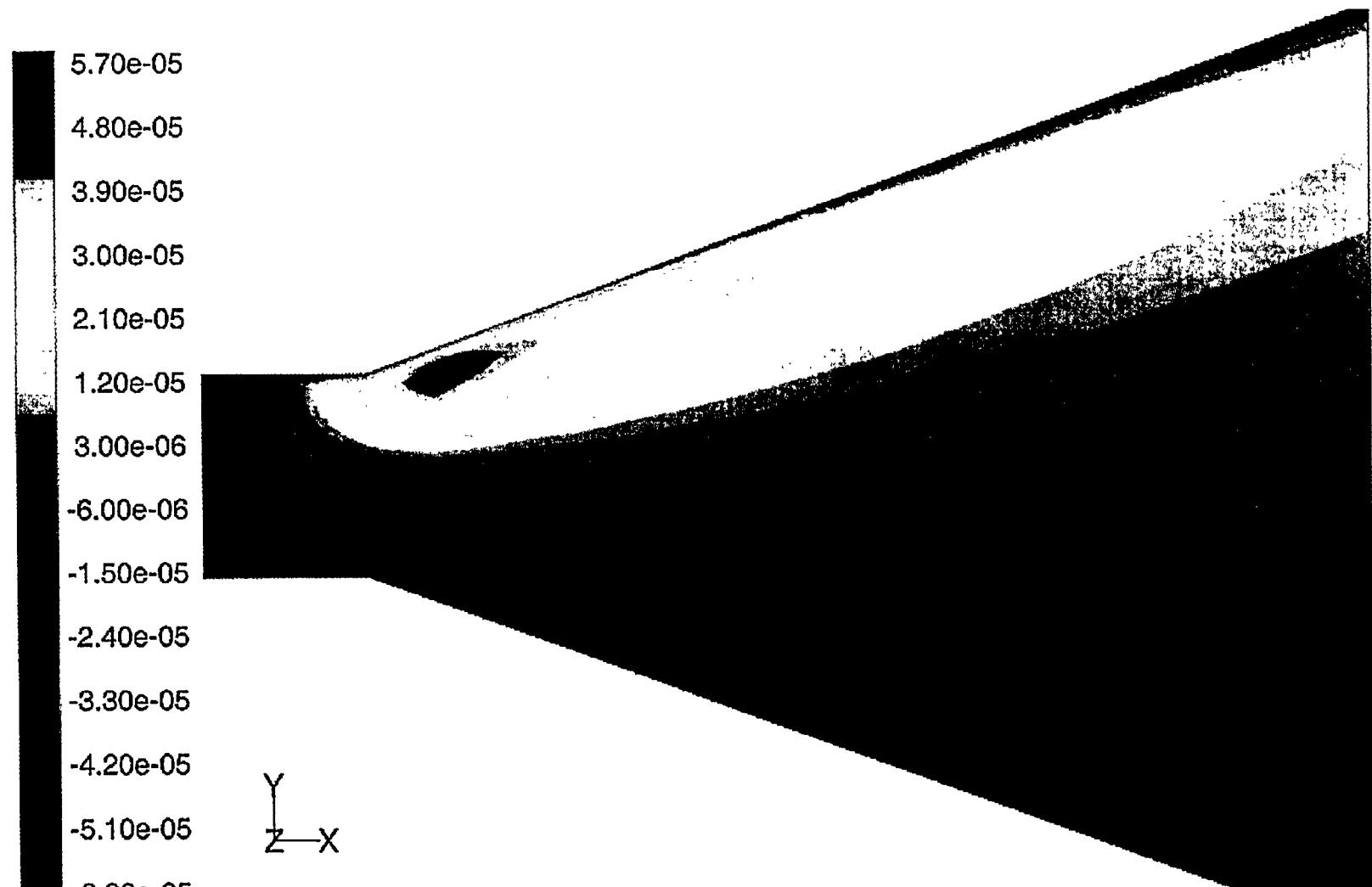
| 5.70e-05 |
| 4.80e-05 |
| 3.90e-05 |
| 3.00e-05 |
| 2.10e-05 |
| 1.20e-05 |
| 3.00e-06 |
| -6.00e-06 |
| -1.50e-05 |
| -2.40e-05 |
| -3.30e-05 |
| -4.20e-05 |
| -5.10e-05 |
| -6.00e-05 |

Y
Z—X

Contours of Y Velocity (m/s)

Feb 25, 2000
FLUENT 5.0 (3d, segregated, lam)

Figure 14a.

1.34e-03	
1.23e-03	
1.11e-03	
1.00e-03	
8.92e-04	
7.80e-04	
6.69e-04	
5.57e-04	
4.46e-04	
3.34e-04	
2.23e-04	
1.11e-04	
0.00e+00	
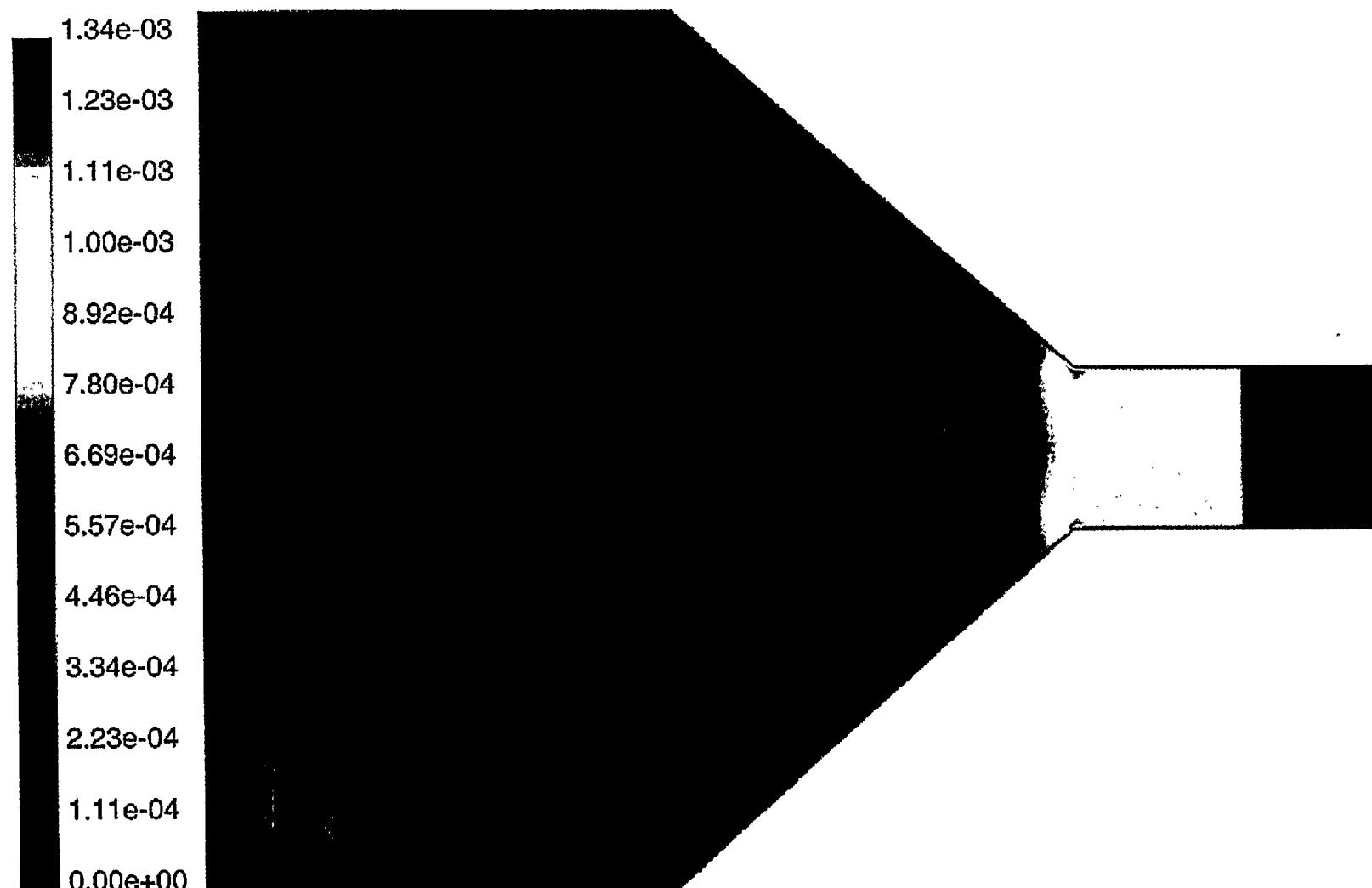
Contours of Velocity Magnitude (m/s)

Mar 10, 2000
FLUENT 5.0 (3d, segregated, lam)
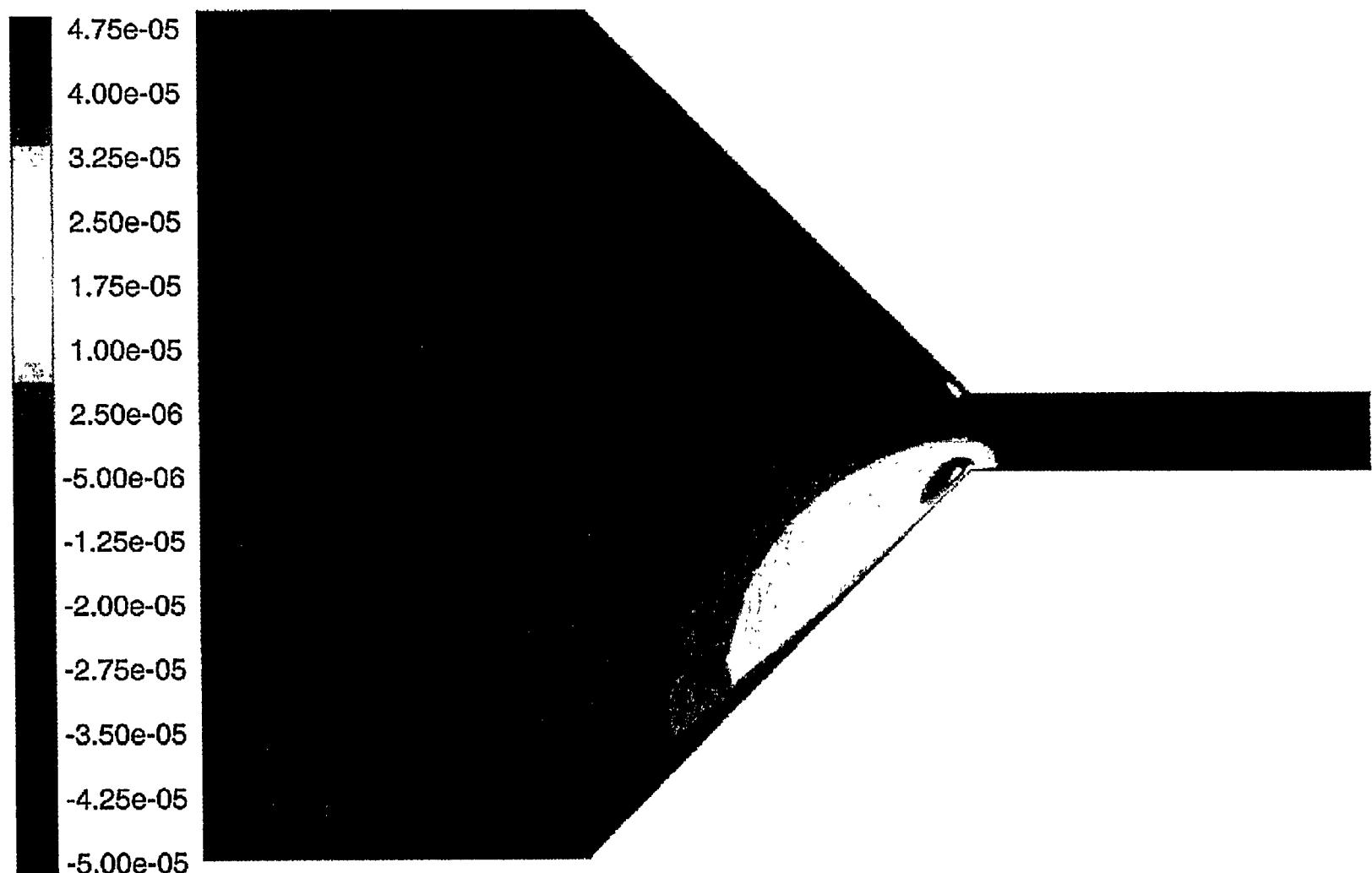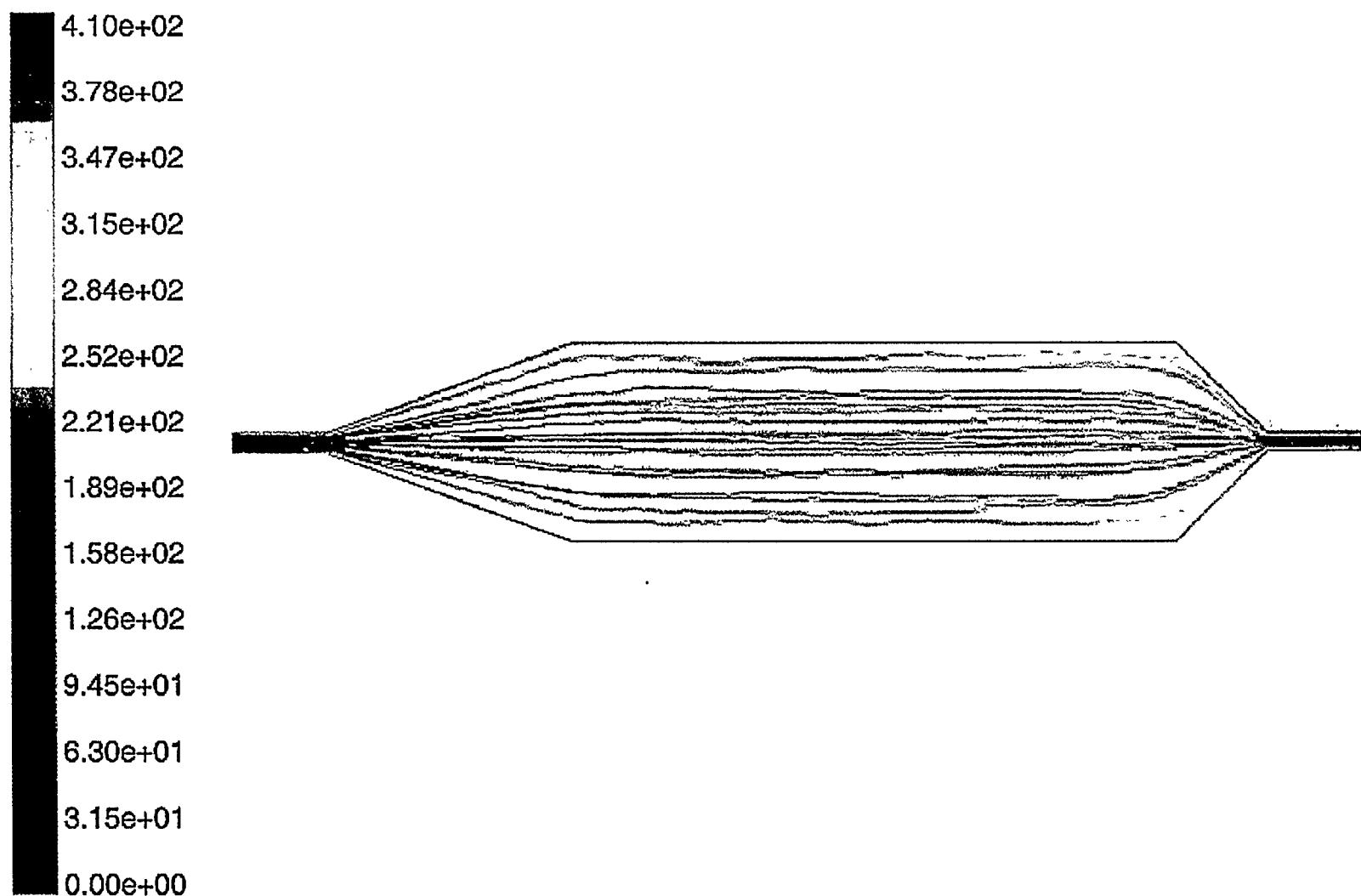
Figure 14b.

Contours of Y Velocity (m/s)

Feb 25, 2000
FLUENT 5.0 (3d, segregated, lam)

Figure 14c.

4.10e+02	
3.78e+02	
3.47e+02	
3.15e+02	
2.84e+02	
2.52e+02	
2.21e+02	
1.89e+02	
1.58e+02	
1.26e+02	
9.45e+01	
6.30e+01	
3.15e+01	
0.00e+00	

Particle Traces Colored by Particle Residence Time (s)

Mar 08, 2000
FLUENT 5.0 (2d, segregated, lam)

Figure 15a.

6.87e+02	
6.34e+02	
5.81e+02	
5.28e+02	
4.75e+02	
4.23e+02	
3.70e+02	
3.17e+02	
2.64e+02	
2.11e+02	
1.58e+02	
1.06e+02	
5.28e+01	
0.00e+00	
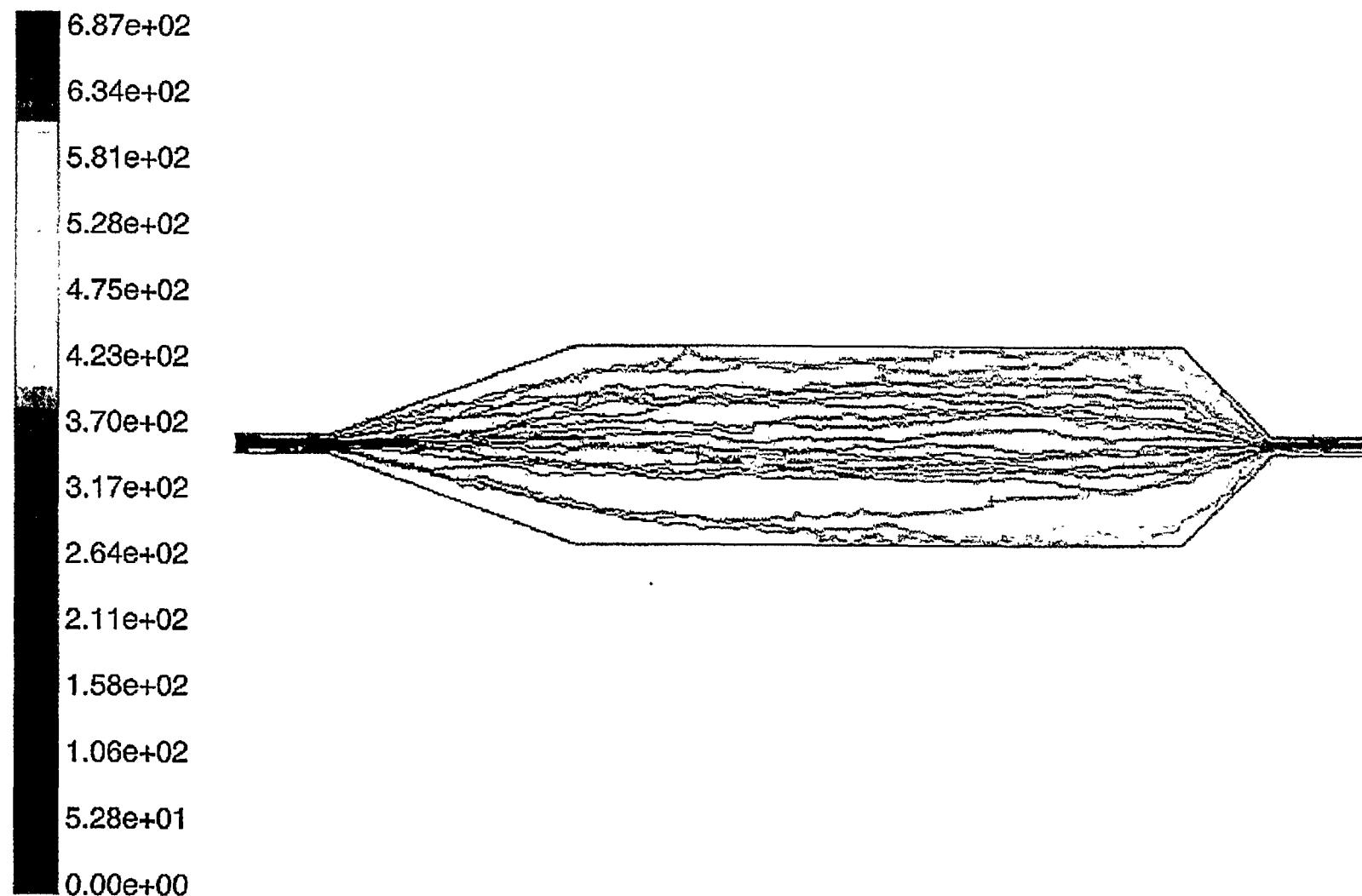
Particle Traces Colored by Particle Residence Time (s)

Mar 08, 2000
FLUENT 5.0 (2d, segregated, lam)
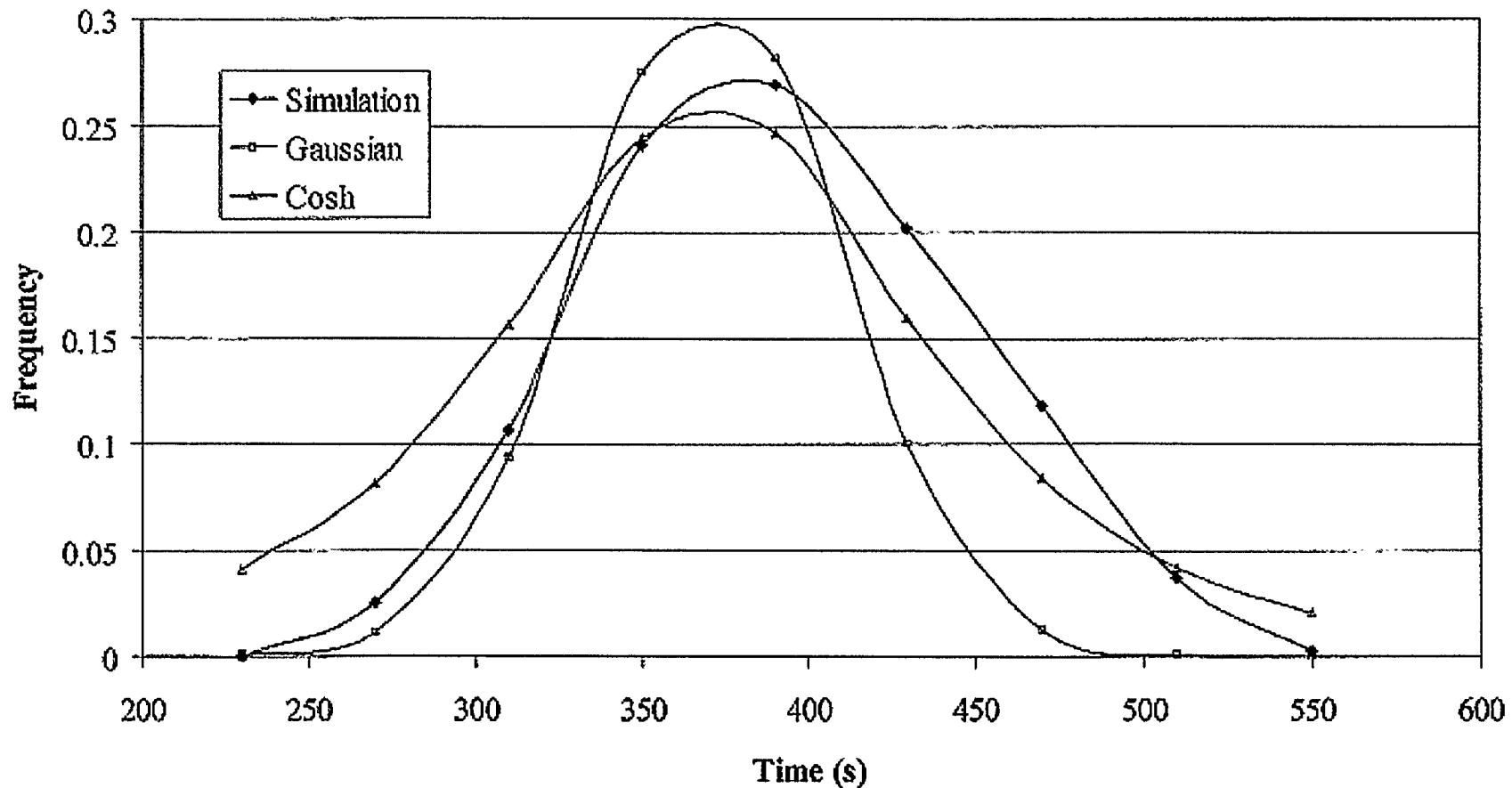
Figure 15b.

Figure 16a. Exit times at section x=60.4 mm for particles of diameter 1 μm, with Brownian motion; Simulation and Gaussian and hyperbolic cosine models with the sample statistics.
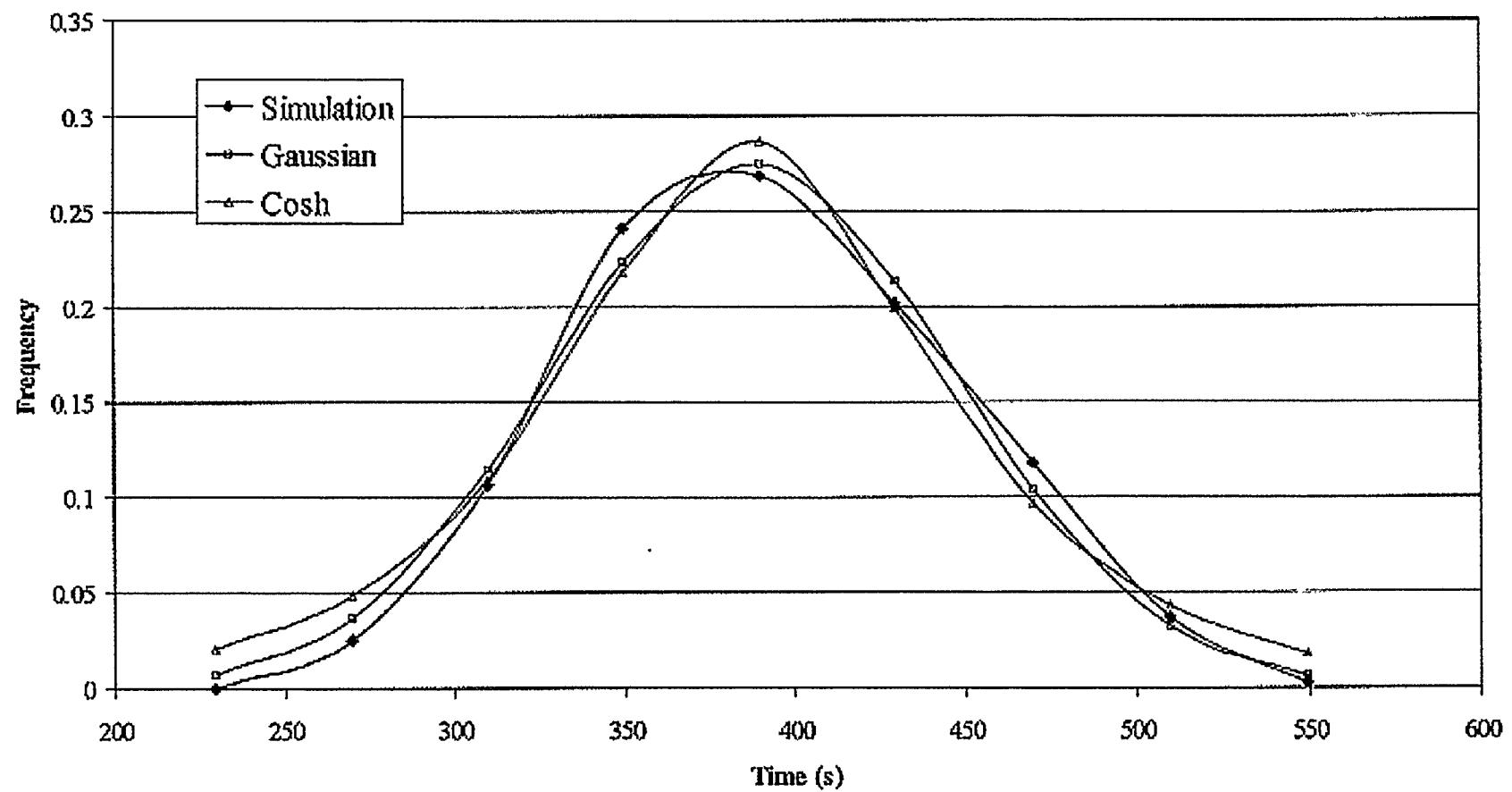
Figure 16b. Exit times at section x=60.4 mm for particles of diameter 1 μm, with Brownian motion; Simulated and Gaussian and hyperbolic cosine models with best fit statistical parameters.

Figure 18a.

83
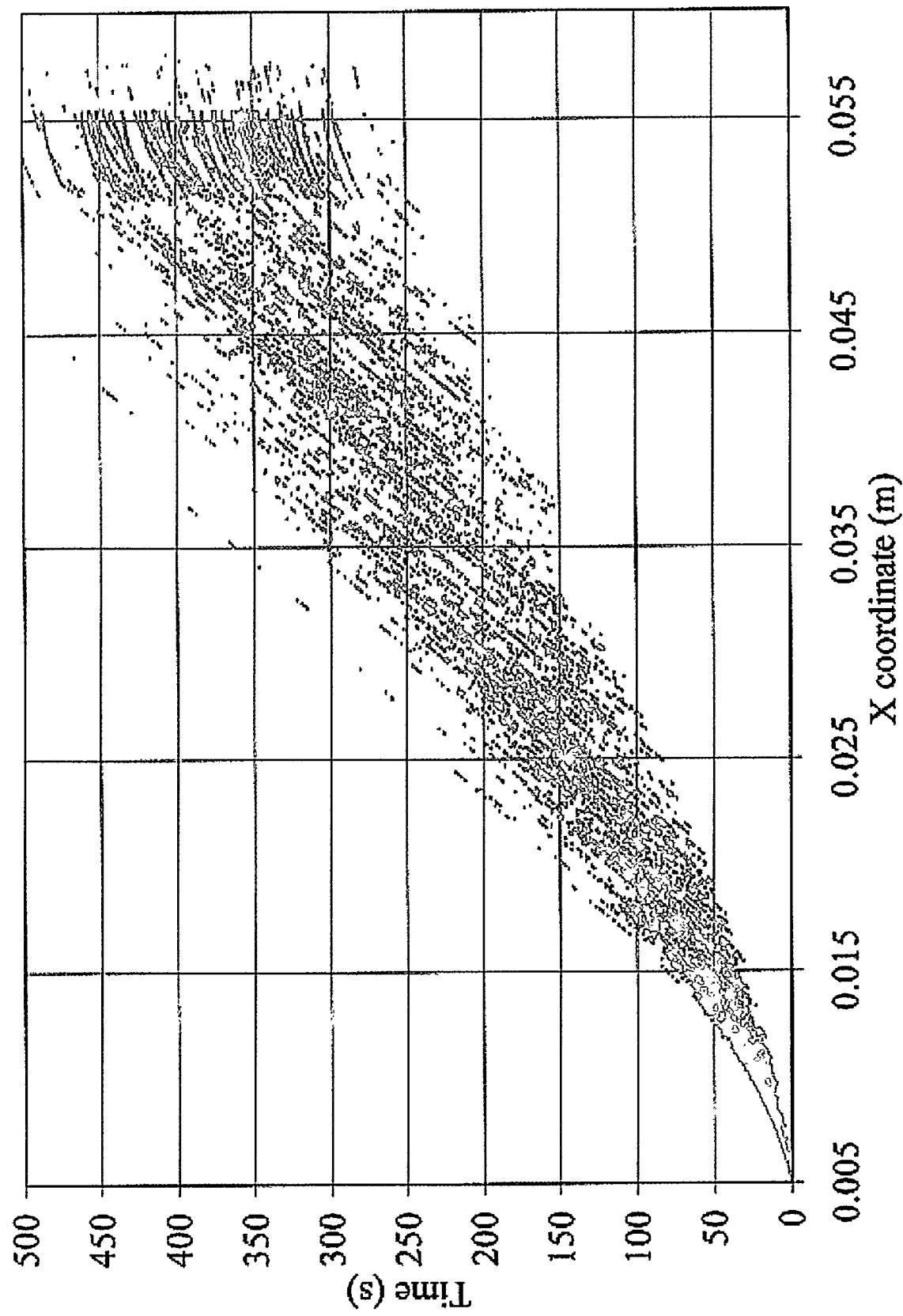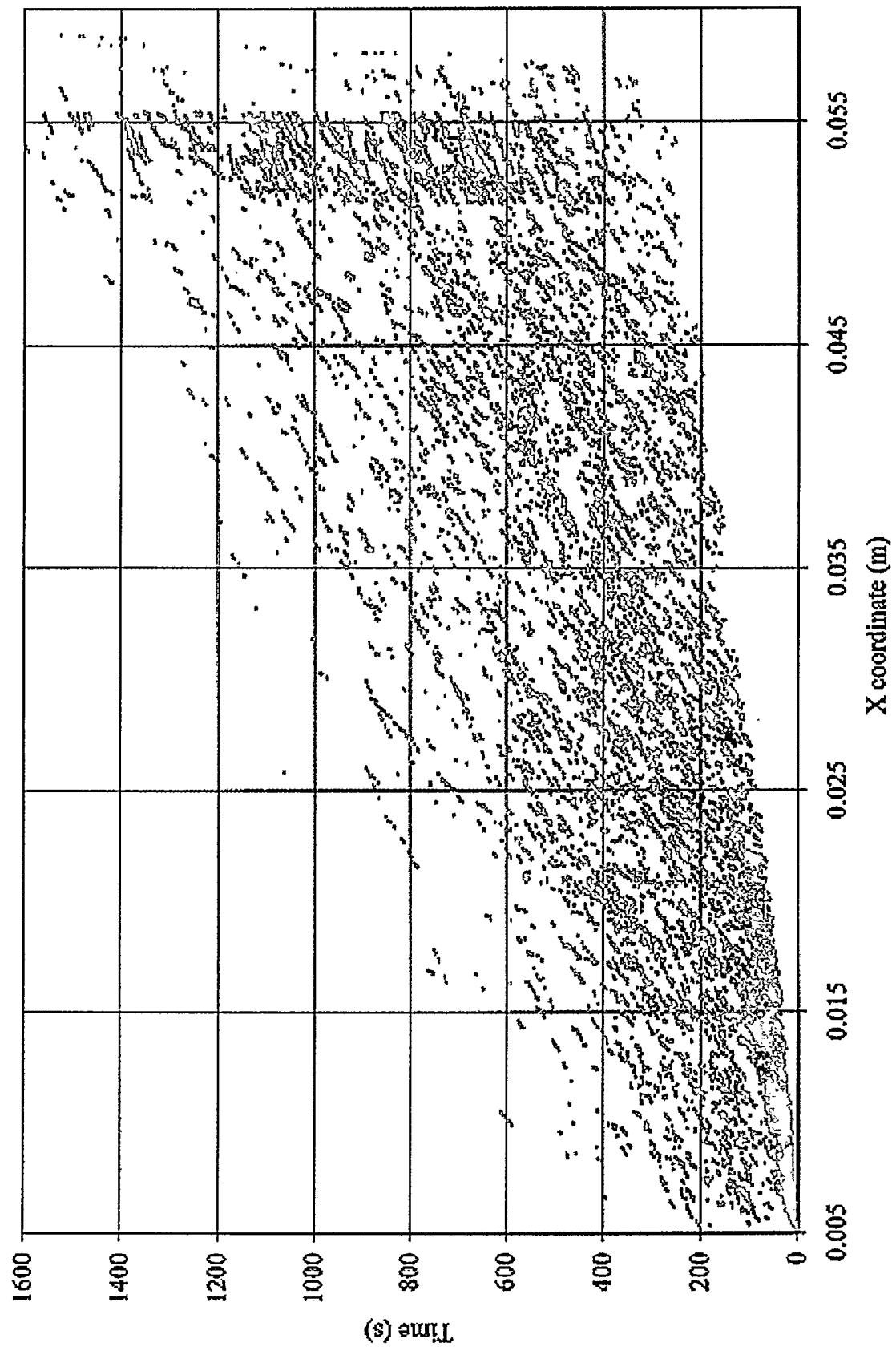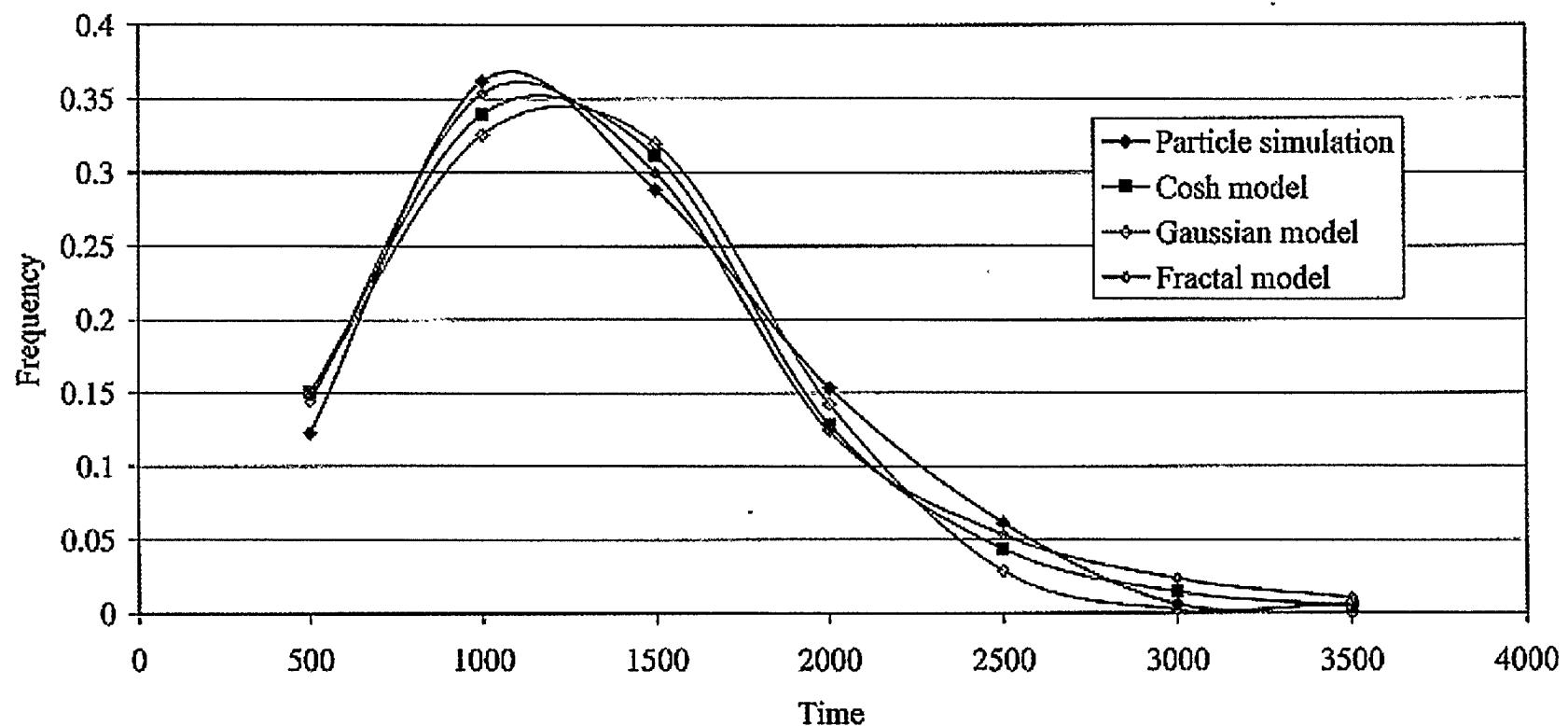
Figure 18b.

Figure 18c. Exit times at section x=60.4 mm for Brownian particles of diameter 1 μm, with bimodeal attachment. Simulated and Gaussian, hyperbolic cosine, and exponential-fractal models with best fit statistical parameters.

Figure 19.

86
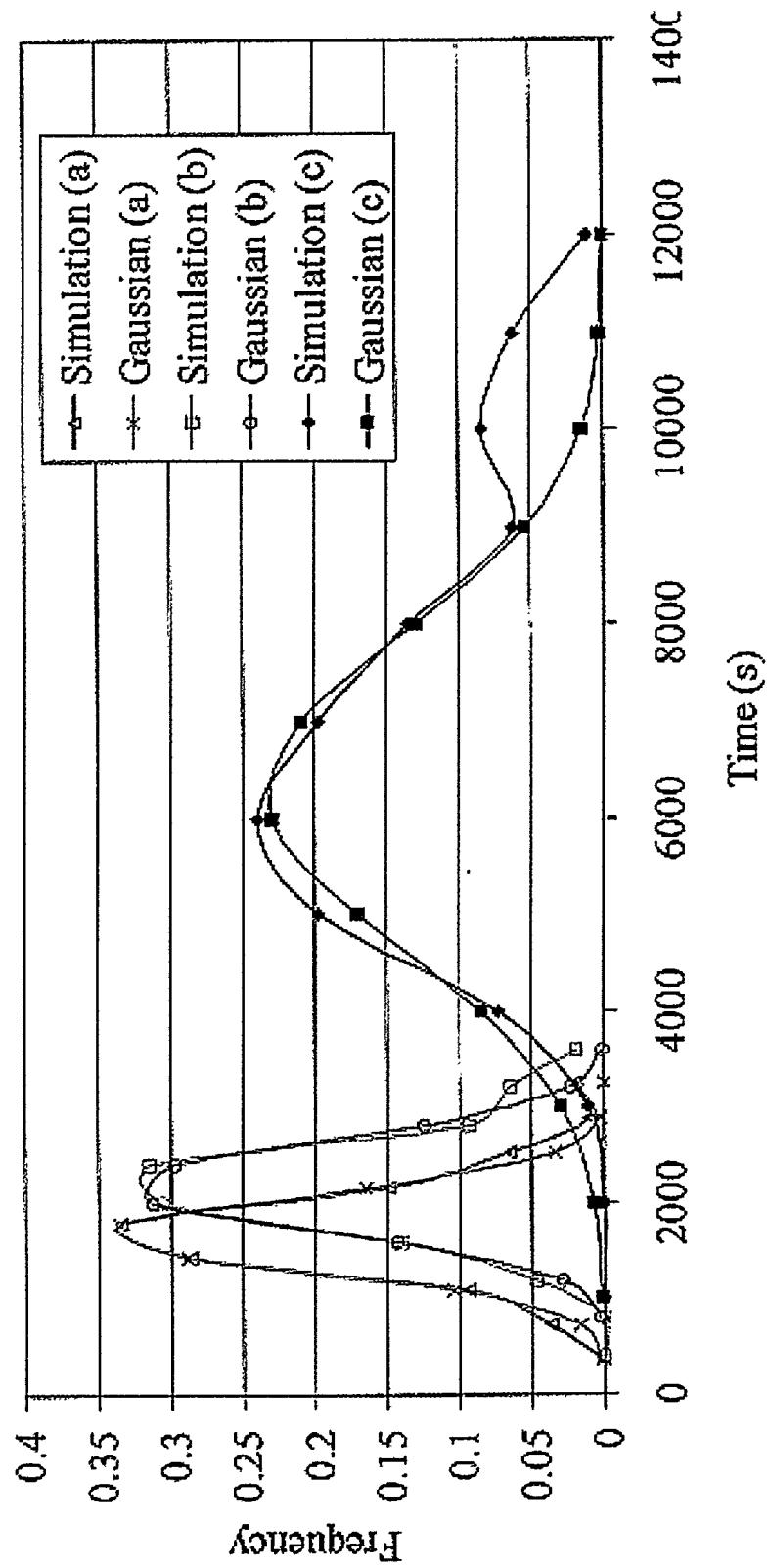
2.4. Recommendations

1. Study the effect of shear wall stress by locating coverslips in the entrance and exit regions.

2. Study the effect of wall collision frequency by comparing inlet and outlet funnel attachment (Important for pore clogging).

3. Obtaining several images per second and developing a computer algorithm to follow the bacteria and compute the statistics. It is necessary to find the ratio of number of collisions to successful attachments, and the statistics of the attachment times.

4. Consider the effect of vorticity and bacteria rotation. The observations for different vorticities can be performed in the current flow cell by locating coverslips in the entrance and exit funnels.

Warning. The low velocities in the inlet and outlet pipes change add another length scale affecting breakthrough. When breakthrough is simulated at a section at the end of the outlet pipe, the time statistics (mean and variance) are significantly different. It is recommended that concentrations samples are taken as close as possible to the flow cell's exit section at x=60.4 mm. Also an optical method to measure concentrations at the exit sections may be considered if possible.

2.5. Appendix A

Haider and Levenspiel (1989) provide a drag force model for non-spherical particles

$$C_D = \frac{24}{Re}(1 + b_1 Re^{b_2}) + \frac{b_3 Re}{b_4 + Re} \qquad (A1)$$

where the coefficients b_1, b_2, b_3, and b_4 are defined through the empirical relationships

$$b_1 = 2.3288 - 6.4581\phi + 2.4486\phi^2 \qquad (A2)$$

$$b_2 = 0.0964 + 0.5565\phi \tag{A3}$$

$$b_3 = 4.905 - 13.8944\phi + 18.4222\phi^2 - 10.26\phi^3 \tag{A4}$$

$$b_4 = 1.4681 - 12.2584\phi - 20.7322\phi^2 + 15.8855\phi^3 \tag{A5}$$

where ϕ is the factor shape, defined as the ratio of the surface area of a sphere having the same

volume as the particle (s), to the actual surface area of the particle (S), $\phi = \dfrac{s}{S}$

3.   Application of Sticky Brownian Motion to Microbial Dynamics in a Microflow Cell

3.1. Introduction

An important factor in the engineering of biobarriers/bioremediation is the microbial partitioning that goes on between the aqueous and solid phase of the porous media. The factors which affect such partitioning are numerous, but include such things as growth and starvation conditions (Dawson et al. 1981; van Loosdrecht et al. 1987, 1990), limiting of nutrients (Fletcher and Marshall, 1982), potential toxicity in the aqueous phase (Chen et al., 1993) as well as local surface properties of the porous medium. The importance of the representation of the biomass in a porous medium cannot be underestimated since it plays an important role in the degradation rates of contaminants as important nutrients necessary for the process may not be available in the solid phase.

Here we present an alternative model for the dynamics of a microorganism undergoing random forces in addition to a convective transport. Since the proper representation of the biological phase is a matter without consensus as noted in the exchanges of Widdowson (1991) and Jaffee and Taylor (1992), and since we do not want to restrict ourselves to clogging and permeability changes which are the focus of continuous biofilm models, we give a model which will also serve as a basis for an unstructured biological population. We will focus on the individual dynamics of a single microbe, or perhaps a system of such particles in a relatively low concentration so that they have little effect on the surrounding environment and each other. One may think of this as the initial stage before a type of colonization of the surface occurs. The random forces can be thought of as a sum of Brownian forces together with random swimming forces generated by a bacteria in a homogeneous liquid. We assume the random forces are normally distributed and independent. The normality assumption is an averaging of sorts over

different particle trajectories, but we comment that the model can be extended to include chemotactic behavior if one assumes that it is of the same order as either the molecular Brownian forces, in which case one replaces the normality of the random walk assumption with a non-symmetric random walk or on the same order as the convective forces, in which case one can superimpose the vector fields arising from the chemotaxis and convection to get a net vector field for the average movement. In particular the run and tumble behavior of certain types of bacteria (Berg and Brown, 1972) can be taken into effect. In addition to the random forces in the liquid phase our model introduces a stickiness parameter which relates the attachment/detachment process resulting from physico-chemical interactions between microbes and the solid matrix. The need for incorporation of time lags due to interaction with the soil matrix is crucial if one hopes to understand the effects a microbial population would have on a contaminant convecting through the matrix.

Model. Here we discuss the mathematical model for the transport of bacteria which react with the boundary of a domain. The movement of bacteria is well documented (Berg and Brown, 1972) and is best described by a run and tumble (or twiddle) behavior. Basically put this behavior consists of a sequence of runs, that is a linear movement in a particular direction, followed by tumbles which are random changes of direction following some distribution. The mechanism by which bacteria responds to a chemical gradient or chemotaxis is to increase/decrease run times between tumbles. The actual tumbling distribution appears unaffected by the environment. If a chemical potential $a(X,t)$ is introduced into a medium containing bacteria, receptors on the microbial surface can detect the change up to a saturation point at which all receptors are activated. In a large population of bacteria a statistical average can be made for the concentration in the presence of a 1 dimensional gradient. This

homogenization performed in Rivero et al. (1989) leads in one dimension to an equation of the form

$$\frac{\partial C}{\partial t} = \frac{\partial}{\partial x}\left(\mu \frac{\partial C}{\partial x} - V_c C\right) \tag{8}$$

where μ is a coefficient of motility and V_c is a coefficient of chemotactic velocity given by the following formulas

$$V_c = v \tanh\left(\alpha v \frac{\partial a}{\partial z}\right) \tag{9}$$

$$\mu = Cv^2 \exp\left(\alpha \frac{\partial a}{\partial t}\right)\text{sech}\left(\alpha v \frac{\partial a}{\partial z}\right) \tag{10}$$

where v is the running speed of a bacteria, a is the chemical potential, α is a measure of saturation which tends to zero as a gets large. If a is constant or if saturation occurs then μ is a constant multiple of v^2 and V_c equals zero, as it should since there is no chemotactic behavior at this point.

If we think of $C(x,t)$ as a probability density $p(t,x)$ we can rewrite (8) as

$$\frac{\partial p}{\partial t} = \frac{\partial}{\partial x}\left(\mu(x,t)\frac{\partial p}{\partial x}\right) - \frac{\partial}{\partial x}\left(V_c(x,t)p\right) \tag{11}$$

which corresponds to a forward-Kolmogorov or Fokker-Planck equation. We may now associate a stochastic process X_t, with p as its transition density. Another way of describing the behavior is to think of it as the solution of a stochastic differential equation, which is the continuous time version of a random walk. The SDE that it satisfies can be written

$$dX_t = \sqrt{\mu(X_t,t)}dW_t + V_c(X_t,t)dt \tag{12}$$

starting from some initial point x_0. Here W_t is a Brownian motion, which means that if one takes an ensemble of particles starting from x_0 at time zero and advects them according to the scheme

$$X_{t+\Delta t} = X_t + \sqrt{\mu(X_t,t)}Z + V_c(X_t,t)\Delta t \tag{13}$$

where Z is a normal random variable with mean zero and variance Δt, or an approximation by Z with a uniform distribution as is commonly done in particle tracking methods and justified by the central limit theorem, then the distribution of the ensemble follows the transition densities satisfying (11). In a capillary assuming constant flow we can simply add measures of advection and dispersion to get a general motion for bacteria following a stochastic differential equation of the form

$$dX_t = \sigma(X_t)dW_t + \vec{b}(X_t)dt \tag{14}$$

where now σ takes into account the dispersive terms and b is the advective term. The associated Fokker-Planck equation which is the transition density of X, denoted by $p(t,x)$ solves

$$\frac{\partial p}{\partial t} = \frac{1}{2}\frac{\partial^2}{\partial x^2}\left(\sigma^2(x,t)p\right) - \frac{\partial}{\partial x}\left(b(x,t)p\right) \tag{15}$$

If we consider a higher dimensional domain as a set of one dimensional tubes then this equation is generalized to

$$\frac{\partial p(t,x)}{\partial t} = \frac{1}{2}\sum\frac{\partial^2}{\partial x_i \partial x_j}\left(a_{ij}p(t,x)\right) - \sum\frac{\partial}{\partial x}\left(b_i(x,t)p\right) \tag{16}$$

where a_{ij} is a dispersion matrix and $\vec{b}$ is an advection vector. Up to this point we have assumed that the motion of the bacteria is not confined, that is there has been no boundary effects. To study the movement in a capillary tube or porous medium we need to augment (10) or (12) by

some boundary conditions. In the random walk we want to impose physically meaningful boundary conditions which capture the attachment and detachment behavior of microbes. This boundary behavior is crucial in understanding the transport biological agents in porous media. In Boyd and Chakrabarty (1994) the attachment/detachment process is shown to occur regularly in the presence of enzymatic degradation. At each point $x \in \Gamma$ of the boundary we assign a measure of "stickiness" $\rho(x)$. This measure ranges from 0, reflecting, through infinity at which point a microbe is adsorbed to the surface irreversibly. A similar model has been proposed for the flow of a chemical pushed by an inert gas through a tube with liquid state on the boundary (Graham 1988). On a domain E, with a boundary Γ, the stochastic differential equations representing the motion of a sticky bacteria are given by

$$dK_t = 1_\Gamma (X_t) dK_t, X_0 = x, X_t \in E \tag{17}$$

$$\langle N^i, N^i \rangle = \left(t - \int_0^t \rho(X_s) dK_s \right) \tag{18}$$

$$dX_t = \sigma(X_t) dN_t + \vec{b}(X_t)(dt - \rho(X_t) dK_t) + \gamma(X_t) dK_t \tag{19}$$

where X_t is the microbes position, $1_\Gamma = 1$ if x is on Γ and 0 otherwise, K_t is a measure of the time the bacteria is near to, but not on the boundary. N_t is a random directional motion which only changes when X_t is not on the boundary, equation (11), γ is a directional vector which keeps the microbe inside the domain, and the square bracket process $\langle N, N \rangle$ is a measure of the amount of time a particle has spent inside the domain up to time t. With these interpretations (8) says that K_t only increases when X_t is near (at) the boundary and the last equation states that inside the domain X_t acts as a classical Brownian motion. In this model the rate of adsorption and desorption happen relatively quickly and what is important is the ratio of the rates of

adsorption when the microbe is near the boundary and attachment time once on the boundary. This assumption, while rather restrictive leads to numerical schemes which have the appropriate limiting behavior for fast reactions, and which can themselves be modified in case of slower reactions. Moreover, in the above mathematical model the "local time" satisfies the equation

$$K_t = \lim_{\varepsilon \to 0} \int_0^t 1_{0 < d(X_s, \Gamma) < \varepsilon} (X_s) ds \qquad (20)$$

Here we assume that the expected time on the boundary and its variance are both finite. Otherwise the boundary behavior corresponds to adsorption and a scale up or homogenization would only lead to transport with decay. The appropriate boundary conditions for the Fokker-Planck equation (11) is known in one dimension (see Borodin-Salamin 1996) and can be immediately extended to more dimensions. Together with (15) which can be rewritten as

$$\frac{\partial p(t,x)}{\partial t} = Lp(t,x) \qquad (21)$$

where L is a linear operator. We require that at the boundary $p(t,x)$ satisfies

$$\frac{\partial p}{\partial n} + \rho \frac{\partial p}{\partial t} = 0 \qquad (22)$$

where $\frac{\partial p}{\partial n}$ is the normal derivative of p and the value of $\rho \frac{\partial p}{\partial t}$ is taken to be the limit as one approaches the boundary from inside. This is a form of mass balance. Since no concentration is permanently adsorbed, the outflow at the boundary $\frac{\partial p}{\partial n}$ is determined by the loss with respect to time of the concentration near the boundary $\rho \frac{\partial p}{\partial t}$. The usual no flow conditions correspond to $\rho = 0$, which says nothing is even temporarily stored at the boundary.

Formally, we can also write (22)

$$\frac{\partial p}{\partial n} + \rho L p = 0 \qquad (23)$$

The Fokker-Planck equation with these boundary conditions seems not to be well studied, but there is some work for the SDE approach. One of the most fundamentally useful results concerning the sticky boundary conditions is the relationship between solutions of SDE which are the same except for the boundary stickiness. Specifically Graham, 1988 showed [theorem 1.7] that if one has two measures ρ, $\bar{\rho}$, and one is subordinate to the other, that is one has $\rho \leq \bar{\rho}$ then solving the SDE for ρ immediately gives a solution for $\bar{\rho}$, but run with a different "clock" or "time change". More precisely the theorem states that if (X_t, K_t, ρ) is the solution of (10-19) and we let $A_t = t + \int_0^t (\rho - \bar{\rho})(X_s) dK_s$ be an increasing function with inverse A_t^{-1} then $\overline{X}_t = X_{A_t^{-1}}$ and $\overline{K}_t = K_{A_t^{-1}}$ solves the SDE for $\bar{\rho}$. A particular example is taken by letting $\rho = 0$ which is subordinate to any measure of stickiness. Practically this means that solving the reflecting boundary condition and keeping track of the local time allows one to study the sticky boundary problem. This "time change" is important also from a numerical point of view in that it says to approximate the SDE with a random walk model one needs to generate a reflected random walk but with a random insertion of time when it hits the boundary. The reflecting boundary condition has been numerically studied in the case of the half plane by Lepingle (1996) where an Euler scheme with good convergence rate is given. We generalize to other domains this scheme by considering them as approximately polygonal. The distribution for the inserted time can be freely set, but necessarily depends on the time step involved due to the rapidly fluctuating behavior of a Brownian motion (the local time is not differentiable).

In particular the complex behavior remarked upon by McCaulou (1994) can be produced if the inserted time is a mixture of a highly probable small time and a less likely large time. This type of behavior is homogenized at large times and an average or expected residence time is necessary to use when upscaling. Another important characteristic of stickiness is that it depends

on location and time so that by modeling it as depending on local chemistry one can produce a behavior for microbes which mimics active "attachment/detachment", something not previously recoverable. A possible model for an initial distribution of the stickiness as a function on the boundary could be given as random function in which a covariance structure is given. This then gives rise to a stochastic partial differential equation for evolution problems which have been the subject of much recent investigation (see e.g. Cushman 1997), the situation which first interested us was modeling of bacterial attachment through a flow chamber, the upper part of which is formed by a treated slipcover (McEldowney and Fletcher 1998), so in this case a constant on this part of the boundary and a smaller constant on the rest of the boundary.

3.2. The Stickiness

We collect here some analytic results which are useful in determining how to parameterize ρ, as well as some of the limiting behavior of random walks.

We first show that for a time discretized process to have a positive amount of time on the boundary that

$$\frac{\varepsilon}{(1-\varepsilon)^2} = \frac{\rho}{\sqrt{\Delta t}} \tag{24}$$

where ε is the probability of staying on the boundary. From the central limit theorem or the basic properties of Brownian Motion (Protter 1992) the time-scale versus displacement scale is $B_{st} = \sqrt{s}B_t$. This means that if one discretizes the random walk in time and space and time steps are divided as Δt then the corresponding space discretization should be on the order of $\sqrt{\Delta t}$, so for example if dividing time into intervals of length 0.01 one should divide space into intervals of length 0.1. Now if a random walk on the points $\{0, \Delta t, 2\sqrt{\Delta t} \ldots\}$ is at 0 at time zero and stays

at zero with probability ε and if not at zero goes up or down $\sqrt{\Delta t}$ amount with probability 0.5, then one can ask how much time is the random walk at zero on the time interval $\{0, \Delta t, 2\Delta t, ..., \frac{n}{\Delta t}\Delta\}$ that is on $[0, n]$ where n is some large time.

The first question of interest is what is the distribution of the time that it takes for a bacteria executing a Brownian motion to first attach to a flow tubes' boundary. If we assume that the flow is slow relative to the length of the flow tube then the answer is given by integrating the transition density. That is if we let $P(\tau > t)$ denote the probability that a microbe entering a flow cell has not hit the wall by time t, then with D as the cross-sectional area of the flow cell one has

$$P(\tau > t) = \int_D p(t, 0, y) \, dy = \int_D \sum_{n=1}^{\infty} e^{-\lambda_n t} \phi_n(0) \phi_n(y) \, dy$$

$$= \sum_{n=1}^{\infty} e^{-\lambda_n t} \phi_n(0) \int_D \phi_n(y) \, dy = \sum_{n=1}^{\infty} c_n e^{-\lambda_n t}$$

(25)

where ϕ_n are Bessel functions, λ_n are zeroes of Bessel functions and c_n are the integrals of the Bessel functions all of which have been well tabulated. Notice that the long time asymptotics are determined by the leading order term in t.

If we don't assume that the velocity is slow relative to the length of the flow cell then there is a chance that a microbe might never hit the boundary before exiting. The probability of this event happening is approximately given (again letting D be the cross section)

$$P(\tau > t) = P(\tau_D > t \text{ or } \tau_{end} < t)$$

$$\approx P(\tau_D > t) + P(\tau_{end} < t)$$

(26)

The first of these is calculated as before and the latter can be approximated by a volume averaged one-dimensional stochastic process.

Another question of interest is the expected amount of time a microbe spends on the wall. This is given by

$$\langle \tau_{wall} \rangle = \langle \rho K_t \rangle \text{ the local time of the process}$$

$$= \rho \langle K_t \rangle \approx \rho \frac{|\partial \Omega|}{|\Omega|} \langle T \rangle \qquad (27)$$

$$= \rho \langle K_t \rangle \approx \rho \frac{|\partial \Omega|}{|\Omega|} \frac{length}{\langle v \rangle}$$

Here T is the time inside the flow cell.

The final question we are interested in is what is the distribution of the time on the wall for a microbe in a flow chamber given that it stars on a wall. This is an important question since if one is interested in introducing genetic information into a microbial community the transfer of genes takes place when microbes come into contact, a process most likely to occur on boundaries. With $\tilde{\tau}$ representing the amount of time on the boundary we want

$$P\left(\tilde{\tau} > t \mid \tilde{\tau} > 0\right) \approx P\left(K_T > \frac{t}{\rho}\right)$$

$$\approx P\left(K_{\frac{length}{\langle v \rangle}} > \frac{t}{\rho}\right) \qquad (28)$$

This last quantity is finally calculated (using equation 32) as the square root of an exponential distribution.

3.3. Numerical Considerations

At this point we would like to discuss how to numerically implement random walk models to solve transport problems with sticky boundaries. In the homogenized version where the boundaries are not visible, this is essentially a convection-diffusion-reaction (CDR) equation. Traditionally this is solved by a particle tracking scheme (Valocchi 1989) which in each instant calculates probabilities of adsorption/desorption, measures the amount of time (random) in each

phase (sorbed or desorbed) and then performs the random walk only on that portion of time in the desorbed phase. For fast reactions the constant generation of random variables (for small time steps) becomes prohibitive and Valocchi proposes to assume that on any fraction of time a fixed proportion is spent in either phase and then performs a random walk on the relative portion in the desorbed phase. Unfortunately this just has the effect of retarding the flow, that is changing its clock. A more uniform approach suggested by the above analysis of sticky diffusion as a basis for CDR suggests not only should a random displacement take place at each step, but also a random amount of time should be inserted into the clock.

There is not a lot of work for random walks with nonadsorbing boundaries in general and the added condition of wanting to keep track of the local time for a reflecting boundary (to be used for the random time insertion) leaves even fewer. In a paper of Lepingle an Euler Scheme for reflected SDE is proposed which is not based on projecting an escaped particle back into a domain, but is instead based on generating random variable with the same distribution as the local time of the process and using these extra variables to keep the process inside.

The basic scheme of approximating the reflecting SDE on $(0,\infty)$ with a continuous random walk, is

$$dX_t = \sigma(X_t)dW_t + \bar{b}(X_t)dt + dK_t \text{ on } (0,\infty) \tag{29}$$

or in a half space

$$X_0 = x_0 \tag{30}$$

$$Y_{t+\Delta t} = b(X_t)\Delta t + \sigma(X_t)W_{\Delta t} \tag{31}$$

$$K_{t+\Delta t} = K_t + \max\left(0, -X_t + \frac{\sqrt{\sigma(X_t)^2 V + Y_t^2} - Y_t}{2}\right) \tag{32}$$

99

$$X_{t+\Delta t} = X_t + Y_{t+\Delta t} + \gamma \left(K_{t+\Delta t} - K_t \right) \tag{33}$$

Here $W_{\Delta t}$ is a Gaussian random variable with mean zero and variance Δt and V is distributed as an exponential with mean $2\Delta t$. The reason that this scheme approximates correctly a reflected diffusion is that reflection in a line is a simple matter of taking any continuous function and adding another function which together always stays positive (the Skorohod problem see Lepingle 1989). This so called Shorohod problem in the case of random walk Brownian motion is determined by the infinum of the process which in turn is given as an exponential random variable of the type discussed. In a half space each component has a covariance matrix for the dispersion, but this does not change the scheme much. A way of simulating flow through a two dimensional tube with reflecting boundaries is to make the time step small enough so that one cannot during that interval hit both boundaries, then treat the problem only locally, that is one can keep track of a separate local time at each boundary and adjust the random walk accordingly. An obvious problem with this scheme is that it cannot be readily extended to other types of bounded domains in 2 dimensions, much less to a circular capillary in 3 dimensions which are of interest.

The simulation of a sticky process follows the above scheme except that the sets of points making up the trajectories for one realization (t, X_t) are replaced with $\left(t + \int_0^t \rho(X_s) dK_s, X_s \right)$.

If one is interested in the position of a particle at a particular time τ it can be had by finding the time t for which $A_t = \tau$. One usually knows in advance the times of interest and can simply calculate the time t when if first surpasses τ. First passage times are especially easy since one knows the position the particle is at when the time is reached and hence one need only keep track of A_t.

An alternative to this approach, which has "time marching", that is a strick discretization of time is used to construct a simple random walk, which upon hitting the boundary sticks, and then desorbs from the boundary with a probability say ε. However, to capture the boundary behavior of continuous diffusions, which have infinite variation, with a discrete process requires a dependence of ε on the time step. It can be shown that the appropriate order for ε takes the form of

$$\frac{\varepsilon}{\left(1-\varepsilon\right)^2} = \frac{\rho}{\sqrt{\Delta t}} \tag{34}$$

That is as $\Delta t \rightarrow 0$, $\varepsilon \rightarrow 1$. So that a large effort is made in calculating almost certain events. Moreover it is well known that a Poisson random variable is the limit of appropriately scaled binomial random variables (see DeGroot 1980) and so the first exit from a wall is given by the distribution of the interarrival times of a Poisson which has an exponentially decaying distribution. This means that upon averaging the two approaches are equivalent.

For a circular domain with no drift one can write the Laplacian in polar coordinates, that is the Euclidian process X_t, Y_t can be thought of as the product of a radial process R_t and angular process Θ_t. This corresponds to a skew product decomposition of Brownian motion where the radial process satisfies the stochastic differential equation

$$dR_t = \frac{1}{2R_t} dt + dW_t \tag{35}$$

together with reflection on the boundary. While the angular process of interest satisfies

$$d\Theta_t = \frac{1}{R_t^2} dB_t \tag{36}$$

where W_t is a Brownian motion on the line (1 dimensional random walk), and B_t is a Brownian motion on the unit circle. One can now apply Lepingle's ideas to the radial process without

101

much trouble. The angular process can be thought of as taking place on the real number line and then mapped onto the circle. The coefficient of its dispersion, $\frac{1}{R_t^2}$, can be integrated approximately by taking the average of $\frac{1}{R_t^2}$ and $\frac{1}{R_{t+\Delta t}^2}$.

In more complicated polygonal like domains one can perform a decomposition of the domain into overlapping wedges (cones), keep track of the particles position relative to the decomposition and near the boundary reflect the angular part alone. The transition probabilities for random walks in such domains are symbolically given by (35) and (36) but have been studied in the context of heat conduction for decades, e.g. (Carslaw and Jaeger 1959). The actual displacement in euclidean coordinates is not transferred easily into polar coordinates. Instead a random displacement radically is first generated by (35) and then a random angular displacement generated by (36) where however the variance of the angular change necessarily depends on the radial distance. In a general bounded domain one can approximate the boundary polygonally and allow the number of sides to increase.

3.4. Discussion and Summary

We have presented an analytic model for the transport of microbial populations in a porous medium which incorporates the attachment behavior. The stochastic differential equation model assumes fast attachment/detachment for the microbes but the numerical implementation outlined allows a general probability distribution to be chosen as a time scale and hence one can use interpolation. The model can be easily used in situations where porous media are modeled as collections of tubes, e.g. networked models or stream-tube ensembles as in Ginn et al. (1995). The numerical scheme discussed extends the work of Lepingle on simulation of normally reflected processes, in two directions. First "sticky or slowly reflected" conditions are added to allow one to add microbial-boundary interactions as parameters in the transport problem and

second one can model reflections in nonrectangular domains such as capillary tubes. Using this scheme one can also study the small and intermediate time behavior of transport in capillary tubes which has been previously studied for large times using various forms of homogenization (Bhattacharya and Gupta 1984).

4. Fractional Dispersion of Microbes

4.1. Introduction

Quantitative research in fate and transport processes occurring in the natural subsurface commonly deals with transformations associated with complex chemical and/or microbiological reaction networks (cf. *Murphy et al.*, 1997; *Chilakapati et al.*, 1998; *Lichtner et al.*, 1996; and Transport in Porous Media, Vol. 38, Nos. 1-2, 2000), in the presence of multiscale heterogeneities in physical, chemical, and microbiological properties. Yet even the simple setting wherein a conservative tracer is transported in a physically heterogeneous environment is not well quantified from a theoretical perspective, and sophisticated analyses of the phenomenon continue to proliferate in the physics and hydrology literature. Much attention has been and continues to be focused on the development of governing integro-differential equations for the expectation of conservative solute concentration undergoing advective-dispersive transport in flow fields that are nonuniform on multiple scales. Recently, researchers have developed a fractional advection-dispersion equation approach to describe this phenomenon (e.g., *Meerschaert et al.*, 1999; *Benson et al.*, 2000). This approach shows promise in its ability to represent so-called anomalous, or non-Fickian, dispersive fluxes that may describe expected concentration plume evolution in natural media. Here we relate the fractional ADE to the nonlocal dispersive constitutive theory (*Cushman and Ginn*, 1993), by demonstrating that the fractional ADE is obtained as a well-defined special case of the convolution-Fickian form of the nonlocal dispersion equation, which is itself a special case of the general form presented in *Cushman and Ginn* (1993).

4.2. A Hierarchy in Complexity of Fluxes

The nonlocal dependency of flux on constitutive properties is described by Cushman (*Cushman*, 1990, Introduction) as a manifestation of the occurrence of a continuum of scales of heterogeneity and its effect on velocity. In constitutive models nonlocality is manifest in one of two forms: fluxes which are given as integrals on space/ time (integral theories), or fluxes which involve derivatives higher than the first (gradient theories). *Simmons and Kincaid* (1987) provide one of the first examples of gradient theory representations of transport in hydrology, writing a Lagrangian transport equation involving an infinite series of spatial derivatives of the Lagrangian velocity distribution function. Because our interest here is in fractional dispersion, we restrict our discussion to the integral theories. The conventional Fickian (local) constitutive theory maintains that the dispersive flux at a point in space is proportional to the gradient of the expected tracer concentration at that point. That is,

$$\mathbf{q} = \mathbf{D} \cdot \nabla C \tag{37}$$

where $\mathbf{D}$ is a positive-definite tensor.

The generalization to nonlocal constitutive theory holds that the diffusive/dispersive flux at a point in space depends on the conditions in some larger neighborhood of the point in space-time. In this formulation the flux at a point (x,t) is given as a weighted average of concentration gradients in this larger neighborhood. *Cushman* (1991) first developed a general nonlocal theory of diffusion in media with evolving heterogeneity using an equilibrium statistical mechanical approach. The resultant diffusive flux is of convolution form

$$\mathbf{q}(\mathbf{x},t) = -\int_{0}^{t} \int_{R^3} \mathbf{D}(\mathbf{y},\tau) \cdot \nabla_{x-y} C(\mathbf{x}-\mathbf{y},t-\tau) d\mathbf{y} d\tau \tag{38}$$

In a subsequent article *Cushman and Ginn* (1993) generalized this result to provide a nonlocal constitutive theory for dispersive flux in a local-equilibrium statistical mechanical setting. The flux in this case takes the form

$$q(x,t) = \langle v \rangle C - \int_0^t \int_{R^3} D(y,\tau,t) \cdot \nabla_{x-y} C(x-y,t-\tau) dy d\tau \qquad (39)$$

In a later article (Cushman et al., 1994), a more general fully non-equilibrium flux was derived using nonequilibrium statistical mechanical arguments. In this general case the resultant flux is

$$q(x,t) = \int_0^t \int_{R^3} D_1(y,\tau) C(x-y,t-\tau) dy d\tau + \langle v \rangle C$$
$$- \int_0^t \int_{R^3} D_2(y,\tau;t) \cdot \nabla_{x-y} C(x-y,t-\tau) dy d\tau \qquad (40)$$

In these two general forms the nonlocal dependence of the dispersive flux appears in an integral form that is not a convolution on time, but it is always a convolution on space. However under certain constraints the integral form (e.g. in Eq. 39) is a convolution on time, in which case Eq. 39 becomes

$$q(x,t) = \langle v \rangle C - \int_0^t \int_{R^3} D(y,\tau) \cdot \nabla_{x-y} C(x-y,t-\tau) dy d\tau \qquad (41)$$

In this form the dispersion tensor arises as a function of the spatial and temporal lag intervals only, and the resulting dispersive flux is a convolution integral. Nonlocality in the dispersive flux of Eq. 41 is manifest as a convolution of a generalized dispersion tensor with the concentration gradient and so it is called "convolution-Fickian". In this case the dispersion tensor is a weight function conveying the spatiotemporal "memory effect" of concentration gradients in a possibly infinite neighborhood to the dispersive flux at the local point (x,t). This dispersion tensor is known as the memory kernel.

106

A more detailed discussion of these fluxes is summarized in Chapter 2 of *Cushman* (1997).

4.3. The Fractional ADE

Over the last decade there has been considerable effort directed to the study of anomalous diffusion and dispersion in transport domains exhibiting power law scaling rules. One route that has received particular attention involves generalizing the classical advection dispersion equation, which involves classical integer spatial derivatives, to an equation involving fractional derivatives, i.e., derivatives of noninteger power α. The resulting solute mass balance equation can be written as

$$\frac{\partial C}{\partial t} = -\nabla \cdot \mathbf{v}C + \nabla \cdot \left(\mathbf{D}_1 \cdot \nabla_x^{\alpha-1} + \mathbf{D}_2 \cdot \nabla_{(-x)}^{\alpha-1} \right) C \tag{42}$$

where $\alpha \left(1 \leq \alpha \leq 2 \right)$ is the order of the fractional derivative, and where it is common to write $\mathbf{D}_1 = p\mathbf{D}$ and $\mathbf{D}_2 = (1 - p)\mathbf{D}$ with $0 \leq p \leq 1$. The right-hand side of this expression can be written as the gradient of the total flux q, which is then

$$\mathbf{q}\left(\mathbf{x}, t \right) = \mathbf{v}C - \mathbf{D}_1 \cdot \nabla_x^{\alpha-1}C - \mathbf{D}_2 \cdot \nabla_{(-x)}^{\alpha-1}C \tag{43}$$

The purpose of this note is to show that Eq. 43 is in fact a special case of the convolution-Fickian flux appearing in Eq. 41, and as such, the fractional ADE is a special case of the nonlocal transport theory of *Cushman and Ginn* (1993) or *Cushman et al.* (1994). We henceforth restrict our attention to a one-dimensional setting and for simplicity set $p = 1$. The analysis can be carried over to arbitrary p and in 3-D, but it adds little to our discussion, so we omit it here (see *Cushman and Ginn*, 2000 for a much more detailed discussion).

Transformation of the Fractional Flux to Convolution Form. In 1-D with $p = 1$ and

$1 < \alpha \leq 2$ the fractional derivative $\frac{d^\alpha}{dx^\alpha}$ is defined as

$$\frac{d^\alpha f(x)}{dx^\alpha} = \frac{1}{\Gamma(n-\alpha)} \frac{d^n}{dx^n} \int_0^\infty \frac{f(x-y)}{y^{\alpha+1-n}} dy \tag{44}$$

with n the smallest integer larger than α. In this case n = 2 and so

$$\begin{aligned}
D\frac{d^\alpha C}{dx^\alpha} &= \frac{d}{dx} \int_0^\infty \frac{D}{\Gamma(2-\alpha)y^{\alpha-1}} \frac{dC(x-y)}{dx} dy \\
&= \frac{d}{dx} \int_0^\infty \frac{D}{\Gamma(2-\alpha)y^{\alpha-1}} \frac{dC(x-y)}{d(x-y)} dy \\
&= \frac{d}{dx} \int_0^t \int_{-\infty}^\infty \frac{D\delta(\tau)H(y)}{\Gamma(2-\alpha)y^{\alpha-1}} \frac{dC(x-y,t-\tau)}{d(x-y)} dy d\tau
\end{aligned} \tag{45}$$

where $\delta(\tau)$, $0 \leq \tau \leq t$, is the Direct Delta and $H(y)$ is the Heaviside function on $(0,\infty)$.

Finally, define $D(y,\tau)$ by

$$D(y,\tau) = \frac{D\delta(\tau)H(y)}{\Gamma(2-\alpha)y^{\alpha-1}} \tag{46}$$

so that

$$D\frac{d^\alpha C}{dx^\alpha} = \nabla_x \int_0^t \int_{-\infty}^\infty D(y,\tau) \nabla_{x-y} C(x-y,t-\tau) dy d\tau \tag{47}$$

Thus Eq. 43 is equivalent to Eq. 41 with $D(y,\tau)$ defined by Eq. 46 in the 1-D case. That is, in

the fractional dispersion case, the flux q, is given by

$$\begin{aligned}
q(x,t) &= -\int_0^t \int_{-\infty}^\infty D(y,\tau) \cdot \nabla_{x-y} C(x-y,t-\tau) dy d\tau + \langle v \rangle C \\
&= -\int_0^t \int_{-\infty}^\infty \frac{D\delta(\tau)H(y)}{\Gamma(2-\alpha)y^{\alpha-1}} \nabla_{x-y} C(x-y,t-\tau) dy d\tau + \langle v \rangle C
\end{aligned} \tag{48}$$

Thus the fractional ADE is a particular form of the nonlocal ADE, when the memory kernel of the nonlocal form is given by Eq. 46. Some particular aspects of this kernel are physically meaningful. Firstly, the Dirac-delta function serves to localize the flux in time (i.e. it makes the flux Markovian), so that the ADE is only spatially nonlocal. Secondly, the Heaviside serves to restrict the nonlocality in space to positive values of y, which corresponds to an upstream nonlocal domain, x - y, appearing in the integer-ordered space derivative on C. Thus in this case the ADE is nonlocal in the upstream sense. Finally, aside from these two generalized functions, the kernel is inversely proportional to y raised to a power below unity. This weighs the contributions (to the local dispersive flux) of the nonlocal C-gradient, in inverse proportion to the contribution to the dispersive flux. Finally note that in the limiting case where $\alpha \to 1$ this particular nonlocal form reduces to the local first-order derivative (by the fundamental theorem applied to the last term in Eq. 45).

4.4. Summary

The quantitative representation of anomalous dispersion continues to be an unresolved research question in a number of fields, and the explanation of anomalous dispersion is an active field of study in physics, fluid mechanics, and hydrology. Recent results on fractional dispersion are special cases of earlier representations of anomalous dispersion using the convolution-Fickian constitutive theory, which itself is a particular case of nonlocal transport theory. This mathematical equivalence between the fractional derivative and a special nonlocal form implies the physics underlying the former constitutive theory are embedded in the more general nonlocal transport theories. In both cases researchers are investigating the role played by long-range correlations in hydraulic properties.

5. The Effect of System Boundaries on the Upscaling the Flow Problem

5.1. Introduction

Predicting the evolution of microbes in the subsurface and understanding various degradation scenarios associated with their movement, requires knowledge of the role macroscopic system boundaries play in the process. Uncertainty in this boundary data is the rule rather than the exception (as for example the role of rainfall time series). To begin to understand these sinergies we have analysed a stochastic upscaling method for the flow problem with uncertain boundary conditions. Specifically we have studied steady flow through a heterogeneous medium in a bounded domain using a recursive perturbation scheme. Details of this study are found in Bonilla and Cushman (2000a) and the appendix to this report.

We have analyzed the head and velocity moments for a two-dimensional bounded domain (rectangular) in heterogeneous media. Boundary conditions were modeled as the sum of deterministic and stochastic components. This allows for a scheme that permits more elaborate computations than previously studied. We studied the effects of two sets of boundary conditions, deterministic and stochastic, on the fluctuating head which drives the random flow process. The major conclusions are:

1. Randomness (or lack of) of hydraulic controls at domain boundaries significantly affects head and velocity moments. Effects of processes at boundaries are not confined to boundary layers; the head and velocity moments are perturbed everywhere in the domain.

(a) The head variance function is most sensitive to this effect, with differences of up to one order of magnitude. That the effect is not confined to differences within boundary layers can be observed by comparing the central regions which differ by factors varying from 3 in the

longitudinal direction to 10 in the transverse direction. A consequence of this is, the inverse problem may be ill posed if boundary conditions are modeled inadequately.

(b) Velocity variances are less sensitive to stochastic boundary conditions yet differences are present. When comparing longitudinal velocity variances there are differences of a factor of 2 in regions of small zero order-gradient (center of domain), and of a factor of 1.2 to 1.5 within boundary layers. For transverse velocity variances, differences are more important along the boundaries $y = H$ and $y = 0$. The term mostly accountable for this difference is the variance in the fluctuating-head gradient.

The mean head and mean head gradient in both cases differ very little from their zero order counterparts (both cases have the same zero order solution).

2. Perturbation schemes are formally valid for $\sigma_f^2 \ll 1$. However numerical experiments show more robust behavior $\left(\text{convergence with } \sigma_f^2 \geq 1\right)$. Here we show convergence of perturbation schemes relies also on the magnitude of the kernels describing the problem. While the magnitude of heterogeneity plays a role in convergence, the dynamics of each problem, and in particular the boundary conditions will determine the convergence limits for the problem. The milder the gradients present, the larger σ_f can be within the scheme. Dirichlet boundary conditions for the fluctuation h_1 improve convergence, while Neumann boundary conditions (for h_1) decrease the degree of allowable heterogeneity.

3. Generally there is a boundary layer from 3 to 4 integral scales for Dirichlet boundary conditions, and at least 7 to 8 integral scales for mixed Dirichlet and Neumann boundary conditions. Mean velocity differs up to 30 percent from the zero order velocity within the boundary layers, a phenomena that should induce greater mixing when a contaminant is entering through the boundary.

4. Inhomogeneity in head and velocity second moments arises for two reasons: boundary type, and spatially varying zero-order gradients. Both affect the value of the moments across the domain. The first gives rises to a boundary layer. The second manifests itself in inhomogeneity everywhere in the domain. This is of particular relevance when recharge is present at one of the boundaries. For a flow with constant zero order head gradient, first order Dirichlet boundary conditions render approximately homogeneous head and velocity covariance functions beyond 3 to 4 integral scales away from the boundaries. Under the same circumstances, first order Neumann boundary conditions cause inhomogeneity over 3 to 8 integral scales. However gradients applied in the direction normal to a Neumann boundary do not induce inhomogeneity in that direction.

5. Nonlocality acts in different ways according to the type of boundary condition. For the head variance, effects of nonlocality for Neumann boundary conditions are more important and localization renders large errors. Nonlocality for Dirichlet boundary conditions acts within smaller distances than for the Neumann case. Localization is a more suitable option in the former case.

Finite difference schemes (Tartakovsky and Mitkov preprint) have been found to be more efficient in computing head and velocity moments than integral evaluation. However, the integral evaluation is useful for analyzing the various directional contributions of the physics to the moments and gives more insight into the problem of fully two and three dimensional flow and nonconstant gradients.

Careful determination of the nature of processes occurring at boundaries is important to an adequate interpretation of laboratory and field flow and transport problems. Randomness in observed variables is due to both the media's heterogeneity and the surrounding environment

fluctuations (or lack of). The former cannot be reliably estimated without a reasonable model for the later in the context of inverse problems. Nonstationary analysis of the transport problem based on the results presented here for the flow problem is especially relevant for natural gradient experiments where mixing is different within boundary layers, or in presence of vertical and or transverse head gradients.

6.   The Role Played by Various Macroscopic Length Scales on Flow and Transport

6.1.   Introduction

For steady flow in a nondeformable heterogeneous aquifer where σ_f (the fluctuating

log-conductivity standard deviation) is often used as a perturbation parameter, a closed form for

the head can be obtained to $0\left(\sigma_f^2\right)$. Mathematically, the expansion appears to require $\sigma_f^2 < 1$ for

convergence of the expansion. Yet the schemes often work for $\sigma_f^2 > 1$ (cf. Dagan, 1989;

Cushman, 1990; Gelhar, 1993; Cushman, 1997). In this case, disparate length scales (domain

size, anisotropic integral scales, etc.) might explain the robust character of the perturbation

scheme.

There exists extensive research on perturbation solutions to the stochastic flow problem

(see references above). But it is not known how large σ_f can be and yet have a convergent

expansion. For example, Hassan et al. (1998) have reported that small integral scales generate

very slow convergence and sometimes instability in the solution to stochastic flow via Monte

Carlo simulations, even using small values of σ_f. Other researchers (e.g., Hsu et al., 1996;

Zhang and Winter, 1999) have shown this to hold for $\sigma_f^2 = 4.38$. The work presented below

addresses, convergence, and clarifies a commonly misunderstood issue. Further, the parameter

bounds provided here offer a quick way to assess the magnitude of terms of higher order.

Because the processes f and ∇f can often be considered independent, further assumptions on

∇f are necessary. In particular, when the two point correlation function for the conductivity is

assumed to be exponential or Gaussian, it is possible to estimate the magnitude of $\sigma_{\nabla f}$ in terms

of σ_f and various other length scales. The ratio, ρ, of the integral scale in the main direction of

flow, λ, to the total domain length, L, plays an important role in the convergence of the perturbation scheme. For $\rho > \rho_c$, $\varepsilon = \sigma_f / \rho^3$ is the most appropriate for 2-D flow. Here ρ_c is a critical length scale. In addition, the shape of the log-conductivity fluctuation covariance, and boundary conditions influence the convergence of the scheme.

6.2. Example: 2D-Flow

The one dimensional analysis of the previous section sets the stage for the two dimensional problem. We concentrate on bounding the head variance using L^2 convergence. Therefore all the norms below are L^2, that is read $\| \ \|_2$ where $\| \ \|$ is found.

The balance law in 2-D is

$$\frac{\partial f}{\partial x_i'} \frac{\partial h'}{\partial x_i'} + \frac{\partial^2 h'}{\partial x_i' \partial x_i'} = 0 \quad \mathbf{x}' \quad \Omega' \tag{49}$$

The primed notation $\mathbf{x}' = (x_1', x_2')$ (the x_i' has length units) has been introduced for convenience, so that after scaling, a non-primed system, $\mathbf{x}$, is obtained. Introduce the dimensionless system $\mathbf{x} = (x, y)$ with $x = \frac{x_1'}{\sqrt{\lambda_x L_x}}$ and $y = \frac{x_2'}{\sqrt{\lambda_y L_y}}$ where λ_x and λ_y denote the integral scales in the two directions of the unscaled system $((x_1', x_2') = (x', y'))$, and L_x and L_y are the side lengths of a rectangular domain $\Omega' = [(0, L_x)(0, L_y)]$. As in the one dimensional case, the goal is to obtain a dimensionless head that is independent of the length scales of the problem. To make a judicious scaling, it is important to consider gradients in both directions, x, and y. However, for environmental applications it is common to study the case for which mean flow occurs in one direction (say x direction). General mean head gradients with non zero components in both directions and space dependence have been analyzed by Bonilla and Cushman (1999) for steady

saturated flow and by Zhang (1999) for transient unsaturated flow. From their analysis the most

convenient scaling for the hydraulic head is $h = \frac{h'}{L_x}$ where x is the dominant direction of flow.

With this scaling, (49) becomes

$$\xi^2 \frac{\partial^2 h}{\partial x^2} + \frac{\partial^2 h}{\partial y^2} = -\xi^2 \frac{\partial f}{\partial x}\frac{\partial h}{\partial x} - \frac{\partial f}{\partial y}\frac{\partial h}{\partial y} \tag{50}$$

where $\xi^2 = \frac{\lambda_y L_y}{\lambda_x L_x}$ is the square of a modified anisotropy ratio, ξ. Define $\rho_x^2 = \frac{\lambda_x}{L_y}$, and $\rho_y^2 = \frac{\lambda_y}{L_y}$.

Then ξ can be written as $\xi = \frac{\rho_y L_y}{\rho_x L_x}$. Equation (50) must be supplemented with boundary

conditions (BC's), and they may be stochastic or deterministic. These may be Dirichlet,

Neumann or mixed. We consider stochastic Dirichlet and Neumann:

$$h = h^D \qquad \mathbf{x} \; \varepsilon \; \Gamma_D \tag{51}$$

$$-K\frac{\partial h}{\partial \eta} = q \qquad \mathbf{x} \; \varepsilon \; \Gamma_N \tag{52}$$

where h^D is random dimensionless head on Dirichlet boundary Γ_D, $h^D = \frac{h'^D}{L_x}$, and q is random

scaled recharge through Neumann boundary Γ_N with outward unit normal η, $\eta = x$ or $\eta = y$ for

the rectangular domain being considered. $q = q'\rho_x$ if $\eta = x$, and $q = q'\rho_x\xi$ if $\eta = y$.

After this scaling, the two point conductivity fluctuation (multi-Gaussian) is

$$R_{ff}\left(\mathbf{x} - \mathbf{u}\right) = \sigma_f^2 \exp\left(-\frac{(x-u)^2}{\rho_x^2} - \frac{(y-w)^2}{\rho_y^2}\right) \tag{53}$$

with points $\mathbf{x} = \left(x, y\right)$, and $\mathbf{u} = \left(u, w\right)$. The above Poisson equation (50) involves an 'anisotropic'

Laplace operator in the left hand side and a non-zero fluctuation in the right hand side. We use

two parameters for the perturbation expansion, $\sigma_{\nabla fx}$ and $\sigma_{\nabla fy}$

$$\left\|\frac{\partial f}{\partial x}\right\| = \sigma_{\nabla fx} = \frac{\sqrt{2}\sigma_f}{\rho_x} \tag{54}$$

116

$$\left\| \frac{\partial f}{\partial y} \right\| = \sigma_{\nabla fy} = \frac{\sqrt{2}\sigma_f}{\rho_y} \tag{55}$$

Consider the case in which the mean flow is in the x direction, and suppose $\sigma_{\nabla f} = \sigma_{\nabla fx}$.

By substituting the expansion $h = h_0 + h_1 + h_2 + \dots$, with $h_n = O(\sigma_{\nabla f}^n)$ into equations (51) and (52), and separating terms of order $n = 0, 1, 2, \dots$ we obtain the hierarchy of equations

$$O(1): \qquad \xi^2 \frac{\partial^2 h_0}{\partial x^2} + \frac{\partial^2 h_0}{\partial y^2} = 0 \tag{56a}$$

$$n \geq 1 \quad O(\sigma_{\nabla f}^n): \qquad \xi^2 \frac{\partial^2 h_n}{\partial x^2} + \frac{\partial^2 h_n}{\partial y^2} = -\xi^2 \frac{\partial f}{\partial c} \frac{\partial h_{n-1}}{\partial x} - \frac{\partial f}{\partial y} \frac{\partial h_{n-1}}{\partial y} \tag{56b}$$

with associated hierarchical boundary conditions

$$n \geq 0 \qquad h_n = h_n^D \qquad \mathbf{x} \; \varepsilon \; \Gamma_D \tag{57a}$$

$$O(1): \qquad -K_G \frac{\partial h_0}{\partial \eta} = q_0 \qquad \mathbf{x} \; \varepsilon \; \Gamma_N \tag{57b}$$

$$n \geq 1 \quad O(\sigma_{\nabla f}^n): \qquad -K_G \frac{\partial h_n}{\partial \eta} = q_n + K_G \left(\sum_{j=1}^{n} \frac{1}{j!} f^j \frac{\partial h_{n-j}}{\partial \eta} \right) \qquad \mathbf{x} \; \varepsilon \; \Gamma_N \tag{57c}$$

where the random boundary functions h^D and q have the expansions $h^D = h_0^D + h_1^D h_2^D + \dots$ and $q = q_0 + q_1 + q_2 + \dots$ as a result of the expansion for h. The zeroth order, deterministic problem by equations (56a), (57a), and (57b) has solution

$$h_0(x,y) = \int_{x' \varepsilon \Gamma_D} \left[h_0^D \left(x'', y'' \frac{\partial G(x,y|x'',y'')}{\partial x''} \right) \right] \Big|_{x' \varepsilon \Gamma_D} d\Gamma_D$$
$$+ \frac{1}{K_G} \int_{x' \varepsilon \Gamma_N} \left[q_0(x'',y'') G(x,y|x'',y'') \right] \Big|_{x' \varepsilon \Gamma_N} d\Gamma_N \tag{58}$$

117

where $\mathbf{x}''$ denotes an integration variable in the scaled system (not to confuse it with unscaled system previously denoted $\mathbf{x}'$), and the Greens function $G(\mathbf{x}, \mathbf{x}'')$ is obtained by solving the problem

$$\Delta_\xi G(\mathbf{x}, \mathbf{x}'') = \xi^2 \frac{\partial^2 G}{\partial x^2} + \frac{\partial^2 G}{\partial y^2} = \delta(\mathbf{x} - \mathbf{x}'') \quad \mathbf{x} \varepsilon \Omega$$

$$G(\mathbf{x}, \mathbf{x}'') = 0 \quad \text{for } \mathbf{x} \varepsilon \Gamma_D \tag{59}$$

$$\frac{\partial G(\mathbf{x}, \mathbf{x}'')}{\partial \eta} = 0 \quad \text{for } \mathbf{x} \varepsilon \Gamma_N$$

where $\delta(\mathbf{x} - \mathbf{x}'')$ is the two-dimensional delta function.

Problems of order $n \geq 1$ are prescribed by equations (56b), (57a), and (57c). The right hand side of the Poisson equation (56b) is a random forcing term. Using Greens functions the solution is

$$h_n = -\int\int_D G_n\left(x, y \middle| x'', y''\right)\left(\xi^2 \frac{\partial f}{\partial x''}\frac{\partial h_{n-1}}{\partial x''} + \frac{\partial f}{\partial y''}\frac{\partial h_{n-1}}{\partial y''}\right)dx''dy'' + h_{n_{bc}} \tag{60}$$

where $h_{n_{bc}}$ represents the boundary integrals incorporating the conditions given by equations (57a) with $n \geq 1$, and (57c). These are completely analogous to the boundary integrals presented in equation (58). When higher order $(n \geq 1)$ problems have homogeneous boundary conditions then $h_{n_{bc}} = 0$. The Greens function $G_n\left(x, y \middle| x'', y''\right)$ may be different for each n depending on the model for processes occurring at the boundaries.

Consider the case of flow in a rectangular scaled domain $\mathbf{x} \varepsilon \Omega = \left[\left(0, \ell_x\right)\left(0, \ell_y\right)\right]$, with all boundaries Dirichlet. Here $\ell_x = \frac{1}{\rho_x}$ and $\ell_y = \frac{1}{\rho_y}$. To simplify the analysis, consider deterministic boundary conditions, that is, $h_0^D \neq 0$, and $h_n^D = 0$ for $n \geq 1$. The zero order problem for the head is

$$\xi^2 \frac{\partial^2 h_0}{\partial x^2} + \frac{\partial^2 h_0}{\partial y^2} = 0 \quad x \varepsilon \Omega \tag{61a}$$

$$h_0 (x = 0, y) = J \tag{61b}$$

$$h_0 (x = \ell_{x,y}) = 0 \tag{61c}$$

$$h_0 (x, y = 0) = J(1 - \rho_x x) \tag{61d}$$

$$h_0 (x, y = \ell_y) = J(1 - \rho_x x) \tag{61e}$$

so that the flow is in the x direction, with constant gradient $\frac{\partial h_0}{\partial x} = -J\rho_x$. Equations (56b) with

homogeneous boundary conditions $h_n^D = 0$ for $n \geq 1$ complete the statement of the problem. The

Greens function for Dirichlet BC's may be represented as

$$G(x, y | x'', y'') = \frac{2}{\pi} \sum_{n=1}^{\infty} \frac{\sinh(\gamma_n x) \sinh(\gamma_n [\ell_x - x'']) \sin(\alpha_n y'')}{n \sinh(\gamma_n \ell_x)} \quad if \ 0 \leq y < y''$$

$$\tag{62}$$

$$G(x, y | x'', y'') = \frac{2}{\pi} \sum_{n=1}^{\infty} \frac{\sinh(\gamma_n x'') \sinh(\gamma_n [\ell_x - x]) \sin(\alpha_n y) \sin(\alpha_n y'')}{n \sinh(\gamma_n \ell_x)} \quad if \ y'' < y \leq \ell_x$$

where $\alpha_n = \frac{n\pi}{\ell_y}$ and $\gamma_n = \frac{\beta_n}{\xi}$. The above Greens function includes the nonlocal anisotropy, that

without scaling is manifest only in the two point correlation functions for log conductivity

fluctuations, R_{ff}. After the scaling, both the Greens function and R_{ff} are anisotropic with a

different anisotropy ratio, as shown by equation (53).

A solution is obtained for the $O(\sigma_{vf}^2)$ head covariance. First use an exponential two

point correlation function (also named separated exponential in the literature)

$$R_{ff}(\mathbf{x} - \mathbf{u}) = \sigma_f^2 \exp\left(-\frac{|x - u|}{\rho_x} - \frac{|y - w|}{\rho_y} \right) \tag{63}$$

119

The resulting expression is computed using numerical integration techniques including Gaussian quadrature, Romberg integration, and importance sampling. Importance sampling is used to decrease the number of sample points. For instance, equations (63) and (53) suggest that if one integrates first over $u(w)$, for a fixed $x(y)$, one can restrict the sampling points to a region (interval in u) where $\exp\left(-\frac{|x-u|}{\rho_x}\right)\left(\exp\left(-\frac{|y-w|}{\rho_y}\right)\right)$ is not negligible (exponential case). Likewise, Greens function (62) has a singularity when $y \rightarrow y''$, and $x \rightarrow x''$. To address this singularity, when integrating over $x''(y'')$ for $x(y)$ fixed, it is useful to divide the integration interval $[0,\ell_x]([0,\ell_y])$ in two subintervals $[0,x]$ and $[x,\ell_x]([0,y]$ and $[y,\ell_y])$. The subintervals are best handled using Romberg integration excluding the right and left points respectively, where the singularity is found. Once it has been integrated over x'' and y'', a smoother function of x and y is obtained, and it is expensive and unnecessary to use Romberg integration anymore, so a Gaussian quadrature rule is used. A further refinement can be achieved by approximating the Greens function (62)

$$
\begin{aligned}
G(x,y|x'',y'') = \frac{1}{4\pi}&\left[\ln\left(\frac{\cosh(\gamma(x-x''))-\cos(\alpha[y+y''])}{\cosh(\gamma[x-x''])-\cos(\alpha[y-y''])}\right)\right]\\
&+\ln\left(\frac{\cosh(\gamma[x+x''])-\cos(\alpha[y-y''])}{\cosh(\gamma[x+x''])-\cos(\alpha[y+y''])}\right)\\
&+\ln\left(\frac{\cosh(\gamma[\ell_x-(x-x'')])-\cos(\alpha[y-y''])}{\cosh(\gamma[\ell_x-(x-x'')])-\cos(\alpha(y+y''))}\right)\\
&+\ln\left(\frac{\cosh(\gamma[\ell_x+(x+x'')])-\cos(\alpha(y+y''))}{\cosh(\gamma[\ell_x+(x+x'')])-\cos(\alpha(y-y''))}\right)
\end{aligned}
\tag{64}
$$

where $\alpha = \frac{\pi}{\ell_y}$ and $\gamma = \frac{\alpha}{\xi}$. This expression is very accurate (error under 0.05%) for $L_x \geq L_y$. This however is not a restriction as an equivalent expression may be found to approximate the Greens function for the case $L_y \geq L_x$.

For this two dimensional case we have four independent parameters to analyze: the log-conductivity fluctuation standard deviation, σ_f, and three scale-related parameters, $\rho_x = \sqrt{\frac{\lambda_x}{L_x}}$, $\rho_y = \sqrt{\frac{\lambda_y}{L_y}}$, and $\xi = \frac{\rho_y L_y}{\rho_x L_x}$. The dependence of the perturbation expansion on σ_f is similar to the 1D case. For the length scale parameters, start the analysis for dependence on the single parameter ρ_x. Selecting $L_x = L_y$, a "square domain" (in the unscaled system) is considered, so the effect of ρ_x and ρ_y can be studied. First, fixing ρ_y at different values, compute the head covariance norm. The covariance has a maximum at $\mathbf{x} = \mathbf{y}$, i.e. the variance. Under the boundary conditions given, the variance has a maximum at the domain's center, $\mathbf{x} = (x, y) = (\ell_x/2, \ell_y/2)$.

Figure 20 shows the head variance norm $\|h\|$ as a function of the parameter ρ_x for different values of the parameter ρ_y on a log-log scale. An exponential two point correlation function, equation (63) was used. Two linear regions of different slopes are noted to the left and right of the point $\rho_x = \rho_c$ (the transition for the exponential case happens at a very well defined region, unlike the Gaussian case analyzed below), with $0.35 < \rho_c < 0.7$ for different values of ρ_y. Let us first analyze the region $\rho_x < \rho_c$. The straight lines suggest a relationship of the type

$$\frac{\|h\|}{J\sigma_f} = C(\rho_y)\frac{1}{\rho_x^n} \tag{65}$$

holds as in the one dimensional analysis, but, C depends on the parameter ρ_y, $C = C(\rho_y)$, and possibly on the parameter ξ. Performing regressions to fit relationship (65) in the data plotted Figure 20, renders the following relationships

$$\rho_y = 0.01 \qquad \frac{\|h_1\|}{\sigma_f J} = \frac{1}{42000}\left(\frac{1}{\rho_x}\right)^2 \tag{66a}$$

$$\rho_y = 0.05 \qquad \frac{\|h_1\|}{\sigma_f J} = \frac{1}{1700}\left(\frac{1}{\rho_x}\right)^2 \tag{66b}$$

$$\rho_y = 0.15 \qquad \frac{\|h_1\|}{\sigma_f J} = \frac{1}{186}\left(\frac{1}{\rho_x}\right)^2 \tag{66c}$$

$$\rho_y = 0.5 \qquad \frac{\|h_1\|}{\sigma_f J} = \frac{1}{19.5}\left(\frac{1}{\rho_x}\right)^2 \tag{66d}$$

$$\rho_y = 1.0 \qquad \frac{\|h_1\|}{\sigma_f J} = \frac{1}{7.5}\left(\frac{1}{\rho_x}\right)^2 \tag{66e}$$

$$\rho_y = 5.0 \qquad \frac{\|h_1\|}{\sigma_f J} = \frac{1}{1.37}\left(\frac{1}{\rho_x}\right)^2 \tag{66f}$$

Notice that the dependence on $\frac{1}{\rho_x}$ is quadratic ($n = 2$ in equation (65)), unlike the one dimensional case where $\|h_1\|$ depended linearly on $\frac{1}{\rho_x}$. If we are to use the criterion $\frac{\|h_1\|}{J} < 1$ as discussed for the one dimenisonal case, and rely purely on $\|h_1\|$ as the bounding term for setting a convergence criterion, then several conclusions follow. For the discussion, one can think of this 2D case as a vertical section of a confined aquifer. For the limiting case of a "strongly layered" formation, equation (66a) (considering y to be the vertical direction, $\rho_y \ll 1$, that is, very small y integral scale, and the mean flow to be aligned with the horizontal direction x), convergence will

122

be achieved even with very large σ_f. On the other hand, if there exist vertical mean flow, or local gradients in the y direction, a conclusion may be drawn for this "strongly layered" case from the previous analysis. Consider the case $\rho_y = 5.0$ and $\rho_x \ll 1$, equation (66f). This corresponds to flow in a "strongly layered" formation in the direction perpendicular to the layering. The convergence condition for this case is much more restrictive, $\sigma_f < 1.37 \rho_x^2$. For environmental conditions, it is expected the flow will align in the direction of layering, but recharge and boundary conditions will induce vertical gradients, and the bound on σ_f for the perturbation expansion to be convergent will be reduced. Figure 21 shows the dependence of $\|h_1\|$ on ρ_y for fixed $\frac{L_x}{L_y} = 1$ and two different values of ρ_y. A fitted relationship for these two values of ρ_x is

$$\rho_x = 0.018 \qquad \frac{\|h_1\|}{\sigma_f J} = 626 \rho_y^2 \tag{67a}$$

$$\rho_x = 0.28 \qquad \frac{\|h_1\|}{\sigma_f J} = 2.72 \rho_y^2 \tag{67b}$$

For $\rho_x > \rho_c$, a different relationship is observed. If equation (65) is fitted an exponent $n = 3$ is obtained, along with a set of coefficients that guarantee convergence for very large values of σ_f. This case corresponds to the condition in which the integral scale is of the same or greater order of magnitude than the domain size we are looking at, $\lambda_i \approx L_i$. It is intuitively correct, since the domain of interest will exhibit very smooth change in hydraulic conductivity. As an example of such a bound, for $\rho_y = 0.5$, the convergence condition is $\frac{\|h_1\|}{J} = \frac{\sigma_f}{30} \left(\frac{1}{\rho_x}\right)^3 < 1$, with $\rho_x > 0.35$. For example, if $\rho_x = 0.5$, the above convergence condition establishes that the
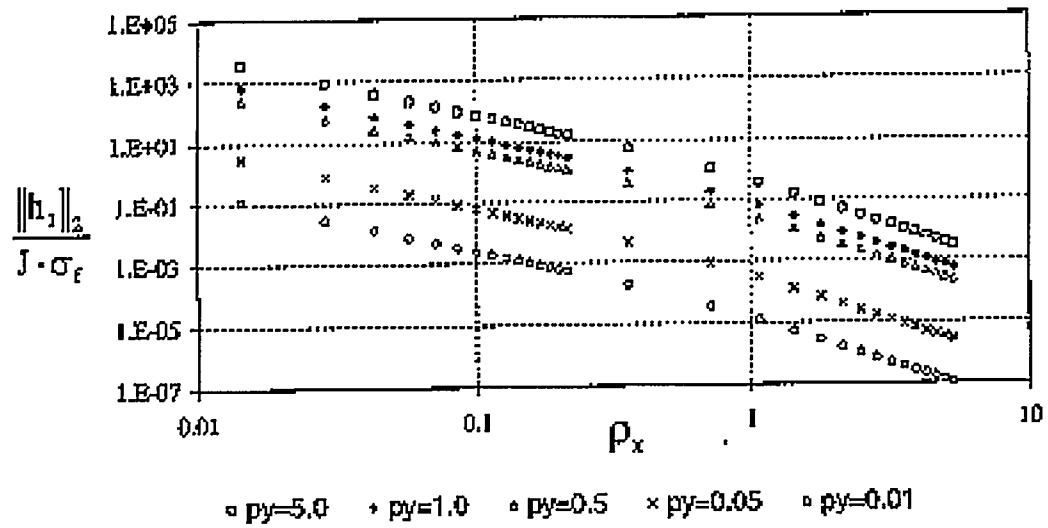
Figure 20. Dependence of $\|h_1\|_2$ on the parameter ρ_x for exponential log conductivity two point correlation function, two dimensional (2D) flow.
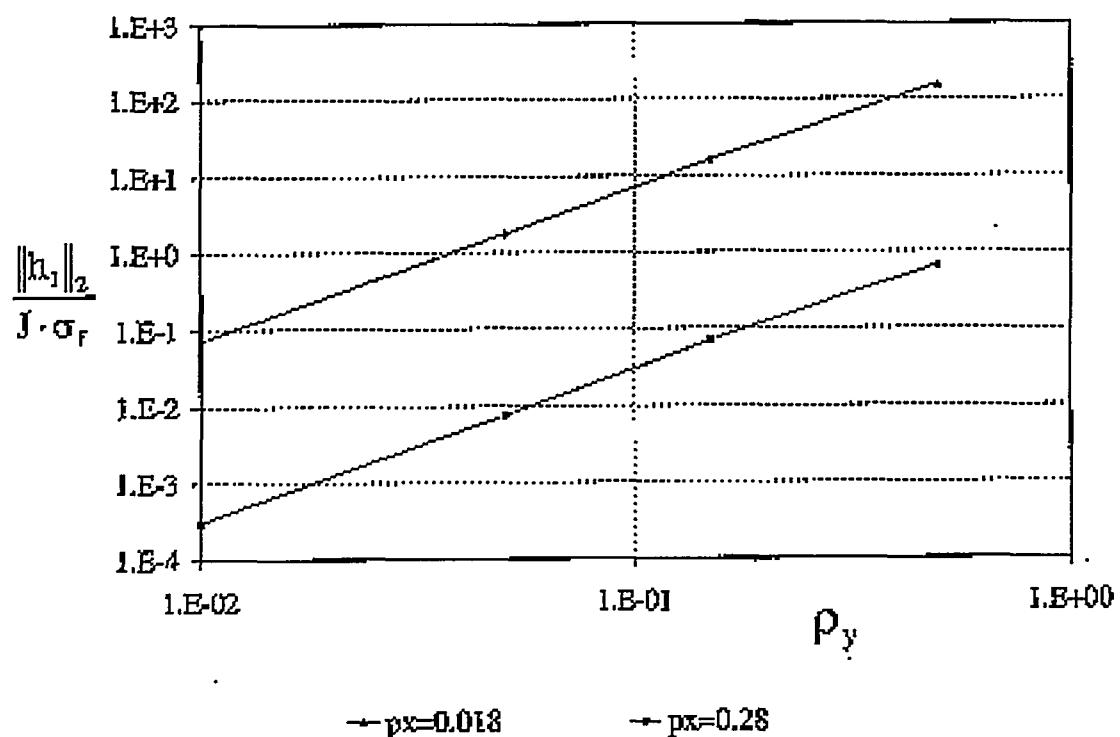
Figure 21. Dependence of $\|h_1\|_2$ on the parameter ρ_y for exponential log conductivity two point correlation function, 2D flow.

solution will be convergent if $\sigma_f < 30(0.5)^3 = 3.75$. Finally the relationship between the

parameter ξ and $\|h_1\|$ is shown in Figure 22. The dependence is also quadratic for large values

of ξ (small values of $\rho_x < \rho_c$) and cubic for small values of $\xi = \frac{\rho_y L_1}{\rho_x L_x}$, and the convergence

condition changes for different values of ρ_y.

If we compute $\|h_1\|$ using a Gaussian two point correlation function, equation (53), we

can see the large impact of this correlation function's shape on the convergence of the

perturbation scheme. Figure 23 shows the dependence of $\|h_1\|$ on ρ_x. A fitted relationship to

powers of $\frac{1}{\rho_x}$ does not seem suitable except at the limits $\rho_x \to 0$ and $\rho_x > 1$ where such fitting

follows a trend (65) with n integer. Figure 23 shows a complex dependence of $\|h_1\|$ on the length

parameters in the transition region $\rho_{cl} = 0.05 < \rho_x < 1.0 = \rho_{cu}$. For the limiting case $\rho_x < 0.05$,

the following convergence relationships are found

$$\rho_y = 0.05 \qquad \frac{\|h_1\|}{\sigma_f J} = \frac{1}{145000} \left(\frac{1}{\rho_x} \right)^2 \qquad (68a)$$

$$\rho_y = 1.0 \qquad \frac{\|h_1\|}{\sigma_f J} = \frac{1}{675} \left(\frac{1}{\rho_x} \right)^2 \qquad (68b)$$

$$\rho_y = 5.0 \qquad \frac{\|h_1\|}{\sigma_f J} = \frac{1}{144} \left(\frac{1}{\rho_x} \right)^2 \qquad (68c)$$

Notice that convergence occurs for much larger values of σ_f, than for the exponential case,

while keeping all the other parameters constant. For a Gaussian two point correlation function,

large values of the anisotropy ratio and/or vertical gradients will render a scheme with greater

convergence bounds than for the exponential case. For the case $\rho_x > 1$, the dependence is again

cubic, e.g., for $\rho_y = 1.0$, $\frac{\|h_1\|}{\sigma_f J} = \frac{1}{20}\left(\frac{1}{\rho_x}\right)^3$, with $\rho_x > 1$. Figure 24 shows the dependence of $\|h_1\|$ on the parameter ξ for different values of ρ_y.

Further analysis for higher head corrections should be performed before the dependence of each one of the terms h_1, h_2, h_3, ... on the parameters ρ_x, ρ_y, and ξ can be fully assessed. However, the preliminary results for h_1 support the findings of numerical Monte Carlo techniques, where it has been found that Gaussian two point correlation functions converge faster than the exponential model, e.g., Hassan et al. (1998). It also reinforces the idea that perturbation schemes for stochastic flow should rely on the gradient of the log conductivity fluctuation for their expansion. $\sigma_{\nabla f}$ is the small parameter needed in the perturbation analysis. However the spatial pattern of the two point correlation is not captured by its value at the maximum point, $\sigma_{\nabla f}$. Additional computations are required to improve knowledge of the 'shape' effect on convergence. Hassan et al. (1998) have also analyzed fractal conductivity fluctuation distributions and have found that convergence is difficult to obtain for that case. The effect of boundary conditions in two dimensional flow will be presented at a later date.

Since the perturbation expansion for the head and velocity is generally consistent (Deng and Cushman, 1995; Hsu et al., 1996) (that is, terms of higher order $O\left(\sigma_f^2\right)$ have been computed and found to be of smaller magnitude as the order increases for parameter values ranging within values of practical interest), some of the conclusions drawn in this paper for the two dimensional case have been based on such consistency and computation of higher order will be performed in the future to further test the outcome of the present research. This does not constitute a proof of convergence but, as pointed out in the literature of perturbation methods, one should be satisfied if the expansion is consistent as far as we have proceeded (Hinch, 1990). For the one

127
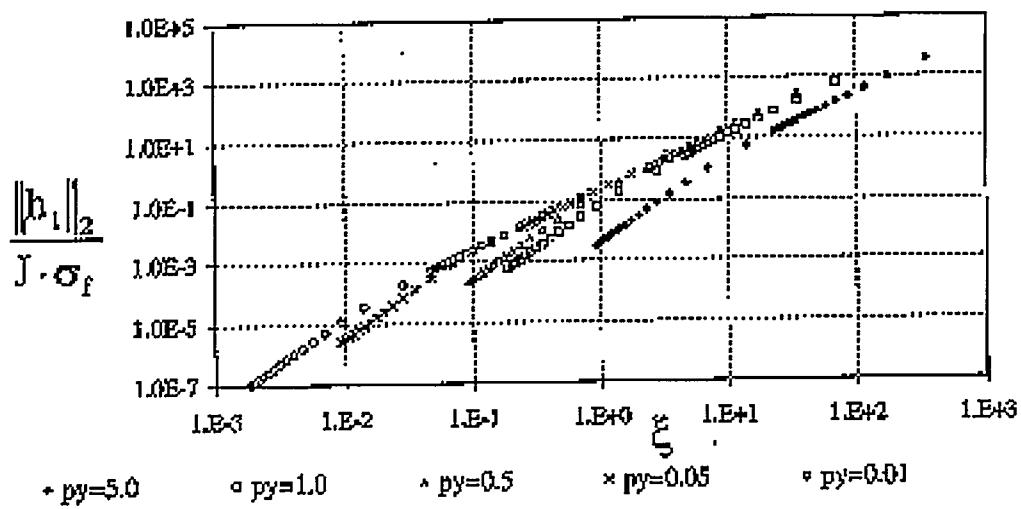
Figure 22. Dependence of $\|h_1\|_2$ on the parameter $\xi = \frac{\rho_y L_y}{\rho_x L_x}$ for exponential log conductivity two point correlation function, 2D flow.
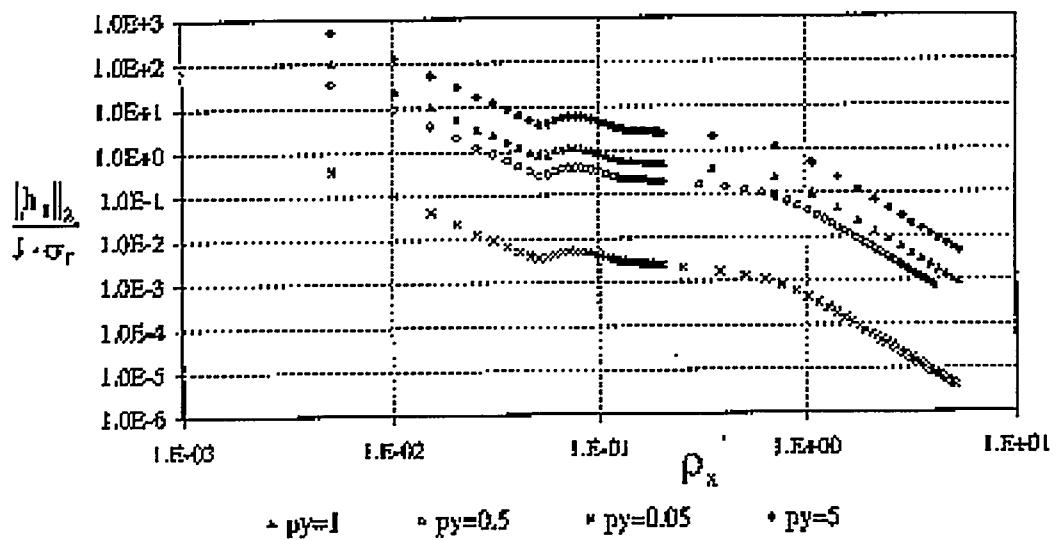
Figure 23. Dependence of $\|h_1\|_2$ on the parameter ρ_x for Gaussian log conductivity two point correlation function, 2D flow.
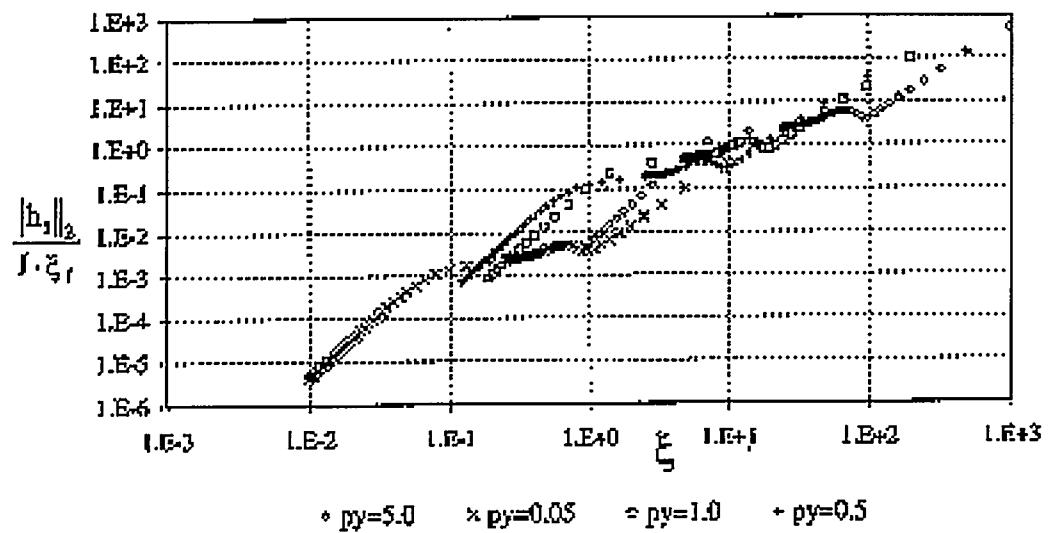
Figure 24. Dependence of $\|h_1\|_2$ on the parameter $\xi = \frac{\rho_y L_y}{\rho_x L_x}$ for Gaussian log conductivity two point correlation function, 2D flow.

dimensional case this consistency is clear, and it is expected that for the two-dimensional case terms of higher order will reinforce these findings. There are significant differences in convergence between one- and two-dimensional flow. Convergence limits for σ_f in two dimensions are greater than those for one dimension. The literature (e.g., Mizell et al. (1982)) suggest convergence for the three dimensional case should be close to the criterion for the two dimensional case. For instance, observe the slopes of Fig. 2 of Mizell et al. (1982).

6.3. Summary

When constructing a macroscale model of the flow field from small scale data (the upscaling problem) various length scales naturally appear in the analysis. We have taken a hard look at this issue from a stochastic perturbation perspective. The goal was to provide a rigorous setting for developing upscaled models.

When looking at steady flow in a heterogeneous medium the log-conductivity appears naturally. Often the log-conductivity is represented by the sum of an average plus a stochastic fluctuation. And to make the problem tractable, the log-conductivity fluctuation, f, about the mean log-conductivity, $\ln K_G$, is assumed to have finite variance, σ_f^2. Historically, perturbation schemes have involved the assumption that $\sigma_f^2 < 1$. We have shown that σ_f may not be the most judicious choice of perturbation parameters for steady flow. Instead, we have examined the variance of the gradient of the conductivity fluctuation, $\sigma_{\nabla f}^2$, is a more appropriate choice. By solving the problem with this parameter and studying the solution, we have found an even more appropriate parameter.

7. The Significance of Porosity Variability to Chemical Transport

7.1. Introduction

It is well known that heterogeneity in natural porous formations controls the flow of liquids and spreading of contaminants in the subsurface. This heterogeneity leads to a nonhomogeneous velocity field that exhibits excitements or fluctuations on many scales. Much of the physical heterogeneity of geologic formations is manifest in the hydraulic conductivity and to a lesser extent in the medium porosity. It is known that conductivity may vary in space by 3-4 orders of magnitude, whereas the porosity changes by at most 1 order of magnitude. Consequently, studies usually regard the conductivity variability as the main factor controlling flow and transport processes in heterogeneous media, and consider the porosity as a deterministic constant. The effect of the spatial variability of the medium porosity has been studied to a small extent as compared to the conductivity variability. Lin (1997) considered transport in porous media with variable porosity but constant volumetric seepage flow rate. He reported that transport predictions using an average porosity are within 15% of those using a linear or slightly nonlinear porosity function, but the discrepancy between the two cases becomes very substantial when the porosity variability is strongly nonlinear. Although this disregards the conductivity variability, it does show the importance of porosity. Shvidler (1985, 1993) studied purely convective transport of nonreactive solutes in porous media with random porosity and conductivity. However, he did not report on the significance of assuming a random porosity rather than a deterministic porosity. Warren and Skiba (1964) and Naff (1978) considered the variability in the porosity field and found it secondary relative to the effect of the conductivity variability. However, these authors did not allow the porosity to be correlated to the conductivity field which is to be expected in natural porous media. They also did not study its

effect when combined with a random reactivity field. It should be mentioned that these aspects, which we try to investigate here, were outside the scope of those studies. To the authors knowledge, no one has studied the effect of correlations between geochemistry, porosity, and conductivity.

In this study we use the Monte Carlo method to simulate flow and transport in random conductivity, porosity, and geochemistry fields. The purpose is to investigate the effect of porosity variability on contaminant transport in heterogeneous porous media. Conductivity, porosity, and reactivity fields are generated from fractional Brownian motion (fBm) and exponential distributions. In some cases we allow cross correlation between these fields. The flow problem is solved over a two-dimensional horizontal cross section using a block-centered finite difference scheme. The transport equation is solved by using a particle-tracking, random-walk method. The solution of the transport equation is then averaged over sufficiently large number of realizations to obtain the mean concentration. Results are presented in terms of concentration contours and spatial moments of the mean plume. The nonlocal stochastic transport theory of Deng et al. (1993) for the conservative case is modified to include a random porosity that may be correlated to the conductivity, and the perturbation results are compared to the case of deterministic porosity.

7.2. Flow and Transport Simulations with Spatially Varying Porosity

Measurements of horizontal distributions of a variety of soil properties, mineral deposits and other environmental data indicate that they often have fractal character with statisstics similar to a fBm (Burrough 1981; Turcotte, 1985 as quoted by Hewett, 1986). Hewett (1986) considered a sequence of 2189 porosity values taken at intervals of 0.5 feet (0.3048 m) from a porosity log in a well. The porosity varies between a minimum of 0.05 to a maximum of ~0.6.

The rescaled range analysis applied to this sequence revealed a fractal character in the vertical porosity distribution with $H = 0.85$, where H is the so-called Hurst exponent. Hewett also argued that in the absence of adequate information about the areal (two-dimensional horizontal) distribution of properties, the value of H determined from well logs also applies to the areal distribution. This may be justified by recognizing that the statistics of the spatial distribution of sediments are determined by the statistics of the processes which formed them and that these processes acted simultaneously over large area influenced by the same changes in weather and climate (Hewett, 1986). It should be recognized that the two-dimensional fBm distribution of a property has a fractal dimension D, which is related to the Hurst exponent $D = 3 - H$.

In the light of the above discussion, although the variation of porosity is much smaller than that of the conductivity, the coupled effect of porosity, conductivity and reactivity may be significant. Therefore it is important to investigate the influence of this variability on the transport and spreading of contaminants in such media. Although the correlation between porosity and conductivity has not yet been established by field measurements, one may expect that some degree of correlation exist in certain geologic media. For example, Archie (1950) suggested a positive correlation between the effective porosity and conductivity. Also, Doyen (1988) found a positive correlation between porosity and conductivity for a certain type of sandstone using laboratory measurements and an empirical formula based on the pore skeleton. Gelhar et al. (1992) compiled conductivity, porosity, and dispersivity data from 59 different field sites. Among these data, 28 porosity-conductivity pairs could be analyzed. A simple correlation analysis indicates a correlation coefficient of –0.259. Removing the lowest four porosity values, which seemed significantly different than the rest of the 28 pairs, and analyzing the remaining pairs yields a coefficient of –0.539. Though not very strong, this empirical evidence show that

porosity could be correlated to the conductivity. Since the type of correlation is not clearly identified in the field, we examine both cases in this study. The scope of this study may be of theoretical interest with the lack of field data needed to support any of the correlation models. However, it indicates the need to consider the porosity variability and its correlation to the conductivity in a more elaborate manner both theoretically and in field studies.

Consider the transport of a tracer under steady groundwater flow in a two-dimensional horizontal cross section. The conductivity field is assumed to obey fBm or exponential statistics. In each case, a spectral method (Voss, 1988) based on the fast Fourier transform (FFT) is used to generate random realizations of the conductivity field. The method uses the spectral density in conjunction with a random number generator to create a field in real space having the statistics of the desired distribution. For a fBm process we use the band-pass-filtered spectrum (Hassan et al., 1997):

$$\widehat{ff}(k) = \frac{\sigma_f^2 (D-3)}{\pi \left[k_{\max}^{2D-6} - k_{\min}^{2D-6} \right] k^{8-2D}} \tag{69}$$

where f is the fluctuating log-conductivity, $\ln K(x) = F + f(x)$ is the expected value of the log-conductivity field, σ_f^2 is the log-conductivity variance, D is the fractal dimension of the two-dimensional distribution which has a value between 2 and 3, $k_{\max}$ is the upper cutoff wave number which is set proportional to the inverse of the measurements spacing or the grid size, and $k_{\min}$ is the lower cutoff number that is proportional to the inverse of the domain size. If an isotropic exponential covariance of the form $\overline{ff}(\mathbf{u}) = \sigma_f^2 e^{-u/\lambda}$ is used, the two-dimensional spectrum (Mantoglou and Wilson, 1982) is

$$\widehat{ff}(k) = \frac{\sigma_f^2 \lambda^2}{2\pi \left(1 + \lambda^2 k^2\right)^{3/2}} \tag{70}$$

where u is the spatial lag at which the correlation is estimated and λ is the integral scale. For more details regarding the properties of fBm and the random field generator used here, the reader is referred to Hassan et al. (1997).

Assuming that the porous medium is incompressible, the Darcy scale steady flow equation is

$$\nabla \cdot q(x) = \nabla \cdot \left[K(x)\nabla\phi(x)\right] = 0 \tag{71}$$

where $\mathbf{q}(x)$ is the specific discharge vector and $\phi(x)$ is the hydraulic head. The flow velocity or $\mathbf{V}$ is computed using Darcy's law, $V_i = -K/n\,\partial\phi/\partial x_i$, where n is the effective porosity. To proceed in the analysis we first discuss the role of the porosity variability in the solution to the flow and transport equations. Since the flow equation (71) is written in terms of the specific discharge $\mathbf{q}$ and solved for the hydraulic head h, the porosity variability does not affect the solution of (71) for the head field. It only plays a role in computing the velocity, sometimes called the seepage velocity, which is obtained by dividing $\mathbf{q}$ by the porosity n. Therefore the velocity field will be influenced by the variations in n. This influence depends on the covariance structure of n and its cross correlation with the hydraulic conductivity. Unlike the flow equation, the transport equations for both conservative and reactive chemicals explicitly involve n.

$$\frac{\partial nC}{\partial t} + \nabla \cdot (nC\mathbf{V}) = \nabla \cdot (n\mathbf{d} \cdot \nabla C) \tag{72}$$

$$\frac{\partial nC}{\partial t} + \frac{\partial nS}{\partial t} + \nabla \cdot (nC\mathbf{V}) = \nabla \cdot (n\mathbf{d} \cdot \nabla C) \tag{73}$$

With linear first-order kinetics, the exchange reactions can be described by

$$\frac{\partial S}{\partial t} = K_r \left(K_d C - S \right) \tag{74}$$

where C is the liquid phase concentration, S is the sorbed concentration (defined as sorbed solute mass per fluid volume), $\mathbf{d}$ is the velocity-dependent local dispersion tensor $d_i = \alpha_i V$, α_i is the local dispersivity, K_r is the reaction rate coefficient, K_d is the partition coefficient, which controls the chemical exchange at the local scale, and V is the magnitude of the velocity.

The solution of the flow and transport problems starts by solving the flow equation (71) for the head field. The two-dimensional domain is divided into a uniform grid of square blocks of length $\Delta x_1 = \Delta x_2 = \Delta$. The values of the spatially varying parameters such as porosity, conductivity, and distribution coefficient are assigned to the center of the block but are not assumed uniform over the block. Interpolation is employed in the solution of the transport equation as will be discussed later. We employ a five-point finite difference scheme to discretize (71) over this uniform grid. The result of this discretization is a system of linear equations that we directly solve by Gaussian elimination to obtain the head field. Darcy's law is then used to compute the velocity components at midpoints between block centers. The interblock conductivity-porosity ratio required to compute the seepage velocity is obtained by harmonic averaging the two adjacent values of K/n. This ensures continuity of the head field and conservation of mass across block boundaries (Aziz and Settari, 1979).

The transport equations in the conservative and reactive cases are solved by a random-walk particle-tracking approach. This approach is computationally efficient because it does not require a grid for the particle-tracking algorithm. It therefore requires little computer storage and running time relative to finite element, finite difference, and method of characteristics models (LaBolle et al., 1996). The reason being the fact that the random walk method does not require

solving large systems of linear equations every time step as do the finite difference and the finite element methods. Another advantage of the random walk method is that it does not suffer from numerical dispersion. A disadvantage, however, is that the obtained concentration distribution is not smooth and usually requires some smoothing. This problem is alleviated to some extent in our Monte Carlo simulations by averaging the concentration over a large number of realizations. We use 2500 particles in all simulations which were found sufficient for the mean concentration and spatial moments we consider here. Any increase in the number of particles does not change the results presented here. The initial areal solute pulse is represented by this number of particles such that the total particles mass is equivalent to the injected mass,

$$\sum_{i=1}^{NP} m_i = \int_\Omega n C_0 d\mathbf{x} \tag{75}$$

where m_i is the mass associated with particle i, NP is the number of particles released, C_0 is the concentration of the initial pulse and Ω is the domain considered. Particles are then traced as they move within the know velocity field. Therefore the solution of (72) or (73) for any time t can be approximated as

$$nC(\mathbf{x},t) = \sum_{np \in NP} m\left[\mathbf{X}_{np}(t),t\right]\eta\left[\mathbf{x} - \mathbf{X}_{np}(t)\right] \tag{76}$$

where $np = 1,2,3,\cdots,NP$ is the particle index, NP is the total number of particles used to simulate the continuous solute mass, $m\left(\mathbf{X}_{np},t\right)$ is the mass associated with the npth particle that is located at $\mathbf{X}_{np}(t)$ at time t and was originally at $\mathbf{X}_{np}(0)$, and $\eta(\mathbf{x})$ is a mollifying function that is used to smooth the concentration distribution. We choose η to be a box of size $\Delta x_1 \times \Delta x_2$ around each grid point and project all particles in this box to that grid point.

For the conservative case, the random walk equation with the variability in the medium porosity is (Tompson and Gelhar, 1990; Tompson, 1993; LaBolle et al., 1996)

$$\mathbf{x}_{t+\Delta t} = \mathbf{x}_t + \left\{ \mathbf{V}(\mathbf{x}_t, t) + \nabla \cdot \mathbf{d}[\mathbf{V}(\mathbf{x}_t, t)] + \frac{1}{n} d[\mathbf{V}(\mathbf{x}_t, t)] \cdot \nabla n \right\} \Delta t$$
$$+ \left\{ 2\mathbf{d}[\mathbf{V}(\mathbf{x}_t, t)] \Delta t \right\}^{1/2} \cdot \mathbf{Z}$$

(77)

where $\mathbf{x}$ is the particle location in space, Δt is the time step, and $\mathbf{Z}$ is a vector of normally distributed random numbers of zero mean and unit variance. The spatial distribution of these particles in the limit of small Δt can be described by a probability density function that satisfies a Fokker-Plank equation (Uffink, 1985; Kinzelbach and Ackerer, 1986) of a form similar to (72). Here C, normalized between zero and one, plays the role of the probability density.

For the reactive transport, the reversible reaction process described by (74) can be handled in a manner similar to Hassan et al. (1997). They extended the approach of Kinzelbach (1988) and Valocchi and Quinodoz (1988) for kinetic reactions with deterministic rate coefficients and one-dimensional simulations to the case of randomly distributed reaction rates and two-dimensional heterogeneous flow field. However, all the previous studies were performed assuming constant porosity. Chemical reactions are included in the particle tracking approach by assigning a state variable to each particle which indicates whether the particle resides in the aqueous or sorbed phase. At the beginning of each time step, particles in the liquid phase are moved in space according to the random walk equation, whereas particles sorbed to the solid matrix are not allowed to move for the entire time step, provided that it is sufficiently small. At the end of the time step the state of each particle is adjusted by employing a Bernoulli trial and using the probability of phase transition as given by Parzen (1962). For more details the reader is referred to Kinzelbach (1988), Valocchi and Quinodoz (1988), and Hassan et al. (1997).

139

To extend the above procedure to the case of random porosity, the only change that needs to be made is in the random-walk equation used to advect and diffuse the particles in the aqueous phase. Equation (77), which has a term that accounts for the porosity variability, is used. The concentration distribution at any time can be obtained using (76).

An important factor when using (77) is the computation of the velocity and dispersion coefficient at the particles location. As pointed out by LaBolle et al. (1996), the accuracy of the random walk method in terms of local mass conservation has been traded for computational efficiency by specifying velocity and dispersion coefficients as block constants in previous studies (e.g., Tompson and Gelhar, 1990; Tompson, 1993). LaBolle et al.'s (1996) results show that this approach does not conserve local mass and may significantly affect solute transport prediction. They also showed that in interpolation scheme to obtain particle velocities is necessary. Their results indicate that the particle velocity in the advective term is not sensitive to the interpolation scheme used, but in the dispersion term

Table 2. Input Parameters

Parameter		Value
Fractal dimension of f	D	2.2
Upper cutoff	k_{max}	2π
Lower cutoff	k_{min}	$2\pi/128$
$<\ln K>$	F	1.0
Initial concentration mass	M	4.2 Kg.
Initial concentration box		$6.0 \times 2.0 \text{ m}^2$
Initial source location	(x_1, x_2)	(0.0, 0.0) m

the velocity interpolation technique may affect the results. Schemes that employ bilinear interpolation for velocities in the dispersion term conserve local mass and disagree with schemes that use block-constant velocities. Consistent with these results our previous simulations (Hassan et al., 1997) use bilinear interpolation for the velocity in both the advection and dispersion terms of the random walk equation. We therefore use the same interpolation scheme in this study to compute the particles velocities from the values obtained at the computational nodes.

Monte Carlo simulations are used by repetitively solving the flow and transport equations for a large number of conductivity, porosity, and reactivity realizations. Ensemble averaging is then used to obtain the mean concentration plume and its spatial moments as they evolve in time. The accuracy of the simulations and the convergence of the ensemble statistics have been established and are discussed by Hassan et al. (1997). In the following section we present the effect of the porosity variability for conservative tracers and then study the combined effect of random K_d and n.

7.3. Conservative Chemicals

Monte Carlo experiments are performed with and without randomness in the porosity using the conductivity distributions presented in the previous section. Table 2 lists the flow and transport parameters that are kept unchanged throughout.

For the purely convective case, two experiments are performed. In the first experiment the porosity is generated from a fBm distribution, $n(x) = n_G e^{rw(x)}$, where n_G is the geometric mean of porosity, $w(x)$ is a fBm process with variance σ_w^2, and r is a scaling factor that is used to guarantee that the porosity range is physically plausible (e.g., within the rage found in

Hewett's sequence) and to adjust the variance of the porosity logarithm, $\sigma^2_{\ln n}$. Thus, for $r = 0.35$

and $\sigma^2_w = 0.15$, $\sigma^2_{\ln n} = 0.018$. The value of r is chosen based on a number of numerical

simulations in which the random porosity is generated from the fBm model. In each simulation,

the parameter r is chosen based on a number of numerical simulations in which the random

porosity is generated from the fBm model. In each simulation, the parameter r is adjusted such

that the porosity values in any single realization are physically reasonable and within the range

mentioned before. Table 3 summarizes the results of these simulations for 600 realizations in

each case. The ranges of K and n in Table 3 are defined using the lowest and highest values in

the 600 realizations. The conductivity is independently generated from a fBm distribution with

variance $\sigma^2_f = 0.15$ such that it is about one order of magnitude higher than the variance in the

natural logarithm of the porosity. The domain size is chosen as 64 m × 40 m with the longer side

aligned along the mean flow direction. The grid size is taken as 0.5 m, which proved to be

sufficient for the local and global mass balance (Hassan et al., 1997). The mean concentration

obtained with spatially varying porosity and conductivity is compared to the mean concentration

obtained by varying conductivity with fixed porosity. $n(x) = n_G = 0.35$.

Table 3. Porosity Range and Values of r

σ^2_f	λ	Range of K	Range of n	r
0.15	1.0	0.55-12.5	0.21-0.62	0.37
0.5	1.0	0.13-37	0.22-0.64	0.22
1.0	1.0	0.5-124	0.24-0.59	0.13
0.15	5.0	0.23-24	0.17-0.60	0.3
0.5	5.0	0.03-117	0.19-0.67	0.15
1.0	5.0	0.02-659	0.21-0.65	0.10

Figure 25a shows the superimposed concentration contours for both cases plotted at 10,

25, 40, and 50 days after the tracer was released into the domain. There are small differences
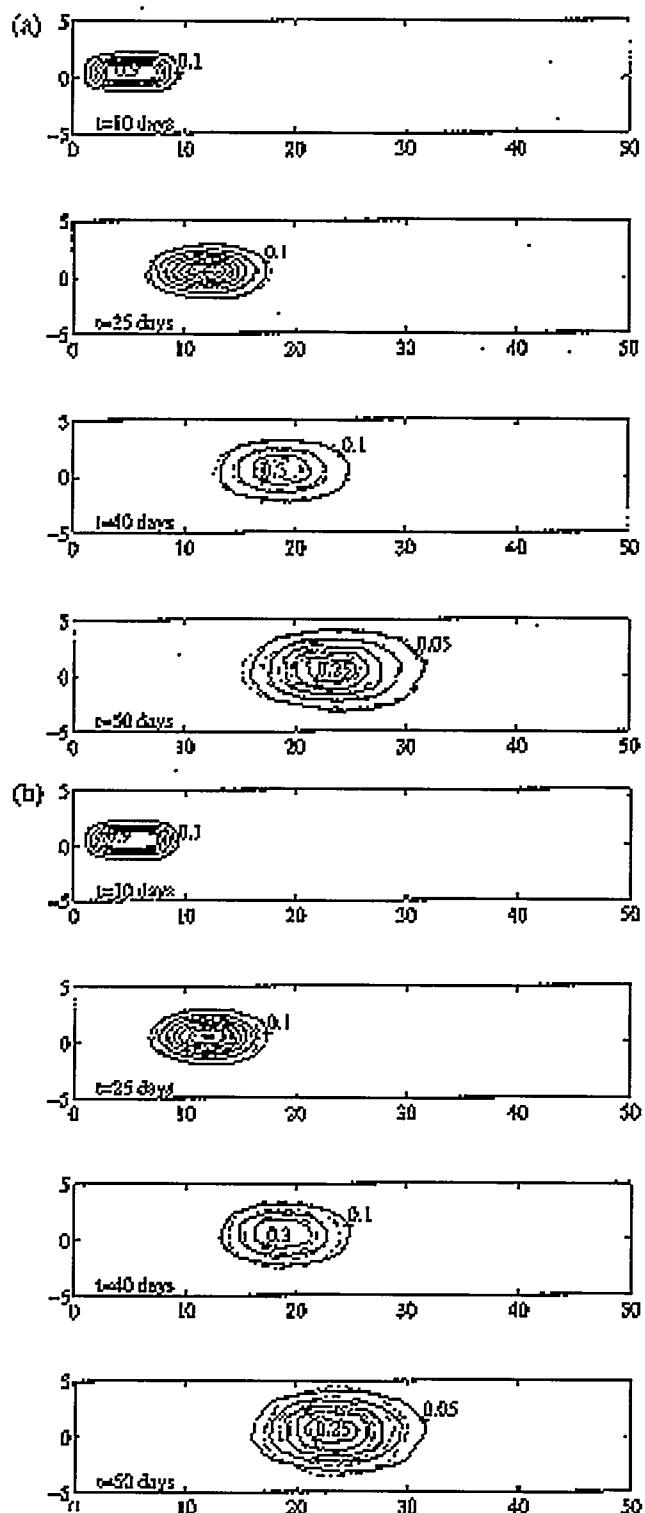
Figure 25a,b. Mean concentrations for purely convective transport with fBm conductivity and porosity, and $\sigma_f^2 = 0.15$ and $\sigma_{\ln n}^2 = 0.018$: (a) Monte Carlo simulation with spatially varying n (solid) which is not correlated to K and with deterministic n (dashed), and (b) Monte Carlo simulation with spatially varying n (solid) which is negatively correlated to K and with deterministic n (dashed).

between the two sets of concentration contours in this case. The spatial variability of n has little effect on the plume dispersion when uncorrelated with K. However, in the second experiment the result is different. Porosity is generated as before, but in addition it is also assumed to be positively correlated to the conductivity field, $n(x) = n_G e^{rf(x)}$, with $r = 0.35$, $\sigma_f^2 = 0.15$ and $\sigma_{\ln n}^2 = 0.018$ as in the first experiment. The positive correlation between K and n is to be expected since the coarse grained sediments such as sand and gravel tend to have higher conductivity and effective porosity than fine sediments such as clays that have very small effective porosity. This is also suggested by Archie (1950). Figure 25b compares the concentration distributions for this case, to the one obtained with constant porosity. Clearly, the variability of the porosity and its positive correlation to the hydraulic conductivity significantly decrease the dispersion in the longitudinal direction. This result is more graphically illustrated by comparing the mean-plume spatial moments. Define these spatial moments as

$$M_i = \frac{1}{M} \int_{R^2} n_G \overline{C} x_i dx \tag{78}$$

$$M_{ii} = \frac{1}{M} \int_{R^2} n_G \overline{C} x_i^2 - M_i^2 \tag{79}$$

$$s = \left(\frac{1}{M} \int_{R^2} n_G \overline{C} (x_i - M_i)^3 dx \right) \Big/ M_{ii}^{3/2} \tag{80}$$

$$\kappa = \left(\frac{1}{M} \int_{R^2} n_G \overline{C} (x_i - M_i)^4 dx \right) \Big/ M_{ii}^2 \tag{81}$$

where $M = \int_{R^2} n_G \overline{C} dx$ is the total mass of the solute, s is the skewness and κ is the kurtosis. Figure 26 shows the second longitudinal moments are significantly lower for n positively correlated with K, than they are for n uncorrelated with K or when n is a deterministic constant.
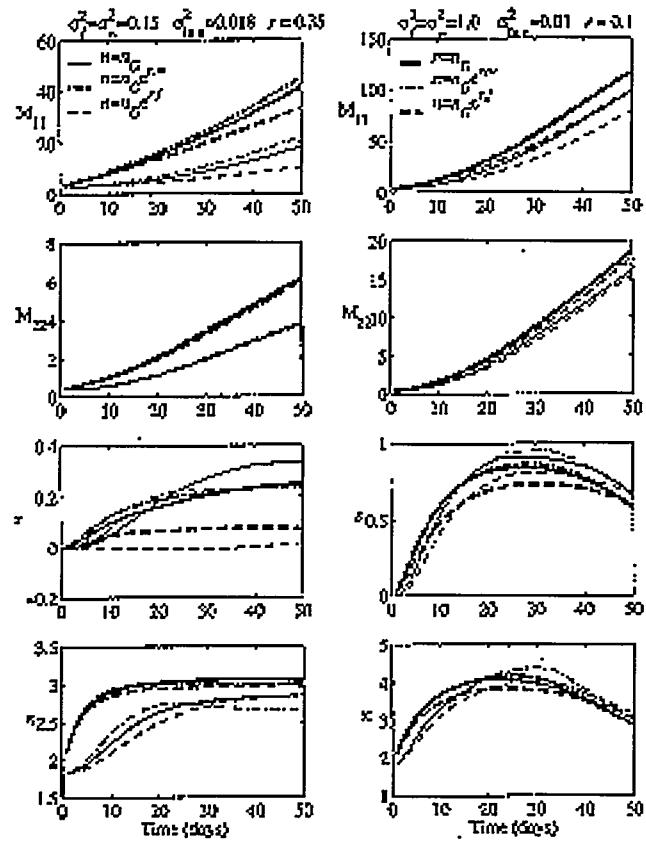
Figure 26. Spatial moments for fBm conductivity and porosity; thick lines indicate convective-dispersive transport, thin lines indicate purely convective transport.

Also, the uncorrelated case yields higher longitudinal dispersion, but the same transverse dispersion, as the case with n a deterministic constant. The significant decrease in dispersion when n is positively correlated to K is due to the fact that the solution of the flow equation with this type of correlation yields velocities with a smaller variance than when the porosity is considered constant. This decreased velocity variance implies smaller velocity fluctuations, which are the main factor driving dispersion and causing this decreased plume spreading. Should the porosity be negatively correlated to the conductivity, the results would have been reversed. This can be easily seen if one substitutes $n = n_G e^w$ in Darcy's law to get,

$V_i = \left[K_G / n_G \right] e^{(f-w)} \left(\partial \phi / \partial x_i \right)$. Assuming a constant head gradient along the x_1 direction, J, and using a first-order analysis yield the variance of the velocity fluctuations as

$$\sigma_{v_i}^2 = \frac{K_G^2}{n_G^2} \left[J^2 \delta_{i1} \left(\overline{ff} + -2\overline{fw} + \overline{ww} \right) + \left(\overline{\frac{\partial \phi'}{\partial x_i}} \right)^2 - 2J \delta_{i1} \overline{(f-w) \frac{\partial \phi'}{\partial x_i}} \right] \tag{82}$$

where ϕ' is the head fluctuation. The positive correlation between f and w leads to lower velocity variance and vice versa. From Fig. 26 it can also be seen that the skewness of the mean plume is significantly affected by the porosity variability and its correlation to K. When n is positively correlated to K, the skewness almost vanishes. The kurtosis is slightly affected by the porosity variability.

The same two experiments are performed for the convective-dispersive case. The longitudinal and transverse horizontal dispersivities are taken as 0.5 and 0.05 m, respectively. These values are chosen in the upper range of values as determined by Klotz et al. (1980). The results are presented in terms of the spatial moments as shown in Fig. 26 with the thick lines. As for the purely convective case, the second longitudinal moment and skewness (corresponding to the correlated case) significantly differ from the other two cases. The longitudinal moments with

random uncorrelated porosity and conductivity start to deviate from the deterministic porosity case only at large times. It is also clear from Fig. 26 that though smaller than the purely convective transport, the influence of the porosity variability in the convective-dispersive case is significant.

These experiments are based on a 1 order of magnitude difference between σ_f^2 and $\sigma_{\ln n}^2$. We repeat the same experiments with 2 orders of magnitude difference between the two variances. The results of this case, shown in the right panels of Figure ___, also reveal the importance of porosity variability when correlated to the conductivity variability. As expected, the effect is less than the previous case when there is only 1 order of magnitude difference between the variances. However, even in this current case, the second moments for the correlated case at 50 days are ~20-25% smaller than the deterministic porosity case.

Figure 27 is similar to Fig. 26, except the conductivity is exponential with integral scale, $\lambda = 3.0$ m. The simulation domain is ~$21\lambda \times 13\lambda$ and the grid resolution is kept at 6 points per integral scale. The same conclusions can be drawn from Fig. 27 as Fig. 26, but with smaller moments and skewness. Since the case of random n uncorrelated to the conductivity has little effect on the plume evolution as compared to the correlated case, we restrict out attention to the latter case in what follows.

We study the effect of porosity with different $n - K$ correlation models. Perfect positive and negative correlations are considered as well as imperfect correlations. Four correlation models are studied in Fig. 28. These models are a perfect positive correlation, $n(x) = n_G e^{\sigma f(x)}$, a positive correlation with noise, $n(x) = n_G e^{\sigma f(x)} + \varepsilon$, a perfect negative correlation, $n(x) = n_G e^{-\sigma f(x)}$, and a negative correlation with noise, $n(x) = n_G e^{-\sigma f(x)} + \varepsilon$, where ε is a random
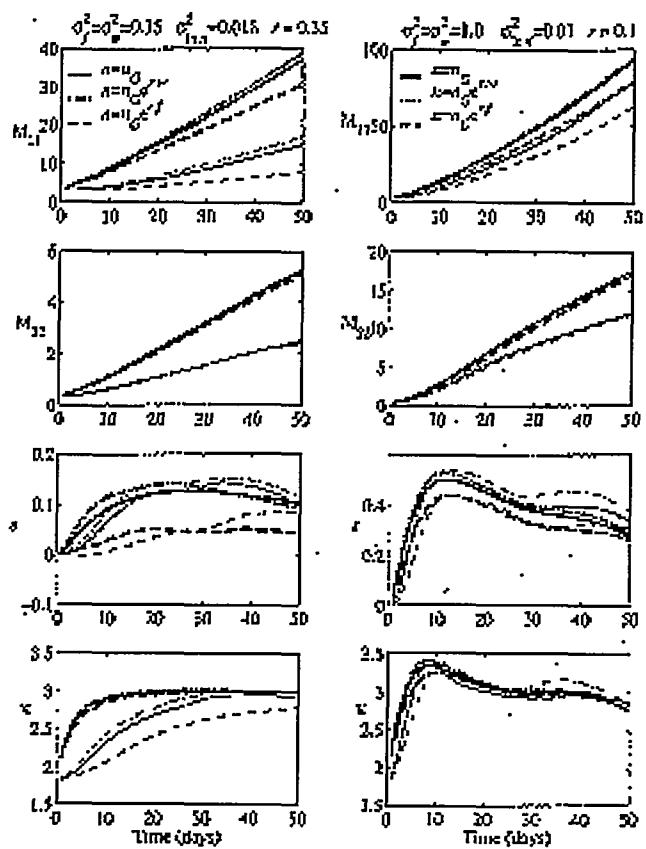
Figure 27. Same as Figure 26 but for the exponential model
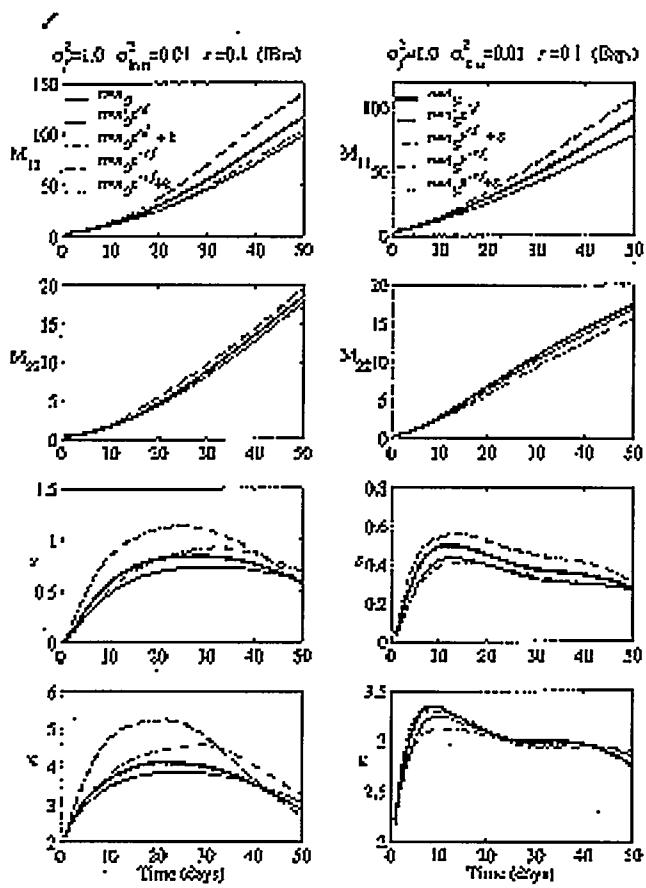
Figure 28. Spatial moments for conservative transport in fBm and exponential conductivity distributions using different $n - K$ correlation models.

number uniformly distributed between −0.05 and 0.05. For $\sigma_f^2 = 1.0$ and $r = 0.1$, the variance of the porosity logarithm, $\sigma_{\ln n}^2$, is 0.01 in the perfect correlation cases and is about 0.017 in the imperfect correlation cases. The results of Fig. 28 indicate that the perfect and imperfect correlations yield the same moments except for minor differences in the plume skewness and kurtosis, especially with the fractal conductivity distribution. Therefore adding a noise to the perfect correlation models does not significantly alter the results. The second transverse moment is least influenced by the porosity variability and its correlation with the conductivity. As alluded to earlier, the negative correlation models increase dispersion in the longitudinal direction.

As reported by Hewett (1986), porosity variability in geologic media exhibit long range correlations. We investigate the effect of the porosity integral scale λ_n relative to the conductivity integral scale $\lambda_K = \lambda$. Conductivity values are generated from the exponential distribution with integral scale λ_K. The same seed for the random number generator is used to generate the porosity with correlation scale λ_n. The correlation structure between n and K is maintained and the porosity correlation scale is allowed to be different from that of the conductivity. Figure 29 compares two deterministic porosity cases, $\lambda_K = 1.0$ and 5.0 m and three random cases with positive correlation to the conductivity, $\left(\lambda_K = \lambda_n = 1.0 \text{ m} \right)$, $\left(\lambda_K = 1.0 \text{ m}, \lambda_n = 5.0 \text{ m} \right)$ and $\left(\lambda_K = 5.0 \text{ m}, \lambda_n = 1.0 \text{ m} \right)$. Changing λ_n only slightly affects the skewness of the plume. The longitudinal second moment is most influenced by the conductivity integral scale.

The results presented for the conservative tracer indicate that porosity variability when correlated to the conductivity significantly affects the plume dispersion, especially in the

longitudinal direction. The effect is more significant for the case of mildly heterogeneous porous media with porosity variance ~1 order of magnitude smaller than σ_f^2, such as encountered at Cape Cod where $\sigma_f^2 = 0.24$ (Hess et al., 1992), and the Borden experiment, $\sigma_f^2 = 0.172$ (Woodbury and Sudicky, 1991). These two sites are mildly heterogeneous, and if porosity variations are considered with variance on the order of 0.1 σ_f^2, the simulation results of these sites can significantly differ from previous simulations with constant porosity.

7.4. Reactive Chemicals

Here we explore the interplay between randomness in the porosity and reactivity fields when they are correlated to the conductivity field. Our aim is to examine the importance of the randomness in the medium porosity relative to the randomness in the distribution coefficients, K_d. For simplicity we assume that K_d is negatively correlated to the conductivity through $K_d = K_d^G e^{(-r_k f)}$, with K_r a deterministic constant. The parameter r_k is used to control the variance of $\ln K_d$. The porosity is assumed to be positively correlated to the conductivity with $n_G = 0.35$. Higher values of $f(x)$ imply higher porosity values and lower values of K_d. This means that porosity and the distribution coefficient are likely to be negatively correlated. This assumption is realistic based on Karickhoff et al. (1979) who found a strong correlation between K_d and the organic carbon content of the sediments. We surmise this content increases as the porosity of the sediments decreases and vice versa. Clay deposits, for instance, have a small porosity but a very high organic carbon content and therefore provide a rich sorptive environment for many chemicals passing through the system.

We consider the four cases: (1) K_d and n both deterministic constant, (2) K_d random and n deterministic constant, (3) K_d deterministic content and n random, and (4) both K_d and n random. Conductivity is generated from fBm and exponential models. Local scale dispersion is considered as before. In the first set of experiments the geometric mean of K_d and the parameter r_k are set to 1.0 yielding $\sigma_{\ln K_d}^2 = \sigma_f^2 = 1.0$, the porosity variance is $\sigma_{\ln n}^2 = 0.01$, and the reaction rate K_r is 0.1. Again, the values of the porosity are checked and found to be within the range found in Hewett's sequence. Figure 30 displays the spatial moments for this case using both heterogeneity models. As is apparent, the second longitudinal moment increases with K_d random and n deterministic and decreases but to a lesser extent for random n and deterministic K_d. When both are random, the second longitudinal moment is closer to that with only K_d random. The second transverse moment exhibits the same behavior, but the skewness and kurtosis are slightly affected by the randomness in the two parameters. It should, however, be remembered that the variance in $\ln n$ is 2 orders of magnitude smaller than $\ln K_d$. In Figure 31 the same set of experiments is repeated with the only difference being the value of K_d^G, which is 0.2. In this case the plume is slightly retarded (approximate retardation factor of 1.2), and therefore the travel distance is larger than in Figure 30 where the retardation factor is ~2.0. The results of Figure 31 show that K_d and n have equal and opposite effects on the plume's second moment. When both variabilities are considered, the moment is no different than when both parameters are deterministic constant. When K_d^G is large and the plume is significantly retarded, K_d variability is more important than that of n. This is due to the fact that the plume has not traveled far enough into the domain to sufficiently experience the porosity variability. Because porosity variability is much smaller than that of the conductivity, the plume has to travel many

integral scales of the porosity before it is affected. Also, because $\sigma^2_{\ln K_d} = 100\sigma^2_{\ln n}$, the effect of

K_d is more significant for such short travel distances. On the other hand, when $K_d^G = 0.2$, the

plume retardation is smaller, and the traveled distance is larger. In this case the plume has

experienced more of the porosity heterogeneity so that its effect is equivalent to that of K_d,

which has a much larger variance.

When the exchange reactions between the liquid phase and the solid matrix are fast, the

effect of K_d variability is more significant (Hu et al., 1995). We show in Figure 32 the same set

of experiments as in Figure 31, but with a much faster reaction rate, $K_r = 10$. Although the

plume has the same K_d^G as in Figure 31, the effect of K_d variability is more apparent than that of

the porosity, especially for the second longitudinal moment. This, however, agrees with the

findings of Hu et al. (1995) that fast reactions enhance the effect of the randomness in the

distribution coefficient, K_d. Figure 32 also indicates that the combined effect of the variability

in K_d and n yields a result significantly different from that when only one field is random. It is

close to that of deterministic K_d and n. Although the $\ln n$ variance in these cases was taken 2

orders of magnitude smaller than the variance in $\ln K_d$, the effect of the porosity variability

seems significant.

We consider in Figure 33 a set of experiments with $\sigma^2_{\ln K_D} = \sigma^2_{\ln n} = 0.01$, $\sigma^2_f = 1.0$,

$K_d^G = 1.0$, and $K_r = 0.1$. Figure 33 shows that the randomness in the porosity field affects all

moments much more than does that of K_d. However, the overall effect of K_d and n on the

second transverse moment is small. Thus considering the variability in one parameter alone may

153

overestimate or underestimate the moments. The combined effect of the random parameters may lead to a completely different result than if the randomness in one parameter alone is considered.

These results indicate dispersion is markedly affected by the porosity variability, especially in the longitudinal direction. Therefore the porosity should be considered as a random space variable in the analysis of flow and transport problems in such media. Thus perturbation theories should have n random. To this end, we extend Deng et al.'s (1993) stochastic transport theory to include the variability in the medium porosity.

7.5. Nonlocal Conservative Transport

We start with Darcy's law at local scale

$$q_i = -K \frac{\partial \phi}{\partial x_i} \tag{83}$$

where q_i is the specific discharge (flow per unit cross-sectional area) component in x_i direction. Following the lead of Deng et al. (1993), it is assumed that a conservative tracer is transported by advection and dispersion under steady, incompressible groundwater flow in a two-dimensional nondeformable porous medium of random conductivity and porosity. The Darcy scale transport equation is

$$n \frac{\partial C}{\partial t} + \frac{\partial (q_i C)}{\partial x_i} - \frac{\partial}{\partial x_i} \left(d_{ij} \frac{\partial C}{\partial x_j} \right) = 0 \tag{84}$$

where d_{ij} is a Darcy scale (local scale) dispersion tensor defined as

$$d_1 \equiv d_{11} = \alpha_L \overline{q}_1$$
$$d_2 \equiv d_{22} = \alpha_{TH} \overline{q}_1$$
$$d_3 \equiv d_{33} = \alpha_{TV} \overline{q}_1$$

154
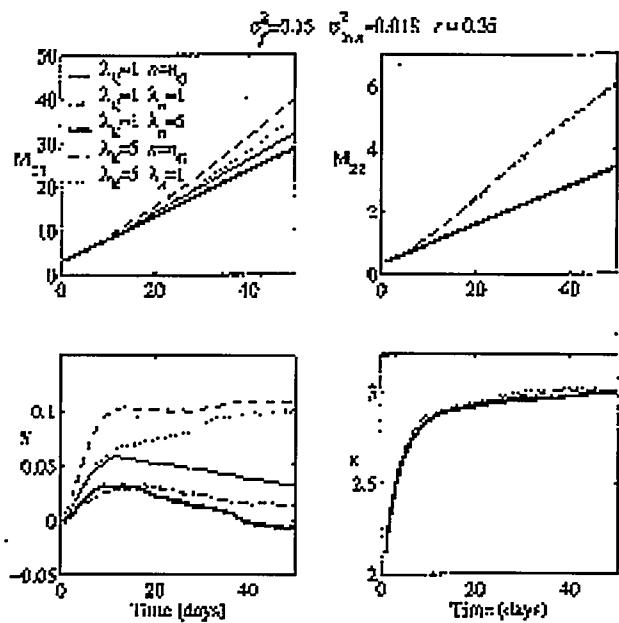
Figure 29. Spatial moments for conservative transport with exponential conductivity using different correlations scales for porosity and conductivity.
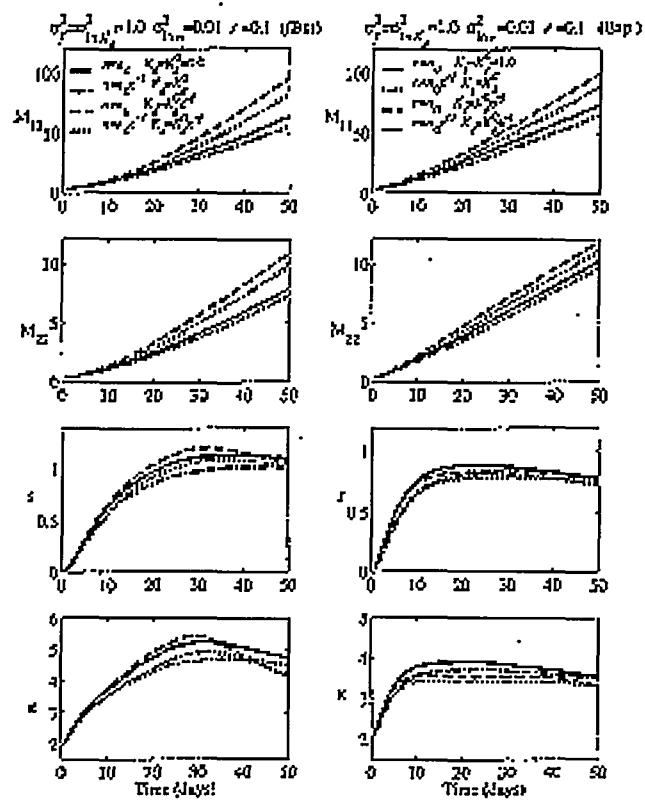
Figure 30. Spatial moments for reactive transport with fBm and exponential conductivity, n and K_d fields with $K_r = 0.1$ and $K_d^G = 1.0$.
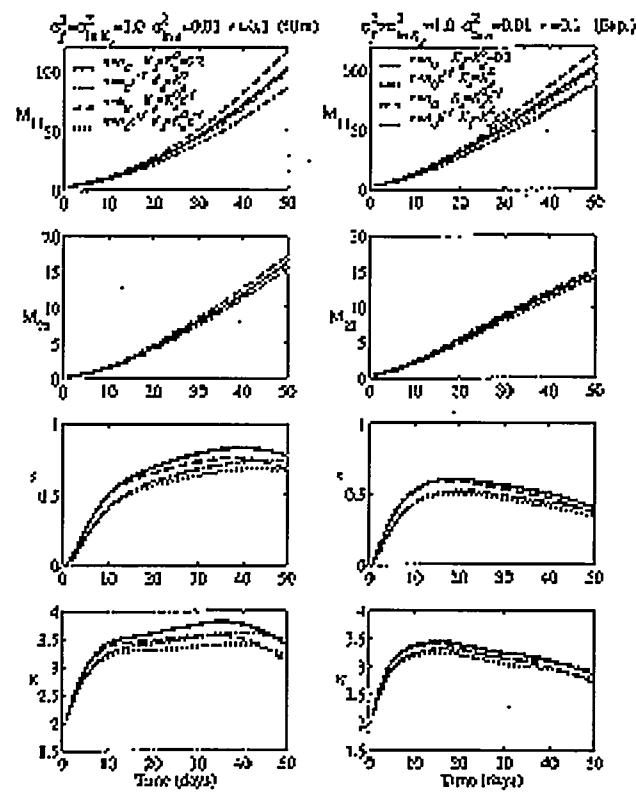
Figure 31. Same as Figure 30 but with $K_d^G = 0.2$.
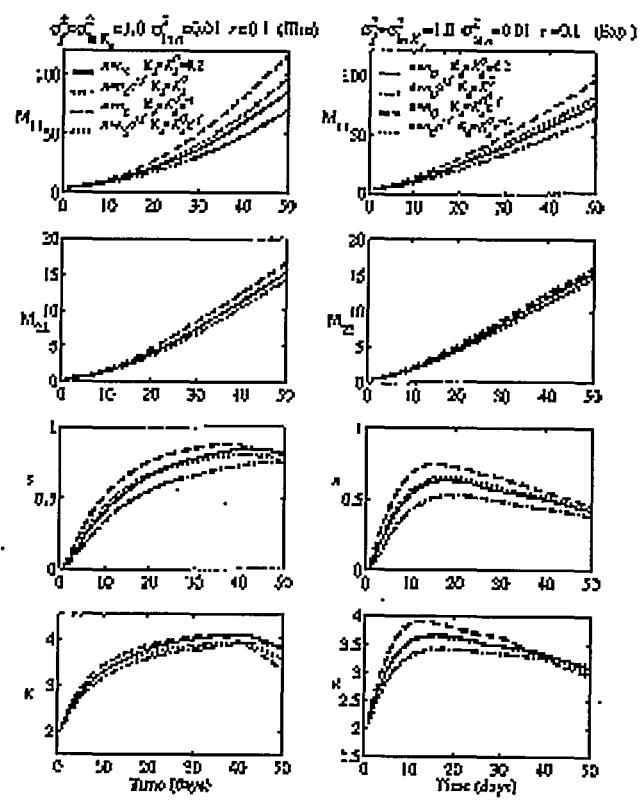
Figure 32. Same as Figure 31 but with $K_r = 10.0$.
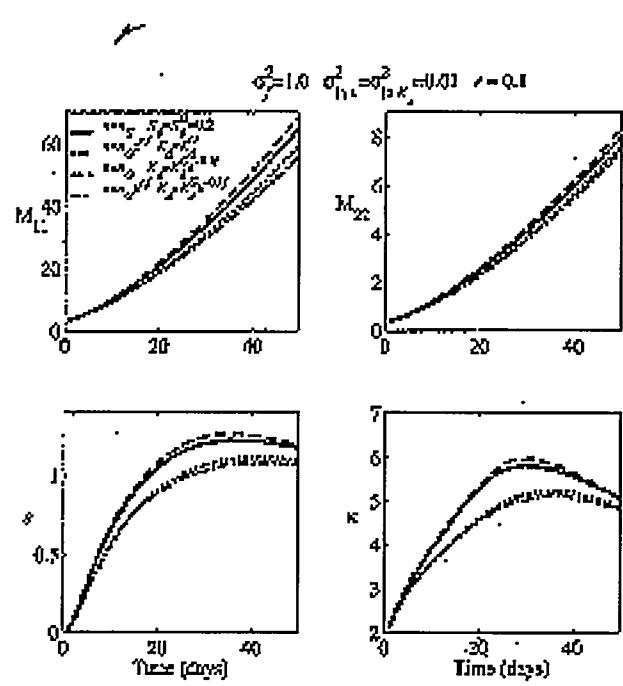
Figure 33. Spatial moments for reactive transport in fBm and exponential conductivity, n and K_d fields with $K_r = 0.1$, $K_d^G = 1.0$, and $\sigma_{\ln K_d}^2 = \sigma_{\ln n}^2 = 0.01$.

where $d_{ij} = 0$ for $i \neq j$, and α_L, α_{TH} and α_{TV} are the so-called local scale longitudinal, transverse-horizontal and transverse-vertical dispersivities, respectively. It is also assumed that the coordinate (Eulerian) system is aligned so that the steady mean flow is in x_1 direction, $\overline{q_1} = \text{const}$, and $\overline{q_2} = \overline{q_3} = 0$. In addition, the hydraulic conductivity is assumed to be a stationary random field with known covariance structure. It is clear that the randomness in the porosity field affects the transport equation. Decomposing the spatially varying parameters in the transport equation into means and fluctuations about the means, $n = \overline{n} + n$, $q_i = \overline{q_i} + q_i$ and $C = \overline{C} + c$, one can write (84) as

$$(\overline{n} + n)\frac{\partial(\overline{C} + c)}{\partial t} + \frac{\partial}{\partial x_i}(\overline{q_i} + q_i)(\overline{C} + c) - d_i \frac{\partial^2(\overline{C} + c)}{\partial x_i^2} = 0 \tag{85}$$

which upon taking expectations becomes

$$\overline{n}\frac{\partial\overline{C}}{\partial t} + \overline{q_1}\frac{\partial\overline{C}}{\partial x_i} - d_i\frac{\partial^2\overline{C}}{\partial x_i^2} = -\frac{\partial\overline{q_i c}}{\partial x_i} - \frac{\partial\overline{nc}}{\partial t} \tag{86}$$

with the mean-removed equation

$$\overline{n}\frac{\partial c}{\partial t} + \overline{q_i}\frac{\partial c}{\partial x_i} - d_i\frac{\partial^2 c}{\partial x_i^2} = \frac{\partial\overline{nc}}{\partial t} + \frac{\partial\overline{q_i c}}{\partial x_i} - n\frac{\partial\overline{C}}{\partial t} - \frac{\partial nc}{\partial t} - q_i\frac{\partial\overline{C}}{\partial x_i} - \frac{\partial q_i c}{\partial x_i} \tag{87}$$

Taking the space Fourier and the time Laplace transforms of (86) and (87)

$$\overline{n}\left(\omega\overline{C}^o - \hat{C}_0\right) + ik_1\overline{q_1}\overline{C}^o + d_i k_i^2 \overline{C}^o = -\left[\frac{\partial\overline{q_i c}}{\partial x_i} - \frac{\partial\overline{nc}}{\partial t}\right]^o \tag{88}$$

$$\overline{n}\left(\omega c^o\right) + ik_1\overline{q_1}c^o + d_i k_i^2 c^o = \left[\frac{\partial\overline{nc}}{\partial t} + \frac{\partial\overline{q_i c}}{\partial x_i} - n\frac{\partial\overline{C}}{\partial t} - \frac{\partial nc}{\partial t} - q_i\frac{\partial\overline{C}}{\partial x_i} - \frac{\partial q_i c}{\partial x_i}\right]^o \tag{89}$$

In driving (89) we assumed that $c(x,0) = 0$. If we define the deterministic function B,

$$B^o(k,\omega) = \left[\omega\overline{n} + ik_1\overline{q_1} + d_i k_i^2\right]^{-1}$$

then (88) and (89) become

$$\overline{C}^o = B^o \overline{n} \hat{C}_0 - B^o \left[\frac{\partial \overline{q_i c}}{\partial x_i} - \frac{\partial \overline{nc}}{\partial t} \right]^o \tag{90}$$

$$c^o = -B^o \left[\frac{\partial \overline{nc}}{\partial t} + \frac{\partial \overline{q_i c}}{\partial x_i} - n \frac{\partial \overline{C}}{\partial t} - \frac{\partial nc}{\partial t} - q_i \frac{\partial \overline{C}}{\partial x_i} - \frac{\partial q_i c}{\partial x_i} \right] \tag{91}$$

Take inverse Fourier and Laplace transforms of (91) to obtain

$$c(x,t) = -B *_{x,t} \left[n \frac{\partial \overline{C}}{\partial t} + q_i \frac{\partial \overline{C}}{\partial x_i} + \frac{\partial (q_i c)}{\partial x_i} - \frac{\partial \overline{q_i c}}{\partial x_i} + \frac{\partial (nc)}{\partial t} - \frac{\partial \overline{nc}}{\partial t} \right] \tag{92}$$

Multiply the above equation by $q_j(\mathbf{x})$, take expectations and neglect triplet flux terms to yield

$$\overline{cq_j}(\mathbf{x},t) = -\int_0^t \int_{R^2} \left[B(\mathbf{x}-\mathbf{y},t-\tau) \overline{q_j(\mathbf{x})q_i(\mathbf{y})} \frac{\partial \overline{C}}{\partial y_i}(y,\tau) + \overline{q_j(\mathbf{x})n(\mathbf{y})} \frac{\partial \overline{C}(\mathbf{y},\tau)}{\partial \tau} \right] dy d\tau \tag{93}$$

Similarly,

$$\overline{cn}(x,t) = -\int_0^t \int_{R^2} \left[B(\mathbf{x}-\mathbf{y},t-\tau) \overline{n(\mathbf{x})q_i(\mathbf{y})} \frac{\partial \overline{C}}{\partial y_i}(\mathbf{y},\tau) + \overline{n(\mathbf{x})n(\mathbf{y})} \frac{\partial \overline{C}(\mathbf{y},\tau)}{\partial \tau} \right] dy d\tau \tag{94}$$

It is clear that these two equations exhibit nonlocality in both space and time. Taking the space-Fourier and the time-Laplace transforms of (93) and (94), assuming $\overline{q_i q_j}$, $\overline{nq_i}$, and $\overline{nn}$ are stationary yields

$$\overline{cq_j}^o = -\left(\frac{1}{2\pi} \right)^3 \left[\left(ik_i \overline{C}^o \right) \left(B^o *_k \widehat{q_j q_i} \right) + \left(\omega \overline{C}^o - \hat{C}_0 \right) \left(B^o *_k \widehat{q_j n} \right) \right] \tag{95}$$

$$\overline{cn}^o = -\left(\frac{1}{2\pi} \right)^3 \left[ik_i \overline{C}^o \left(B^o *_k \widehat{nq_i} \right) + \left(\omega \overline{C}^o - \hat{C}_0 \right) \left(B^o *_k \widehat{nn} \right) \right] \tag{96}$$

Substituting (95) and (96) into (90)

161

$$\bar{C}^o = B^o \bar{n} \hat{C}_0 + B^o \left(\frac{1}{2\pi}\right)^3 \left[\omega\left(\left(\omega\bar{C}^o - \hat{C}_0\right)\left(B^0 *_k \widehat{nn}\right) \right. \right.$$

$$\left. +ik_i\bar{C}^o\left(B^o *_k \widehat{nq_i}\right) \right) + ik_i\left(\left(\omega\bar{C}^o - \hat{C}_0\right)\left(B^o *_k \widehat{q_i n}\right) \right)$$

$$\left. +ik_j\bar{C}_o\left(B^o *_k \widehat{q_j q_i}\right) \right) \bigg] \tag{97}$$

Rearranging the above equation gives the final solution for the mean concentration as

$$\bar{C}^o = \left\{ B^{o-1} + \left(\frac{1}{2\pi}\right)^3 \left(k_i k_j \left(B^o *_k \widehat{q_j q_i}\right) - 2ik_i\omega\left(B^o *_k \widehat{q_i n}\right) - \omega^2\left(B^o *_k \widehat{nn}\right) \right) \right\}^{-1}$$

$$\cdot \left\{ \bar{n} - \left(\frac{1}{2\pi}\right)^3 \left(\omega\left(B^o *_k \widehat{nn}\right) + ik_i\left(B^o *_k \widehat{nq_i}\right) \right) \right\} \hat{C}_0 \tag{98}$$

This equation can be solved exactly in Fourier-Laplace space, and subsequently inverted to real space to yield the mean concentrations for random conductivity and porosity. If the porosity is considered deterministic, (98) reduces to Deng et al.'s (1993) result (equation (90)). Following this latter study, the FFT is used to obtain numerical estimates of the mean concentrations in (38) and hence the mean-plume spatial moments. Figure 34 compares the second spatial moments for purely convective and convective dispersive transport cases obtained with random n positively correlated to the conductivity, to the case of deterministic n. The effect of porosity variability is very significant for the longitudinal moment and increases with time. The transverse moment is slightly affected by the porosity variability which agrees with our Monte Carlo results presented in the previous section.

These findings indicate the flow and transport analysis that is based on the assumption that the porosity is a deterministic constant, may be misleading and can cause large errors. It should be mentioned that the results presented herein cannot be generalized before a detailed study using different covariance structures for the porosity variability and a sensitivity analysis
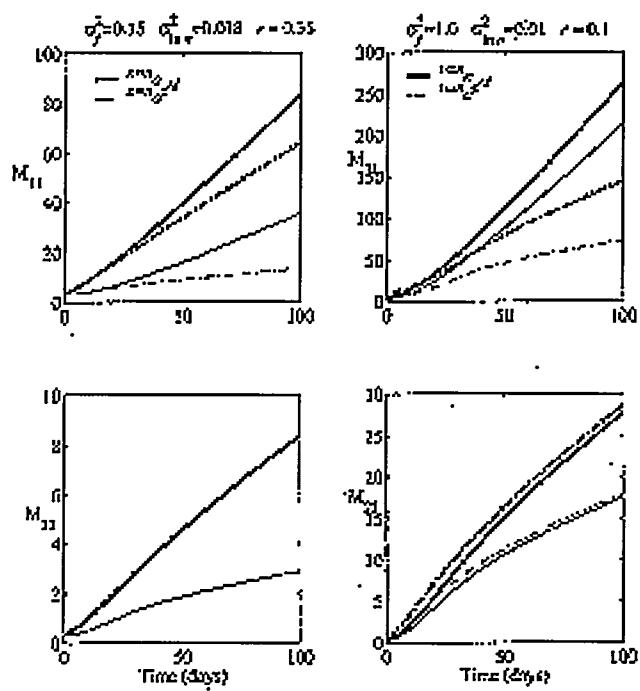
Figure 34. Spatial moments for exponential conductivity and porosity; thick lines indicate convective-dispersive transport, thin lines indicate purely convective transport.

163

are performed. We present here the initial results that indicate the importance of porosity variability and that its effect may be significant and continuously increasing with time.

7.6. Conclusions

The purpose of this paper was to address the significance of the spatial variability in the porous mediums porosity to flow and transport in heterogeneous systems. Numerical simulations were performed using the Monte Carlo method to solve the flow and transport equations over heterogeneous conductivity, porosity, and reactivity fields generated with a fractional Brownian or exponential spectrum. The realized concentrations are averaged to obtain the mean concentration plume and results are presented in terms of concentration contours and/or spatial moments. It was found that the spatial variability of the medium porosity has a significant influence on the plume evolution when it is correlated to the conductivity field. To the authors knowledge, this is the first observation of such an effect. Positive correlation leads to decreased dispersion as a result of smaller variance in the fluctuating velocity, especially in the longitudinal direction. Transverse dispersion is slightly affected by the porosity variability. Negative correlation is shown to increase the plume spreading. The porosity variability has the same effect in both purely convective and convective-dispersive models, but the purely convective case is influenced more by the porosity variability than the convective-dispersive case. For reactive transport in physically and chemically heterogeneous media, the porosity variability, when added to the chemical heterogeneity, significantly affects the results. The importance of the randomness in the porosity and the distribution coefficient depends to a great extent on the variances of $\ln n$ and $\ln K_d$. With K_d more heterogeneous than n, porosity variability has an equal and opposite effect on the plume dispersion as the distribution coefficient for slow exchange reactions. When the reactions are fast, the K_d variability affects dispersion

more than does that of the porosity. When n is as heterogeneous as K_d, the effect of porosity variability dominates the plume spreading. The numerical results suggest that it is important to consider the spatial variability in the porosity of a porous medium and analyze the role its covariance structure plays in flow and transport processes in such media. A first step in this regard was taken where the nonlocal stochastic transport theory developed by Deng et al. (1993) was modified to account for the porosity spatial variability and its cross correlation to the hydraulic conductivity. Results of the modified stochastic theory supported the Monte Carlo results and showed that longitudinal dispersion is significantly affected by the porosity variability with the effect increasing as time increases. The importance of these findings and the implications of the study for dispersion in real aquifers can be assessed when the cross correlation between porosity and conductivity is established.

8. Higher-Order Eulerian Solutions to the Stochastic Chemical Transport Problem

8.1. Introduction

It is generally recognized that transport of conservative chemicals in the subsurface is to a large extent dictated by the velocity profile of the water in which the chemical is dissolved. The velocity of the water, in turn, is governed by natural geologic heterogeneity and boundary conditions. Over the last two decades many stochastic approaches have been devised to study this problem. There are essentially two reference frames adopted, eulerian and lagrangian (see, Gelhar 1993; Cushman, 1990; 1997; Dagan, 1989). In the eulerian frame one fixes oneself in space and watches the contaminant pass by. This is in contrast to the lagrangian frame wherein the observer views the world while riding a contaminant particle. Most eulerian methods are a modification of that set out by Gelhar and Axness (1983), and most lagrangian methods are extensions of Simmons' (1982) and Taylor's (1921) work. The problem with classical eulerian perturbation schemes is closure and the degree of accuracy of the closure (Dagan and Neuman, 1991; Hassan et al., 1998). It is generally known that eulerian closure schemes underestimate higher-order moments (e.g., the forth-order eulerian moment for conservative tracers is 1/3 of that in the lagrangian approach (Dagan and Neuman, 1991)). From a practical perspective the eulerian approach can be used to study the effect of local-scale dispersion and nonlocal macrodispersion. Further, the eulerian methods can be used to calculate not only the various spatial moments, but also the mean concentration. The lagrangian approach on the other hand can be used to calculate the spatial moments, and, with significant difficulty, the mean concentration. In addition the influence of local dispersion on plume development is commonly neglected in lagrangian method, which may lead to underestimation of the spatial moments, especially in transverse directions (Cushman et al., 1996; Hu and Cushman, 1997), and further it

may lead to serious errors in dilution (Kapoor and Gelhar, 1994 a,b). However, if analysis is performed consistently, using either frame, results should be equivalent with the two approaches. In this study we provide a recursive perturbation solution to the eulerian transport problem for a conservative chemical in a random conductivity field. The method applied here overcomes the closure weaknesses in classical eulerian approaches and provides a systematic closure approach to any arbitrary order.

Recently second-order solutions have been developed to investigate the accuracy of the first-order solution. Dagan (1994) developed a second-order correction for the second transverse moment using the lagrangian approach in two dimensions. Although the transport closure was second-order, the flow closure he employed was only first-order. His results suggested that the second-order correction to the transport problem had little effect on the transverse moment. Based on Dagan's (1994) second-order correction to the transport problem and Deng and Cushman's (1995) second-order correction to the flow problem, Hsu et al. (1996) investigated the combined effects of second-order corrections to both flow and transport on the second transverse moment for a simplified case in two dimensions. Their results indicate the second-order correction to the flow problem has a profound effect on transverse transport. These results, however, are in stark contrast to the Monte Carlo results of Chin and Wang (1992) and Bellin et al. (1992) wherein such an effect on transverse transport was not observed. Based on their findings, Hsu et al. (1996) questioned the accuracy of the Monte Carlo simulations and suggested these simulations may only be $O(\sigma_f^2)$. Employing a classical eulerian perspective, Naff (1994) developed consistent second-order corrections to both the flow and transport problems for a special type of heterogeneity. His results suggested second-order corrections to both the flow and transport problems may lead to a plume evolution with strongly non-Gaussian character at

late time. He also showed that if the eulerian analysis is consistent with lagrangian, the fourth moments obtained by eulerian and lagrangian methods are same.

In this study we would like to take advantage of the recursive perturbation method to obtain the $O(\sigma_v^4)$ correction to the transport equation and apply Deng and Cushman's (1995) approach to get the $O(\sigma_f^4)$ correction to the flow equation. These two corrections are combined to investigate their influence on plume evolution. The results are then compared with those obtained via a classical method (Deng et al., 1993) and Monte Carlo simulation (Hassan et al., 1997). We begin by following Cushman and Hu (1997) and Deng and Cushman (1995), and subsequently perform a detailed analysis of mean concentration.

8.2. The Closure Problem Induced by the Classical Eulerian Approach to Chemical Transport

Classically, a conservative chemical in a nondeformable porous medium of constant porosity with constant local-scale dispersivities satisfies

$$HC \equiv \frac{\partial C}{\partial t} + V_i \frac{\partial C}{\partial x_i} - d_i \frac{\partial^2 C}{\partial x_i^2} = 0 \tag{99}$$

in an unbounded domain with diagonal local dispersion tensor. Geologic heterogeneity forces us to consider the hydraulic conductivity to be a random space function, and this in turn implies that both the Darcy velocity, V_i, and solution concentration, C, are random space functions. Following Gelhar and Axness's [1983] pioneering work one now decomposes the concentration and velocity into their means and fluctuations about the means:

$$C = \bar{C} + c_i \tag{100a}$$

$$V_i = \bar{V}_i + v_i \tag{100b}$$

For simplicity we assume $\overline{V_i} = (V, 0, 0)$ is constant, and then write the equations for the mean concentration and its fluctuation as

$$\overline{H}\overline{C} \equiv \frac{\partial \overline{C}}{\partial t} + \overline{V_i} \frac{\partial \overline{C}}{\partial x_i} - d_i \frac{\partial^2 \overline{C}}{\partial x_i^2} = -\frac{\partial \overline{cv_i}}{\partial x_i} \qquad (101)$$

$$\overline{H}c = -\left(v_i \frac{\partial \overline{C}}{\partial x_i} + \frac{\partial v_i c}{\partial x_i} - \frac{\partial \overline{v_i c}}{\partial x_i} \right) \qquad (102)$$

Several approaches can be followed to close (101) using (102) and the Green's function for H. Classically, this was done (Gelhar and Axness, 1983) with a spectral decomposition of a weakly stationary process. Here, however, we follow Deng et al. (1993) using a more transparent transform approach. With similar assumptions Deng et al.'s (1993) result reduces to Gelhar and Axness's (1983).

Let G be the Green's function for the deterministic operator $\overline{H}$ with $G \downarrow 0$ as $|\mathbf{x}| \to \infty$ and initial data

$$HG = \delta(\mathbf{x}, t) \qquad (103)$$

An implicit solution for c is given by

$$c(\mathbf{x}, t) = -\int_0^t \int_{R^3} G(\mathbf{x} - \mathbf{y}, t - t') \left[v_i(\mathbf{y}) \frac{\partial \overline{C}(\mathbf{y}, t')}{\partial y_i} + \frac{\partial v_i(\mathbf{y})c(\mathbf{y}, t')}{\partial y_i} - \frac{\partial \overline{v_i(\mathbf{y})c(\mathbf{y}, t')}}{\partial y_i} \right] d\mathbf{y} dt' \qquad (104)$$

with

$$G(\mathbf{x}, t) = \prod_{k=1}^3 \exp\left[-\frac{(x_k - \overline{V_k}t)^2}{4d_k t} \right] (4\pi d_k t)^{-1/2} \qquad (105)$$

To obtain the macroscale dispersive flux, $\overline{v_j c}(\mathbf{x}, t)$, multiply (104) by $v_j(\mathbf{x})$ and take expected values to obtain

169

$$\overline{c(\mathbf{x},t)v_j(\mathbf{x})} = -\int_0^t \int_{R^3} G(\mathbf{x}-\mathbf{y},t-t') \left[\overline{v_j(\mathbf{x})v_i(\mathbf{y})} \frac{\partial \overline{C}(\mathbf{y},t')}{\partial y_i} + \frac{\partial \overline{v_j(\mathbf{x})v_i(\mathbf{y})c(\mathbf{y},t')}}{\partial y_i} \right] d\mathbf{y}dt' \quad (106)$$

If one next assumes the term involving the triplet correlation is small compared to that involving the two-point correlation on RHS (106), and in addition if one assumes the velocity covariance is weakly stationary, then one finally arrives at a convolution-Fickian macroscale flux

$$\overline{c(\mathbf{x},t)v_j(\mathbf{x})} = -\int_0^t \int_{R^3} D_{ij}(\mathbf{x}-\mathbf{y},t-t') \frac{\partial \overline{C}(\mathbf{y},t')}{\partial y_i} d\mathbf{y}dt' \quad (107)$$

where D_{ij} has its obvious definition. If one further assumes the gradient of $\overline{C}$ varies slowly in comparison to D_{ij} then one arrives at a quasi-Fickian flux:

$$\overline{c(\mathbf{x},t)v_j(\mathbf{x})} \approx -D_{ij}'(t) \frac{\partial \overline{C}(\mathbf{x},t)}{\partial x_i} \quad (108)$$

with

$$D_{ij}'(t) = \int_0^t \int_{R^3} D_{ij}(\mathbf{y},t-t') d\mathbf{y}dt' \quad (109)$$

Either (107) or (108) may be used to close (101).

The reader should note a significant problem with (107) and (108): we do not, a priori, know the error induced by neglecting the triplet flux. Dagan and Neuman (1991) and others criticize the eulerian closure schemes presented. They argue that the truncated triplet term may be of the same order as those retained and further that it will significantly influence the fourth spatial moments. A numerical study by Hassan et al. (1998) shows that if $\ln K$'s variance is small and $\ln K$'s correlation structure is chosen to be exponential, the neglected triplet term is small in comparison to the retained terms. However, in the other cases, such as large variance and/or power law $\ln K$ correlation structure, this may not be true. In the next section we

illustrate an alternative perturbation approach that does not rely on the balance for mean concentration, and further does not require a closure scheme for the so-called "macro-scale dispersive flux", $\overline{cv_j}$. That is, we believe there is no need to define a macroscale dispersive flux, and in fact, such a definition clouds the picture of large scale transport.

8.3. A Systematic Real Space Closure Model for Chemical Transport

Again assume the validity of (99) locally, but do not decompose C into its mean and fluctuation. The authors believe it is that decomposition that leads to the closure debate associated the eulerian approach. Rather we decompose V_i as before and introduce an infinite series decomposition for C. Normally we set (Cushman and Hu, 1997)

$$C = \sum_{j=0}^{\infty} C^j \tag{110}$$

where C^0 satisfies the sure problem

$$HC^0 = 0 \tag{111}$$

subject to $C^0\big|_{t=0} = C_0$, where C_0 is the initial data, and further assume

$$C^j \approx O(\sigma_v^j) \quad j \geq 1 \tag{112}$$

with $\left(\sigma_v/\|V\|\right)^2 < 1$. For simplicity in exposition we further take $\|V\| \approx O(1)$, so that our previous assumption requires

$$\sigma_v^2 < 1 \tag{113}$$

Equating terms of the same order in σ_v, we find the following recursive hierarchy in an infinite spatial domain

$$\bar{H}C^1 = -v_i \frac{\partial C^0}{\partial x_i}$$

$$\vdots$$

$$\bar{H}C^N = -v_i \frac{\partial C^{N-1}}{\partial x_i}$$

(114)

with the initial condition $C^N\big|_{t=0} = 0 \;\; (N = 1,2,3,\cdots)$.

Again letting G be the deterministic Green's function for $\bar{H}$, we find

$$C^0(\mathbf{x},t) = \int\limits_{R^3} G(\mathbf{x}-\mathbf{y},t)C_0(\mathbf{y})d\mathbf{y}$$

(115)

$$C^1(\mathbf{x},t) = -\int\limits_0^t \int\limits_{R^3} G(\mathbf{x}-\mathbf{y},t-t')v_i(\mathbf{y})\frac{\partial C^0(\mathbf{y},t')}{\partial y_i}d\mathbf{y}dt'$$

(116)

$$\vdots$$

$$C^N(\mathbf{x},t) = -\int\limits_0^t \int\limits_{R^3} G(\mathbf{x}-\mathbf{y},t-t')v_i(\mathbf{y})\frac{\partial C^{N-1}(\mathbf{y},t')}{\partial y_i}d\mathbf{y}dt'$$

(117)

The system (115)-(117) is recursive and so a closed form solution for C^N can be obtained in terms of the initial data, the deterministic Green's function for $\bar{H}$, and the stochastic velocity. It is given for $N \geq 1$ by

$$C^N(\mathbf{x},t) = (-1)^N$$
$$\int\limits_0^t \cdots \int\limits_0^{t^{N-1}} \int\limits_{R^{3(N+1)}} G(\mathbf{x}-\mathbf{x}^1,t-t')\left[\prod_{\ell=1}^{N-1}\frac{\partial G}{\partial x_{j\ell}^\ell}(\mathbf{x}^\ell-\mathbf{x}^{\ell+1},t^\ell-t^{\ell+1})\right]\frac{\partial G}{\partial x_{j_N}^N}(\mathbf{x}^N-\mathbf{x}^{N+1},t^N)$$

(118)

$$\left[\prod_{l=1}^N v_{j_l}(\mathbf{x}^\ell)\right]C_0(\mathbf{x}^{N+1})d\mathbf{x}^1\cdots d\mathbf{x}^{N+1}dt^1\cdots dt^N$$

In deriving (67) we have used the assumption $\frac{\partial v_i}{\partial x_i} = 0$.

172

From here we find the stochastic concentration to $O(\sigma_v^M)$ is

$$C(\mathbf{x},t) = \int_{R^3} G(\mathbf{x}-\mathbf{y},t)C_0(\mathbf{y})d\mathbf{y} + \sum_{k=1}^{M}(-1)^k$$

$$\int_0^t \cdots \int_0^{t^{k-1}} \int_{R^{3(k+1)}} \left\{ G\left(\mathbf{x}-\mathbf{x}^\ell,t-t^\ell\right) \right.$$

$$\left[\sum_{\ell=1}^{k-1} \frac{\partial G}{\partial x_{j\ell}^\ell} \cdot \left(\mathbf{x}^\ell - \mathbf{x}^{\ell+1},t^\ell - t^{\ell+1}\right) \right] \frac{\partial G}{\partial x_{jk}^k}\left(\mathbf{x}^k - \mathbf{x}^{k+1},t^k\right)$$

$$\left. \left[\prod_{\ell=1}^{k} v_{j\ell}\left(\mathbf{x}^\ell\right) \right] C_0\left(\mathbf{x}^{k+1}\right) \right\} d\mathbf{x}^1 \cdots d\mathbf{x}^{k+1} dt^1 \cdots dt^k \tag{119}$$

and its mean is

$$\overline{C}(\mathbf{x},t) = \int_{R^3} G(\mathbf{x}-\mathbf{y},t)C_0(\mathbf{y})d\mathbf{y} + \sum_{k=1}^{M}(-1)^k$$

$$\int_0^t \cdots \int_0^{t^{k-1}} \int_{R^{3(k+1)}} \left\{ G(\mathbf{x}-\mathbf{x}^\ell,t-t^1) \right.$$

$$\left[\sum_{\ell=1}^{k-1} \frac{\partial G}{\partial x_{j_\ell}^\ell}(\mathbf{x}^\ell - \mathbf{x}^{\ell+1},t^\ell - t^{\ell+1}) \right] \frac{\partial G}{\partial x_{j\ell}^k}(\mathbf{x}^k - \mathbf{x}^{k+1},t^k)$$

$$\left. \left[\overline{\prod_{\ell=1}^{k} v_{j\ell}(\mathbf{x}^\ell)} \right] C_0(\mathbf{x}^{k+1}) \right\} d\mathbf{x}^1 \cdots d\mathbf{x}^{k+1} dt^1 \cdots dt^k \tag{120}$$

There are several important points to note in (120). First, to arrive at the mean concentration we never need the mean balance law of the Gelhar and Axness's (1983) approach (we just use the mean operator); secondly, we obtain the actual stochastic concentration so that given a realization of the velocity field, one can use (119) in a Monte Carlo approach without solving the CDE; third, we have included the effects of local dispersion; and fourth, the solution can be implemented via fast Fourier Transform (FFT).

8.4. Monte Carlo vs. Perturbation: Numerical Results

For comparison and to shed more light on the significance of flow and transport corrections, we perform Monte Carlo simulations in two-dimensional horizontal domains and compare ensemble mean concentrations and spatial moments from the two solutions. Monte Carlo analysis is performed in a manner similar to Hassan et al. (1997, 1998). For completeness we briefly review the numerical approach employed , and for more details the reader is referred to Hassan et al. (1998).

Conductivity realizations are generated based on a Gaussian through an FFT-based approach. A uniform mean head gradient is imposed on the domain along the x_1-direction by fixing the heads at the two boundaries normal to x_1. The other two boundaries are assumed to be impervious. The flow equation, subject to these boundary conditions, is solved via a finite difference method which yields the head values at the grid points of the modeled domain. Darcy's law is then applied to obtain the pore velocities based on the generated conductivity, the obtained head, and the assumed constant effective porosity. The transport equation is solved for each individual realization using a random walk particle tracking approach discussed earlier. The transport solutions are ensemble averaged to obtain the mean concentrations and the spatial moments.

The FFT method developed by Deng et al. (1993), and subsequently elaborated on in Deng and Cushman (1995) and Hu et al. (1995, 1997), is adapted here and used to obtain numerical estimates of the mean concentrations given in Eq. (106). We compute the mean concentrations and spatial moments using the deterministic solution, C_0, the first-order flow and transport solution, $C_{[1, 1]}$, the first-order flow and second-order transport, $C_{[1, 2]}$, the second-order

174

flow and first-order transport solution, $C_{[2, 1]}$, the second-order flow and transport, $C_{[2, 2]}$, and the convolution Fickian solution, C_{NL}, of Deng et al. (1993).

Previous studies that deal with second-order solutions to the flow and transport problems usually assume that the velocity distribution is Gaussian (e.g., Dagan, 1994; Deng and Cushman, 1995, 1998; Hsu et al., 1996), and as such the three-point velocity correlations are dropped from the analysis. We present in this study the general solution that does not require the Gaussian assumption. This leads to additional terms in the second-order solution. However, for simplicity and to permit direct comparison between our results and previous studies we drop these terms in our numerical computations. In our first case we set $\sigma_f^2 = 0.4$. Figure 35 shows four comparisons of mean-concentration distributions. In each case, the Monte Carlo results (solid contours) are superimposed on the theoretical solution (dashed-dotted contours) for two dimensionless times. In the first panel of Fig. 35 we compare Monte Carlo results to the deterministic solution, $\overline{C}_0$. Figure 35B compares Monte Carlo results to $\overline{C}_{[1,1]}$. The solution with transport correction, $\overline{C}_{[1,2]}$ is presented in Fig. 35C, the solution with the corrections to the flow, $\overline{C}_{[2,1]}$ is shown in Fig. 35D, and the correction to both flow and transport is in Fig. 35E. For the purpose of comparison, the convolution Fickian result, $\overline{C}_{NL}$, is calculated and shown in Fig. 35F. As can be seen from these comparisons, the deterministic solution significantly underestimates the dispersion whereas the first-order solution leads to an increased dispersion as compared to the Monte Carlo results. The convolution Fickian solution, on the other hand, leads to a slightly more dispersed plume than the Monte Carlo results. The solution with transport corrections gives the closest results to the Monte Carlo simulations. When the velocity corrections are added, dispersion slightly changes in the longitudinal direction, but significantly increases in the transverse direction. This is due to the significant increase of transverse velocity

covariance, $\overline{v_2 v_2}$, resulting from the second-order correction to flow equation. However, the second-order correction to flow will not significantly change $\overline{v_1 v_1}$ (Deng and Cushman, 1998). These comparisons become more transparent using the spatial moments (Fig. 36). As expected, the first spatial moment is not influenced by the order of the solution. The second longitudinal moment shows that $\overline{C}_{[2,2]}$ is consistent wit almost produces the Monte Carlo results. The first-order solution, $\overline{C}_{[1,1]}$, and the convolution Fickian solution lead to a higher second longitudinal moment. This result is consistent with Hsu et al. (1996) and Bellin et al. (1992) where the longitudinal second moment obtained using a Monte Carlo approach was significantly below the predictions of first-order Lagrangian transport (advection only) theories. The second transverse moment presented in Fig. 36 reveals a different picture. It indicates that the first-order and the convolution Fickian solutions are the closest to the Monte Carlo results, whereas the second-order solution, $\overline{C}_{[2,2]}$, leads to substantially higher moments. This result is also similar to the findings of Hsu et al. (1996) whose second-order flow and advective transport solution give significantly higher transverse moments than the Monte Carlo results. The Monte Carlo simulations underestimate the second-order predictions of transverse moments to a greater extent than do the first-order predictions (Hsu et al., 1996). The theoretical results for the skewness show a pattern that is consistent with the Monte Carlo solution, though more negative. These results also indicate that including the second-order flow correction reduces the magnitude of the skewness, leading to closer results to the Monte Carlo simulations. Figure 37 is similar to Fig. 36, but with a log-conductivity variance of 1.0. Qualitatively, the results are similar to Fig. 36 and same conclusions can be drawn.

It should be noted that the above results are based on a specific form of the Gaussian covariance function. Several previous studies of second-order corrections to flow and transport (Deng and

Cushman, 1995; Dagan, 1994; Naff, 1994; Hsu et al., 1996) are also based on the Gaussian covariance of log-conductivity. We next would like to investigate the influence of the second-order corrections to spatial moments based on a different log-conductivity structure. The conductivity model we choose here qualitatively behaves like the spectrum inferred from measurements (Kapoor and Kitanidis, 1998). The two-dimensional version of the spectrum is

$$\hat{\overline{ff}}(k) = \sigma_f^2 \prod_{i=1}^{2} \frac{2\ell_i^3 k_i^2}{\sqrt{\pi}} \exp(-\ell_i^2 k_i^2) \tag{121}$$

where ℓ_i is a characteristic length, which can be thought of as the correlation length. Figure 38 shows the spatial moments with for this log-conductivity structure and with σ_f^2 of 1.0. Comparing Fig. 38 with Fig. 37 we see no significant differences for the second moments. However, the skewness results are different. Velocity corrections lead to a significant deviation from Monte Carlo results. The plume is strongly negatively distributed at early time and approaches the Monte Carlo results at late time.

It is important to note that our theoretical derivation does not assume any distribution for the velocity field. We simplified the solution and dropped the three-point velocity correlation to allow a direct comparison with the studies that have a Gaussian distribution assumption for the triplet correlation terms (Hsu et al., 1996; Dagan, 1994; Naff, 1994). In a subsequent article we intend to investigate the influence of this assumption on transport behavior. In this regard it was shown in Bellin et al. (1992) that the velocity distribution is not necessarily Gaussian even if the underlying conductivity distribution is. This is not a surprise since the transformation relating the two is nonlinear.

The key question that arises from the previous results is why the solution with both flow and transport corrections deviates more from Monte Carlo results than does the first-order

177

solution, especially for the transverse moment. As mentioned earlier, the higher-order corrections to the velocity covariance significantly increase transverse covariance, and slightly increase the longitudinal. For example, Hsu et al. (1996) found that second-order flow corrections in two dimensions increase longitudinal velocity variance by 8% whereas transverse velocity variance is increased by 34%. Deng and Cushman (1995, 1998) reported even stronger effects for three-dimension case. By increasing the transverse velocity variability through higher covariance values, one would expect enhanced dispersion normal to mean flow direction. Numerical studies also showed that the transverse covariance obtained through Monte Carlo is higher than that predicted by first-order flow theories (Bellin et al., 1992; Chin and Wang, 1992; Hassan et al., 1998). However, it can be seen from these studies that the deviations between Monte Carlo results and the first-order predictions are not as large as predicted by the second-order theory. For example, the Monte Carlo results of Hassan et al. (1998, Fig. 38) predict a transverse velocity variance that is only 2% higher than the first-order prediction for $\sigma_f^2 = 0.15$ and about 14% higher for $\sigma_f^2 = 0.95$. In addition, the same study showed that the deviations of the first-order prediction from the Monte Carlo solution diminish considerably after one conductivity correlation length. In a similar study, Bellin et al. (1992, Fig. 39) reports a Monte Carlo estimate of $\overline{v_2 v_2}(0)$ that is about 10% higher than first-order prediction for $\sigma_f^2 = 0.8$ and about 28% higher for $\sigma_f^2 = 1.6$. Therefore, it is clear that although the effects of second-order corrections to the velocity covariance seem to be consistent with the fact the Monte Carlo predictions are higher than the first-order results, these corrections increase the covariances to a much larger extent than what is indicated by Monte Carlo simulations.

In order to clarify and elaborate on this aspect, we use our transport theory (both first- and second-order) to predict mean-concentration spatial moments, but utilizing velocity

covariances generated numerically by Monte Carlo simulations of the flow problem. The two-dimensional velocity covariances are generated numerically for the Gaussian log-conductivity distribution at the same two heterogeneity levels employed before. These covariances are used in the transport solution instead of using the analytical velocity covariances. The results of this case and the comparison with the Monte Carlo spatial moments are presented in Figure 39. The results with the numerical velocity, labeled as C[MC, 1] and C[MC, 2], are for the first-order transport model with numerical velocity covariance and the second-order transport model with same covariances. It is clear that these new cases are very similar to the solutions without flow corrections shown in Figures 36 and 37. The results in Figure 39 supports our argument that second-order flow corrections contribute to the transverse velocity covariance. From these results, one can conclude that either the second-order corrections are not sufficient, and even higher corrections are needed. Or the Monte Carlo simulations are limited to an accuracy to between first and second order. Future efforts should be devoted to explore the issue.

8.5. Summary

In this study we have presented systematic closures to the eulerian flow and transport problems for conservative tracers in heterogeneous media. The transport solution is N^{th}-order accurate in σ_y, and it includes the effects of local-scale dispersion. General closed form expressions were presented for the mean concentration to arbitrary order of σ_y. The solution combines the best attributes of classical eulerian and lagrangian approaches to transport. A more detailed form of mean concentration is derived to σ_y^4. The algorithm followed lays a path to general closure schemes of arbitrary order, and overcomes the closure weakness of classical eulerian methods (Dagan and Neuman, 1991). The analysis can be extended in a straight-
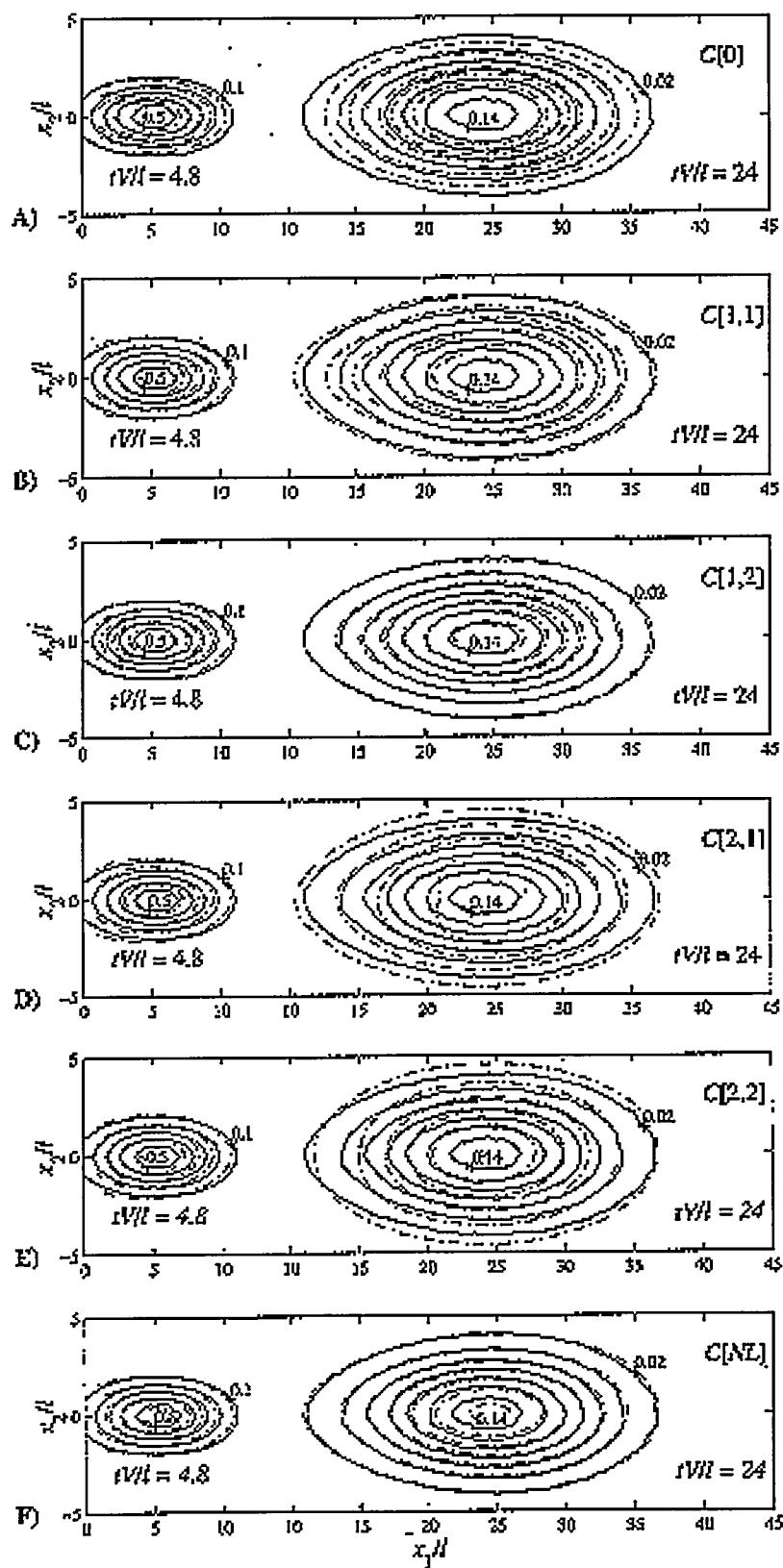
Figure 35. Comparison between Monte Carlo solution (solid contours) and theoretical predictions (dash-dotted contours) for (a) deterministic $\overline{C}$, (b) first-order $\overline{C}$, (c) first-order flow and second-order transport $\overline{C}$, (d) second-order flow and first-order transport $\overline{C}$, (e) second-order $\overline{C}$, where $\sigma_f^2 = 0.4$, and (f) nonlocal prediction of $\overline{C}$.

180
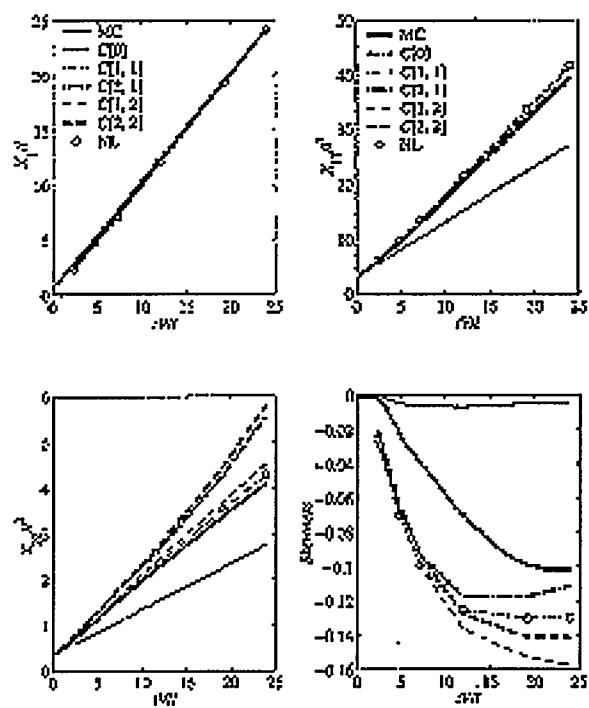
Figure 36. Comparison between spatial moments obtained via the Monte Carlo solution and theoretical predictions for $\sigma_f^2 = 0.4$.
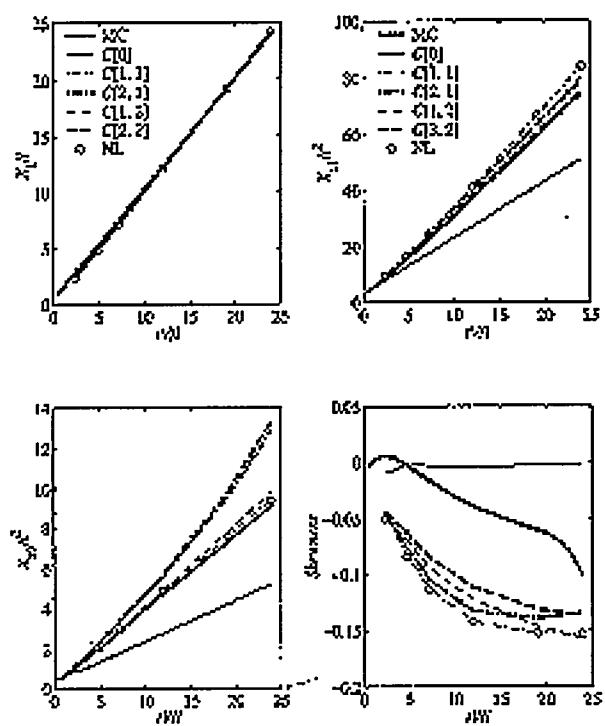
Figure 37. Same as Figure 36 but for $\sigma_f^2 = 1.0$.
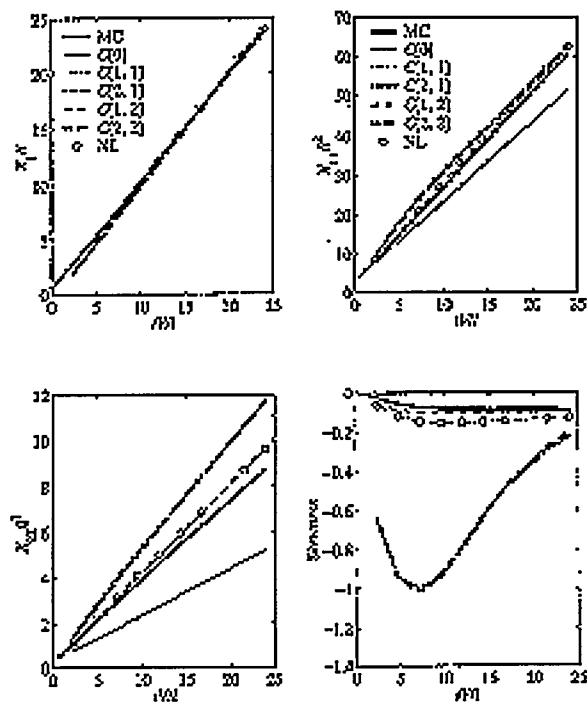
Figure 38. Same as Figure 37 but using the log conductivity spectrum of (53) instead of (51).
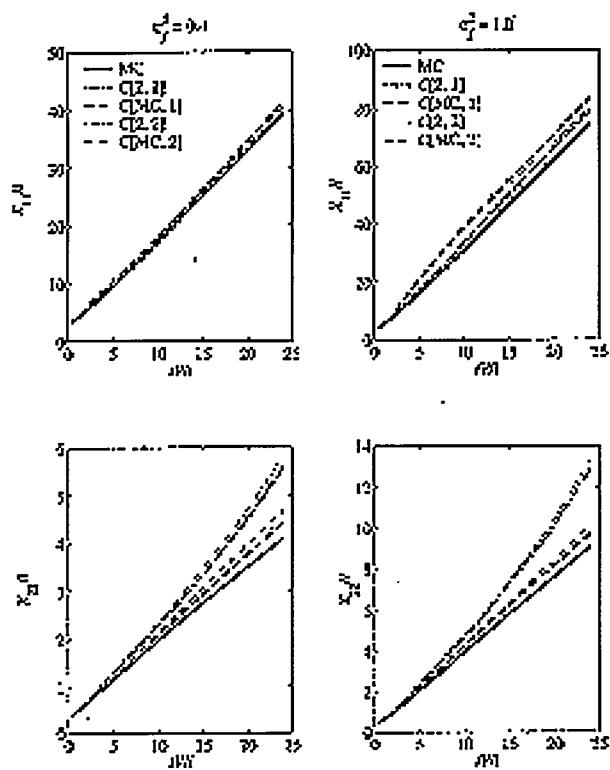
Figure 39. Comparison between Monte Carlo results and analytical moment solutions with numerical velocity covariance.

forward fashion to handle linear reactions and to examine the concentration variance (dilution problems).

Two spatial correlation structures of log hydraulic conductivity shown in (50) and (52) were chosen for this study. The triplet velocity correlation is assumed to be zero. Based on these assumptions we have the following conclusions:

1. From the spatial moments in Figs. 36, 37 and 38, it appears $C_{[1,1]}$ is comparable to Deng et al's (1993) nonlocal theory. This shows the low-order method provided here is equivalent to the nonlocal model.

2. Corrections to the transport equation do not significantly impact the second spatial moments. Higher-order moments may be impacted but evaluating this impact is fraught with numerical difficulties.

3. Corrections to flow equation may significantly affect the transport behavior. Second-order corrections only significantly influence the second spatial moments in transverse directions, not in longitudinal direction, which is consistent with previous studies (Hsu et al., 1996; Dagan, 1994; Naff, 1994).

4. The skewness obtained by the Monte Carlo simulation is less negative than those obtained via the perturbation methods. However, the influence of second-order correction to flow or transport on skewness is not obvious, which may be attributed to the accuracy of the numerical method applied in this study. In addition, the influence of corrections to skewness also depends on the chosen conductivity structure.

5. The significant difference between the second transverse moments obtained through second-order corrections and Monte Carlo simulation suggests that a more accurate Monte Carlo simulator is needed or an analysis of the order of the Monte Carlo method. This point stems

from the fact that transport solutions with velocity covariances generated via Monte Carlo simulations agree very closely with transport solutions based on first-order flow models, which in turn are close to Monte Carlo simulations.

References

Benson, D., R. Schumer, S.W. Wheatcraft, and M.M. Meerschaert (2000) Fractional dispersion, Lévy motion, and the MADE tracer tests, Trans. Por. Media (In Press).

Chilakapati, A., T.R. Ginn, and J. Szecsody. An analysis of complex reaction networks in groundwater modeling, Water Resources Research, 34:1767-1780, 1998.

Cushman, J.H. (1991) On Diffusion in Fractal Porous Media, Water Resour. Res. 27:643-644.

Cushman, J.H. (1997) The Physics of Fluids in Hierarchical Porous Media: Angstroms to Miles, Kluwer, 480pp.

Cushman, J.H. (Ed) (1990) Dynamics of Fluids in Hierarchical Porous Media, Academic, 500pp.

Cushman, J.H. and T.R. Ginn (1993) Nonlocal Dispersion in Media with Continuously Evolving Scales of Heterogeneity, Trans. Por. Media 13:123-138.

Benson, D., R. Schumer, S.W. Wheatcraft, and M.M. Meerschaert (2000) Fractional dispersion, Lévy motion, and the MADE tracer tests. Trans. Por. Media (In Press).

Chilakapati, A., T.R Ginn, and J. Szecsody (1998) An analysis of complex reaction networks in groundwater modeling, Water Resour. Res. 34:1767-1790.

Cushman, J.H. (1991) On Diffusion in Fractal Porous Media, Water Resour. Res. 27:643-644.

Cushman, J.H. (1997) The Physics of Fluids in Hierarchical Porous Media: Angstroms to Miles, Kluwer, 480pp.

Cushman, J.H. (Ed) (1990) Dynamics of Fluids in Hierarchical Porous Media, Academic, 500pp.

Cushman, J.H. and T.R. Ginn (1993) Nonlocal Dispersion in Media with Continuously Evolving Scales of Heterogeneity, Trans. Por. Media 13:123-138.

Barton J.W., and R.M. Ford (1997) Mathematical model for characterization of bacterial migration through sand cores. Biotechnol. Bioeng. 53:(5) 487-496.

Berg, H.C. and L. Turner (1990) Chermotaxis of bacteria in glass capillary arrays. Biophysics J. 58:(4)919-930.

Berg, H.C. (2000) Motile behavior of bacteria. Phys. Today 53:(1) 24-29.

Berg, H.C. and D.A. Brown (1972) Chermotaxis in Escherichia coli analysed by three-dimensional tracking. Nature 239:500-504.

187

Biondi, S.A., J.A. Quinn, and H. Goldfine (1998) Random motility of swimming bacteria in restricted geometries. AIChE Journal 44:(8)1923-1929.

Busscher H.J., A.T. Poortinga, and R. Bos (1998) Lateral and perpendicular interaction forces involved in mobile and immobile adhesion of microorganism on model solid surfaces. Curr. Microbiol. 37:(5)319-323.

Camesano, T.A., and B.E. Logan (1998) Influence of fluid velocity and cell concentration on the transport of motile and nomnotile bacteria in porous media. Env. Science & Tech. 32:(11) 1699-1708.

Camper, A.K., J.T. Hayes, P.J. Sturman, W.L. Jones and A.B. Cunningham (1993) Effects of Motility and Adsorption Rate Coefficient on Transport of Bacteria Through Saturated Porous Media. Appl. Environ. Microb. 59:(10)3455-3462.

Chen, C.I., M.A. Reinsel, and R.F. Mueller (1994) Kinetic Investigation of Microbial Souring in Porous Media Using Microbial Consortia from oil Reservoirs. Biotech. & Bioeng. 44:(3)263-269.

Dawson, M.P., B.A. Humphrey, and K.C. Marshall (1981) Adhesion: A Tactic in the Survival of a Marine Vibrio During Starvation. Curr. Microbiol. 6:195-199.

Fletcher, M., and K.C. Marshall (1982) Are solid surfaces of ecological significance to aquatic bacteria?, In K.C. Marshall (ed), *Advances in Microbial Ecology*, Vol. 6, Plenum Press, New York, pp. 199-236.

Haider A., and O. Levenspiel (1989) Drag Coefficient and Terminal Velocity of Spherical and Nonspherical Particles. Powder Technology 58:63-70.

Jaffe, P.R., and S.W. Taylor (1992) Biofilm Growth and the Related Changes in the Physical-Properties of a Porous Medium 1. Investigation Reply. Water Resour. Res. 28(5)1483-1484.

Li, A. and G. Ahmadi (1992) Dispersion and deposition of spherical particles from point sources in a turbulent channel flow. Aerosol Science and Technology 16:209-226.

Othmer, H.G., S.R. Dunbar, and W. Alt (1988) Models of dispersal in biological systems. J. Math. Biol. 26:(3)263-298.

Phillips, B.R., J.A. Quinn, and H. Goldfine (1994) Random Motility od Swimming Bacteria: Single Cells Compared to Cell Populations. AIChE 40:(2)334-348.

Rivero, M.A., R.T. Tranquillo, H.M. Buettner, and D.A. Lauffenberger (1989) Transport models for chemotactic cell populations based on individual cell behavior. Chem. End. Sci. 44:2881-2897.

Segre, G., and A. Silberberg (1961) Nature 189:209.

Van Loosdrecht, M.C.M., J. Lyklema, W. Norde, G. Schraa, and A.J.B. Zehnder (1987) Electrophoretic mobility and hydrophobicity as a measure to predict the initial steps of bacterial adhesion. Appl. Environ. Microbiol. 53:1898-1901.

Van Loosdrecht, M.C.M., J. Lyklema, W. Norde and AJ.B. Zehnder (1990) Influence of interfaces on microbial activity. Microbiological Reviews 54(l):75-87.

Van Schie, P.M., and M. Fletcher (1999) Adhesion of biodegradative anaerobic bacteria to solid surfaces. Appl. & Env. Microb. 65:(11)5082-5088.

Widdowson, MA. (1991) An Evaluation of Mathematical Models of the Transport of Biologically Reacting Solutes in Saturated and Aquifers –Comment. Water Resour. Res. 27:(6)1375-1378.

Benson, D., R. Schumer, S.W. Wheatcraft, and M.M. Meerschaert (2000) Fractional dispersion, Lévy motion, and the MADE tracer tests. Trans. Por. Media (In Press).

Chilakapati, A., T.R. Ginn, and I Szecsody (1998) An analysis of complex reaction networks in groundwater modeling. Water Resour. Res. 34:1767-1780.

Cushman, J.H. (1991) On Diffusion in Fractal Porous Media, Water Resour. Res. 27:643-644.

Cushman, J.H. (1997) The Physics of Fluids in Hierarchical Porous Media: Angstroms to Miles, Kluwer, 480pp.

Cushman, J.H. (Ed) (1990) Dynamics of Fluids in Hierarchical Porous Media, Academic, 500pp.

Cushman, J.H. and T.R. Ginn (1993) Nonlocal Dispersion in Media with Continuously Evolving Scales of Heterogeneity, Trans. Por. Media 13:123-138.

Cushman, J.H. and T.R. Ginn (2000) On Fractional Dispersion and Diflusion, Physical Rev. E (In Preparation).

Cushman, J.H., BX Hu and T.R. Ginn (1994) Nonequilibrium Statistical Mechanics of Preasymptotic Dispersion, I Stat. Phys. 75:859-878.

Eringen, A.C. (1976) Continuum Physics, Vol. 4, Academic Press, NY, 274pp.

Lichtner, P.C., C.I. Steefel and E.H. Oelkers, eds. (1996) Reactive Transport in Porous Media. Reviews in Mineralogy, Vol. 34, Mineralogical Society of America, 438pp.

Meerschaert, M, D. Benson and R. Bäumer (1999) Multidimensional advection and fractional dispersion, Phys. Rev. E, 59(5), 5026-5028.

Murphy, E.M., T.R. Ginn, A. Chilakapati, T. Resch, J. Phillips, T. Wietsma, and C.M. Spadoni (1997) The Influence of Physical Heterogeneity on Microbial Degradation and Distribution in Porous Media, Water Resources Research, 33:1087-1104.

Simmons, C.S. and C.T. Kincaid (1987) Scale-dependent effective dispersion coefficients for one-dimensional solute transport, Proceedings of the 7th Annual AGU Front Range Branch Hydrology Days, 21-23 April, 1987, Colorado State University, Fort Collins, CO, ed. J.H. Morel-Seytoux and T. G. Sanders, pages 140-155.

Ash, R.B. (1972) Real Analysis and Probability. Academic Press, London, San Diego.

Benson, D.A., S.W. Wheatcraft, and M.M. Meerschaert (1999) Development and Application of the Fractional Advection-Dispersion Equation. Water Resour. Res. (Submitted).

Bonilla, F.A. and J.H. Cushman (1999) Role of boundary conditions on convergence and nonlocality of solutions to stochastic flow problems in bounded domains. Water Resour. Res. (In Press).

Carrier, G.F. and C.E. Pearson (1988) Partial Differential Equations Theory and Technique. Academic Press, Boston, San Diego.

Cushman, J.H., editor (1990) Dynamics of fluids in hierarchical porous media. Academic Press, London, San Diego.

Cushman, J.H. (1997) The Physics of Fluids in Hierarchical Porous Media: Angstroms to Miles. Kluwer Academic Pub., N.Y.

Cushman, J.H., B.X. Hu and F.W. Deng (1995) Nonlocal reactive transport with physical and chemical heterogeneity: Localization errors. Water Resour. Res. 31(9):2219-2237.

Dagan, G. (1982) Stochastic modeling of groundwater flow by unconditional and conditional probabilities 1. Conditional simulation and the direct problem. Water Resour. Res. 18(4):813-833.

Dagan, G. (1989) Flow and Transport in Porous Formations. Springer-Verlag, New York.

Dagan, G. (1993) Higher-Order correction of effective permeability of heterogeneous isotropic formations of lognormal conductivity distribution. Trans. Porous Media 12:279-290.

Deng, F.W. and J.H. Cushman (1995) On higher-order corrections to the flow velocity covariance tensor. Water Resour. Res. 31(7):1659-1672.

Eckhaus, W. (1973) Matched Asymptotic Expansions and Singular Perturbations. North-Holland Pub. Co., American Elsevier Pub. Co., Amsterdam, New York.

Gelhar, L.W. (1993) Stochastic Subsurface Hydrology. Prentice-Hall, Englewood Cliffs, N.J.

Gómez-Hernández, J.J. and X.H. Wen (1998) To be or not to be multi-Gaussian? A reflection on stochastic hydrogeology. Adv. In Water Resour. 21:47-61.

Hassan, A., J.H. Cushman and J.W. Delleur (1998) A Monte Carlo assessment of Eulerian flow and transport perturbation models. Water Resour. Res. 34(5):1143-1163.

Hinch, E.J. (1990) Perturbation Methods. Cambridge University Press, Cambridge, New York.

Hsu, K.C., D.X. Zhang and S.P. Neuman (1996) Higher-order effects on flow and transport in randomly heterogeneous porous media. Water Resour. Res. 32(3):571-582.

Magnus, W., F. Oberhettinger, and R.P. Soni (1966) Formulas and Theorems for the Special Functions of Mathematical Physics. Springer-Verlag, New York.

Mizell, S.A., A.L. Gutjahr, and L.W. Gelhar (1982) Stochastic Analysis of Spatial Variability in Two-Dimensional Steady Groundwater Flow Assuming Stationary and Nonstationary Heads. Water Resour. Res. 18(4):1053-1067.

Mukhopadhyay, S. and J.H. Cushman (1998) Diffusive transport of volatile pollutants in nonaqueous-phase liquid contaminated soil: A fractal model. Trans. Porous Media 30:125-154.

Neuman, S.P. (1995) On advective transport in fractal permeability and velocity fields. Water Resour. Res. 31(6):1455-1460.

Neuman, S.P. and S. Orr (1993) Prediction of steady state flow in nonuniform geologic media by conditional moments -exact nonlocal formalism, effective conductivities, and weak approximation. Water Resour. Res. 29(2):341-364.

Roach, G.F. (1982) Green's Functions. Cambridge University Press, London.

Rubin, Y. and G. Dagan (1992) A note on Head and Velocity Covariances in Three-Dimensional Flow Through Heterogeneous Anisotropic Porous Media. Water Resour. Res. 28:1463-1470.

SanchezVila, X., I Carrera and I.P. Girardi (1996) Scale effects in transmissivity. Journal of Hydrology 183(1-2):1-22.

Serrano, S.E. (1992) Semianalytical methods in stochastic groundwater transport. Applied Mathematical Modeling 16(4):181-191.

Zhang, D.X. (1999) Nonstationary stochastic analysis of transient unsaturated flow in randomly heterogeneous media. Water Resour. Res. 35:1127-1141.

Zhang, D.X. and C.L. Winter (1999) Moment-Equation Approach to Single-Phase Fluid Flow in Heterogeneous Reservoirs. Soc. Petroleum Eng. Journal 3(2).

Fletcher, M. and K.C. Marshall (1982) "Are solid surfaces of ecological significance to aquatic bacteria?" In: K.C. Marshall (ed), Advances in Microbial Ecology, vol. 6, Plenum Press, New York, pp. 199-236.

Jaffe, P.R., and S.W. Taylor (1992) "Reply." Water Resources Research 28(5):1483-1484

Graham, C. (1988) "The martingale problem with sticky reflection conditions and a system of particles interacting at the boundary." Ann. Inst. H. Poincare Probab. Statist. 24:45-72

Borodin, A. N. and Paavo Salminen (1996) "Handbook of Brownian motion: facts and formulae", Birkhauser Verlag.

McCaulou, D.R., R.C. Bales, and J.F. McCarthy (1994) Use of short-pulse experiments to study bacterial transport through porous media. J. Contaminant Hydrol. 15:1-14.

Bhattacharya, R. N. (1982) On the Functional Central Limit Theorem and the Law of the Iterated Logarithm for Markov Processes. Z. Wahrs. Verw. Geb. 60:185-201.

Bhattacharya, R.N. and Vijay K. Gupta (1984) On the Taylor-Aris Theory of Solute Transport in a Capillary. SIAM J. Appl. M. vol 44 pg33-39.

Lepingle, D. (1995) Euler scheme for reflected stochastic differential equations. Mathematics and Computers in Simulation 38:119-126.

McEldowney, S. and M. Fletcher (1988) Effect of pH, Temperature and Growth Conditions on the Adhesion of a Gliding Bacterium and Three Nongliding Bacteria to Polystyrene. Microbial Ecology 16:183-195.

Valocchi and Quinodoz (1989) Application of the random walk method to simulate the transport of kinetically adsorbing solutes. In: Groundwater contamination, edited by L.M. Abriola, IAHS publ. 185, pp. 35-42.

Ginn, T.R., C.S. Simmons and B.D. Wood (1995) Stochastic-convective transport with nonlinear reaction: Biodegradation with microbial growth. Water Res. Research 31(11):2689- 2700.

Johnson, W.P., K.A. Blue, B.E. Logan and R.G. Arnold (1995) Modelling bacterial detachment during transport through porous media as a residence-time-dependent process. Water Res. Research 31(11):2649-2658.

Philip Protter (1992) Stochastic Integration and Differential Equations. Springer-Verlag.

Arroyo, M. P. and C.A. Greated (1991) Stereoscopic particle image velocimetry. Meas. Sci. Technol. 2:1181-1186.

Berne, B.J. and G.D. Harp (1970) On the Calculation of Time Correlation Functions. Adv. Chem. Phys. 17:63-227.

Berne, B.J. and R. Pecora (1976) *Dynamic Light Scattering,* Wiley, New York.

Campbell, G.M. and J. T. Day (1970) The Numerical Solution of Nonlinear Volterra Integral Equations. BIT 10:10-19.

Cenedese, A., M. Moroni and P. Viotti (1997) Lagrangian analysis of dispersion in porous media by means of three-dimensional particle tracking velocimetry. XXVII IAHR Congress, "Water for a Changing Global Community", 10-15 Aug. 1997, San Francisco, CA USA.

Cenedese, A. and P. Viotti (1996) Lagrangian analysis of nonreactive pollutant dispersion in porous media by means of the particle image velocimetry technique. Water Resour. Res. 32(8):2329-2343.

Cushman, J.H. (1990) *Dynamics of Fluids in Hierarchical Porous Media,* J.H. Cushman (eds.) Academic Press Inc., San Diego.

Cushman, J.H. and T. R. Ginn (1993) Nonlocal Dispersion in Media with Continuously Evolving Scales of Heterogeneity. Trans. Porous Media 13:123-138.

Cushman,J.H., X. Hu and T.R. Ginn (1994) Nonequilibrium Statistical Mechanics of Preasympotic Dispersion. J. Stat. Phys., 75(5/6):859-878.

Cushman, J.H. (1997) *The Physics of Fluids in Hierarchical Porous Media: Angstroms to Miles,* Kluwer Academic Publishers, The Netherlands.

Dagan, G. (1989) Flow and Transport in Porous Formations, Springer-Verlag eds.

Dracos, T.A., M. Virant, H.G. Maas and A.W. Gruen (1995) Photogrammetric approach to PIV (PTV), Proceedings of The International Workshop on PIV, Fukui, Japan.

Gelhar, L.W. (1993) *Stochastic Subsurface Hydrology,* Prentice-Hall, Englewood Cliffs, N.J.

Guezennec, Y.G., R.S. Brodkey, N. Trigui and J.C. Kent (1994) Algorithms for fully automated three-dimensional particle tracking velocimetry. Exp. Fluids, 17:209-219.

Hamming, R.W. (1962) *Numerical Methods for Scientists and Engineers,* McGraw-Hill.

Iguchi, K. (1972) A Starting Method for Solving Nonlinear Volterra Integral Equations of the Second Kind. ACM Communications 15(6):460-46 1.

Irwin, N.C., R.A. Greenkorn, S.A. Altobelli and J.H. Cushman (1999) Examination of Transport Theory of Arbitrary Order in Velocity Variance by MRI. AIChE J., 45(6):1351-1354.

Khalili, A., A.J. Basu and U. Pietrzyk (1998) Flow visualization in porous media via positron emission tomography. Phys. Fluids 10 (4):1031-103 3.

Kutsovsky, Y.E., L.E. Scriven and H.T. Davis (1996) NMR imaging of velocity profiles and velocity distributions in bead packs. Phys. Fluids 8(4):863-871.

Lebon, L., L. Oger, J. Leblond and J.P. Hulin (1996) Pulsed gradient NMR measurements and numerical simulation of flow velocity distribution in sphere packings. Phys. Fluids 8(2):293-301.

Lebon, L., J. Leblond and J.P. Hulin (1997) Experimental measurements of dispersion processes at short times using a pulsed field gradient NMR technique. Phys. Fluids 9(3):481-490.

Moroni, M. and J.H. Cushman. 3D-PTV Studies of Asymptotic limits to Classical Stochastic Theories of Porous Media Transport. Water Resour. Res. (Submitted).

Moroni, M. and J.H. Cushman. 3D-PTV Comparison with Statistical Mechanical Theories of Steady Conservative Tracer Transport in Porous Media. Phys. Fluids (Submitted).

Northrup, M.A., T.J. Kulp, S.M. Angel and G.F. Pinder (1993) Direct measurement of interstitial velocity field variations in a porous medium using fluorescent particle imaging velocimetry. Chem. Engng. Sci. 48:13-21.

Park, J. and S.J. Gibbs (1999) Mapping Flow and Dispersion in a Packed Column by MRI. AIChE J. 45(3):655-660.

Peurrung, L.M., M. Rashidi and T.J. Kulp (1995) Measurements of the porous medium velocity fields and their volumetric averaging characteristics using particle tracking velocimetry. Chem. Engng. Sci. 50(14):2243-2253.

Rashidi, M., L. Peurrung, A.F.B. Tompson and T.J. Kulp (1996) Experimental analysis of pore-scale flow and transport in porous media. Adv. Water Resour. 19(3):163-180.

Saleh, S., J.F. Thovert and P.M. Adler (1993) Flow along porous-media by partial image velocimetry. AIChE J. 39(11):1765-1776.

Bales, R.C., S.R. Hinkle, T.W. Kroeger, and K. Stocking (1991) Bacteriophage adsorption during transport through porous media: chemical perturbations and reversibility. Environ. Sci. Technol. 25:2088-2095.

Bales, R.C., S. Li, K.M. Maguire, M.T. Yahya, C.P. Gerba, and R.W. Harvey (1995) Virus and bacteria transport in a sandy aquifer, Cape Cod, Massachusetts. Groundwater 33:653-661.

Baveye, P. and A. Valocchi (1989) An Evaluation of Mathematical Models of the Transport of Biologically. Reacting Solutes in Saturated Soils and Aquifers. Water Resources Research 25:1413-1421.

Baveye, P., P. Vandevivere, and D. Lozada (1992) Comment on biofilm growth and the related changes in the physical properties of a porous medium. 1. Experimental investigation by S.W. Taylor and P.R. Jaffe. Water Resour. Res. 28:1481-1482.

Bellin, A., A. Rinaldo, W.J.P. Bosma, S.E.A.T.M. Van Der Zee, and Y. Rubin. (1993) Linear equilibrium adsorbing solute transport in physically and chemically heterogeneous porous formations. 1. Analytical solutions. Water Resources Research 29(12):40 19-4030.

Bengtsson, G. (1989) Growth and metabolic flexibility in groundwater bacteria. Microb. Ecol., 18:235-248.

Bennethum, L.W., and J.H. Cushman (1996) Multiscale hybrid mixture theory for swelling systems. II: Constitutive theory. Int. J. Eng. Sci. 34:147-169.

Borden, R.C. and P.B. Bedient (1986) Transport of dissolved hydrocarbons influenced by oxygen-limited biodegradation. Water Resour. Res. 22:1973-1982.

Bosma, W.J.P., A. Bellin, S.E.A.T.M. Van Der Zee, and A. Rinaldo (1993) Linear equilibrium adsorbing solute transport in physically and chemically heterogeneous porous formations. 2. Numerical results. Water Resources Research 29(12):4031-4043.

Bower, E.J., and G.D. Cobb (1986) Modeling of biological processes in the subsurface. IAWPRC Water Sci. Technol. 19:769-779.

Bouwer, E.J. and P.L. McCarty (1983) Transformations of 1- and 2-carbon halogeneated aliphatic organic compounds under methanogenic conditions. Appl. Environ Microbial. 45:1296-1294.

Boyd, A. and A.M. Chakmbarty (1994) Role of alginate lyase in cell detachment of Pseudomonas aeruginosa. Appl. Environ. Microbiol. 60:2355-2359.

Brown, M.R.W., and J. Melling (1969) Role of divalent cations in the action of polymyxin B and EDTA on Pseudomonas aeruginosa. J. Gen. Microbiol. 59:263-274.

Brusseau, M.L., and P.S.C. Rao (1989) Sorption non-ideality during organic contaminant transport in porous media. CRC Crit. Rev. Environ. Control 19:22-99.

Cheeseman, P., A. Toms-Wood, and R.S. Wolfe (1972) Isolation and properties of a fluorescent compound, factor 420, from Methanobacterium strain M.o.H. J. Bacterial. 112:527-531.

Chen, Ching-I., T. Griebe, and W.G. Characklis. (1993) Biocide action of monochloramine on biofilm systems of Pseudomonas aeruginosa. Biofouling 7:1-26.

Chen, Y., L.M. Abriola, P.J.J. Alvarez, P.J. Anid, and T.M. Vogel (1992) Modeling transport and biodegradation of benzene and toluene in sandy aquifer material: Comparison with experimental measurements. Water Resour. Res. 28:1833-1847.

Chiang, C.Y., J.V. Salanitro, E.Y. Chai, J.D. Colthart, and C.L. Klein (1989) Aerobic biodegradation of benzene, toluene, and xylene in a sandy aquifer - Data analysis and computer modeling. Ground Water 27:823-834.

Chilakapati, A. (1995) RAFT: A Simulator for ReActive Flow and Transport of Groundwater Contaminants, PNNL-10636, Pacific Northwest National Laboratory.

Chrysikopoulos, C.V., P.K. Kitanidis, and P.V. Roberts (1992) Macrodispersion of sorbing solutes in heterogeneous porous formations with spatially periodic retardation factor and velocity field. Water Resources Research 28 (6):1517-1529.

Clark, D.P. (1984) The number of anaerobically regulated genes in Escherichia coli. FEMS Microbiol. Lett. 24:251-254.

Clausen, J.L., K.R. Davis, J.W. Douthitt, and B.E. Phillips (1992) Report of the Paducah Gaseous Diffusion Plant Groundwater Investigation Phase III. Martin Marietta Energy Systems. Paducah, KY. KY/E-150.

Clement, T.P., B.S. Hooker, and R.S. Skeen (1996) Macroscopic models for predicting changes in saturated porous media properties caused by microbial growth. Ground Water (in press).

Clement, T.P, B.M. Peyton, R.S. Skeen, D.A. Jennings, and J.N. Petersen (1996) Microbial growth and transport in porous media under denitrification conditions: Experiment and simulations. J. Contaminant Hydrol. (In press).

Cobb, G.D., and E.J. Bower (1991) Effects of electron acceptors on halogenated organic compound biotransformations in a biofilm column. Environ. Sci. Technol. 25:1068-1074.

Corapcioglu, Y.M., and A. Haridas (1984) Transport and fate of microorganisms in porous media: A theoretical investigation. J. of Hydrol. 72:149-169.

Cressie, N. (1991) Statistics for Spatial Data. Wiley-Interscience, New York, New York.

Cunningham, A.B., W.G. Characklis, F. Abeeden, and D.J. Crawford (1991) Influence of biofilm on porous media hydrodynamics. Environ. Sci. Technol. 25:1304-1311.

Cushman, J.H., and T.R. Ginn (1993) Nonlocal Dispersion in Media with Continuously Evolving Scales of Heterogeneity. Transport in Porous Media 13:123-138.

Cushman, J.H. (ed.) (1990) Dynamics of Fluids in Hierarchical Porous Media. New York, Academic Press.

Cushman, J.H. (1996) Physics of Fluids in Hierarchial Porous Media: Angstroms to Miles. Cambridge University Press (In press).

Cvetkovic, V. and G. Dagan (1994) Transport of kinetically sorbing solute by steady random velocity in heterogeneous porous formations. Journal of Fluid Mechanics 265:189-215.

Dagan, G. (1989) Flow and Transport in Porous Formations. New York: Springer-Verlag.

Dagostino, L., A.E. Goodman, and K.C. Marshall (1991) Physiological responses induced in bacteria adhering to surfaces. Biofouling 4:113-119.

Davies, D.G., A.M. Chakrabarty, and G.G. Geesey (1993) Exopolysaccharide production in biofilms: substratum activation of alginate gene expression by Pseudomonas aeruginosa. Appl. Environ. Micrbiol. 59:1181-1186.

Davis, T.A., and I.S. Duff (1995) An unsymmetric-pattern multifrontal method for sparse LU factorization, CISE Department, University of Florida.

Dawson, M.P., B.A. Humphrey, and K.C. Marshall (1981) Adhesion: A tactic in the survival strategy of a marine vibrio during starvation. Curr. Microbial. 6:195-199.

De Bruin, W.P., M.J.J. Kotterman, M.A. Posthumus, G. Schraa, and A.J.B. Zehnder (1992) Complete biological reductive transformation of tetrachloroethene to ethane. Appl. Environ. Microbiol. 58(6):1996-2000.

DeMarsily, G. (1986) Quantitative Hydrogeology. Academic Press, New York.

Deng. F.W., and J.H. Cushman (1995) On higher order corrections to the flow velocity covariance tensor. Water Resour. Res. 31:1659-1672.

DiMarco, A.A., T.A. Bobik, and R.S., Wolfe (1990) Unusual coenzymes of methanogenesis. Annu. Rev. Biochem. 59:355-394.

DiStefano, T.D., J.M. Gossett, and S.H. Zinder (1991) Reductive dechlorination of high concentrations of tetrachlorethene to ethene by an anaerobic enrichment culture in the absence of methanogenesis. Appl. Environ. Microbiol. 57:2287-2292.

Dodds, J. (1982) La chromatographie hydrodynamique. Analysis 10:109-119.

Dykaar, B.B., and P.K. Kitanidis (1996) Macrotransport of a biologically reacting solute through porous media. Water Resour. Res. 32:307-320.

Eirich, L.D., G.D. Vogels, and R.S. W olfe (1979) Proposed structure for coenzyme F420 from Methanobacterium. Biochemistry 17:4583-4593.

Ellwood, D.C. and D.W. Tempest (1972) Effects of environment on bacterial cell wall content and composition. Adv. Microb. Physiol. 7:83-117.

197

Engfield, C.G., and G. Bengtsson (1988) Macromolecular transport of hydrophobic contaminants in aqueous environments. Groundwater 26:64-70.

Fathepure, B.Z. and S.A. Boyd (1988) Dependence of tetrachloroethylene dechlorination on methanogenic substrate consumption by *Methanosarcina* sp. Strain DCM. Appl. Environ. Microbiol. 54:2976-2980.

Fletcher, M. (1991) Bacterial Colonization of Solid Surfaces in Subsurface Environments. In Proceedings of the *First International Symposium on Microbiology* of *the Deep Subsurface,* eds. C.B. Fliermans and T.C. Hazen. WSRC Information Services, Aiken, South Carolina.

Fletcher, M., and G.I. Loeb (1979) Influence of Substratum Characteristics on the Attachment of a Marine Pseudomonad to Solid Surfaces. Appl. Environ Microbiol. 37:67-72.

Fletcher, M., and K.C. Marshall (1982) Are solid surfaces of ecological significance to aquatic bacteria? In: K.C. Marshall (ed), Advances in Microbial Ecology, vol. 6, Plenum Press, New York, pp. 199-236.

Fontes, D., A.L. Mills, G.M. Hornberger, and J.S. Herman (1991) Physical and chemical factors influencing transport of microorganisms through porous media. Appl. Environ. Microbiol. 57:2473-2481.

Freedman, D.L., and J.M. Gossett (1989) Biological reductive dechlorination of tetrachloroethylene and trichloroethylene to ethylene under methanogenic conditions. Appl. Environ. Microbiol. 55:2144-2151.

Gilbert, P. and M.R.W. Brown (1995) Mechanisms of the protection of bacterial biofilms from antimicrobial agents. In *Microbial Biofilms,* H.M. Lappin-Scott and J.W. Costerton, Eds., pp, 118-130. Cambridge University Press, Cambridge.

Ginn, T.R., C.S. Simmons, and B.D. Wood (1995) Stochastic-convective transport with nonlinear reaction: Biodegradation with microbial growth. Water Resour. Res. 31:2689-2700.

Goodman, A.E., and K.C. Marshall (1995) Genetic responses of bacteria at surfaces. In *Microbial Biofilms,* H.M. Lappin-Scott and J.W. Costerton, eds., pp. 80-98. Cambridge University Press, Cambridge.

Gordon, A.S., and F.J. Millero (1985) Adsorption mediated decrease in the biodegradation rate of organic compounds. Microb. Ecol. 11:289-298.

Griffith, P.C., and M. Fletcher (1991) Hydrolysis of protein and model dipeptide substrates by attached and nonattached marine Pseudomonas sp. strain NCIMB 2021. Appl. Environ. Microbial. 57:2186-2191.

Griffith, P.C., and M. Fletcher (1991) Hydrolysis of protein and model dipeptide substrates by attached and nonattached marine Pseudomonas sp. strain NCIMB 2021. Appl. Environ. Microbial. 57:2186-2191.

Guerin, W.F., and S.A. Boyd (1992) Differential bioavailability of soil-sorbed napthalene to two bacterial species. Appl. Environ. Microbiol. 58:1142-1152.

Gupta, A.D., L.W. Lake, G.A. Pope, K. Sephemoori, and M.J. King (1991) High-resolution monotonic schemes for reservoir fluid flow simulation. In Situ 15:289-317.

Harvey, J.W. (1993) Measurement of variation in soil solute tracer concentration across a range of effective pore sizes. Water Resour. Res. 29:1831-1837.

Harvey, R.W., R.L. Smith, and L. George (1984) Effect of organic contamination upon microbial distribution and heterotrophic uptake in a Cape Cod, Massachusetts, aquifer. Appl. Environ. Biol. 48:1197-1202.

Harvey, R.W., L.H. George, R.L. Smith, D.R. LeBlanc, S.P. Garabedian, and B.L. Howes (1987) Transport of bacteria through a contaminated freshwater aquifer. Open File Report 87-109, B31-B33, U.S. Geological Surveys.

Harvey, R.W., N.E. Kinner, D. MacDonald, D.W. Metge, and A. Bunn (1993) Role of physical heterogeneity in the interpretation of small-scale laboratory and field observations of bacteria, microbial-sized microsphere, and bromide transport through aquifer sediments. Water Resources Research 29:2713-2721.

Harvey, R.W., and S.P. Garabedian (1991) Use of colloid filtration theory in modeling movement of bacterial through a contaminated sandy aquifer. Environ. Sci. Technol. 25:178-185.

Hassan, A, J.H. Cushman, and J.W. Delleur (1996) Monte Carlo studies of flow and transport in fractal conductivity fields: Comparison with stochastic perturbation theory. Water Resour. Res. (Submitted).

Herzig, J.P., D.M. Leclerc, and P. LeGoff (1970) Flow of suspension through porous media: Application to deep filtration. Industr. Eng. Chem. 62:129-157.

Hermansson, M., and K.C. Marshall (1985) Utilization of surface localized substrate by non-adhesive marine bacteria. Microb. Ecol. 11:91-105.

Hindmarsh, A.C., ODEPACK (1983) A systemetized collection of ODE solvers, in *Scientific Computing*, edited by R.S. Stepleman, pp. 55-64, North-Holland, Amsterdam.

Holme, T. (1972) Influence of the environment on the content and composition of bacterial envelopes. J. Appl. Chem. Biotech. 22:391-399.

Hornberger, G. M., A.L. Mills, and J.S. Herman (1992) Bacterial transport in porous media: Evaluation of a model using laboratory observations. Water Resour. Res. 28:915-938.

Hu, B.X., F.W. Deng, and J.H. Cushman (1995) A nonlocal theory of reactive transport with physical and chemical heterogeneity: Linear nonequilibrium sorption with random Kd. Water Resour. Res. 31:2219-2237.

Jaffe, P.R., and S.W. Taylor (1992) Reply. Water Resources Research 28(5):1483-1484.

James, A.M (1991) Charge properties of microbial cell surfaces. In *Microbial Cell Surface Analysis*, N. Mozes, P.S. Handley, H.J. Busscher, and P.G. Rouxhet, eds., pp. 221-262. VCH Publishers, New York, New York.

Jenneman, G.E., M.J. McInerney, and R.M. Knapp (1985) Microbial penetration through nutrient-saturated berea sandstone. Appl. Environ. Microbiol. 50(2):383-391.

Jenneman, G.E., M.J. McInerney, M.E. Crocker, and R.M. Knapp (1986) Effect of sterilization by dry heat or autoclaving on bacterial penetration through berea sandstone. Appl. Environ. Microbial. 51(1):39-43.

Jennings, D.A. (1994) *Microbial Transport in Porous Media*. M.S. Thesis, Washington State University, Pullman, Washington.

Jewett, D.G., T.A. Hilbert, B.E. Logan, R.G. Arnold, and R.C. Bales (1995) Bacterial transport in laboratory columns and filters: Influence of ionic strength and pH on collision efficiency. Water Res. 29:1673-1680.

Kefford, B., S. Kjelleberg, and K.C. Marshall (1982) Bacterial scavenging: Utilization of fatty acids localized at a solid-liquid interface. Arch. Microbiol. 133:257-260.

Kerner, E. (1971) Statistical-mechanical theories in biology. Adv. Chem. Phys. 19:325-352.

Kindred, J.S., and M.A. Celia (1989) Contaminant transport and biodegradation: 2. Conceptual model and test as simulations. Water Resour. Res. 25:1149-1159.

Kinoshita, T., R.C. Bales, M.T. Yahya, and C.P. Gerba (1993) Bacteria transport in a porous medium: retention of bacillus and pseudomonas on silica surfaces. Water Res. 27:1295-1301.

Kinzelbach, W., W. Schafer, and J. Herzer (1991) Numerical modeling of natural and enhanced denitrification processes in aquifers. Water Resour. Res. 27:1123-1135.

Kissel, J.L., P.L. McCarty, and R.L. Street (1994) Numerical modeling of mixed-culture biofilm. J. Environ. Eng. 110:393-411.

Kjelleberg, S. and M. Hermansson (1984) Starvation-induced effects on bacterial surface characteristics. Appl. Environ. Microbiol. 48:497-503.

Kjelleberg, S., K.C. Marshall, and M. Hermansson (1985) Oligotrophic and copiotrophic marine bacteria-observations related to attachmen. FEMS Microb. Ecol. 31:89-96.

Lambert, P.A. (1988) Enterobacteriaceae: Composition, structure and function of the cell envelope. J Appl. Bacteriol. 65(Suppl.):21S-34S.

Lappin-Scott, H.M., F. Cusack, and J.W. Costerton (1988) Nutrient resuscitation and growth of starved cells in sandstone cores: A novel approach to enhanced oil recovery. Appl. Environ. Microbiol. 54:1373-1382.

Lawrence, J.R., and D.E. Caldwell (1987) Behavior of bacterial stream populations within the hydrodynamic boundary layers of surface microenvironments. Microb. Ecol. 24:15-27.

Leff, L.G., J.V. McArthur, J.L. Meyer, and L.J. Shimikets (1994) Effect of macroinvertebrates on detachment of bacteria from biofilms in stream microcosms. The North American Benthological Society, 13(1):74-79.

Lindqvist, R. and G. Bengtsson (1991) Dispersal dynamics of groundwater bacteria. Microb. Ecol. 21:49-72.

Lindqvist, R., J.S. Choo, and C.G. Enfield (1994) A kinetic model for cell density dependent bacterial transport in porous media. Water Resources Research 30:3291-3299.

Lovley, D.R., M.J. Baedecker, D.J. Lonergan, E.J. Cozzarelli, P. Phillips, and D.I. Siegel (1989) Oxidation of aromatic contaminants coupled to microbial iron reduction. Nature 339:297-299.

Lundman, R.E. (1992) *Transport of Substrate and Biomass in a Packed Bed Reactor.* M.S. Thesis, State University, Kalispell, Montana.

Mayotte, T.J., M.J. Dybas, and C.S. Criddle (1996) Bench-scale evaluation of bioaugumentation to remediate carbon tetrachloride contaminated aquifer materials. Ground Water 34:358-367.

MacQuarrie, K.T.B., E.A. Sudicky, and E.0. Frind (1990) Simulation of biodegradable organic contaminants in groundwater. 1. Numerical formulation in principal directions. Water Resour. Res. 26:207-222.

Marshall, K.C., R. Stout, and R. Mitchell (1971) Mechanisms of the initial events in the sorption of marine bacteria to surfaces. J. Gen. Microbiol. 68:337-348.

Marshall, P.A., G.I. Loeb, M.M. Cowan, and M. Fletcher (1989) Response of microbial adhesives and biofilm matrix polymers to chemical treatments as determined by interference reflection microscopy and light section microscopy. Appl. Environ. Microbiol. 55:2827-2831.

McCaulou, D.R., R.C. Bales, and J.F. McCarthy (1994) Use of short-pulse experiments to study bacterial transport through porous media. J. Contaminant Hydrol. 15:1-14.

McCleary, H. (1996) Fluorescing microbes may shed light on how to improve bioremediation. The Biocleanup Report, January 1, 1996 issue, page 2.

McDowell-Boyer, L.M. (1992) Chemical mobilization of micron-sized particles in saturated porous media under steady flow conditions. Environ. Sci. Technol. 26:586-593.

McDowell-Boyer, L.M., J.R. Hunt, and N. Sitar (1986) Particle transport through porous media. Water Resour. Res. 22:1901-1921.

McEldowney, S., and M. Fletcher (1986) Physicochemical factors affecting bacterial adhesion to polystyrene substrate. Appl. Environ. Microbiol. 52:460-465.

McEldowney, S., and M. Fletcher (1988) Effect of pH, Temperature, and Growth Conditions on the Adhesion of a Gliding Bacterium and Three Nongliding Bacteria to Polystyrene. Microbiol. Ecol. 16:183-195.

McFeters, G.A., T. Egli, and E. Wilberg (1990) Activity and adaptation of nitrilotriacetate (NTA)-degrading bacteria: Field and laboratory studies. Water Res. 24:875-881.

Mills, A.L., and W.D. Eaton (1984) Biodegradation of bromobenzene in simulated groundwater conditions. In Biodegradation 6, G.C. Llewellyn and C.E. O'Rear, eds., pp. 9-13. C.A.B. International, Slough U.K.

Mills, A.L., J.S. Herman, G.M. Hornberger, and T.H. DeJesus (1994) Effect of ionic strength and iron coatings on mineral grains on sorption of bacterial cells to quartz sand. Envirm. Microbiol. 60:3300-3306.

Mills, W.B., S. Liu, and F.K. Fong (1991) Literature review and model (comet) for colloid/metals transport in porous media. Ground Water. 29:199-208.

Molz, F.J., M.A. Widdowson, and L.D. Benefield (1996) Simulation of microbial growth dynamics coupled to nutrient oxygen transport in porous media. Water Resour. Res. 22:1207-1216.

Mukhopadhay, S., and J.H. Cushman (1996) Transport of contaminants in groundwater: A fracture network model. Water Resour. Res. (Submitted).

Murad, M., L.W. Bennethum, and J.H. Cushman (1995) A multiscale theory for swelling porous media. I. Application to one-dimensional consolidation. J. Trans. Porous Media 19:93-122.

Murad, M., and J.H. Cushman (1996) Multiscale flow and deformation in hydrophilic swelling porous media. Int. J. Eng. Sci. 34:313-338.

Murphy, E.M., J.A. Schramke, J.K. Fredrickson, H.W. Bledsoe, D.S. Sklarew, and J.C. Linehan (1992) The Influence of Microbial Activity and Sedimentary Organic Carbon on the Isotope Geochemistry of the Middendorf Aquifer. Water Resour. Res. 28(3):723-740.

Myers, C.W., and S.M. Price (1979) *Geologic studies of the Columbia Plateaw A status report.* RHO-BWI-ST-4, Rockwell Hanford Operations, Richland, WA.

Ogram, A.V., R.E. Jessup, L.T. Lou, and P.S.C. Rao (1985) Effects of sorption on biological degradation rates of (2,4-dichlorophenoxy) acetic acid in soils. Appl. Environ. Microbiol. 49:582-587.

Parsons, F., P.R. Wood, and J. DeMarco (1984) Transformations of tetrachloroethene and trichloroethene in microcosms and groundwater. J. Am. Water Works Assoc. 76:56-59.

Peyton, B.M., and W.G. Characklis (1993) A statistical analysis of the effects of substrate utilization and shear stress on the kinetics of biofilm detachment. Biotechnol. Bioeng. 41:728-735.

Peyton, B.M., R.S. Skeen, B.S. Hooker, R.W. Ludman, and A.B. Cunningham (1995) Evaluation of bacterial detachment rates in porous media. Appl. Biochem. Biotechnol. 51:785-797.

Peyton, B.M. (1996) Improved biomass distributions using pulsed injections of electron donor and acceptor. Water Resour. 30(3):756-758.

Poeter, E., and D.R. Gaylord (1990) Influence of aquifer heterogeneity on contaminant transport at the Hanford Site. Ground Water 28(6):900-909.

Pyle, B.H. (1979) *Technical Publication No. 2.* Lincoln College Department of Agriculture Microbiology, Canterbury, New Zealand.

Pyle, B.H., and H.R. Thorpe (1981) Evaluation of the potential for microbiological contamination of an aquifer using a bacterial tracer. Proceedings of Ground-Water Pollution Conference, 1979. Australian Water Resources Council Conference Series, No. 1, 213-224.

Quinodoz, H.A.M., and A.J. Valocchi (1993) Stochastic analysis of the transport of kinetically sorbing solutes in aquifers with randomly heterogeneous hydraulic conductivity. Water Resources Research 29(9):3227-3240.

Reynolds, P.J., P. Sharma, G.E. Jenneman, and M.J. McInerney (1989) Mechanisms of microbial movement in subsurface materials. Appl. Environ. Microbiol. 55(9):2280-2286.

Rifai, S.H., P.B. Bedient, R.C. Borden, and J.F. Haasbeek (1997) *BIOPLUME II – Computer model of two-dimensional contaminant transport under the influence of oxygen limited biodegradation in ground water.* National Center for Ground Water Research, Rice University, Houston, Texas.

Rifai, S.H., and P.B. Bedient (1990) Comparison of biodegradation kinetics with an instantaneous reaction model for groundwater. Water Resour. Res. 26:637-645.

Riley, R.G., J.M. Zachara, and F.J. Wobber (1992) *Chemical Contaminants on DOE Lands and Selection of Contaminant Mixtures for Subsurface Science Research.* DOE/ER-0547T, U.S. Department of Energy, Office of Energy Research, Washington, D.C.

Rittmann, B.E. (1993) The significance of biofilms in porous media. Water Resour. Res. 29:2195-2202.

Rosenberg, E., A. Gottlieb, and M. Rosenberg (1983) Inhibition of bacterial adherence to epithelial cells and hydrocarbons by emulsan. Infect. Immun. 39:1024-1028.

Ryan, J.N., and P.M. Gschwend (1990) Colloid mobilization in two Atlantic coastal plain aquifers: Field studies. Water Resour. Res. 26:307-322.

Saiers, J.E., G.M. Hornberger and L. Liang (1994) First- and second-order kinetics approaches for modeling the transport of colloidal particles in porous media. Water Resources Research 30(9):2499-2506.

Samuelsson, M.0. and D.L. Kirchman (1990) Degradation of adsorbed protein by attached bacteria in relationship to surface hydrophobicity. Appl. Environ. Microbiol. 56:3643-3648.

Sakthivadivel, R. (1966) *Theory and mechanism of filtration of non-colloidal fines through a porous medium.* Report HEL 15-5, Hydraulic Engineering Lab., U.C. Berkeley, Berkeley, California.

Sakthivadivel, R. (1969) *Clogging of a granular porous medium by sediment.* Report HEL 15-7, Hydraulic Engineering Lab., U.C. Berkeley, Berkeley, California.

Sakthivadivel, R., and S. Irmay (1966) *A review of filtration theories.* Inter. Report HEL IS-4, U.C. Berkeley, Berkeley, California.

Sargent, K.A., and C.B. Fliermans (1989) Geology and Hydrology of the Deep Subsurface Microbiology Sampling Sites at the Savannah River Plant, South Carolina. Geomicroblol. J. 7:3-13.

Scheibe, T.D., and C.R. Cole (1994) Non-gaussian particle tracking: application to scaling of transport processes in heterogeneous porous media. Water Resources Research 30:2027-2041.

Scholl, M.A., A.L. Mills, J.S. Herman, and G.M. Hornberger (1990) The influence of mineralogy and solution chemistry on the attachment of bacteria to representative aquifer materials. J. Contaminant Hydrol. 6:321-336.

Schwertman, U. and R.M. Cornell (1991) *Iron oxides in the laboratory.* VCH Publishers, New York, N.Y. 137 pages.

Selroos, J.-O., and V. Cvetkovic (1994) Mass-flux statistics of kinetically sorbing solute in heterogeneous aquifers: analytical solution and comparison with simulations. Water Resources Research 30(1):63-69.

Semprini, L., G.D. Hopkins, D.B. Janssen, M. Lang, P.V. Roberts, and P.L. McCarty (1991) *In situ biotransformation of carbon tetrachloride under anoxic conditions*. EPA Rep. No. EPA 2-90/060, U.S. Environmental Protection Agency, Ada, Oklahoma.

Sharma, M.M., Y.I. Chang, and T.F. Yen (1985) Reversible and Irreversible Surface Charge Modification of Bacteria for Facilitating Transport through Porous Media. Colloids Surfaces 16:193-206.

Sharma, P.K., M.J. McInerney, and R.M. Knapp (1993) In situ growth and activity and modes of penetration of *escherichia coli* in unconsolidated porous materials. Appl. Environ. Microbial. 59(11):3686-3694.

Shaw, D.J. (1976) Introduction to colloid and surface chemistry. Butterworth 2:168-177.

Shonnard, D.R., R.T. Taylor, M.L. Hanna, C.O. Boro, and A.G. Duba (1994) Injection-attachment of Methylosinus trichosporium 0B3b in a two-dimensional miniature sand-filled aquifer simulator. Water Resour. Res. 30:25-36.

Simmons, C.S., T.R. Ginn, B.D. Wood (1995) Stochastic-convective transport with nonlinear reaction: Mathematical framework. Water Resour. Res. 31: 2675-2688.

Smith, M.W., and F.C. Neidhardt (1983) Proteins induced by anaerobiosis in Escherichia coli. J. Bacterial. 154:336-343.

Smith, P.K., R.I. Drohn; G.T. Hermanson, A.K. Mallia, F.H. Mallia, F.H. Gartner, M.D. Provenzano, E.K. Fujimoto, N.M. Goeke, B.J. Olson, and D.C. Klenk (1985) Measurement of protein using bicinchoninic acid. Anal. Biochem. 150:76-85.

Sturman, P.J, P.S. Stewart, A.B. Cunningham, E.J. Bower; and J.H. Wolfram (1995) Engineering scale-up of in situ bioremediation processes: A review. J. Contaminant Hydrol. 19:171-203.

Sudicky, E.A., S.L. Schellenberg, and K.T.B. MacQuarrie (1990) Assessment of the behavior of conservative and biodegradable solutes in heterogeneous porous media. In *Dynamics of fluids in Hierarchical Porous Media*, J.H. Cushman, ed., pp. 429-462. Academic Press, New York, New York.

Tan, Y., J.T. Gannon, P. Baveye, and M. Alexander (1994) Transport of bacteria in an aquifer sand: Experiment and model simulations. Water Resour. Res. 30:3243-3252.

Taylor, S.W., P.C.D. Milly, and P.R. Jaffe (1990) Biofilm, growth and the related changes in the physical properties of a porous medium. 2. Permeability. Water Resour. Res. 26:2161-2169.

Taylor, S.W., and P.R. Jaffe (1990a) Biofilm growth and the related changes in the physical properties of a porous medium. 3. Dispersivity and Model Verifications. Water Resour. Res. 26:2171-2180.

Taylor, S.W., and P.R. Jaffe (1990b) Substrate and biomass transport in a porous medium. Water Resour. Res. 26:2181-2194.

Tien, C.R., R M. Turian, and H. Pandse (1979) Simulation of the dynamics of deep bed filters. *AICHE Journal*, 25:385-395.

U.S. Department of Energy (DOE) (1993) *Cleanup of VOC's in non-arid soils - The Savannah River Integrated Demonstration*. U.S. Department of Energy, Environmental Restoration and Waste Management, Office of Technology Development.

van der Mei, H.C., M. Rosenberg, and H.J. Busscher (1991) Assessment of microbial cell surface hydrophobicity. In *Microbial Cell Surface Analysis*, N. Mozes, P.S. Handley, H.J. Busscher, and P.G. Rouxhet, eds., pp. 263-287. VCH Publishers, New York, New York.

Vandevivere, P., and P. Baveye (1992a) Saturated hydraulic conductivity reduction caused by aerobic bacteria in sand columns. Soil Sci. Soc. Am. J. 56:1-13.

Vandevivere, P., and P. Baveye (1992b) Effect of bacterial extracellular polymers on the saturated hydraulic conductivity of sand columns. Appl. Environ, Microbial. 58:1690-1698.

Vandevivere, P. and D.L. Kirchman (1993) Attachment stimulates exopolysaccharide synthesis by a bacterium. Appl. Environ. Microbiol. 59:3280-3286.

van Loosdrecht, M.C.M., J. Lyklema, W. Norde, G. Schraa, and A.J.B. Zehnder (1987) Electrophoretic mobility and hydrophobicity as a measure to predict the initial steps of bacterial adhesion. Appl. Environ. Microbial. 53:1898-1901.

van Loosdrecht, M.C.M., J. Lyklema, W. Norde, and A.J.B. Zehnder (1989) Bacterial Adhesion: A Physiochemical Approach. Microbiol. Ecol. 17:1-15.

van Loosdrecht, M.C.M., J. Lyklema, W. Norde, and A.J.B. Zehnder (1990) Influence of interfaces on microbial activity. Microbiological Reviews 54(1):75-87.

Vogel, T.M., and P.L. McCarty (1985) Biotransformation of tetrachloroethylene to trichloroethylene, dichloroethylene, vinylchloride, and carbon dioxide under methanogenic conditions. Appl. Environ. Miciobiol. 49:1080-1083.

Wiechelman, K., R. Braun, and J. Fitzpatrick (1988) Investigation of the bicinchoninic acid protein assay: Identification of the groups responsible for color formation. Anal. Biochem. 175:231-237.

Wiencek, K.M. and M. Fletcher (1995) Bacterial adhesion to hydroxyl- and methyl-terminated alkanethiol self-assembled monolayers. J. Bacteriology 177:1959-1966.

Widdowson, M.A. (1991) Comment on "An evaluation of mathematical models of the transport of biologically reacting solutes in saturated soils and aquifers" by P. Baveye and A. Valocchi. Water Resour. Res. 27:1375-1378.

Widdowson, M.A., F.J. Molz, and L.D. Benefield (1988) A numerical transport model for oxygen- and nitrate-based respiration linked to substrate and nutrient availability in porous media. Water Resour. Res. 24:1553-1565.

Williams, F.M. (1967) A model of cell growth dynamics. J. Theor. Biol. 15:190-207.

Williamson K. and P.L: McCarty (1976) A model of substrate utilization by bacterial films. J. Water Pollution Control Federation 48:9-24.

Wood, B.D., C.N. Dawson, J.E. Szecsody, and G.P. Streile (1994) Modeling contaminant transport and biodegradation in a layered porous media system. Water Resour. Res. 30:1833-1845.

Wood, B.D., T.R. Ginn, and C.N. Dawson (1995) Effects of Microbial Lag in Contaminant Transport and Biodegradation Modeling. Water Resour. Res. 31:553-563.

Wood, W.W. and G.G. Ehrlich (1978) Use of baker's yeast to trace microbial movement in ground water. Ground Water 16:398-403.

Wrangstadh, M., U. Szewzyk, J. Oestling, and S. Kjelleberg (1990) Starvation-specific formation of a peripheral exopolysaccharide by a marine Pseudomonas sp., strain S9. Appl. Environ. Microbial. 56:2065-2072.

Yao, K.M., M.T. Habibian, and C.R. O'Melia (1971) Water and wastewater filtration: Concepts and applications. Environ. Sci. Technol. 5:1105-1112.

Zysset, A., F. Stauffer, and T. Dracos (1994) Modeling of reactive groundwater transport governed by biodegradation. Water Resour. Res. 30:2423-2434.

Deng, F.-W., J.H. Cushman, and J.W. Delleur (1993) A fast Fourier transform of the contaminant transport problem. Water Resour. Res. 29(9):3241-3247.

Doyen, P.M. (1988) Permeability, conductivity, and pore geometry of sandstone. J. Geophys. Res. 93(B7):7729-7740.

Gelhar, L.W., C. Welty, and K.R. Rehfeldt (1992) A critical review of data on field-scale dispersion in aquifers. Water Resour. Res. 28(7):1955-1974.

Hassan, A.E., J.H. Cushman, and J.W. Delleur (1997) Monte Carlo studies of flow and transport in fractal conductivity fields: Comparison with stochastic perturbation theory. Water Resour. Res. 33(11):2519-2534.

Hess, K.M., S.H. Wolf, and M.A. Celia (1992) Large-scale natural gradient tracer test in sand and gravel, Cape Cod, Massachusetts, 3, Hydraulic conductivity variability and calculated macrodispersivities. Water Resour. Res. 28(8):2011-2027.

Hewett, T.A. (1986) Fractal distribution of reservoir heterogeneity and their influence on fluid transport, paper presented at SPE Annual Technical Conference and Exhibition, Soc. of Petrol. Eng., New Orleans, LA.

Hu, B.X., F.-W. Deng, and J.H. Cushman (1995) Nonlocal reactive transport with physical and chemical heterogeneity: Linear nonequilibrium sorption with random K_d. Water Resour. Res. 31(9):2239-2252.

Karickhoff, S.W., D.S. Brown, and T.A. Scott (1979) Sorption of hydrophobic pollutants on natural sediments. Water Res. 13:241-248.

Kinzelbach, W. (1988) The random walk method in pollutant transport simulation, in *Groundwater Flow and Quality Modeling,* edited by E. Custodio, A. Gurgui, and J.P. Lobo Ferreira, pp. 227-246, D. Reidel, Norwell, Mass.

Kinzelbach, W., and P. Ackerer (1986) Modelisation du transport de contaminant dans un champ d'ecoulement non-permanent. Hydrogeologie, 2:197-206.

Klotz, D., K.P. Seiler, H. Moser, and F. Neumaier (1980) Dispersivity and velocity relationships from laboratory and field experiments. J. Hydrol. 45:169-184.

LaBolle, E.M., G.E. Fogg, and A.F.B. Tompson (1996) Random-walk simulation of transport in heterogeneous porous media: Local mass-conservation problem and implementation methods. Water Resour. Res. 32(3):583-593.

Lin, S.H. (1977) Longitudinal dispersion in porous media with variable porosity. J. Hydrol. 34:13-19.

Mantoglou A., and J.L. Wilson (1982) The turning bands method for simulation of random fields using line generation by a spectral method. Water Resour. Res. 18(5):1370-1394.

Naff, R.L. (1978) A continuum approach to the study and determination of field longitudinal dispersion coefficients, Ph.D. dissertation, N.M. Inst. of Mining and Technol., Socorro.

Parzen, E. (1962) *Stochastic Processes,* Holden-Day, Merrifield, VA.

Shvidler, M.I. (1985) Averaging of transport equations in porous media with random inhomogeneities. Fluid Dyn. 20(l):59-65.

Shvidler, M.I. (1993) Correlation model of transport in random fields. Water Resour. Res. 29(9):3189-3199.

Tompson, A.F.B. (1993) Numerical simulation of chemical migration in physically and chemically heterogeneous porous media. Water Resour. Res. 29(11):3709-3726.

Tompson, A.F.B., and L.W. Gelhar (1990) Numerical simulation of solute transport in three-dimensional, randomly heterogeneous porous media. Water Resour. Res. 26(10):2541-2562.

Turcotte, D.L. (1985) A fractal approach to the relationship between Ore grade and tonnage, Ph.D. thesis, Dept. of Geol. Sci., Cornell Univ., Ithaca, N.Y.

Uffink, G. (1985) Macrodispersie in gelaagde pakketten-deel, 1, een reken-model. RIVM Leidschendam, Leidschendam, Netherlands.

Valocchi, A.J., and A.M. Quinodoz (1988) Application of the random walk method to simulate the transport of kinetically adsorbing solutes, in *Groundwater Contamination,* edited by L.M. Abriola, IA*HS Publ.,* 185:35-42.

Voss, R.F. (1988) Fractals in nature: From characterization to simulation, in *The Science of Fractal Images,* edited by H. Peitgen and D. Saupe, Springer-Verlag, New York.

Warren, J.E., and F.F. Skiba (1964) Macroscopic dispersion. Trans. Am. Inst. Min. Metall. Pet. Eng. 231:215-230.

Woodbury, A.D., and E.A. Sudicky (1991) The geostatistical characteristics of the Borden aquifer. Water Resour. Res. 27(4):533-546.

Bellin, A., P. Salandin, and A. Rinaldo (1992) Simulation of dispersion in heterogeneous porous formations: Statistics first-order theories, convergence of computations. Water Resour. Res. 28(9):2211-2227.

Chin, D.A., and T. Wang (1992) An investigation of the validity of first-order stochastic dispersion theories in isotropic porous media. Water Resour. Res. 28:1531-1542.

Cushman, J.H. (1983) Comment on "Three-dimensional stochastic analysis of macrodispersion in aquifers" by L.W. Gelhar and C.L. Axness. Water Resour. Res. 19:1641-1642.

Cushman, J.H. (1990) *Dynamics of Fluids in Hierarchical Porous Media,* Academic, San Diego, Calif.

Cushman, J.H. (1997) *The Physics of Fluids in Hierarchical Porous Media: Angstroms to Miles,* Kluwer Acad., Norwell, Mass.

Cushman, J.H., and B.X. Hu (1997) Solution to the stochastic transport problem of $O\left(\sigma_v^N\right)$ for conservative solutes. Stochastic Hydrol. Hydraul. 104(2):215-223.

Cushman, J.H., B.X. Hu, and F.-W. Deng (1996) Comparison of Eulerian to Lagrangian expected spatial moments for transport in a heterogeneous porous medium with deterministic linear nonequilibrium sorption. Chem. Eng. Commun. 148-150, 5-21.

Dagan, G. (1989) *Flow and Transport in Porous Formations,* Springer-Verlag, New York.

Dagan, G. (1994) An exact nonlinear correction to transverse macrodispersivity for transport in heterogeneous formations. Water Resour. Res. 30(10):2699-2705.

Dagan, G., and S.P. Neuman (1991) Nonasymptotic behavior of a common Eulerian approximation for transport in random velocity fields. Water Resour. Res. 27(12):3249-3256.

Deng, F.-W., and J.H. Cushman (1995) On higher-order corrections to the flow velocity covariance tensor. Water Resour. Res. 31(7):1659-1672.

Deng, F.-W., and J.H. Cushman (1998) Higher-order corrections to the flow velocity covariance tensor, revisited. Water Resour. Res. 34(1):103-106.

Deng, F.-W., J.H. Cushman, and J.W. Delleur (1993) A fast Fourier transform stochastic analysis of the contaminant transport problem. Water Resour. Res. 29(9):3241-3247.

Gelhar, L.W. (1993) *Stochastic Subsurface Hydrology,* Prentice-Hall, Englewood Cliffs, N. J.

Gelhar, L.W., and C.L. Axness (1983) Three-dimensional stochastic analysis of macrodispersion in aquifers. Water Resour. Res. 19(1):161-180.

Hassan, A.E., J.H. Cushman, and J.W. Delleur (1997) Monte Carlo studies of flow and transport in fractal conductivity fields: Comparison with stochastic perturbation theory. Water Resour. Res. 33(11):2519-2534.

Hassan, A.E., J.H. Cushman, and J.W. Delleur (1998) A Monte Carlo assessment of Eulerian flow and transport perturbation models. WaterResour. Res. 34(5):1143-1164.

Hsu, K., D. Zhang, and S.P. Neuman (1996) Higher-order effects on flow and transport in randomly heterogeneous porous media. Water Resour. Res. 32(3):571-582.

Hu, B.X., and J.H. Cushman (1997) Comparison of nonlocal Eulerian to Lagrangian moments for transport in an anisotropic heterogeneous aquifer with deterministic linear nonequilibrium sorption. Water Resour. Res. 33(4):891-896.

Hu, B.X., F.-W. Deng, and J.H. Cushman (1995) Nonlocal reactive transport with physical and chemical heterogeneity: Linear nonequilibrium sorption with random K_d. Water Resour. Res. 31(9):2239-2252.

Hu, B.X., F.-W. Deng, and J.H. Cushman (1997) Nonlocal reactive transport with physical and chemical heterogeneity: Linear nonequilibrium sorption with random rate coefficients, in *Recent*

Advances in Subsurface Stochastic Hydrolog, edited by G. Dagan and S.P. Neuman, pp. 891-896, U.N. Educ. Sci. and Cult. Org., Paris.

Kapoor, V., and L.W. Gelhar (1994a) Transport in three-dimensionally het-erogeneous aquifers, 1, Dynamics of concentration fluctuations. Water Resour. Res. 30(6):1775-1788.

Kapoor, V., and L.W. Gelhar (1994b) Transport in three-dimensionally heterogeneous aquifers, 2, Predictions and observations of concentration fluctuations. Water Resour. Res. 30(6):1789-1802.

Kapoor, V., and P.K. Kitanidis (1998) Concentration fluctuations and dilusion in aquifers. Water Resour. Res. 34(5):1181-1193.

Kinzelbach, W. (1988) The random walk method in pollutant transport simulation, in *Groundwater Flow and Quality Modeling,* edited by E. Custodio, A. Gurgui, and J.P. Lobo Ferreira, pp. 227-246, D. Reidel, Norwell, Mass.

LaBolle, E.M., G.E. Fogg, and A.F.B. Tompson (1996) Random-walk simulation of transport in heterogeneous porous media: Local mass-conservation problem and implementation methods. Water Resour. Res. 32(3):583-593.

Naff, R.N. (1994) An Eulerian scheme for the second-order approximation of subsurface transport moments. Water Resour. Res. 30(5):1439-1455.

Simmons, C.S. (1982) A stochastic-convective transport representation of dispersion in one-dimension porous media systems. Water Resour. Res. 18(4):1193-1214.

Taylor, G.I. (1921) Diffusion by continuous movements, *Proc. London Math. Soc., Ser. A,* 20:196-211.

Tompson, A.F.B. (1993) Numerical simulation of chemical migration in physically and chemically heterogeneous porous media. Water Resour. Res. 29(11):3709-3726.

Tompson, A.F.B., and L.W. Gelhar (1990) Numerical simulation of solute transport in three-dimensional, randomly heterogeneous porous media. Water Resour. Res. 26(10):2541-2562.

Archie, G.E. (1950) Introduction to petrophysics of reservoir rocks. Bull. Am. Assoc. Petrol. Geophys. 34(5):943-961.

Aziz, K. and A. Settari (1979) *Petroleum Reservoir Simulation,* 476 pp., Appl. Sci., London.

Burrough, P.A. (1981) Fractal dimensions of landscapes and other environmental data. Nature 294:240-242.

IV. Publications

1. M. Moroni and J.H. Cushman (2000) Anomalous dispersion of conservative tracters: Theory and 3-DPTV experiments. In Stochastic Methods in Subsurface Hydrology, ed. R.S. Govindaraju (In Press) AICE.

2. M. Moroni and J.H. Cushman (2000) Asymptotic limits for anomalous dispersion: Nonequilibrium statistical mechanical theories and 3-DPTV experiments: Physics of Fluids (Submitted).

3. M. Moroni and J.H. Cushman (2000) Pore-scale dispersion in the asymptotic limit: Comparison of theory and 3-DPTV experiments. Water Resour. Res. (Submitted).

4. F. Bonilla and J.H. Cushman (2000) Role of boundary conditions on convergence and nonlocality of solutions to stochastic flow problems in bounded domains. Water Resour. Res. 36(4):981-997.

5. F. Bonilla and J.H. Cushman (2000) On perturbative expansions to the stochastic flow problem. Trans. Porous Media (In Press).

6. R. Smits and J.H. Cushman (2000) Application of sticky Brownian motion to microbial dynamics in porous media. 1. Random walks. AIChE (Submitted).

7. J.H. Cushman and T.R. Ginn (2000) The fractional ADE is a classical mass balance with convolution-Fickian flux. Water Resour. Res. (Submitted).

8. A. Hassan, J.H. Cushman and J.W. Delleur (1998) The significance of porosity variability to transport in heterogeneous media. Water Resour. Res. 34(9):2249-2259.

9. B.X. Hu, A. Hassan and J.H. Cushman (1999) Eulerian solutions of $O\left(\sigma_v^N\right)$ for the stochastic transport problem for conservative tracers coupled with $O\left(\sigma_p^2\right)$ solutions for the flow problem in an infinite domain. Water Resour. Res. 35(12):3687-3698.